Empleo de Nuevas Tecnologías Aplicadas a la Química Analítica

Kevin Urbano Antela

Doctorado en Técnicas Experimentales en Química

Directores:
M. Luisa Cervera Sanz
Ángel Morales Rubio

Universitat de València [ó ʒ] Facultad de Química

Empleo de Nuevas Tecnologías Aplicadas a la Química Analítica

MEMORIA PRESENTADA PARA OPTAR AL TITULO DE DOCTOR POR

Kevin U. Antela

Programa de doctorado

"Técnicas Experimentales en Química"

Directores:

Dra. M. Luisa Cervera Sanz

Dr. Ángel Morales Rubio

Valencia, Marzo 2023

El Prof. Dr. Ángel Morales Rubio, Catedrático de Universidad, y la Prof. Dra. M. Luisa Cervera Sanz, Catedrática de Universidad del Departamento de Química Analítica de la Universitat de València (Estudi General)

CERTIFICAN

Que D. Kevin Urbano Antela ha realizado la presente Tesis Doctoral titulada "Empleo de Nuevas Tecnologías Aplicadas a la Química Analítica" bajo su dirección en el Departamento de Química Analítica de la Universitat de València, y autorizan su presentación para optar al Grado de Doctor en Técnicas Experimentales en Química.

Y para que así conste, firman la presente en Burjassot a 31 de Marzo de 2023.

Prof. Dr. Ángel Morales Rubio   Prof. Dra. M. Luisa Cervera Sanz

A los que con el tiempo se volvieron mi familia

Si haces una promesa, la cumples, si cometes un error, te disculpas...

y si le das un sueño a alguien, lo proteges hasta el final...

Agradecimientos

Me gustaría agradecer a mis directores de tesis M. Luisa Cervera y Ángel Morales Rubio, por todo el apoyo recibido y por los conocimientos que me han inculcado, y al departamento de Química Analítica de la Universitat de València, así como a la propia universidad, por haberme permitido cursar mis estudios de Doctorado. Me gustaría agradecer a la Conselleria d´Innovació, Universitats, Ciència i Societat Digital de la Generalitat Valenciana por el proyecto GVA-PROMETEO-2019-056 y por la subvención para estancias de contractos predoctorales en centros de investigación fuera de la Comunitat Valenciana CIBEFP/2021/07 y poder así optar a la mención internacional. También al Servei de Formació Permanent i Innovació Educativa de la Universitat de València por los proyectos de innovación docente UV-SFPIE_PID-1356255, UV-SFPIE_PID-1641484 y UV-SFPIE_PID-2079679.

Fuera de los agradecimientos formales me gustaría dar las gracias a varias personas. Me gustaría que estos agradecimientos quedasen entre ellos y yo, por ello, no voy a especificar ningún nombre, pero todo tiene relación con algún recuerdo que tengo con ellos o lo que más me ha marcado con ellos.

A lo largo de estos 3 años, no solo he aprendido de la investigación, ya sea por mis tutores, por lo que he ido leyendo o por mi propia experiencia, sino que además he aprendido a tener diferentes puntos de vista y formas de afrontar diferentes situaciones.

Entre las personas a las que más tengo que agradecer esta tesis es a un fénix, que me ha apoyado durante todo este viaje y siempre me ha escuchado y sin su ayuda nunca podría estar donde estoy. Muchas gracias por todo. Además, sé que jamás lo entenderá, pero hay 3 puntos negros que son muy importantes para mí y aunque no lo sepa, ha hecho por mí más de lo que jamás podría imaginarse y quiero que eso quede aquí reflejado. Muchas gracias.

Siguiendo entre la gente a la que siento que le debo mucho están mis 5 pilares, una flor de cerezo, un copo de nieve, un paparajote, una abejita y una policía. Estas personas son lo más importante que tengo y que he forjado a lo largo de estos más de 3 años de doctorado. Son personas que han estado ahí para todo; para lo bueno, pero sobre todo para lo malo, para mis momentos de desesperación, en aquellas situaciones en las que de verdad he pensado que no podría salir airoso. Es cierto que las personas están siempre en lo bueno, pero en esos momentos en los que uno solo quiere llorar, normalmente está solo y es ahí cuando te das cuenta de la calidad de tus alrededores. Por ello, gracias por no abandonarme cuando más os

necesitaba. Muchísimas gracias de verdad. Son las primeras personas con las que de verdad he podido ser yo. Son personas que han logrado que me pudiera enfrentar a las cosas. Son personas que siempre me han apoyado y siempre han sabido que podría enfrentarme a este doctorado y mucho más. Los recuerdos que tengo con ellos son increíblemente preciados para mí.

Entre otras personas, están un atún rojo, una piedra blanca-negra, un diente rojo y un amigurumi. Esta gente ha estado conmigo durante los momentos de frustración y de "eureka" del laboratorio. Cada uno de ellos me ha enseñado maneras mejores de trabajar y de cómo poder sacar más provecho a los resultados. No solo eso, sino que han sido mi fuga en momentos de desesperación, ya sea con un café o con una broma. Cada uno de ellos es diferente, pero siento que en mi trabajo siempre habrá un pedacito de ellos, pues mi trabajo esta influenciado por su experiencia y sus consejos. Además de hacerme ver la vida con otros puntos de vista y a pensar en aspectos del entorno laboral desde otra perspectiva. Muchas gracias.

Por supuesto tengo que agradecer a la persona de los melocotones, al de la basura espacial y la que me enseño 1500 cartas de colores. Durante estos 3 años he trabajado con ellos codo con codo para intentar sacar todo lo posible adelante. Me han ayudado muchísimo tanto en el trabajo como fuera, algo que he valorado mucho al ser una persona que no tiene ningún familiar en Valencia. Además, siempre han intentado, desde el primer día, integrarme y hacerme sentir como si siempre hubiera pertenecido allí. Ha habido proyectos, congresos, docencia… Muchísimas gracias por estos tres años de enseñanza y experiencia.

Si bien es cierto que estas son las personas que más han estado a mi lado durante estos 3 años hay otras personas a las que tengo que agradecerles muchísimo. La que me dio un túper de huevos cocidos me enseñó muchísimo de la investigación. Fuera de lo puramente químico aprendí mucho del análisis fisicoquímico y del análisis organoléptico. Por mostrarme ese mundo y enseñarme sobre él quisiera darle las gracias. También hay un señor que no quiere comida en el laboratorio que si bien es muy estricto y demasiado trabajador es un gran investigador y me ha mostrado cómo aplicar la química para saber más sobre la historia.

Aunque los conocí tarde, también hay un grupo de personas bastante cinéfilas que se han vuelto importantes para mí con los que he podido tener diferentes experiencias. Ellos también han estado para escucharme y para animarme cuando lo necesité, muchas gracias.

He tenido que irme fuera de mi país para lograr la mención internacional y eso me ha llevado a conocer una cantidad de personas que me han ayudado muchísimo. Una mujer que me ha acogido como uno más de la familia, un aprendiz de robótica que me ha hecho sentirme integrado dentro de un lugar nuevo aún con la dificultad de la barrera del idioma y la promotora de toda esta aventura italiana que me ha ayudado a enfrentarme a todos los problemas que me he encontrado. Muchísimas gracias a todos por facilitarme la vida en unos momentos tan complicados.

Tres años son demasiados, muchas experiencias, muchas personas, momentos buenos, momentos malos… todo ha sido una enseñanza, aunque no puedo comentar todos y cada uno de ellos, muchísimas gracias a todo lo que me ha pasado, a todos los que he conocido. De una manera o de otra todo me ha ayudado, ya sea por las buenas o por las malas, y si estoy aquí ahora es gracias a que todo ha pasado de la manera en la que ha pasado y estoy muy agradecido por ello.

INDEX

FIGURES

TABLES

ABBREVIATIONS

ABSTRACT

FIGURES

Figure R.1: Brief chronology of advances in instrumental techniques (Clark et al., 1925; Engelhardt, 1999; Karayannis & Efstathiou, 2012; Pyke, 1937; Raman & Krishnan, 1928).

Figure R.2: Arrangement of the source-sample-detector for a determination by reflectance (A) or by transmittance (B).

Figure R.3: Visual representation of the RGB colour model.

Figure R.4: Spectral locus with the representation of a triangle of colours generated from a green pixel, a red pixel and a blue pixel (gamut).

Figure R.5: Visual representation of L*a*b* colour space.

Figure R.6: Visual representation of L*h*C* colour space.

Figure R.7: Screenshot of the program loading screen.

Figure 1.1. Representation of the colours of the chips of the glossy Munsell Atlas in the CIELAB space, with different reference whites: the Minolta's reference white (A and B) and the highest-reflectance achromatic sample of the Munsell Atlas (C and D). Representations A and C show that the chips are organized in constant lightness planes. In a plane of constant lightness (B and D), the distribution of the chips in constant Munsell chroma rings (which do not exactly coincide with CIELAB constant chroma loci) and in constant tone loci, approximately equispaced, is appreciated.

Figure 1.2. Methacrylate support employed to obtain the images by the smartphone devices.

Figure 1.3. Passing-Bablok correlation diagrams for RGB values of the Munsell Atlas, obtained by a Xiaomi device and a Samsung device. The violet dotted define the 95% prediction interval of the sample; the central line of the interval is the best fitting line, and is surrounded by its confidence interval (magenta region). The black line is the reference line x = y.

Figure 1.4. ΔE2000 colour differences between the RGB images captured by two mobile phones (Samsung and Xiaomi), using the same standard (sRGB) to calculate the CIELAB description of the samples.

Figure 1.5. Contributions of differences in lightness (L), chroma (C) and hue (H) to the colour difference between devices, as a function of the main tone of the sample.

Figure 1.6. Distribution of the errors obtained when predicting the real CIELab descriptors of the samples, obtained with a spectrophotometer, with a standard transform (sRGB) of the RGB values obtained with two different smartphones.

Figure 1.7. Comparison of the actual chromaticity of the pieces (A) and the chromaticities predicted with the sRGB transformation from the RGB values captured by the Samsung smartphone (B) and Xiaomi (C).

TABLES

Table 2.1: Correlation and Root Mean Square Error values obtained with the best model using regression learner for each combination of data.

Table 2.2: Values of parameters m and n of the equation ($y = m \cdot x^n$) of the power model and R^2 values.

Table 2.3: Correlation between the L* parameter of the leaf and iron obtained by HCl extraction for each of the power models modified with new leaves species.

Table 2.4: Statistical parameters of the validation of the method.

Table 3.1. RMSE and coefficients of determination obtained for the different models calculated for the RGB colour space in peach leaves.

Table 3.2. Summary of the best models for the chlorophyll prediction in peach leaves according to the chlorophyll content units and the colour space. The table specify the colour parameters combination that provides the best prediction model, the lower RMSE and the higher R^2.

Table 3.3. Summary of the best models for the chlorophyll prediction in apricot leaves according to the chlorophyll content units employed and the colour space. The table specify the colour parameters combination that provides the best prediction model, the lower RMSE and the higher R^2.

Table 3.4. Summary of the best models for the chlorophyll prediction in persimmon leaves according to the chlorophyll content units employed and the colour space. The table specify the colour parameters combination that provides the best prediction model, the lower RMSE and the higher R^2.

Table 3.5. Summary of the best models for the chlorophyll prediction in loquat leaves according to the chlorophyll content units employed and the colour space. The table specify the colour parameters combination that provides the best prediction model, the lower RMSE and the higher R^2.

Table 3.6. Summary of the developed models, the combination of parameters employed for each colour space, and estimation of the appropriate prediction: Green - suitable; Orange- not suitable; Yellow-suitable but the 95% confidence interval adjust is too wide. Pea.: Peach; Apr.: Apricot; Per.: Persimmon; Loq.: Loquat.

Table 3.7. Parameters of the joint model of the four fruit species for chlorophyll in µg g^{-1} in the RGB colour space.

Table 3.8. Parameters of the joint model of the four fruit species for chlorophyll in µg g^{-1} in the RGB colour space.

Table 3.9. Summary of the functions for the chlorophyll content prediction of the join models and the values of the parameters in the function.

Table 3.A.1. RMSE and coefficients of determination obtained for the different models calculated for the CIELab colour space in peach leaves.

Table 3.A.2. RMSE and coefficients of determination obtained for the different models calculated for the CIELhC colour space in peach leaves.

Table 3.A.3. RMSE and coefficients of determination obtained for the different models calculated for the RGB colour space in apricot leaves.

ABBREVIATIONS

A: absorbancia (Absobance)

AAS: Espectrometría de absorción atómica (atomic absorption spectrometry)

ADHD: Trastorno de déficit de atención e hiperactividad (attention déficit and hyperactivity disorder)

ADI: Ingesta diaria recomendada (aceptable daily intake)

ALA: Ácido α-linolenico (α-linolenic acid)

AOPs: Procesos de oxidación avanzados (Advance Oxidation Processes)

B: Azul (Blue)

BG: Azul-Verde (Blue-Green)

C: Croma // Incolora (Chroma // Clear)

CCI: índice de contenido de cloroifla (chlorophyll content index)

CCM: Medidor de contenido de clorofila (Chlorophyll content meter)

Chl: clorofila (Chlorophyll)

CIE: Comisión Internacional de la Iluminación (Commission internationale de l'éclairage)

DoE: Diseño de experimentos (design of experiments)

DPASV: Voltamperometría de redisolución anódica de pulso diferencial (differential pulse anodic stripping voltammetry)

EFSA: Autoridad de seguridad alimentaria europea (European Food Safety Authority)

FAAS: Espectroscopia de absorción atómica de llama (flame atomic absorption spectroscopy)

G: Verde (Green)

GND: Tierra (ground)

GY: Verde-Amarillo (Green-Yellow)

GBL: Game-Based Learning

GPIO: conexión de entrada salida de propósito general (general-purpose input output)

H: Tono (Hue)

HPLC: Cromatografía líquida de alta eficiencia (high-performance liquid chromatography)

ICP-MS: Plasma de acoplamiento inductivo- espectrómetro de masas (inductively coupled plasma - mass spectrometry)

ICP-OES: Plasma de acoplamiento inductivo- espectrofotómetro de emisión óptico (iductive coupled plasma- optic emission spectrofotometer)

IDE: Entorno de desarrollo integrado (integrated development environment)

IFR: Federación internacional de robótica (International Federation of Robotics)

Jpeg: Joint Photographic Experts Group

L: Luminosidad (Lightness)

LDR: Resistencia dependiente de la luz (light-dependant resistor)

LED: Diodo emisor de luz (Light emission diode)

LMC: Concentración máxima legislada (Legislated máximum concentration)

LOD: Limite de detección (Limit of Detection)

LOQ: Límite de cuantificación (Limit of Quantification)

min: minutos (minutes)

NA: No disponible (not available)

o-phen: o-fenantrolina (o-phenanthroline)

P: Púrpura (Purple)

PB: Púrpura-Azul (Purple-Blue)

PFOA: Ácido perfluorooctanoico (perfluorooctanoic acid)

PLG: Gas licuado de petróleo (petroleum liquid gas)

R: Rojo (Red)

RGB: Rojo, Verde y Azul (Red, Green & Blue)

RP: Rojo-Púrpura (Red-Purple)

rpm: revoluciones por minuto (Revolutions per minute)

RMSE: Error cuadrático medio (Root mean square error)

SC: Escáner (scanner)

SCL: Señal de reloj (serial clock)

SDA: Señal de datos (serial data)

sLab: standard Lab

SP: *Smartphone*

sRGB: standard RGB

V: valor (Value)

VCC: Colector común de tensión (voltaje common collector)

WC: Cámara web (webcam)

XRF: Espectrometría de fluorescencia de rayos X (X-ray fluorescence spectrometry)

Y: Amarillo (Yellow)

YR: Amarillo-Rojo (Yellow-Red)
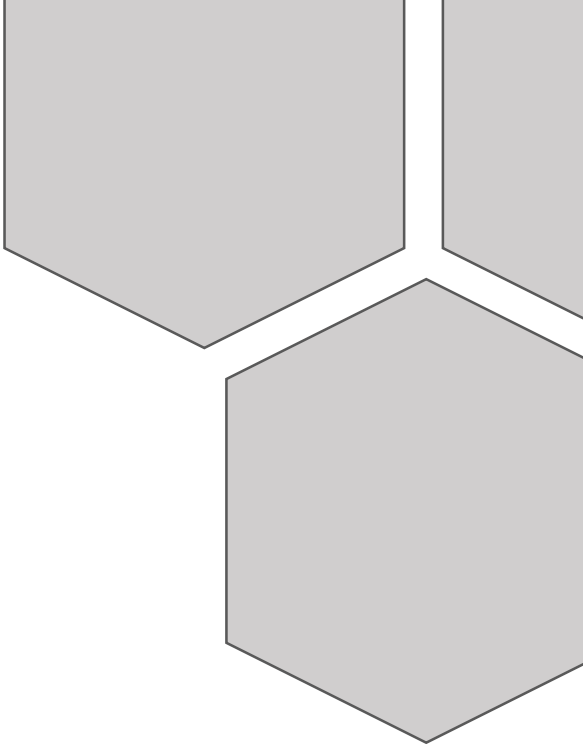
ABSTRACT
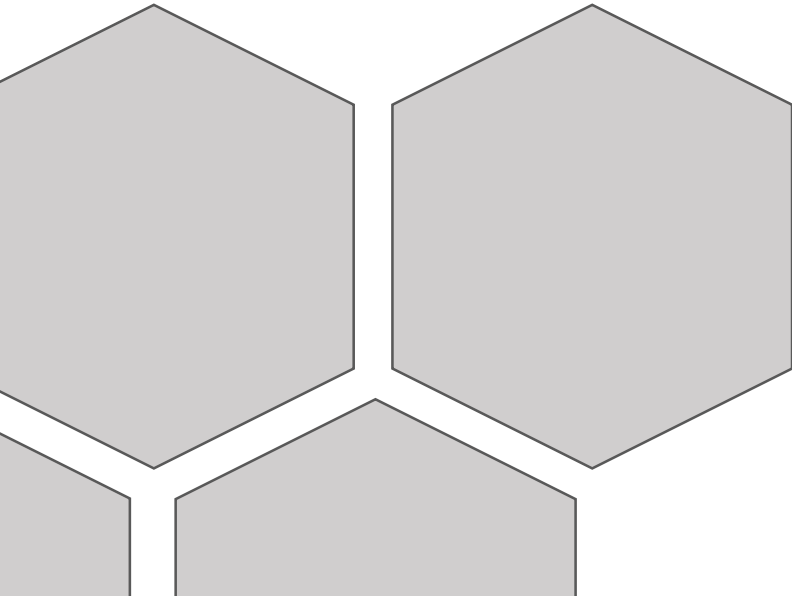
The advance of technology in recent years has been very remarkable, and its development continues to accelerate. Situations that were unthinkable 30 years ago are not only a reality but also are within reach of any user. This can be exemplified in the use of smartphones, which allow citizens to have multiple tools in their hands that would normally need a specific instrument. It has also been seen that robotics has gone from being essential complex tools and specialised personnel to simply requiring curiosity and interest to learn its operation, having available several induction courses of robotics, even for children.

This thesis aims to demonstrate the advantages of the interconnection between chemistry and new technologies, drawing attention to the importance of programming, image colour treatment, and 3D printing. The thesis is divided into 15 chapters, organised into 3 sections:

1. The first section is based on the use of smartphones as an analytical tool and is divided into 10 chapters. One of the most notable aspects of a smartphone is its camera, which captures information about the colour of the environment. By filtering and processing the information collected in the images, using appropriate programming codes, colorimetric analyses can be performed.
2. The second section comprises 4 chapters and is focused on the development of robots for automated analysis. Technological development has led to the emergence of simple platforms for programming, such as Arduino boards and Raspberry Pi devices that even novice users can use to create electronic devices. With the correct programming of these boards and the appropriate connections to sensors and other devices, laboratory automation can be achieved at low cost and tailored to the operator's needs.
3. Finally, the third section is centred on a single chapter related to educational research. Within the university community, teaching is considering one of the most significant aptitudes, in addition to basic knowledge or its application. For this reason, the development and evaluation of a video game as a teaching tool from the perspective of gamification and Game-Based Learning (GBL) has been proposed.

The first chapter of this thesis addresses the issue of colour information received by smartphones, comparing the information captured by various phones with the information obtained by reference colour measuring instruments. The following

four chapters are based on obtaining information through direct image capture with the smartphone. In these chapters, foliar iron and chlorophyll content in leaves and aquatic environments is measured without any further sample treatments. The next four chapters illustrate the data obtained from the image after performing a treatment or a chemical reaction on the sample. This work encompasses the study of food dyes and quinine in food samples and the development of a kit for quantifying copper in treated waters. The last chapter is based on the development of an image transformation captured with the phone to allow the establishment of organoleptic differences in tomato ripeness by dichromatic individuals.

The first chapter of the second block (Chapter 11) reviews the electronic sensors that can be coupled with Arduino and Raspberry Pi that are being applied in the performance of analysis. In this chapter, not only is the review of these sensors presented, but also their assembly and programming. The second chapter of this block a device for colour analysis with a colour sensor using Raspberry Pi is developed. This device not only performs automated analysis, but also has been coupled with a sampler built with 3D printing and programmed with the Raspberry Pi board to perform automated analysis of various samples. The next two chapters deal with devices to automate the preparation and analysis of samples using Arduino. In these cases, the analyses are performed using colour sensors.

The last chapter of the thesis (Chapter 15) focuses on educational research with a GBL. A video game has been programmed to contain simulated laboratory practices and exercises to help students to reinforce their knowledge. In addition, the video game presents a mini-game for laboratory waste management and videos to explain ~~the~~ more complex sections of the educational planning contents.

1.   The smartphone in instrumental analysis

The great development of instrumental techniques dates to World War II. Since then, instrumental methods of analysis have been used more frequently than classical ones (Karayannis & Efstathiou, 2012). In an analysis, the instruments utilise electromagnetic radiations or some physical properties of matter to obtain information which, after being manipulated and interpreted, leads to the parameters of interest. According to this definition, it can be understood that the devices used to obtain this data serve as a mean of communication between the sample and the operator (Skoog et al., 2017; Robinson et al., 2005). In Figure R.1, a brief chronology of the evolution in the development of some of the different known techniques can be observed.
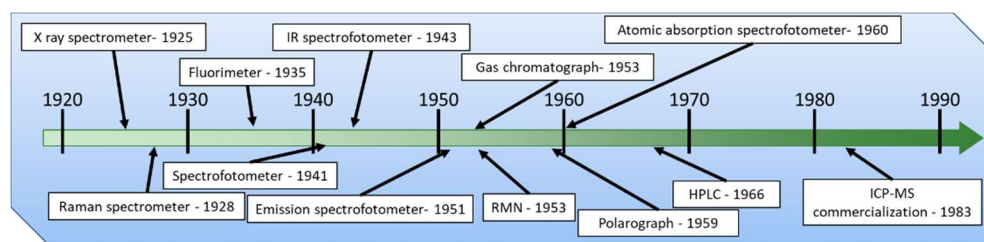
Figure R.1: Brief chronology of advances in instrumental techniques (Clark et al., 1925; Engelhardt, 1999; Karayannis & Efstathiou, 2012; Pyke, 1937; Raman & Krishnan, 1928).

Due to the aforementioned, it is safe to say that smartphones can fit that definition. This device, also known as a mobile phone, has made information and social networks more accessible to people. Given its characteristics, it is a widely distributed object among the population (Organista-Sandoval et al., 2013). A smartphone is defined as a mobile phone that offers similar features to those provided by a computer and stands out for its ability to connect to the network. These phones usually include a QWERTY keyboard, with the possibility of accessing internet search servers or personal email, making calls, sending messages, among others. However, the most remarkable feature of these types of phones is the presence of different kinds of sensors and the ability to work in different applications accessible from the phone store.

If these devices had sensors, they could collect information from the environment, and with this information, a user could interpret the surroundings. Therefore, this device could act as an intermediary between the information provided by the object under study and the operator. Thus, the smartphone could be an important tool in instrumental techniques. Among the different possibilities offered by a smartphone to obtain information from the environment, the photographic camera

stands out stands out owing to its inherent ability of taking high quality and low-cost photos quickly.

According to the International Commission on Illumination (CIE), colorimetry is "The measurement of colour stimuli based on a series of conventions" (CIE, 2011). In chemistry, colorimetry is a technique used to determine the concentration of different compounds from the colour of the sample (Housecroft & Constable, 2010). To evaluate the colour of an object, it must be illuminated and the reflected light measured (Figure R.2A). However, in the case of transparent liquids, colour is evaluated by transmitting light through the fluid (Figure R.2B). This is reflected in the equation of Lambert-Beer's Law (Equation 1), which shows a relationship between the absorbance of the liquid sample and the concentration of the compound that absorbs radiation (Shellhammer, 2009). This can be translated into a correlation between the compounds found in the sample and the colour that the sample presents. The smartphone, by having a photographic camera, is capable of obtaining information about the colour of the environment, therefore it ought to be capable of obtaining information about its chemical composition as well. Ergo, smartphones can be used as a colorimetric instrument through image analysis of photographs.

When taking a photograph with a smartphone, it usually provides an image in jpg or jpeg format (Joint Photographic Experts Group). These formats are a type of compression of the image file that allows to store colour data through the RGB channels and the same data in grayscale. There are numerous applications and software programs that permit to obtain information from the different channels of the image to work with that data. In this way, from an image, we can acquire the colour parameters decomposed into Red, Green, and Blue (RGB) components (Rezazadeh et al., 2019). With these colour parameters and the known concentration of an analyte, calibration lines can be set up to calculate the content of that analyte in a real sample. Despite the numerous programs to obtain colour parameters, this thesis employs Matlab software. By using this software and the ColorLab library (Malo & Luque, 2002), not only can we obtain the information encoded in the RGB colour space, but we can also make transformations to get information in other colour spaces such as CIELab or CIELhC, which express the same information in different ways, which, depending on the situation, can be more useful when creating calibration models.
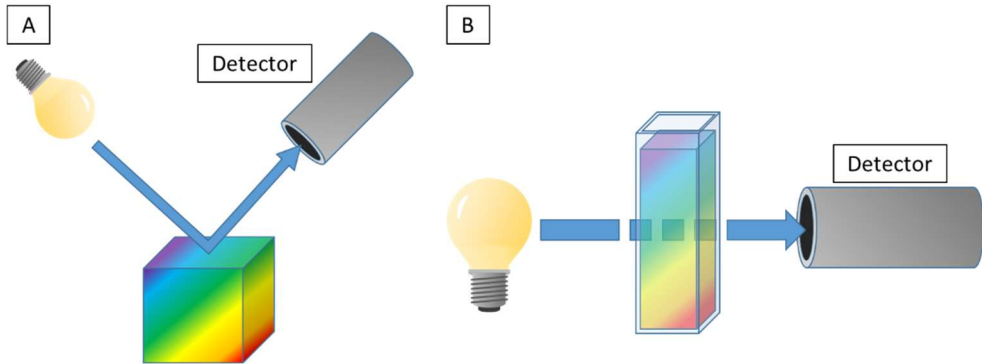
Figure R.2: Arrangement of the source-sample-detector for a determination by reflectance (A) or by transmittance (B).

$$A = \propto \cdot \, l \cdot c \qquad\qquad \text{(Equation 1)}$$

A=absorbance; α= molar absorptivity; k=molar extinction coefficient; λ= wavelength; l= optical path; c= compound concentration.

1.1. Colour spaces

A colour space is a specific organization of colours (Kerr, 2010; Ragain, 2016). Colour is not a primary physical property of matter, and what provides colour is the spectrum of absorbance/reflectance that is dependent on the characteristics of the light source (Kerr, 2010). These spectra can be described as functions of wavelength across the visible spectrum. However, describing these functions would require a practically infinite number of parameters. Despite this, several authors have suggested that spectral reflectance curves could be fitted to a linear model with a reduced number of parameters (Billmeyer & Fairman, 1987). Over the years, a series of colour spaces have been developed that, using 3 parameters, are able to describe a colour, with the most commonly used being RGB, CIELab, and CIELhC.

1.1.1. RGB

The most common colour expression in capture devices is through RGB. This model describes colour using 3 channels, corresponding to Red (R), Green (G), and Blue (B). The values that each channel can take vary between [0, 0, 0], which corresponds to black, and [2n-1, 2n-1, 2n-1], which corresponds to white. The value of n stands for the number of bits used for colour digitisation. The RGB model is additive, meaning that colours are obtained by adding the components of the 3 channels (Capitán-Vallvey et al., 2015). The visual representation of how this model works is shown in Figure R.3.
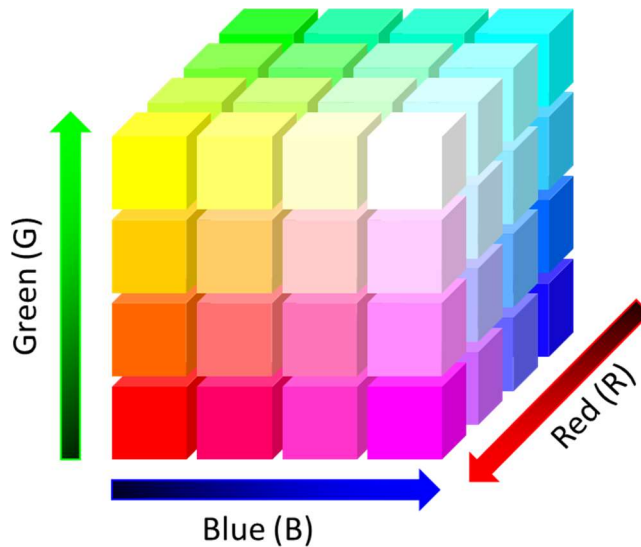
Figure R.3: Visual representation of the RGB colour model.

In this thesis, the RGB colour model has been used in the calibration of dyes using wool (Chapter 7) and in the creation of models for obtaining chlorophyll content in solid support water samples (Chapter 4). In the context of digital devices that provide information about colour expressed in RGB, delimited by the device's Red, Green, and Blue pixels, the colours perceived by these devices are restricted to the colours that can be generated from the combination of these pixels. Figure R.4 shows the spectral locus with the colour generation triangle from the three pixels of a random device. The spectral locus is a representation of the spectral tristimulus values of the monochromatic colours between 380 and 780 nm. Within this represented region are all the colours obtained by combining different wavelengths (Zharinov & Zharinov, 2017).

As can be observed, pixels are not pure colours, therefore, there are many existing colours that cannot be captured or reproduced by devices. In this case, devices perceive the closest generable or capturable colour to the real one. This could be an issue when using different smartphones. Each device is capable of perceiving different colours depending on the camera used, so it would be necessary to always use the same lighting conditions to have reproducibility in the measurements. However, even with these conditions, the use of other devices could provide

different results. This not only applies between devices but could also differ from the results obtained with reference devices such as a colorimeter or a spectroradiometer. The study of the colour data obtained by different devices and their potential use to acquire real colours is discussed in chapter 1 of this thesis.
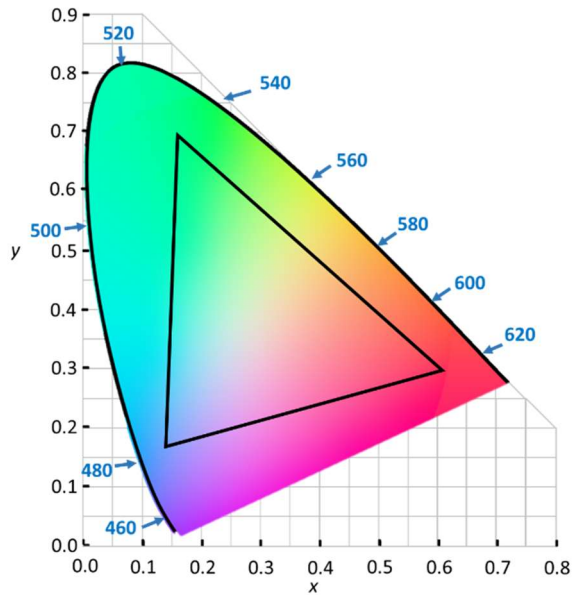
Figure R.4: Spectral locus with the representation of a triangle of colours generated from a green pixel, a red pixel and a blue pixel (gamut).

1.1.2. CIELab

To work in terms of uniformity, the CIE has recommended certain colour spaces, including CIELab (Robertson, 1977). This is a three-dimensional space designed to approximate human vision (Bansal & Aggarwal, 2011). The three coordinates of this space are L*, a*, and b*. The first one refers to luminosity, with a value of L*=0 for black and L*=100 for diffuse white. The a* coordinate stands for the difference in reflected light between green and red, with a value of a*=-100 for green and a*=+100 for red. The last coordinate refers to the difference in reflected light between blue and yellow, with a value of b*=-100 for blue and b*=+100 for yellow (Bansal & Aggarwal, 2011; Robertson, 1977). As shown in Figure R.5, it is a three-dimensional space with spherical geometry. Although this colour space is overly useful, digital devices are not capable of providing data in this format. To address

this issue in the studies presented in the thesis, colour data is transformed utilising Matlab with the use of the ColorLab library (Malo & Luque, 2002). The employment of the equation 2 function in a program script allows for the transformation of colour parameters from RGB to L*a*b*, with "rgb" being our Nx3 matrix of colours in RGB.
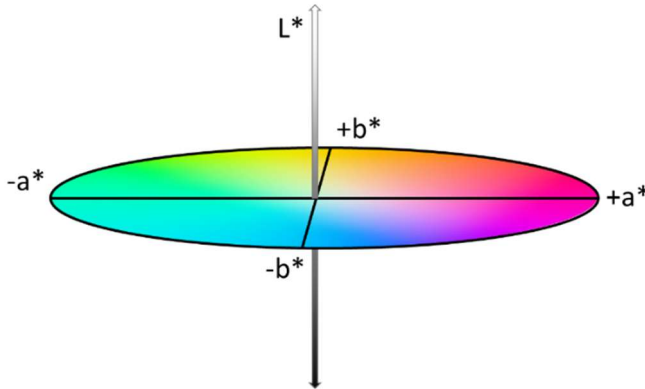
*Figure R.5: Visual representation of L*a*b* colour space.*

$$lab = rgb2lab\ (rgb) \qquad \text{(Equation 2)}$$

To properly perform this analysis, the next procedure must be followed. First, the area of the photograph we are interested in analysing is selected, either manually or using masks that choose a region based on the desired characteristics. Once our study area is separated, the average colour is obtained by taking into account the colour of all pixels in that area. This is achieved using an indexed image, which consists of two parts: on one hand, we have the image in which each area that presents a specific colour is identified with a code, and on the other hand, we have the colour palette in which each code is identified with the colour that governs those pixels/regions. This is achieved utilising the use of the function represented in equation 3, where: 1) "im" is the data matrix corresponding to our study region, 2) "col" would be the number of colours we want our palette to have, 3) "imind" would be the data matrix of our study region, but associating each pixel with a code, and 4) "palRGB" would be our colour palette in the form of an N*3 matrix, with N being the number of colours, associated with our indexed image.

$$[imind, palRGB] = true2pal(im, col) \qquad \text{(Equation 3)}$$

Having the indexed image, we could obtain the colour average using the RGB colour space, however, in this space it is not possible since it is additive, and it is necessary to switch to an intermediate colour space, in this case, XYZ, which corresponds to tristimulus values. To do this, it would be necessary to apply the colour space change to the RGB colour palette and perform the colour average in the XYZ colour space, as shown in equations 4 and 5. In equation 4, "palXYZ" corresponds to our colour palette in the XYZ colour space. In equation 6, the colour average is being performed in the XYZ colour space, using all the pixels corresponding to the indexed image that belong to the region we want to study (masc == 1). In this way, if a colour is present in a certain number of pixels, in the average, that colour is used as many times as pixels with that colour are found. When we have the colour average in XYZ, we only need to convert it to the Lab* colour space using the function presented in equation 6, where "xyz" is our Nx3 matrix of colours and "xyzb" is our reference white value in the XYZ colour space.

$$palXYZ = rgb2xyz(palRGB) \qquad \text{(Equation 4)}$$
$$xyz = mean(palXYZ(imind(masc == 1), :)) \qquad \text{(Equation 5)}$$
$$lab = xyz2lab(xyz, xyzb) \qquad \text{(Equation 6)}$$

This colour space has been useful when working with a specific colour or with a specific amount of light. In chapter 2 of this thesis, the iron content in leaves was determined using a photograph and the L* parameter of the image. The lack of iron in the leaves causes a condition called iron chlorosis, which results in a yellowing of the leaves and therefore in an increase in colour brightness. The L* parameter has also been useful in the fluorometric determination of quinine through image analysis, since a higher content of quinine leads to greater fluorescence. This colour space not only provides good information about brightness, but also about colour, as can be seen in chapters 5 and 10. In chapter 5, chlorophyll was quantified in water by direct photography of a water column using the a* parameter, which corresponds to the green colour of the analyte. On the other hand, in chapter 10, the issue of distinguishing between green and red colours, associated with tomato ripeness, in dichromatic individuals was addressed. This difficulty corresponds to the a* coordinate of this colour space. By swapping the values of the a* and b* coordinates of the image, it is possible for these individuals to perceive differences in tomato ripeness with blue-yellow colours.

1.1.3. CIELhC

The CIELhC colour space has the same shape as the CIELab one. Nevertheless, the difference is that in the former, the coordinates are cylindrical, whereas in the latter, the coordinates are Cartesian (Rossel et al., 2006). In this colour space, L* represents luminosity, h* represents hue, and C* represents chroma. Figure R.6 shows a representation of this colour space. To obtain colour data in this colour space using Matlab, the function in equation 7 needs to be applied, which simply transforms Cartesian coordinates to polar coordinates.

This colour space was used in chapters 6 and 9 of this thesis, where it was necessary to work with colour quantity, associated with chroma, and colour tone, studied with the h* parameter. In chapter 6, this colour space was fundamental for obtaining good results since food dyes were used in sweets. Typically, sweets contain one or two dyes to create the entire range of colours. To evaluate a single colour, it is only necessary to work with chroma. However, in cases where there was a mixture of dyes, the proportion of dyes was given by the hue. Once the proportion of dyes was obtained, it was only necessary to use chroma to acquire the total content of dyes. In chapter 9 of this thesis, the parameter used to perform the chemical analysis through image analysis was the C* one. In this case, the aim was to evaluate the colour of a chemical reaction in the presence of copper. The solution without copper was colourless, and the solution became more violet when increasing copper content. Since we are dealing with an increment in colour, chroma is the parameter of choice for this analysis.
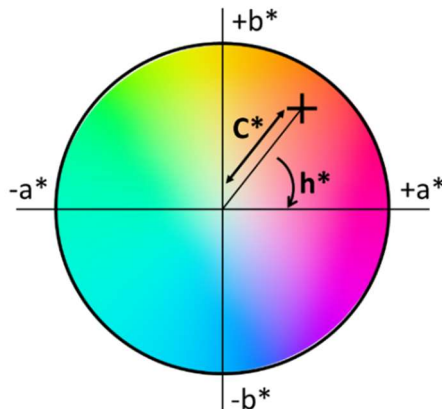
*Figure R.6: Visual representation of L*h*C* colour space.*

$$lhc = lab2perc(lab) \qquad \text{(Equation 7)}$$

2.   Electronic sensors in chemical analysis

The smartphone is a suitable instrument for taking colorimetric measurements, as has been observed in this thesis, but it is necessary to carry out appropriate image processing to perform chemical analysis. While these devices are common among the population, there are other types of tools that are less widespread: electronic sensors. Sensors are devices that convert a physical variable into another variable that can be interpreted. In the case of electronic sensors, we would be talking about electrical signals (Ebel & Nestel, 1993). There is a wide variety of sensors, including physical sensors such as pressure (Hetprostore, 2022) or tilt ones (Llamas, 2022). However, these sensors are not widely used when it comes to performing chemical analysis. On the other hand, another type of sensors that can be found, such as temperature (Parihnar et al., 2017), gas (Sahu et al., 2017), humidity (Bhadani & Vashisht, 2019), or, the focus of this thesis, light (Ashwin & Harish, 2020) and colour sensors (de Carvalho et al., 2022). Chapter 11 of this thesis provides a more in-depth review of the different sensors that can be used for monitoring or analysis of various types.

Among light and colour sensors, the simplest one would be the photoresistor. This tool allows to obtain information from light. Photoresistors are devices that vary their resistance according to the amount of light that falls upon them (Llamas, 2022). At first glance, these devices could be useful; however, they have a large number of disadvantages. Despite being economic, less than €1, they can only measure the amount of light. This could be a significant issue since a change of colour does not necessary have to modify the amount of light, therefore the sensor's resistance would not vary thus the value of the analog signal would remain the same. On the other hand, the range of values that it can adopt is limited to 1024 (10 bits). As an alternative to this light sensor, the BH1750 sensor can be found, which does not give the analog value of the current intensity but directly provides the measurement of light in lumens/m^2 and has a range of values between 1 and 65535 (16 bits) (Naylampmechatronics, 2022). In spite still being affordable and presenting greater accuracy and precision, we again encounter the problem that these devices can only detect changes associated with the amount of light. To make more efficient measurements of the variation of light, whether it is the amount of light or the colour of light, the use of colour sensors such as the TCS34725 would be recommended. This sensor has 3 filters for receiving information corresponding to each channel (red, green, blue, and clear), so it is capable not only of differentiating the amount of light but also the colour (Ams, 2022).

When it comes to working with sensors, it is necessary to have a support that allows the programming of these instruments to be able to obtain the appropriate information from them. In order to develop a programming code and to work on the various available platforms, it is usually believed that extensive knowledge of the field is required; however, this is not really the case. In recent years, and with the rapid growth of new technologies, programming environments are becoming more accessible to a user who is starting out in this world. Such is the situation that anyone can find at their disposal a large number of induction courses in various programming languages such as C++ (Carrillo, 2005), Python (Challenger-Pérez et al., 2014) or R (García et al., 2010). Despite the importance of the code, the physical support with which one is going to work is also important. To be able to program, a device to be programmed is needed and for this, a support that translates the code into orders. Among the most suitable supports for a user without any expertise are the Arduino and Raspberry Pi devices, which are overly versatile due to their application in companies or in the development of prototypes.

Arduino is a reprogrammable microcontroller board that has different connection pins (female type) that facilitate the creation of circuits and the connection of sensors and controllers. Arduino emerged in 2005 from the Interactive Design Institute of Ivrea, Italy, to favour an affordable communication between students and different devices (Artero, 2013). Arduino was created with the intention that non-specialised users could use it to achieve different objectives. It was a platform for designers and artists so that they could modify and use hardware elements in a simple and economical way (Gibb, 2010). On the other hand, the Raspberry Pi device is a small, single-board computer that has an operating system such as a computer, but on a small scale. It is also possible to connect peripherals, such as a monitor, and work within the board. In addition to acting as a computer, it has connection pins like Arduino and, therefore, different sensors and controllers can be connected that are programmed by the Raspberry itself (Zhao et al., 2015).

Both the TCS34725 colour sensor and Arduino and Raspberry Pi boards have been used as tools to obtain the necessary information for carrying out chemical analysis in chapters 12, 13, and 14 of this thesis. In chapter 12, this sensor was programmed using a Raspberry Pi4 single-board computer utilising the Python language. The developed device consisted of a servo-controlled auto-sampler, a peristaltic pump to drive the solution through the circuit, and a TCS34725 sensor. This device allows the automation of the colorimetric measurement of different samples, obtaining a

report with the colour values of the solution. The analytes studied were food colorants such as Tartrazine, Brilliant Blue FCF, and Allura Red AC. In chapter 13 of this thesis, this sensor was coupled to a device used to perform colorimetric reactions automatically. The robot was controlled using the C++ language employing an Arduino UNO board. This device drives the sample and different reagents to the detector through sequences of programming codes by utilising micro-pumps. In the detector, the result of the colorimetric reaction is obtained, and using the TCS34725 sensor, it is possible to calibrate and chemically analyse different samples. The capacity of these robotic devices was studied in the model reaction between copper and bicinchoninic acid and it is described in chapter 9 of this thesis. Finally, in chapter 14 of this thesis, both the TCS34725 sensor and the Arduino board and C++ programming code were used to monitor the consumption of hydrogen peroxide in a photo-Fenton degradation reaction of pollutants. In this process, iron and hydrogen peroxide are used to carry out an advanced oxidation process to degrade organic contaminants. Hydrogen peroxide acts as a precursor of hydroxyl radicals that initiate the degradation reaction. In this sense, the utilisation of these techniques allows to rehabilitate water for a later use. All these investigations show the importance of interdisciplinary work with other fields. The incorporation of basic programming knowledge allows the development of robots that can be applied in analytical chemistry. However, this is not the only technology that can be used as support; 3D printing is a type of technological advance widely distributed both at the professional and user level, which allows to create different structures with PLA plastic, mainly according to the user's requirements. In this thesis, throughout the different chapters, its usefulness for the development of customised supports that facilitate analysis tasks or allow to measure more challenging data that otherwise would be more complicated or costly in terms of time invested can be observed.

3.   Teaching research and GBL

As can be observed, interdisciplinarity is something that is at the forefront when it comes to research. However, this not only applies to basic knowledge research. Universities, as places of knowledge dissemination, also have the function of transmitting knowledge to future researchers (Turugare & Rudhumbu, 2020). Therefore, teaching is something that takes up a large part of the time invested in the university institution. This can be seen in the number of classes taught by researchers from different fields, the final research papers that students have to

carry out in connection with one of the departments associated with the studies taught, or in teaching innovation projects. Educational innovation projects involve the development and implementation of new teaching tools in order to improve students' acquisition of the content taught (Feixas et al., 2018).

One of the most discussed strategies in recent years within educational innovation research is gamification (Kapp, 2012; Pegalajar, 2021). Gamification is a learning methodology in which the teacher applies traditional game techniques, such as points, prizes, missions, or scoreboards, within the classroom and therefore outside the context of a game itself (Pivec et al., 2003). Game-Based Learning (GBL) is a methodology that, unlike gamification, uses games as a teaching tool to transmit and facilitate the acquisition of knowledge (Hartt et al., 2020; Perez, 2015).

Chapter 15 of this thesis discusses a teaching innovation project that involves the development of a GBL as a teaching tool in chemistry studies. This video game has been created using the RPGMaker MZ® program (Figure R.7). When talking about a video game, we are considering the need to write programming codes to carry out the actions of the game. This program is based on the Ruby language (Muñoz Alejandre, 2022), even though basic programming knowledge is somewhat required, the program itself is designed thus anyone can develop a video game without being a professional. This has been achieved by coding pre-established codes called actions. In this way, the user only must select the actions they want the character to carry out to obtain the code of the game. The developed game attempts to address topics such as the preparation and reinforcement of laboratory practices, the formalisation of concepts and procedures for solving numerical exercises, and the incorporation of support material to reinforce the contents of the syllabus. The teaching innovation project is in its third year, which are: UV-SFPIE_PID-1356255 (first year), UV-SFPIE_PID-1641484 (second year), and UV-SFPIE_PID-2079679 (third year).

Figure R.7: Screenshot of the program loading screen.

4. Conclusions

As it can be checked, this thesis reveals the usefulness of computer knowledge in an era ruled by technological advances. Given the large number of tools available to users for device control and content creation, basic programming knowledge can provide the foundation for projects that could not be carried out without these concepts. This technological growth of society makes the interrelation between chemical and computer knowledge more palpable. Owing to basic programming skills, image analysis procedures have been developed, automation devices have been created, and teaching tools have been updated and made more relevant to students, all focused on the chemical viewpoint and created by amateur personnel. This demonstrates the usefulness of computer science and new technologies in any research field for the development of customised equipment or software adapted to the needs of the researcher.

5. References

Ams. (Accessed September 26, 2022). Colour Sensor – Colour Light-To-Digital Converter – TCS34725 ams | ams, (n.d.). https://ams.com/tcs34725#tab/description

Artero, Ó. T. (2013). Arduino. Curso práctico de formación. RC libros. Madrid.

Ashwin, S. H., & Harish, S. V. (2020). Titration machine: A new approach using Arduino. In Kalam, A., Niazi, K.R., Soni, A., Siddiqui, S.A., & Mundra, A. (Eds.), Intelligent Computing Techniques for Smart Energy Systems. Springer, Singapore.

Bansal, S., & Aggarwal, D. (2011). Colour image segmentation using CIELab colour space using ant colony optimization. *International Journal of Computer Applications*, 29(9), 28-34. DOI:10.5120/3590-4978.

Bhadani, P., & Vashisht, V. (2019). Soil moisture, temperature and humidity measurement using arduino. In 9th International Conference on Cloud Computing, Data Science & Engineering. IEEE.

Billmeyer Jr, F. W., & Fairman, H. S. (1987). CIE method for calculating tristimulus values. *Colour Research & Application*, 12(1), 27-36. DOI:10.1002/col.5080120106.

Capitán-Vallvey, L. F., Lopez-Ruiz, N., Martinez-Olmos, A., Erenas, M. M., & Palma, A. J. (2015). Recent developments in computer vision-based analytical chemistry: A tutorial review. *Analytica Chimica Acta*, 899, 23-56. DOI: 10.1016/j.aca.2015.10.009.

Carrillo, A. G. (2005). Fundamentos de programación en C++. Primera edición. García, F. M. (Ed.). Delta Publicaciones. Madrid.

Challenger-Pérez, I., Díaz-Ricardo, Y., & Becerra-García, R. A. (2014). El lenguaje de programación Python. *Ciencias Holguín*, 20(2), 1-13.

CIE. (accessed july 20, 2022). https://cie.co.at/eilvterm/17-25-014

Clark, G. L., Weber, H. C., & Hershey, R. L. (1925). A Precision X-Ray Spectrometer for Chemical Investigations. *Industrial & Engineering Chemistry*, 17(11), 1147-1150.

de Carvalho, G., Machado, C. C. S., Inácio, D. K., da Silveira Petruci, J. F., & Silva, S. G. (2022). RGB colour sensor for colorimetric determinations: Evaluation and quantitative analysis of coloured liquid samples. *Talanta*, 241, 123244. DOI: 10.1016/j.talanta.2022.123244.

Ebel, F., & Nestel, S. (1993). Sensores para la técnica de procesos y manipulación: sensores de proximidad. Festo Didactic. Esslingen.

Engelhardt, H. (1999). GC und HPLC—die letzten 50 Jahre. *Nachrichten aus Chemie, Technik und Laboratorium*, 47(12), 1451-1452. DOI: 10.1002/nadc.19990471229.

Feixas, M., Martínez-Usarralde, M. J., & López-Martín, R. (2018). Do teaching innovation projects make a difference? Assessing the impact of small-scale funding. *Tertiary Education and Management*, 24(4), 267-283. DOI: 10.1080/13583883.2017.1417470.

García, J. M. C., Portillo, E. M., & Cezón, P. A. (2010). Introducción a la programación estadística con R para Profesores.

Gibb, A. M. (2010). New media art, design, and the Arduino microcontroller: A malleable tool. Thesis. Pratt Institute.

Hartt, M., Hosseini, H., & Mostafapour, M. (2020). Game on: Exploring the Effectiveness of Game-based Learning. *Planning Practice & Research*, 35(5), 589-604. DOI: 10.1080/02697459.2020.1778859.

Hetprostore. (Accessed September 26, 2022). Sensor de Fuerza o Presión MF01. https://hetpro-store.com/TUTORIALES/sensor-de-fuerza-o-presion-mf01/#:~:text=El%20sensor%20de%20fuerza%20o,sensor%20cambia%20su%20resistencia%20interna.

Housecroft, C. E., & Constable, E. C. (2010). Chemistry: an introduction to organic, inorganic and physical chemistry. Fourth edition. Pearson education. Harlow.

Kapp, K. M. (2012). The gamification of learning and instruction: game-based methods and strategies for training and education. Taff, R. (Ed.). John Wiley & Sons. San Francisco.

Karayannis, M. I., & Efstathiou, C. E. (2012). Significant steps in the evolution of analytical chemistry—Is the today's analytical chemistry only chemistry? *Talanta*, 102, 7-15. DOI: 10.1016/j.talanta.2012.06.003.

Kerr, D. A. (2010). The CIE XYZ and xyY colour spaces. *Colourimetry*, 1(1), 1-16.

Llamas, L. (Accessed September 26, 2022). Medir inclinación con arduino y sensor TILT SW-520D. https://www.luisllamas.es/medir-inclinacion-con-arduino-y-sensor-tilt-sw-520d/#:~:text=%C2%BFQue%20es%20un%20sensor%20tilt,partir%20de%20una%20cierta%20inclinaci%C3%B3n.

Llamas, L. (Accessed September 26, 2022). https://www.luisllamas.es/medir-nivel-luz-con-arduino-y-fotoresistencia-ldr/.

Malo, J., & Luque, M. J. (2002). ColourLab: the Matlab toolbox for Colourimetry and Colour Vision. Univ. Valencia. http://isp.uv.es/code/visioncolour/colourlab.html.

Muñoz Alejandre, S. (2022). PAWN: Del tablero a videojuego en 3D con UnityDesarrollo del modo multijugador online, Tesis doctoral, Universitat Politècnica de València.

Naylampmechatronics. (Accessed September 26, 2022https://naylampmechatronics.com/blog/44_tutorial-modulo-sensor-de-luz-bh1750.html.

Organista-Sandoval, J., McAnally-Salas, L., & Lavigne, G. (2013). El teléfono inteligente (smartphone) como herramienta pedagógica. *Apertura*, 5(1), 6-19.

Parihar, V. R., Tonge, A. Y., & Ganorkar, P. D. (2017). Heartbeat and temperature monitoring system for remote patients using Arduino. *International Journal of Advanced Engineering Research and Science*, 4(5), 237161. DOI: 10.22161/ijaers.4.5.10.

Pegalajar, M. C. (2021) Implicaciones de la gamificación en Educación Superior: una revisión sistemática sobre la percepción del estudiante. *Revista de Investigación Educativa*, 39(1), 169-188. DOI: 10.6018/rie.419481

Perez, D. (2015). Make a 2D RPG in a Weekend: With RPG Maker MV. Second edition. Renow-Clarke B. (Ed.) Apress.

Pivec, M., Dziabenko, O., & Schinnerl, I. (2003). Aspects of game-based learning. In 3rd International Conference on Knowledge Management, Graz, Austria.

Pyke, M. A. (1937). The chemical measurement of vitamin B1 in foodstuffs and biological material by means of the thiochrome reaction. *Biochemical Journal*, 31(11), 1958. DOI: 10.1042/bj0311958.

Ragain, J. C. (2016). A review of colour science in dentistry: Colourimetry and colour space. *Journal of Dentistry, Oral Disorders & Therapy*, *4*, 1-5. DOI: 10.15226/jdodt.2016.00148.

Raman, C. V., & Krishnan, K. S. (1928). A new class of spectra due to secondary radiation. *Indian Journal of Physics*, 2, 399-419.

Rezazadeh, M., Seidi, S., Lid, M., Pedersen-Bjergaard, S., & Yamini, Y. (2019). The modern role of smartphones in analytical chemistry. *Trends in Analytical Chemistry,* 118*,* 548-555. DOI: 10.1016/j.trac.2019.06.019.

Robertson, A. R. (1977). The CIE 1976 colour-difference formulae. *Colour Research & Application*, 2(1), 7-11. DOI: 10.1002/j.1520-6378.1977.tb00104.x.

Robinson, J. W., Frame, E. M. S., Frame, G. M., Eileen, M., & Skelly, F. (2005). Undergraduate instrumental analysis. Seventh edition. CRC Press. Boca Raton.

Rossel, R. V., Minasny, B., Roudier, P., & Mcbratney, A. B. (2006). Colour space models for soil science. *Geoderma*, 133(3-4), 320-337. DOI: 10.1016/j.geoderma.2005.07.017.

Sahu, P., Dixit, S., Mishra, S., & Srivastava, S. (2017). Alcohol detection based engine locking system using MQ-3 sensor. *International Research Journal of Engineering and Technology*, 4(4), 979-981.

Shellhammer, T. H. (2009). Beer colour. In Bamforth, C.W. (Ed.). Beer: a quality perspective (pp. 213-227). Elsevier Inc.

Skoog, D. A., Holler, F. J., & Crouch, S. R. (2017). Principles of instrumental analysis. Seventh edition. Cengage learning. Boston.

Turugare, M., & Rudhumbu, N. (2020). Integrating technology in teaching and learning in universities in Lesotho: opportunities and challenges. *Education and Information Technologies*, 25(5), 3593-3612. DOI: 10.1007/s10639-019-10093-3.

Zhao, C. W., Jegatheesan, J., & Loon, S. C. (2015). Exploring iot application using raspberry pi. *International Journal of Computer Networks and Applications*, 2(1), 27-34.

Zharinov, I. O., & Zharinov, O. O. (2017). Spectral locus interpolation with splines in optical instruments. In IOP Conference Series: *Materials Science and Engineering* (286, 012013). DOI 10.1088/1757-899X/286/1/012013.

SECTION 1

SMARTPHONE AND IMAGE PROCESSING
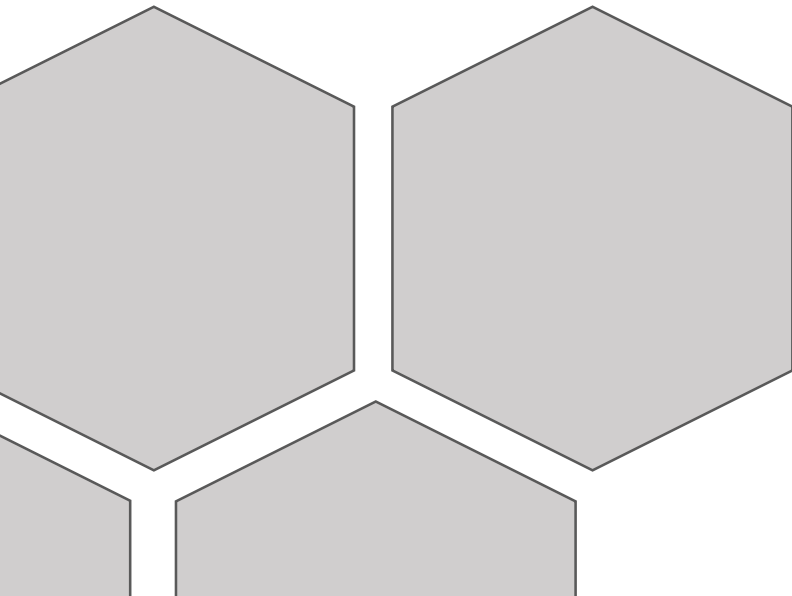
CHAPTER 1: Studies of the employment of characterization models for obtain the colour from a mobile device
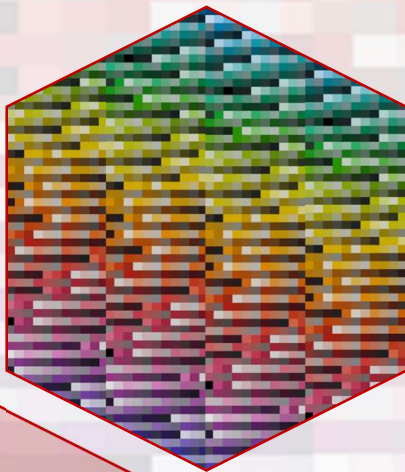
ABSTRACT

In the present chapter, a study has been carried out on the effect of smartphone device characterization on the capture of colour parameters. To accomplish this, 765 Munsell chips, a reference colorimeter, and two smartphones (Xiaomi and Samsung) were employed. Colour difference studies (CIEDE2000) were conducted between the colour detected by the smartphones and the colour captured by the reference device. Subsequently, the samples were divided into a training group and a testing group. Characterization models were designed for both devices using the training group, and the efficiency of the generated model was tested with the testing group. The best characterization model found was with Xiaomi using the XYZ descriptors of the samples and a third-degree polynomial. Other similar models were obtained with Samsung using the XYZ descriptors and third- and fourth-degree polynomials, and with the LAB descriptors using a third-degree polynomial. The use of these device characterization models allowed the colour difference to be reduced from over 10 units without using the characterization model to less than 4 units using said model. In addition to this study, tests have been conducted to evaluate the ability of neural networks to design characterization models for smartphones. The results of these studies indicate that the use of neural network models can be an effective alternative to the use of polynomial models.

Keywords: CIEDE2000, CIELab, Neural networks, RGB, Smartphone, XYZ

1. Introduction

Colour measurement and colourimetry are important techniques used in a variety of fields, including graphic arts, textile manufacturing, and quality control (Gooby, 2020; Wickström et al., 2017). Colour is one of the dimensions of visual perception and is affected by many factors, including the wavelength of light, the spectral power distribution of the light source, and the surface properties of the object being viewed (Caivano, 2022; Fairchild, 2013; Hunt, 1985; Tanaka & Horiuchi, 2018).

A colourimeter is a device that measures the colour of an object by analysing the light that is reflected or transmitted by the object. Colourimeters work by capturing a small portion of the light that is being emitted or reflected by an object and then analysing the spectral power distribution of that light. This information is then used to determine the colour of the object (Ly et al., 2020; Tomasević et al., 2019). There are different types of colourimeters available, such as tristimulus colourimeters, which measure the amount of red, green, and blue light reflected or transmitted by an object, and spectrophotometers, which measure the entire spectrum of light.

Smartphones have increasingly become a popular tool for colour measurement and colourimetry. Many smartphones are equipped with image and video capture devices, and we have already developed applications to analytical chemistry based in colour information extracted from images (Antela et al., 2022; Sáez-Hernández et al., 2022 a-d). Additionally, there are a number of apps available that have been specifically designed for colour measurement and colourimetry, which can be downloaded and used on a smartphone (Shrivas et al., 2021; Wu & Federico, 2019).

One of the ways that smartphones can be used as colourimeters is through the use of the device's camera. The camera can be used to take a picture of an object, and then the colours within the image can be analysed using image processing algorithms. This can be done through apps that are specifically designed for colour measurement, or through the use of third-party image processing software. Some apps use the device's camera to estimate colour descriptors of a sample in different colour representation spaces. In this way, the colour of an object may be compared to a known standard or colour information may be used to adjust colours in a digital image (Antela et al., 2022; Sáez-Hernández et al., 2022 a,c).

The colour measured by a smartphone compared to the colour measured by a professional colourimeter or spectroradiometer can be quite different. This is due to a number of factors, including the limitations of the sensors and camera on the

smartphone and the different methods used by smartphones and colourimeters to measure colour (Abebe et al., 2021; Gómez-Robledo et al., 2013).

One of the main differences between the colour measured by a smartphone and that measured by a colourimeter is the accuracy of the measurement. Professional colourimeters and spectroradiometers are specifically designed for colour measurement, and they use advanced sensors and optics to accurately measure the colours of objects. Smartphones, on the other hand, use cameras and sensors that are not specifically designed for colour measurement, which can lead to inaccuracies in the colour measurements. These inaccuracies could appear when the device collect a colour out of the gamut´s range. Additionally, smartphones have limited dynamic range and are not able to capture the colour information in the same range of brightness as professional devices (Wang et al., 2020).

Another difference is in the way colour is measured. Professional colourimeters and spectroradiometers measure colour using a tristimulus or spectrophotometric method, which takes into account the spectral distribution of the light reflected or emitted by the sample (Tomasević et al., 2019). Smartphones, on the other hand, typically provides a RGB response, where colour is represented by a combination of red, green and blue channel. Those values are obtained by sensors with tunning curves having peaks in the red, green and blue region of the spectrum respectively. This response is normalized between 0 and 2^n-1 for each channel, where n is the resolution of the sensor in bits. This representation is not lineal and depends on the device (Hong et al., 2001; Poynton & Funt, 2014) and on the capture setting. As in any colour measurement, final colour depends on the lighting conditions (Berns, 2019; Linhares et al., 2020; Phuangsaijai et al., 2021). All these factors must be taken into account when transforming device dependent RGB responses to standard colour spaces, such as CIELAB.

It is possible to use a smartphone to obtain an approximation of the real colour descriptors of an object in a standard colour space, as long as the device has been colorimetrically characterized and the illumination and capture conditions are well defined and fixed. RGB values from a smartphone image can be mathematically transformed into colour values expressed in colour spaces such as CIELAB. This can be achieved with standard transformations such as Adobe or sLab (Chmutin, 2022; Fdhal et al., 2009; Kumah et al., 2019; Taghadomi-Saberi et al., 2015). These transformations do not contain information about the sensitivies of the sensors of each particular capture device, introducing errors in the estimation of real colour (Maali Amiri & Fairchild, 2018). By properly characterizing a smartphone, the

inaccuracies and variations in colour measurements may be reduced and more accurate colour descriptors obtained (Leon et al., 2006; Westland et al., 2012; Yang et al., 2021).

One way to characterize a smartphone is to use it in combination with a professional reference colourimeter or spectroradiometer to obtain colour values, and then try reproducing the values of the standard descriptors obtained from the reference device using the smartphone RGB response. This reproduction can be carried out through a mathematical transformation of the RGB values that minimize the difference between descriptors obtained with this model and those measured by the reference devices. This can help to identify any discrepancies between the values obtained by the smartphone and the values obtained by the professional device, and it allows to identify any issues in the camera or light sensor of the smartphone (Martínez-Verdú et al., 2003).

Once the smartphone is characterized, it can be used as a colourimeter, by transforming the RGB values of images of the samples to be measured using the colorimetric characterization software derived for the device. It is important to repeat this process under the same lighting conditions and on the same surface finish as the original characterization process (Abebe et al., 2021).

Even after the colorimetric characterization process, the smartphone is still not as accurate as a professional colourimeter or spectroradiometer, but it can be a useful tool for colour measurement in many everyday situations where a high level of accuracy is not required. Since camera responses are not only influenced by the camera optics, the light sensor sensitivities and architecture and the image enhancement software, but also by the conditions of use and the environment, the device should be used under the same conditions as during the characterization process (Antela et al., 2022; Sáez-Hernández et al., 2022 a-d).

The aim of this work is to study how colour is measured by different smartphones and compare it with reference colorimetric devices such as a Minolta colourimeter and a spectroradiometer. Moreover, it will be studied if a characterization of the smartphones can accurately estimate samples colour.

2.   Materials and methods

2.1.   Instruments

To obtain the reference data about the colour parameters of the samples, a Macbeth spectrocolourimeter (CM-26d Konica Minolta) (Tokyo, Japan) was used.

Sample images were taken with a Samsung Galay S7 Edge smartphone, Samsung (Seoul, South Korea) and a Smartphone Xiaomi Mi T10 smartphone, Xiaomi (Pekín, China).

2.2.   Software

Colour data was processed in Matlab®, using the ColorLab library (Malo & Luque, 2002). Neural models were implemented in Rstudio, with the *h2o* (LeDell et al., 2018) and *skimr* (Waring et al., 2022) packages.

2.3.   Data base

Colour samples for the colorimetric characterization process were extracted from the Munsell Colour Atlas, glossy edition (GretaMacbeth). This Atlas contains a set of 1601 colour chips, organized by hues, with the condition that the perceptual distance between two adjacent chips is always constant. It constitutes a colour ordering system (Fairchild, 2013). The colour of each chip is described with four variables:

-The main hue, Blue, Blue-Green, Green, Green-Yellow, Yellow, Yellow-Red, Red, Red-Purple, Purple, and Purple-Bluish, described by its English initial (B, BG, G, GY, Y, YR, R, RP, P, and PB).

-The secondary hue (H). The space between two main hues is divided into eight hue angles, identified by the values 1.25, 2.5, 3.75, 5 (the main hue), 6.25, 7.5, 8.75, and 10.

-The chroma (C), which evaluates the perceptual distance to white, and that takes the values 0 (achromatic), 1, 2, 4, 6, 8, 10, and 12

-The lightness or value (V). The scale of lightness includes values between 0 (black) and 10 (maximum reflectance white), in unit steps.

Due to its perceptual uniformity properties, the Munsell Atlas has become one of the basic training and testing databases in the development of colour vision spaces and in the analysis of the properties of its metrics (Fairchild, 2013). In this thesis, it will be used to train the colorimetric characterization models of smartphone cameras, accepting the hypothesis that, by covering the range of colours that can be generated by reflection, the characterization model obtained would be valid for the different problems that will be addressed in this thesis.

Using the Macbeth spectrocolourimeter (CM-26d) the reflectance of each of the Munsell chips has been measured, as well as their CIELAB values, obtaining the

results summarized in Figure 1.1. The CIELAB values depend on the reference white used. For the calculations made in the colorimetric characterization model of the smartphone, we will use the most luminous achromatic stimulus present in the scene and illuminated as our samples.
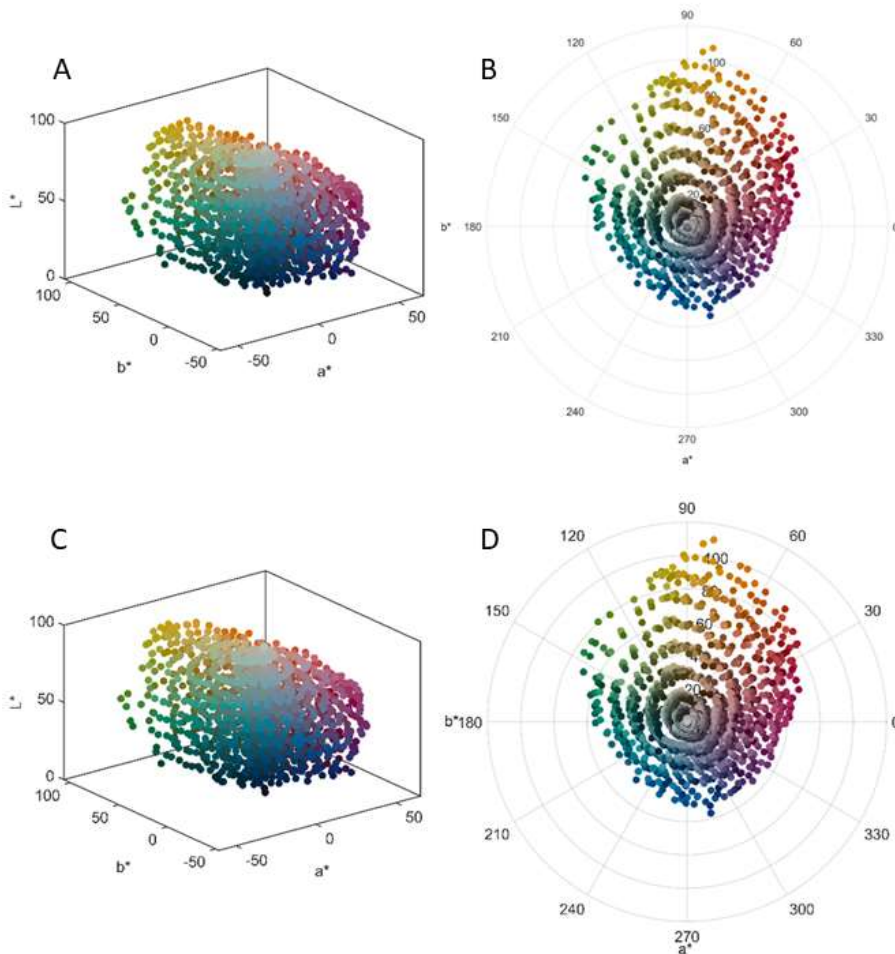
Figure 1.1: Representation of the colours of the chips of the glossy Munsell Atlas in the CIELAB space, with different reference whites: the Minolta's reference white (A and B) and the highest-reflectance achromatic sample of the Munsell Atlas (C and D). Representations A and C show that the chips are organized in constant lightness planes. In a plane of constant lightness (B and D), the distribution of the chips in constant Munsell chroma rings (which do not exactly coincide with CIELAB constant chroma loci) and in constant tone loci, approximately equispaced, is appreciated.

2.4.   Illumination conditions

To capture the images of each Munsell chip, a methacrylate support is used (Figure 1.2). In this support a white expanded polystyrene sphere of 14.5 cm inside diameter and 20 cm outside diameter, painted externally in black is placed at the bottom, to be used as lightning booth. The light sources are placed in the middle of the sphere to allow a homogeneous illumination of the sample. The Munsell chip is placed in the middle of the sphere and photos are taken placing the smartphone at the top of the support at 16 cm.

To take the photo, fixed conditions are employed using the pro mode of the mobile phone. The conditions for the Xiaomi device are 1/f=1/250, iso=80 and Temperature=5200 K. For the Samsung device, the conditions are 1/f=1/350, iso=150 and Temperature=5200 K.

Figure 1.2: Methacrylate support employed to obtain the images by the smartphone devices.

3.   Results and discussion

3.1.   Errors in reproduction on smartphones that are not colourimetrically characterized

The captured images were processed to select a uniform portion of the coloured chip, and the RGB values of the same were averaged. This RGB description is device dependent, as it varies with the characteristics of the optics, sensitivity and sensor geometry. Figure 1.3 shows, as an example, the Passing-Bablok correlation diagrams for R, G and B measured with two devices (Samsung and Xiaomi). It is

shown that there is no concordance between the values and that the measures obtained with the Samsung device are significantly higher than those of Xiaomi (the reference line x = y is always below the lower limit of the 95% confidence interval of the fit and even below the lower limit of the 95% prediction interval of the sample, for R>80, G = 50 and B >100, approximately).
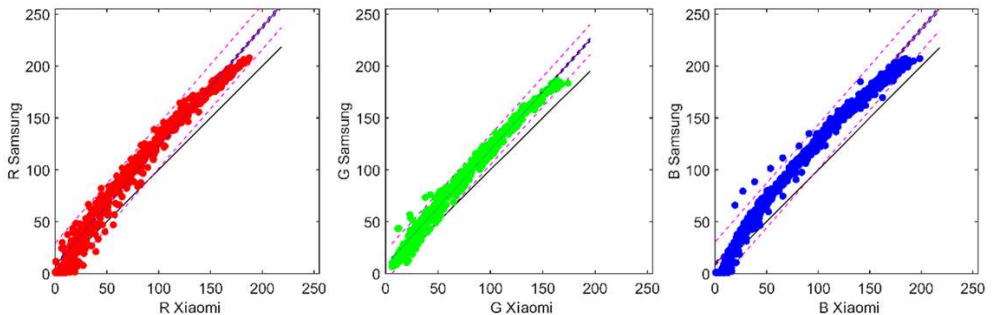
Figure 1.3: Passing-Bablok correlation diagrams for RGB values of the Munsell Atlas, obtained by a Xiaomi device and a Samsung device. The violet dotted define the 95% prediction interval of the sample; the central line of the interval is the best fitting line, and is surrounded by its confidence interval (magenta region). The black line is the reference line x = y.

To evaluate the effect of these differences between devices, we calculated the CIELAB values corresponding to the RGB values, using a standard transformation (sRGB), and, from these values, the CIE ΔE2000 colour difference (Luo et al., 2001) between the colours estimated by these devices. Figure 1.4 shows that the colour differences are greater than 4 ΔE2000 units, which has been proposed as a tolerance margin (Liu et al., 2012). A trend towards greater differences between devices is observed for yellowish stimuli (GY, Y and YR) with moderate or high lightness (Munsell Value between 6 and 8), without apparent influence of chroma.

The changes in the perceptual attributes linked to these colour differences are not systematic. Figure 1.5 shows that the Samsung device would systematically provide higher lightness values than the Xaiomi. Although the chroma values of the Samsung are also higher on average, their variability is much greater and for certain colours the situation can be the reverse. In general, changes in hue contribute the least to the colour difference between the samples captured by the two devices.
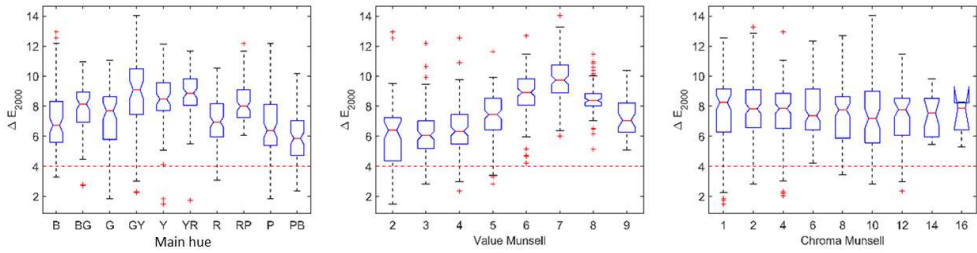
Figure 1.4: ΔE2000 colour differences between the RGB images captured by two mobile phones (Samsung and Xiaomi), using the same standard (sRGB) to calculate the CIELAB description of the samples.
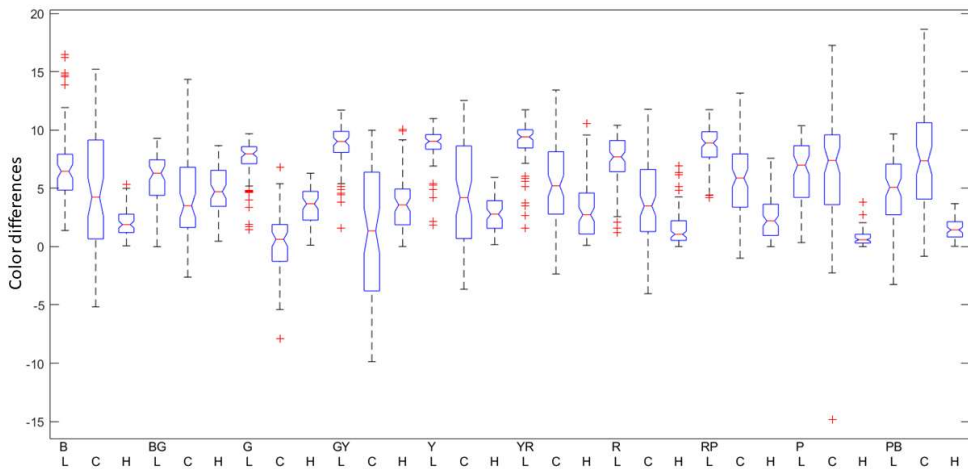
Figure 1.5: Contributions of differences in lightness (L), chroma (C) and hue (H) to the colour difference between devices, as a function of the main tone of the sample.

This analysis shows that the colour descriptions of objects obtained by different devices, assuming a standard characterization, are not concordant. The differences between the real colour and the colour predicted by this standard characterization are even greater, as can be seen in Figure 1.6. In this figure, we represent the CIEDE2000 colour difference between the Lab values measured by the spectrophotometer and the one estimated from the RGB values obtained with the two smartphones, using the Matlab's rgb2lab function, assuming the D65 illuminant white and the standard sRGB transformation. These differences are much higher than the maximum recommended tolerance of 4 CIEDE2000 units (Liu et al., 2012), which makes it clear the need to colourimetrically characterize the image capture device. In this way, we move from the RGB description, dependent

on the device, to a description in a standard colorimetric space, independent of the device.
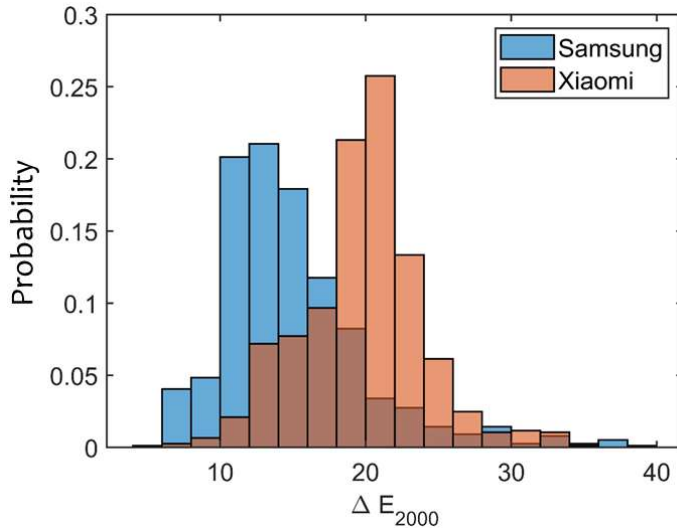
Figure 1.6: Distribution of the errors obtained when predicting the real CIELab descriptors of the samples, obtained with a spectrophotometer, with a standard transform (sRGB) of the RGB values obtained with two different smartphones.

Qualitatively, the image captured by the device reproduces the main hue of the stimuli, but as shown in Figure 1.7, it does not maintain neither the lightness, nor the chroma, nor the relative difference between different stimuli.

The use of standard transformations such as sRGB, explicitly or implicitly, appears recurrently in literature of applications of smartphone-captured images to analytical chemistry problems. While the final result obtained may be valid for the particular capture device used, nothing ensures that it can be generalized to other devices (Cebrián et al., 2022; Soda & Bakker, 2019, Yusufu & Mills, 2018).
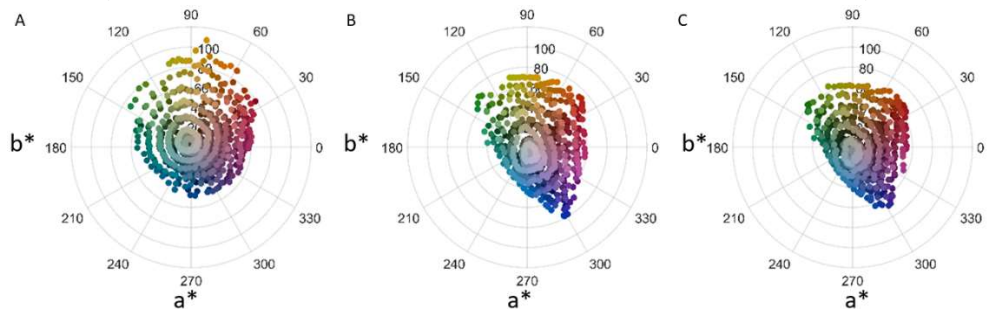
Figure 1.7: Comparison of the actual chromaticity of the pieces (A) and the chromaticities predicted with the sRGB transformation from the RGB values captured by the Samsung smartphone (B) and Xiaomi (C).

3.2. Colorimetric characterization of smartphone device

With the RGB values extracted from the Munsell sample images and their CIELAB values, measured with the Minolta spectrophotometer, simple polynomial models for colorimetric characterization have been derived. Each model for device D is defined by a matrix, $M_{(t,n)}{}^D$, which verifies:

$$H_t = P_n(R_D G_D B_D) \cdot M_{t,n}^D$$

where Pn is a polynomial of degree n of the RGB variables obtained with device D, and Ht are the colorimetric descriptors of the samples. Two sets of descriptors have been tested: the tristimulus values XYZ of the samples (t=1) and their Lab* descriptors (t=2). The matrix of the model $M_{(t,n)}{}^D$ as:

$$M_{t,n}^D = \left(P_n{}^T(R_D G_D B_D) P_n(R_D G_D B_D) \right)^{-1} \left(P_n{}^T(R_D G_D B_D) H_t \right)$$

For the calculation, the set of 765 colours of the Munsell Atlas of Figure 6 was divided into a testing group, with 216 elements, consisting of the Value 2, 5, 7 and 9 samples, with Chromas 2, 6, and 8, and a training group, with all the others. For the testing group, the CIEDE2000 colour difference between the experimental CIELAB descriptors and those obtained with models with n between 1 and 5 was calculated, obtaining the results of Figure 1.8. For both devices, the models with the best results (lower global errors and lower dispersion) are those of degrees 2 to 4. In the case of the degree 3 models, the error committed is within the tolerance of 4 CIEDE2000 units for all samples, excepting the outliers.
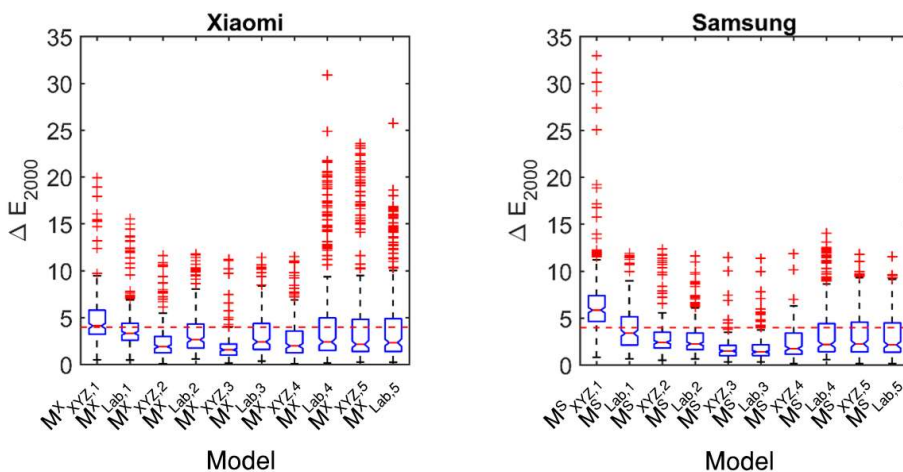
Figure 1.8: Errors of the different polynomial models for the two compared smartphone devices. Models of degrees 2 to 4 show a lower global error and less dispersion.

If we compare the error distributions of all the models and both devices, the Friedman test validates the existence of significant differences ($p \ll 0.0001$, $\chi^2 = 1198.43$) between the models and devices considered. A post-hoc with the Dunn-Sidak correction for multiple comparisons (Figure 1.9) shows that the model $M_{1,3}^{Xiaomi}$ is significantly better than the rest of the models for that device, and that it does not present significant differences with the models $M_{1,3}^{Samsung}$, $M_{2,3}^{Samsung}$, and $M_{1,4}^{Samsung}$, which are, in turn, the best for this second device.

When we consider the complete set of Munsell chips measured, when comparing the colour differences between the experimental Lab* descriptors and those calculated with the third-degree polynomial models, as well as the differences between the predictions of the models for both devices (Figure 1.10), the improvement over the use of a standard transformation model, such as sRGB, is evident.
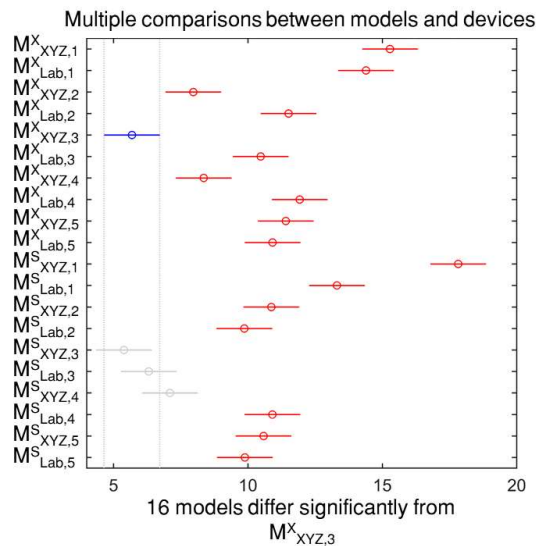
Figure 1.9: Results of the post-hoc of the multiple comparisons between the error distributions obtained for the different polynomial models in the two smartphone devices. The x-axis represents the ranges and the y-axis, the groups. With the Dunn-Sidak criterion for multiple comparisons, the distributions in red show statistically significant differences with the distribution of the degree 3 model.
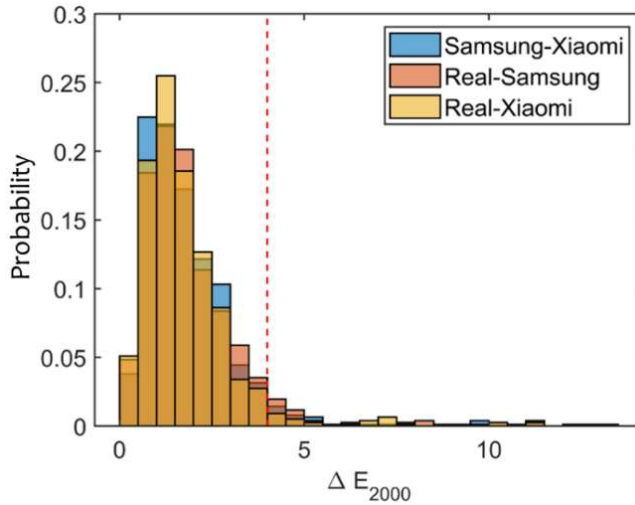
Figure 1.10: Distribution of differences between experimental Lab* values and those obtained with the $M_{1,3}^D$ models, as well as differences between the predictions of the two devices. The red line represents the maximum tolerance of 4 CIEDE2000 units.

3.3.   Development of neural networks for the creation of models

As it has been demonstrated, colorimetric characterized phones can estimate sample colour with acceptable errors in comparison with a standard device. However, a subfield of computer science could provide another way to solve the problem of characterizing smartphone devices: deep learning.

Deep learning is a technique of automatic learning based on a neural network model. Thanks to this distribution of the neural model, deep learning may imitate the actions of the human brain. In this way, by connecting neurons and layers of neurons that perform simple mathematical operations, complex models can be developed for classification and prediction of results through the distribution of weights in the information provided by each one (Kuhn & Johnson, 2013).

In Rstudio, neural network models can be obtained by using the h2o package (LeDell et al., 2018). A preliminary study of this type of prediction methodology can be shown in Figure 1.11. In this figure, the value of ΔE2000 between the real colour and the predicted colour for a given colour using 20%, 50%, or 80% of the total device dataset (Xiaomi) is shown, with the remaining dataset being the test group.

The results obtained from this test indicate that deep learning/neural network algorithms could be useful for the development of prediction models for colour measurement. On the other hand, they could be used to study the optimal number

of parameters for the development of prediction models and avoid problems of overfitting and training groups with a high number of samples. In this way, the most accurate models would be achieved using the smallest possible training dataset.
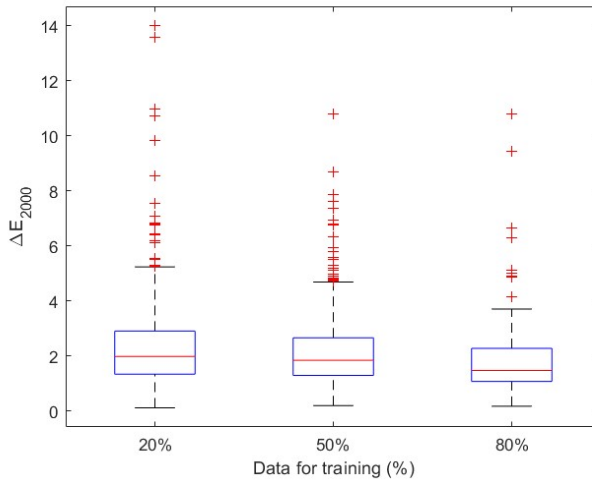
Figure 1.11: ΔE2000 obtained between the real colour and the colour predicted by the neural network model made with the Xiaomi database. The model is tested with the percentage not employed for the creation of the model.

4. Conclusions

This work presents the results of comparing colour measurements obtained through image processing using a smartphone and a reference device. It has been found that the colours obtained by smartphones are significantly different from those obtained by professional colourimeters. While these measurements may be sufficient for analytical determinations, they are not accurate representations of the true colours.

However, characterizing the smartphone can alleviate this issue. As shown in Figure 1.10, this characterization allows for a difference of less than 4 units between the real colour obtained by the reference device and the colour obtained by the characterized device, using the CIEDE2000 formula. Additionally, advances in computational technologies, such as the use of neural networks, offer new solutions for this problem. Initial studies using this approach suggest that it may be a viable alternative, allowing for characterization of smartphones with a lower amount of data and high accuracy.

5.   References

Abebe, M. A., Hardeberg, J. Y., & Vartdal, G. (2021). Smartphones' Skin Colour Reproduction Analysis for Neonatal Jaundice Detection. *Journal of Imaging Science and Technology*, 65(6), 60407-1-60407-15. DOI: 10.2352/J.ImagingSci.Technol.2021.65.6.060407.

Antela, K.U., Ochoa Ballesteros, A., Sáez Hernández, R., Cervera Sanz, M. L., Pastor García, A., Luque Cobija, M. J., & Morales Rubio, Á. (2022). Determinación de quinina en tónicas mediante tratamiento de imagen. In XIII Congreso Nacional del Colour, Terrassa.

Berns, R. S. (2019). Billmeyer and Saltzman's principles of color technology. Fourth Edition. John Wiley & Sons. New Jersey.

Caivano, J. L. (2022). Black, white, and grays: Are they colors, absence of color or the sum of all colors? *Color Research & Application*, 47(2), 252-270. DOI: 10.1002/col.22727.

Cebrián, P., Pérez-Sienes, L., Sanz-Vicente, I., López-Molinero, Á., de Marcos, S., & Galbán, J. (2022). Solving Colour Reproducibility between Digital Devices: A Robust Approach of Smartphones Colour Management for Chemical (Bio) Sensors. *Biosensors*, 12(5), 341. DOI: 10.3390/bios12050341.

Chmutin, A. M. (2022). Contrast and Contrast Enhancement (in Logic of Visual Perception of Graphic Information). *International Journal of Open Information Technologies*, 10(5), 44-52.

Fairchild, M. D. (2013). Colour Appearance Models. Third Edition. John Wiley & Sons. New Jersey.

Fdhal, N., Kyan, M., Androutsos, D., & Sharma, A. (2009). Color space transformation from RGB to CIELAB using neural networks. In Advances in Multimedia Information Processing-PCM: 10th Pacific Rim Conference on Multimedia. Bangkok.

Gómez-Robledo, L., López-Ruiz, N., Melgosa, M., Palma, A. J., Capitán-Vallvey, L. F., & Sánchez-Marañón, M. (2013). Using the mobile phone as Munsell soil-colour sensor: An experiment under controlled illumination conditions. *Computers and electronics in agriculture*, 99, 200-208. DOI: 10.1016/j.compag.2013.10.002.

Gooby, B. (2020). The development of methodologies for colour printing in digital inkjet textile printing and the application of colour knowledge in the ways of making

project. *Journal of Textile Design Research and Practice*, 8(3), 358-383. DOI: 10.1080/20511787.2020.1827802.

Hong, G., Luo, M. R., & Rhodes, P. A. (2001). A study of digital camera colorimetric characterization based on polynomial modeling. *Color Research & Application*, 26(1), 76-84. DOI: 10.1002/1520-6378(200102)26:1<76::AID-COL8>3.0.CO;2-3.

Hunt, R. W. (1985). Perceptual factors affecting colour order systems. *Color Research & Application*, 10(1), 12-19. DOI: 10.1002/col.5080100105.

Kuhn, M., & Johnson, K. (2013). Applied predictive modelling. Fifth edition. Springer. New York.

Kumah, C., Zhang, N., Raji, R. K., & Pan, R. (2019). Color measurement of segmented printed fabric patterns in lab color space from RGB digital images. *Journal of Textile Science and Technology*, 5(1), 1-18. DOI: 10.4236/jtst.2019.51001.

LeDell, E., Gill, N., Aiello, S., Fu, A., Candel, A., Click, C., ... & H2O. ai. (2018). Package 'h2o'. *dim*, *2*, 17.

Leon, K., Mery, D., Pedreschi, F., & Leon, J. (2006). Color measurement in L∗ a∗ b∗ units from RGB digital images. *Food Research International*, 39(10), 1084-1091. DOI: 10.1016/j.foodres.2006.03.006.

Linhares, J. M. M., Monteiro, J. A. R., Bailão, A., Cardeira, L., Kondo, T., Nakauchi, S., Picollo, M., Cucci, C., Casini, A., Stefani, L., & Nascimento, S. M. C. (2020). How good are RGB cameras retrieving colors of natural scenes and paintings? - A study based on hyperspectral imaging. *Sensors*, 20(21), 6242. DOI: 10.3390/s20216242.

Liu, H. X., Wu, B., Liu, Y., Huang, M., & Xu, Y. F. (2012). A discussion on printing colour difference tolerance by CIEDE2000 colour difference formula. *Applied Mechanics and Materials*, 262, 96. DOI: 10.4028/www.scientific.net/AMM.262.96.

Luo M. R., Cui G., & Rigg B. (2001). The development of the CIE 2000 colour difference formula: CIEDE2000. *Color Research & Application*, 26, 340 - 350. DOI: 10.1002/col.1049.

Ly, B. C. K., Dyer, E. B., Feig, J. L., Chien, A. L., & Del Bino, S. (2020). Research techniques made simple: cutaneous colourimetry: a reliable technique for objective skin colour measurement. *Journal of Investigative Dermatology*, 140(1), 3-12. DOI: 10.1016/j.jid.2019.11.003.

Maali Amiri, M., & Fairchild, M. D. (2018). A strategy toward spectral and colorimetric color reproduction using ordinary digital cameras. *Color Research & Application*, 43, 675– 684. DOI: 10.1002/col.22231.

Malo, J., & Luque, M. J. (2002). ColourLab: the Matlab toolbox for Colourimetry and Colour Vision. Univ. Valencia. http://isp.uv.es/code/visioncolour/colourlab.html.

Martínez-Verdú, F., Pujol, J., Vilaseca, M., & Capilla, P. (2003). Characterization of a digital camera as an absolute tristimulus colorimeter. In Color Imaging VIII: Processing, Hardcopy, and Applications. SPIE.

Phuangsaijai, N., Jakmunee, J., & Kittiwachana, S. (2021). Investigation into the predictive performance of colorimetric sensor strips using RGB, CMYK, HSV, and CIELAB coupled with various data preprocessing methods: A case study on an analysis of water quality parameters. *Journal of Analytical Science and Technology*, 12(1), 1-16. DOI: 10.1186/s40543-021-00271-9.

Poynton, C., & Funt, B. (2014). Perceptual uniformity in digital image representation and display. *Color Research & Application*, 39(1), 6-15. DOI:10.1002/col.21768.

[a]Sáez-Hernández, R., Ruiz, P., Mauri-Aucejo, A. R., Yusa, V., & Cervera, M. L. (2022). Determination of acrylamide in toasts using digital image colourimetry by smartphone. *Food Control*, 141, 109163. DOI: 10.1016/j.foodcont.2022.109163.

[b]Sáez-Hernández, R., Antela, K. U., Mauri-Aucejo, A. R., Morales-Rubio, A., & Cervera, M. L. (2022). Smartphone-based colorimetric study of adulterated tuna samples. *Food Chemistry*, 389, 133063. DOI: 10.1016/j.foodchem.2022.133063.

[c]Sáez-Hernández, R., Mauri-Aucejo, A. R., Morales-Rubio, A., Pastor, A., & Cervera, M. L. (2022). Phosphate determination in environmental, biological and industrial samples using a smartphone as a capture device. *New Journal of Chemistry*, 46(3), 1286-1294. DOI: 10.1039/D1NJ05425B.

[d]Sáez-Hernández, R., Antela, K. U., Gallello, G., Cervera, M. L., & Mauri-Aucejo, A. R. (2022). A smartphone-based innovative approach to discriminate red pigments in roman frescoes mock-ups. *Journal of Cultural Heritage*, 58, 156-166. DOI: 10.1016/j.culher.2022.10.003.

Shrivas, K., Kant, T., Patel, S., Devi, R., Dahariya, N. S., Pervez, S., Deb, M. K., Rai, M. K., & Rai, J. (2021). Inkjet-printed paper-based colorimetric sensor coupled with smartphone for determination of mercury (Hg2+). *Journal of Hazardous Materials*, 414, 125440. DOI: 10.1016/j.jhazmat.2021.125440.

Soda, Y., & Bakker, E. (2019). Quantification of colorimetric data for paper-based analytical devices. *ACS sensors*, 4(12), 3093-3101. DOI: 10.1021/acssensors.9b01802

Taghadomi-Saberi, S., Omid, M., Emam-Djomeh, Z., & Faraji-Mahyari, K. (2015). Determination of Cherry Color Parameters during Ripening by Artificial Neural Network Assisted Image Processing Technique. *Journal of Agricultural Science and Technology*, 17(3), 589-600.

Tanaka, M., & Horiuchi, T. (2018). Investigation of metallic color perception using real-world materials. *Color Research & Application*, 43(5), 697-712. DOI: 10.1002/col.22245.

Tomasević, I., Tomović, V., Milovanović, B., Lorenzo, J., Đorđević, V., Karabasil, N., & Đekić, I. (2019). Comparison of a computer vision system *vs*. traditional colourimeter for colour evaluation of meat products with various physical properties. *Meat science*, 148, 5-12. DOI: DOI: 10.1016/j.meatsci.2018.09.015.

Wang, X., Bao, Z., Chang, Y. C., & Liu, R. S. (2020). Perovskite quantum dots for application in high colour gamut backlighting display of light-emitting diodes. *ACS Energy Letters*, 5(11), 3374-3396. DOI: 10.1021/acsenergylett.0c01860.

Waring, E., Quinn, M., McNamara, A., de la Rubia, E. A., Zhu, H., & Ellis, S. (2022). skimr: Compact and Flexible Summaries of Data [Online]. Available: https://cran.r-project.org/web/packages/skimr/skimr.pdf

Westland, S., Ripamonti, C., & Cheung, V. (2012). Computational colour science using MATLAB. Second edition. John Wiley & Sons. United Kingdom.

Wickström, H., Nyman, J. O., Indola, M., Sundelin, H., Kronberg, L., Preis, M., & Sandler, N. (2017). Colourimetry as quality control tool for individual inkjet-printed pediatric formulations. *AAPS PharmSciTech*, 18(2), 293-302. DOI: 10.1208/s12249-016-0620-1.

Wu, W., & Federico, M. A. J. (2019). The APD Skin Monitoring App for wound monitoring: image processing, area plot, and colour histogram. *Scientific Phone Apps and Mobile Devices*, 5, 3. DOI:10.30943/2019/28052019.

Yang, J., Shen, F., Wang, T., Luo, M., Li, N., & Que, S. (2021). Effect of smart phone cameras on color-based prediction of soil organic matter content. *Geoderma*, 402, 115365. DOI: 10.1016/j.geoderma.2021.115365.

Yusufu, D., & Mills, A. (2018). Spectrophotometric and Digital Colour Colorimetric (DCC) analysis of colour-based indicators. *Sensors and Actuators B: Chemical*, 273, 1187-1194. DOI: 10.1016/j.snb.2018.06.131.

CHAPTER 2: A Smartphone-based application for the direct analysis of foliar iron

ABSTRACT

Iron chlorosis induces a homogeneous yellowing of the leaf that keeps nerves green and may compromise the plant's health and productivity. Iron participates in chlorophyll biosynthesis and therefore, the green leaf colour and its iron content could be correlated. The aims of this study were to characterize the leaves' green colour by capturing images by a Smartphone and to correlate them with their iron content. Three different chemical methods for iron determination in the leaves have been studied: total iron by calcination, Fe(II) o-phenantroline extraction and active iron by HCl extraction. Likewise, image capture by a colorimetrically characterized Smartphone was used to measure the leaves' colour. It has been studied which parameter of the CIELab colour space correlates best with the iron of the leaves. The method which best correlates the iron content with leaves' colour is iron extracted by HCl, named active iron. In addition, lightness (L*) proved to be the parameter which best correlated to the active iron content, and the relationship between both variables was modelled by a power equation. A fast and easy method to determine the active iron content in leaves has been developed, and an improvement in the current methodologies was achieved in terms of cost/time/reagents/safety due to the possibility of carrying out an analysis through a photograph taken with a Smartphone. Moreover, the results obtained by image processing are in concordance with those obtained by the reference method.

Keywords: Analytical Chemistry, CIElab, Foliar active iron, Smartphone.

1.   Introduction

The role of iron in the synthesis of chlorophyll can be seen in Figure 2.1, which shows that this micronutrient also activates some enzymes, including aminolevulinic acid synthetase and coproporphyrinogene oxidase, and illustrates the need of the iron's presence in the biosynthesis of the chlorophyll (Kyrkby & Römheld, 2008).
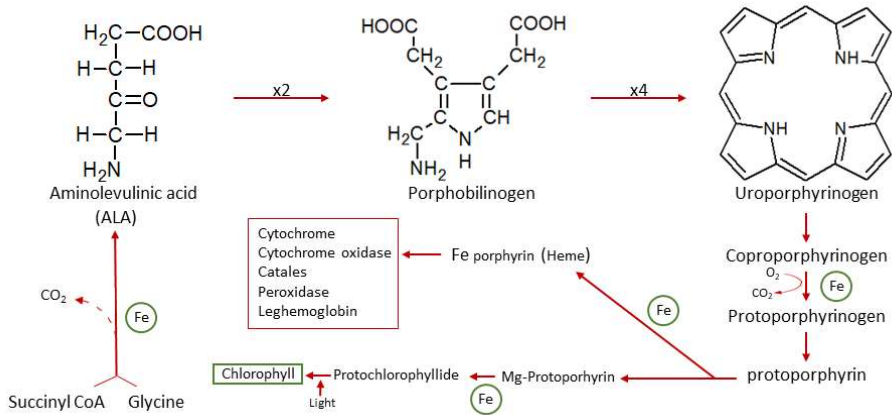
Figure 2.1: Scheme of chlorophyll biosynthesis in vegetables (Adapted from Kyrkby & Römheld, 2008).

Iron takes an active part in the oxidative decarboxylation of coproporphyrinogen to form protoporphyrin. It has also been reported the need of iron in the transformation of Mg-protoporphyrin to protochlorophyllide, which is evident when supplying α-linolenic acid (ALA) to iron-deficient leaves and verifying that there is an increase in Mg-protoporphyrin levels while the concentration of protochlorophyllide and chlorophyll does not suffer variation (Fernández et al., 1994). Fernández et al. (1994) reported that Zhiznevskaya proved in 1972 the involvement of iron in the esterification of chlorophyllide with phytol to form chlorophyll and that Chereskin and Castelfranco (1982) and Pushnik (1984) found that a "feedback" inhibition on the synthesis of α-linolenic acid occurred in Fe-deficient plants. All these relationships reveal the complexity of the interrelation between iron and chlorophyll.

The most characteristic symptom of iron chlorosis is the progressive loss of green leaf colour. This effect is linked to the decrease in chlorophyll content, for that, some studies have tried to correlate iron deficiency with photosynthetic pigment content (Fernández et al., 1994). As can be seen in Figure 2.2, the first visible symptoms of Fe deficiency appear as chlorosis in the young leaves. Chlorosis is

characterized by a homogeneous yellowing of the leaves keeping the green nerves (Merry et al., 2022; Zebec et al., 2021). Two enzymes with heme group, catalase and peroxidase, suffer significantly activity decreases under iron deficiency conditions, in a greater degree in the case of catalase, which can be taken as a biochemical indicator of iron chlorosis (Fernández et al., 1994).

Figure 2.2: Leaf with symptoms of iron chlorosis (left) and control leaf (right).

Due to the importance of iron in leaves, different extraction procedures to achieve quantification in the plant have been proposed. These procedures entail a high reagent consumption, long extraction times (reaching 24 h) or a high sample manipulation, which can lead to an increased risk of contamination (Abadía et al., 1984; Köseoğlu and Açikgöz, 1995; Lang and Reed, 1987; Sadzawka et al., 2007; Takkar and Kaur, 1984). However, currently, direct analysis methods by image processing have appeared, smartphone's cameras are a tool with a significant potential, which are accessible to everyone at an affordable price, total portability and easy to use (Li et al., 2020).

In literature, there are a lot of applications in terms of interest parameters that are determined on different types of samples. For example, tuna adulteration was assessed with the use of smartphone to capture the colour change due to the use of different adulterants (Sáez-Hernández et al., 2022). Also, some applications in archaeometry for the identification of different characteristics in ancient mortars (Ramacciotti et al., 2022). Another example is the creation of a monitoring tool for the detection of fluorosurfactant PFOA employing methylene blue (Fang et al., 2018).

In these works, the processing was carried out using colour descriptors in the CIELab colour space (CIE Technical Committee, 2018), that employs the three-dimensional coordinates, L*, a*, b* of the colour space, in which L* is lightness – luminosity

relative to a reference white, and a* and b* measure red-green and blue-yellow opponency, respectively.

One of the main issues presented by the interpretation of foliar iron content is the controversy associated with which kind of iron causes iron chlorosis. Currently, agrochemical companies analyse, by default, the total iron content by flame atomic absorption spectroscopy (FAAS) or atomic emission with inductively coupled plasma (ICP-OES), although at the request of the costumer they also determine iron(II) content by extraction with o-phenanthroline (o-phen), that are in concordance with the literature (Katyal and Sharma, 1980; Lang and Reed, 1987; Mohammad et al., 1998; Takkar and Kaur, 1984). However, despite the fact that these authors agree on the determination of iron by both the total iron method and the use of o-phenanthroline to quantify the iron(II) in the leaf and associate them with iron chlorosis, it has been argued that the most appropriate method for the determination of iron in the plant is the determination of active iron by other methods (Köseoğlu and Açikgöz, 1995; Lang and Reed, 1987; Razeto and Valdés, 2006; Takkar and Kaur, 1984).

Regarding the functions of iron in the plant and the distinction between active/soluble iron and total iron, it is not clear which iron should be measured to establish the connection with iron chlorosis. This is because of the complex interactions that iron has in the metabolism of the plant (Bidwell, 1990; Puente-Ramírez et al., 2022; Torres et al., 2018; Wang et al., 2022). Although agrochemical companies focus on the analysis of total iron, since 1980 Katyal and Sharma (1980) established that it was necessary to quantify the active iron in the plant, which is the one that really has an influence on iron chlorosis. Since these authors stated that the appropriate method was the quantification of active iron, numerous authors have cited it as the main reference (Köseoğlu and Açikgöz, 1995; Lang and Reed, 1987; Sadzawka et al., 2007; Takkar and Kaur, 1984).

However, obtaining active iron is a complex process and some authors have found no relationship between the colour of the leaf and its iron content (Palacios, 2003). On the other hand, Navarro and Navarro (2013) reported a study by Oserkowsky (1932), in which numerous trials trying to correlate chlorophyll with the iron content of the leaf were carried out and in which was demonstrated that only a relationship was found when iron was extracted with HCl.

The objective of this work is to find a relationship between the iron content in the leaf and its colour, and therefore with chlorosis. The content of the different types

of iron in the leaf has been studied: total iron by calcination and FAAS determination, iron(II) by o-phenanthroline extraction and UV-Vis determination and active iron by HCl extraction and FAAS determination. Finally, a relationship between the iron content and the L*a*b* parameters has been studied via Smartphone and spectroradiometer measurements. A prediction model has been created in order to predict the iron content in the leaves.

2. Materials and methods

2.1. Instrumentation

An 8452A Hewlett Packard spectrophotometer (Germany) was used for the colorimetric determination of iron(II) at 510 nm by o-phen complex formation. Alternatively, a S2 AA Thermo Fisher spectrophotometer (Cambridge, UK) was used for the determination of total Fe by flame atomic absorption at 248.3 nm using a burner of 5 cm and a multielement hollow cathode lamp Photron for Cu/Co/Mg/Ni/Fe (Victoria, Australia), deuterium background corrector and a flow rate of 0.9 L/min of acetylene.

Leaf colour was measured by a SpectraScan® PR655 Photo Research® (Syracuse, NY, USA) spectroradiometer. The photographs were taken with a smartphone Samsung (Seoul, South Korea) Galaxy S7 edge model SM-G935F with a 12.2 MP camera.

Sample illumination was controlled using different illumination booths, designed, and built for this study. For the circular leaf cuttings, a white expanded polystyrene sphere of 14.5 cm inside diameter and 20 cm outside diameter, painted externally in black was used. For the coloured solutions, the lightning booth was a white expanded polystyrene box which dimensions are 27.5x27.5x27.5 cm of inside side. In both cases, the light sources were white 5700 K LED lights.

For the preparation of the samples, thermostatic sand baths J.P. Selecta, S.A. combiplac-sand model 6000709 (Barcelona, Spain) and Ovan model SB400E (EU) were used. To obtain ashes, a Lenton Furnaces Thermal Designs LTD muffle oven model Eurotherm 2416CG Biometa (Llanera, Asturias) was used.

2.2. Instrumentation

All solutions were prepared in water (18.2 MΩ cm of resistivity) obtained from a system of ultrapure water 1 Adrona (Latvia). The standard solution of iron(II) 200 mg/L was prepared from pure ammonium iron(II) sulphate hexahydrate (Panreac, Barcelona, Spain) and a standard iron solution of 1000 mg/L for AA (Scharlab,

Sentmenat, Spain) was used for the atomic absorption iron calibration. For the calcination process, 69 % ultratrace nitric acid (Scharlau) and 37 % ultratrace hydrochloric acid (Scharlau) were used.

For iron extraction tests a 1.5 % o-phen solution was prepared using 1,10-Phenanthroline hydrochloride monohydrate 97 % (Acros Organics, New Jersey, USA). To prepare the solution, 1.65 g of reagent are taken and dissolved in 85 mL of water, the pH is adjusted to 3 using NaOH and subsequent make up to 100 mL.

2.3. Experimental design

2.3.1. Samples

For the realization of these experiments, loquat leaves with different hues and saturations were used due to its high size. These leaves were used to make several tests with the same sample, since each leaf constitutes an independent sample. Citrus, persimmon, apricot, and peach leaves were also used to verify the validity of the mathematical model in other species.

2.3.2. Sample preparation

Collected leaves were cleaned with water with the help of a brush, rinsed with distilled water and gently dried by contact on paper at room temperature. Approximately 1.0 g of leaf sample (always belonging to the same leaf) is weighed. From the weighed leaf sample, 3 circles of 1.1 cm in diameter are taken with the use of a punch for colour measurement. Afterwards, the circles are collected and, together with the rest of the weighed sample, to proceed to the determination of iron.

2.3.3. Measurement of colour parameters using the spectroradiometer

The spectroradiometer is placed 50 cm above the location of the samples to have a zenithally view. The circles belonging to the leaf are placed, one by one and separately, within the sphere of expanded polystyrene. Once the device is in place and the light sources are warmed up, a measurement of the white background is taken as blank, and then the measurements of the samples are taken, making a blank every 10 measurements. The XYZ tristimulus values of the blank are used as reference white in the CIELab formulae.

2.3.4. Measurement of colour parameters using the Smartphone.

The Smartphone is placed at a height of 16 cm above the sample using a methacrylate platform. Circles of the leaves sample are placed within the sphere of expanded polystyrene. Once the device is in place and the light sources are warmed

up, a photo of the light background is taken as blank, and the measurement of the sample is taken, taking a blank every 10 measurements. The RGB data of the photographs are processed through Matlab.

2.3.5. Determination of total iron.

To determine total iron, the iron content in the ashes of the samples obtained by calcination is measured. To perform this procedure, each sample is weighed and placed in a 150 mL beaker. Then, 4 mL of 50 % HNO_3 is added to the sample and left in a sand bath until dryness. Once the sample has dried, it is introduced into the muffle furnace to calcine at 450 °C with the following program: temperature increase up to 150 °C in half an hour, 30 minutes at 150 °C, temperature increase up to 450 °C at 1 °C/min, 12 h at 450 °C, and let to cool to room temperature.

If the ashes of the sample are grey, 3 mL of 50 % HNO_3 are added to moisten them, dried in the sand bath, and are introduced again in the muffle furnace. The process is repeated until the ashes are white.

The white ashes are dissolved with 2.5 mL of 1 M HCl and are transferred to a plastic test tube, washing the beaker glass with 2.5 mL water, and collecting in the tube to have a total volume of 5 mL.

The iron measurement is performed by flame atomic absorption spectroscopy (FAAS) using iron calibration standards between 0 and 5 mg/L, measuring one of the calibration standards every 10 samples to check the stability of the signal.

2.3.6. Determination of iron(II) by extraction with o-phenanthroline

To perform this procedure, the weighed sample is taken and cut sideways into 1-2 mm squares. Once the sample has been chopped, 9 mL of 1.5% o-phen solution at pH=3 is added, since this is the method that has been proposed as the most suitable for complex formation with iron(II) (Abadía et al. 1984; Katyal and Sharma 1980; Köseoğlu and Açikgöz 1995; Mohammad et al. 1998; Pierson and Clark 1984). It is let stand 16 h and then filtered using filter paper. The filtered extract is then passed through a C18 solid phase extraction cartridge to eliminate interference as recommended by certain authors (Takkar and Kaur 1984).

To measure iron, the derivative of the spectra of the samples is recorded in order to eliminate possible interferences due to the additive property of absorbance. The calibration curve was prepared between 0.4 and 2 mg/L, and a solution of o-phen was used as a blank.

2.3.7. Determination of active iron.

Once the image measurements of the leaves have been taken, these are cut into squares of 1-2 mm sideways. A mortar is then taken and 10 mL of 1 M HCl is added, the leaves are introduced and ground for 3 minutes. Then it remains at rest for an additional 17 minutes, making a total of 20 minutes, and finally the solution is filtered through a filter paper. The iron measurement is carried out by the flame atomic absorption spectrophotometer as explained in the total iron determination section. This is the recommended method for the determination of iron with biological activity.

3. Results

3.1. Relationship between different types of iron and leaf colour in loquat.

Firstly, we tried to correlate the different types of Fe; total iron obtained by calcination and FAAS measurement, iron(II) extraction with o-phen with subsequent measurement in UV-vis and active iron extracted with HCl with subsequent measurement in FAAS, with the colour of the leaves obtained by the spectroradiometer.

Since the loquat leaves were large enough to take several subsamples, the different types of iron were determined using 8 leaves of this type of variety. Thus, the iron values obtained could be compared with each other.

In order to evaluate the correlation between the different colour parameters and combination of them with the content of different types of iron, "regression learner" Matlab app was used. The Table 2.1 shows the best correlation and the corresponding RMSE (Root Mean Square Error) obtained for each combination of colour parameters and iron type.

As it can be seen, the best correlation found is between the L parameter of the leaf image and the active Fe extracted with HCl. This leads us to deduce that the iron extracted with HCl is indeed the active iron, that has a catalytic function in the chlorophyll biosynthesis, and therefore it could be correlated with the colour of the plant.

Table 2.1: Correlation and Root Mean Square Error values obtained with the best model using regression learner for each combination of data.

R^2

Iron type	o-phen UV-Vis	o-phen UV-Vis derivative	HCl	Ashes
L*a*b*	0.56	0.57	0.74	0.75
L*a*	0.55	0.45	0.78	0.68
L*b*	0.72	0.65	0.89	0.75
a*b*	0.67	0.39	0.86	0.46
L*	0.60	0.60	**0.95**	0.47
a*	0.37	0.29	0.09	0.17
b*	0.53	0.59	0.91	0.54

RMSE *

Iron type	o-phen UV-Vis	o-phen UV-Vis derivative	HCl	Ashes
L*a*b*	1.733	1.235	3.142	10.794
L*a*	1.892	1.233	2.835	10.260
L*b*	1.509	1.128	2.158	9.368
a*b*	1.645	1.333	1.993	15.524
L*	1.646	1.291	**1.239**	14.639
a*	2.181	1.581	5.201	18.432
b*	1.718	1.195	1.544	12.438

3.2.   Mathematical model for iron prediction

Once the type of iron that correlates with CIELab parameters of the spectroradiometer was found, we proceeded to find the mathematical model that correlated the active iron content with the L* parameter, obtained by the Smartphone, using 11 loquat leaf samples. For this purpose, the "curve fitting" tool of the Matlab program was used to mathematically check which model fit better and also find out what values were out of the adjustment. This tool allows to create models correlating 2 variables and provides parameters such as the equation or the R^2. These models could be polynomial, gaussian, exponential, linear or power models, among others. After checking the L* and active iron values, the model based on a power equation ($y = m \cdot x^n$) is the best to correlate the lightness, L*, versus iron concentration, and provides a $R^2 = 0.882$ (Table 2.2).

Table 2.2: Values of parameters m and n of the equation (y = m·x^n) of the power model and R^2 values.

	Loquat model	Loquat-citrus model	Citrus model
m	96.35	92.05	91.45
n	-0.4169	-0.4083	-0.4142
R²	0.8820	0.8429	0.8131

3.3.   Incorporation of different leaves species to the power model

It was found that the mathematical model created did not work for other species of leaves. When trying to incorporate 10 samples of 4 new species (apricot, persimmon, citrus and peach tree) it was observed that the fact that the leaves of the different species have different optical properties causes that would be necessary create a mathematical model for each specie. Table 2.3 shows the correlations between the L* parameter of the leaves and their corresponding iron obtained by HCl extraction for each power models modified with leaves species. It is only possible to apply the same mathematical model for different species if the optical properties, such as gloss, texture or global reflectance of the leaves are similar, as in the case of loquat and citrus leaves (See Table 2.2).

Table 2.3: Correlation between the L parameter of the leaf and iron obtained by HCl extraction for each of the power models modified with new leaves species.*

Model	R²
Loquat	0.88
Loquat and citrus	0.84
Loquat, citrus and persimmon	0.58
Loquat, citrus and peach	0.67
Loquat, citrus and apricot	0.62
All 5 species	0.42

3.4.   Validation of optical methods

Finally, it was studied whether the prediction of iron in the leaf from its colour, measured with a spectroradiometer and with Smartphone, were statistically comparable.

Once the mathematical model was set up using the spectroradiometer, the colour measurement of 20 samples was taken with the Smartphone. From the photos of

the leaves samples the parameter L* was obtained, and the mathematical model was applied to obtain the prediction of iron concentration of them.

For the methods to be comparable, they must be validated with a reference method (the iron extracted with HCl measured in FAAS), fulfilling 3 conditions: that the confidence interval includes 0, that the p-value is greater than 0.05 and the t student be less than 2.086. In this case, as can be seen in Table 2.4, these three conditions are met for the three validations, giving us the assurance that the three methods are comparable.

Table 2.4: Statistical parameters of the validation of the method.

Parameter	Active Fe vs Spectroradiometer	Active Fe vs Smartphone	Spectroradiometer vs Smartphone
Confidence Interval 95%	[-0.1622 ; 2.5586]	[-0.1072 ; 2.5877]	[-0.9931 ; 1.0772]
P	0.08092	0.06913	0.93313
T student	1.84342	1.92653	0.08502

4.   Discussion

Until now the iron determinations carried out by agrochemical companies are performed to obtain the total iron or iron extracted with o-phen, since some authors have argued that the lack of these types of iron are the cause of chlorosis. These methods are consistent with those reported in literature (Katyal and Sharma, 1980; Lang and Reed, 1987; Mohammad et al., 1998; Takkar and Kaur, 1984), implying that by determining these parameters the deficiency of this nutrient in the plant can be estimated. Therefore, the first attempt was to correlate these types of iron with the colour of the leaf. Nevertheless, the results show that these types of iron have no direct relationship with the leaf colour. However, the iron extracted by HCl does show a direct relationship with the colour of the leaf. This fact could suggest that the iron extracted with HCl could be related to chlorosis. These results demonstrate that the iron extracted following the official methodologies is unlikely to correlate with iron chlorosis since these methods are not providing real information about the possible deficiency of this nutrient in the plant nor about the so-called active iron

Several authors refer to differentiate of iron in the plant between active iron and total iron (Katyal and Sharma, 1980; Köseoğlu and Açikgöz, 1995; Lang and Reed, 1987; Mehrotra et al., 1985; Navarro and Navarro, 2013; Palacios, 2003; Razeto and

Valdés, 2006; Sadzawka et al., 2007; Takkar and Kaur, 1984). The results abovementioned suggest that the iron obtained by HCl extraction, is the one that really correlates with the colour of the leaf, and therefore, provides information about iron active with biological activity, and hence, by quantifying the HCl-extractable iron, information about the potential iron deficiency in the plant can be estimated.

However, the main method used for the determination of iron in leaves is o-phen extraction. This method was already studied against HCl, and it was concluded that active iron was more adequately extracted with HCl (Mehrotra et al., 1985; Navarro and Navarro, 2013).

This is due to the fact that, in the first place, the plant has both, iron(III) and iron(II). Despite this fact, it has been studied that the form of iron that really participates in the chlorophyll biosynthetic pathway is active iron, although it is not known with certainty what forms of iron it includes. Therefore, the plant may have high iron contents, being only a fraction of it active iron. If a proportion was maintained between these types of iron, total iron could be used to establish the state of need for iron in the plant. However, this is not the case, whether due to no controlled cultivation conditions, such as in wild crops, or because the plant uses some mechanism to obtain iron to avoid this deficiency.

If we consider the active iron, the o-phen method should provide results that correlate to leaf colour, but this was not found. The determination o-phen is based on the formation of a Fe-o-phenanthroline colorimetric complex, using o-phen itself as an extractant. The results show that this method extracts iron, but also extracts chlorophyll and degradation products that act as interfering agents, making the measurement difficult. In addition, this complex is formed with iron(II) species exclusively. Considering that no certain information about the type of iron that forms the so-called active iron is available, this extraction method cannot be considered as representative of this fraction. Based on these two factors, it could be justified that the o-phen method does not provide iron values that correlate with the colour of the leaf.

In 1932 Oserkowsky found that active iron was correctly extracted using HCl, and some ulterior literature (Mehrotra et al., 1985) also compared different extractants to assess the active iron, corroborating that an extraction using HCl was the most suitable one to quantify this parameter. Nonetheless, up to this day, the reference methods are still those based on the total iron, and the o-phen extracted iron. The

results of this study confirm that the iron values obtained with HCl do correlate with the colour of the leaf, implying that the method proposed as early as 1932 was adequate and is the one that gives information about iron with biological activity.

Once the different types of iron content in the leaf was determined, a correlation study was carried out between the CIELab colour space and the iron content. The starting hypothesis was that, since iron chlorosis causes a homogeneous yellowing of the leaf due to the decrease in chlorophyll, the parameter that would correlate with iron would be parameter a*, which is the one that measures the difference between the green-red colour. However, the parameter that best correlates with iron is the L* parameter associated with the lightness of the leaf. This can be explained by observing a healthy leaf and a leaf that suffers from iron chlorosis. As can be seen in Figure 2.2, a decrease in chlorophyll content causes the leaf to acquire a yellow colour that is associated with an increase in brightness, which has a direct relationship with the iron content.

After having determined which CIELab parameter was correlated with active iron, the mathematical model based on a power function, was obtained using Matlab software applications, "regression learner" and "curve fitting". This type of equation implies that, at high concentrations of iron, little changes in lightness are observed, since enough chlorophyl is available. However, as the iron content decreases, a perceptual change is readily observed in the leaf, increasing the L* parameter.

Observing this power model in Figure 2.3, it could be seen that it could be broken down into two linear models, one for low iron content and the other for high iron content. This was done for the joint model and for the individual loquat and the citrus models (Table 2.2). It was observed that in all three cases the cut-off points of both linear models of each power model were similar and around 5.8 µg Fe/g of leaf. This point could be indicative of the moment from which the leaf begins to suffer iron chlorosis, since it is the point from which the parameter L* undergoes a faster increase with the iron decrease.
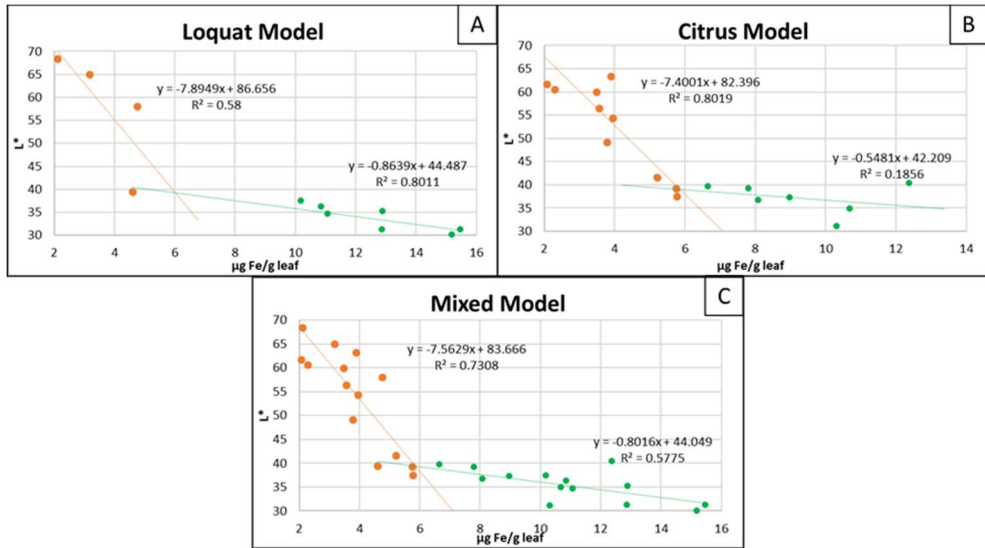
Figure 2.3: Linear models obtained by the fragmentation of the power model for Loquat model (A), Citrus model (B) and the model obtained for combination of both species(C).

Finally, once the mathematical model was obtained, it was considered whether a single model was capable of being used for all leaf varieties or each species required a different model. As observed in the results, the predictions for apricot, persimmon and peach leaves were not correctly made using the model obtained, however, the loquat leaves do fit together with the citrus leaves within the same model. Although incorporating the iron data of the new species in the model did not fit properly, it was observed that they did maintain the power behaviour. This fact can be explained according to the optical properties of the leaves. The leaves have different properties such as gloss, texture or global reflectance that can cause differences in the values of L* with respect to other species. For example, peach leaves tend to be brighter, causing the minimum values of L* to high iron contents to be placed in around 40 while those of citrus around 30. This way it can be said that, although the different species behave in a similar way, each species requires an independent model, unless the optical properties of two species are similar.

5.   Conclusions

 From this work different ideas can be extracted in relation to iron and its deficiency associated with the colour of a leaf.

Firstly, about the controversy of active iron or total iron, different methods have been studied to determine iron, either total iron by calcination or the active iron by

extraction with HCl. Among all the methods proposed, the method that best correlates with the colour of the leaf is that of obtaining active iron using HCl. This indicates that if this iron is the one that correlates properly with the colour of the leaf, it is because it is the one that really has biological activity in the plant and, therefore, the important one to properly diagnose iron chlorosis. Although this method was proposed as early as 1932, nowadays, the accepted methods are total iron and iron obtained with the use of o-phen. However, these methods do not provide values that are associated with the colour of the leaf.

Regarding the connection between the colour of the leaf and the iron present in it, it has been found that predictive models can be obtained using smartphone-based imaging in the CIELab colour space. More specifically, the L* parameter showed a good correlation with the active iron (extracted by HCl) through a power equation. Results evidenced that HCl extraction and regression by imaging were statistically comparable. This way, a fast, easy, and safer procedure has been developed to assess iron chlorosis.

However, although a model can be proposed to correlate the L* value of the leaf and the iron it contains, this depends on the plant species. This is because each plant species has leaves with different optical properties such as gloss, brightness, hue… Therefore, if the leaves differ in optical properties, the models must necessarily be different. However, if the leaves have similar optical properties, they can be grouped within the same model, as is the case with loquat and citrus leaves.

6.   References

Abadía, J., Monge, E., Montañés, L., & Heras, L. (1984). Extraction of iron from plant leaves by Fe (II) chelators. *Journal of Plant Nutrition*, 7, 777-784. DOI: 10.1080/01904168409363241.

Bidwell R.G.S. (1990). Fisiología vegetal. Primera edición. A.G.T. Editor, S.A. Mexico.

CIE Technical Committee. (2018). Colourimetry, 4th Edition. Commission Internationale de l'Éclairage. Vienna. DOI: 10.25039/TR.015.2018.

Fang, C., Zhang, X., Dong, Z., Wang, L., Megharaj, M., & Naidu, R. (2018). Smartphone app-based/portable sensor for the detection of fluoro-surfactant PFOA. *Chemosphere*, 191, 381-388. DOI: 10.1016/j.chemosphere.2017.10.057.

Fernández, J. A., Almela, L., & Fernández, J. (1994) La nutrición férrica de las plantas: el problema de la clorosis, Universidad de Murcia (Ed.). Dialnet. España.

Li, C., Adhikari, R., Yao, Y., Miller, A. G., Kalbaugh, K., Li, D., & Nemali, K. (2020). Measuring plant growth characteristics using smartphone based image analysis technique in controlled environment agricultura. *Computers and Electronics in Agriculture*, 168, 105123. DOI: 10.1016/j.compag.2019.105123.

Miller, G. W., Pushnik, J. C., & Welkie, G. W. (1984). Iron chlorosis, a worldwide problem, the relation of chlorophyll biosynthesis to iron. *Journal of Plant Nutrition*, 7(1-5), 1-22.

Katyal, J. C., & Sharma, B. D. (1980). A new technique of plant analysis to resolve iron chlorosis. *Plant and Soil*, 55, 105-119. DOI: 10.1007/BF02149714

Köseoğlu, A. T., & Açikgöz, V. (1995). Determination of iron chlorosis with extractable iron analysis in peach leaves. *Journal of Plant Nutrition*, 18, 153-161. DOI: 10.1080/01904169509364892.

Kyrkby, E. & Römheld, V. (2008). Micronutrientes en la fisiología de las plantas: funciones, absorción y movilidad. *Informaciones Agronómicas*, 68, 1-6.

Lang, H. J., & Reed, D. W. (1987). Comparison of HCl extraction versus total iron analysis for iron tissue analysis. *Journal of Plant Nutrition*, 10, 795-804. DOI: 10.1080/01904168709363610.

Mehrotra, S. C., Sharma, C. P., & Agarwala, S. C. A. (1985). A Search for extractants to evaluate the iron status of plants. *Soils Science and Plant Nutrition*, 31, 155-162. DOI: 10.1080/00380768.1985.10557423

Merry, R., Dobbels, A. A., Sadok, W., Naeve, S., Stupar, R. M., & Lorenz, A. J. (2022). Iron deficiency in soybean. *Crop Science*, 62(1), 36-52. DOI: 10.1002/csc2.20661.

Mohammad, M. J., Najim, H., & Khresat, S. (1998). Nitric acid and o-phenanthroline-extractable iron for diagnosis of iron chlorosis in citrus lemon trees. *Communications in Soil Science and Plant Analysis*, 29, 1035-1043. DOI: 10.1080/00103629809370005.

Navarro, G., & Navarro, S. (2013). Química agrícola: Química del suelo y de los nutrientes esenciales para las plantas. Ediciones Mundi-Prensa. Madrid.

Palacios, J.V. (2003). Clorosis férrica y su relación con el nivel de clorofila y hierro en diferentes órganos en palto. Tesis. Facultad de ciencias Agronómicas (Santiago-Chile).

Pierson, E. E., & Clark, R. B. (1984). Ferrous iron determination in plant tissue. *Journal of Plant Nutrition*, 7,107-116. DOI: 10.1080/01904168409363178.

Puente-Ramírez, J. V., Rivera-Ortiz, P., Silva-Espinosa, J. H., & Andrade-Limas, E. (2022). Chelate EDDHA to correct the iron deficiency in Italian lemon trees (Citrus limon (L.) Osbeck). *Terra Latinoamericana*, 40, e926. DOI: 10.28940/terra.v40i0.926.

Ramacciotti, M., Gallello, G., Lezzerini, M., Pagnotta, S., Aquino, A., Alapont, L., Martín, J. A., Pérez-Malumbres, A., Hiraldo, R., Godoy, D., Morales-Rubio, A., Cervera, M. L., & Pastor, A. (2022). Smartphone application for ancient mortars identification developed by a multi-analytical approach. *Journal of Archaeological Science: Reports*, 43, 103433. DOI: 10.1016/j.jasrep.2022.103433.

Razeto, B., & Valdés, G. (2006). Análisis de hierro soluble en tejidos para diagnosticar el déficit de hierro en nectarino. *Agricultura Técnica*, 66, 216-220. DOI: 10.4067/S0365-28072006000200012.

Sadzawka, A., Carrasco, M. A., Demanet, R., Flores, H., Grez, R., Mora, M. L., & Neaman, A. (2007). Métodos de análisis de tejidos vegetales. *Serie actas INIA*, 40, 140.

Sáez-Hernández, R., Antela, K. U., Mauri-Aucejo, A. R., Morales-Rubio, A., & Cervera, M. L. (2022). Smartphone-based colorimetric study of adulterated tuna samples. *Food Chemistry*, 389, 133063. DOI: 10.1016/j.foodchem.2022.133063.

Takkar, P. N., & Kaur, N.P. (1984). HCL method for Fe2+ estimation to resolve iron chlorosis in plants. *Journal of Plant Nutrition*, 7, 81-90. DOI: 10.1080/01904168409363176.
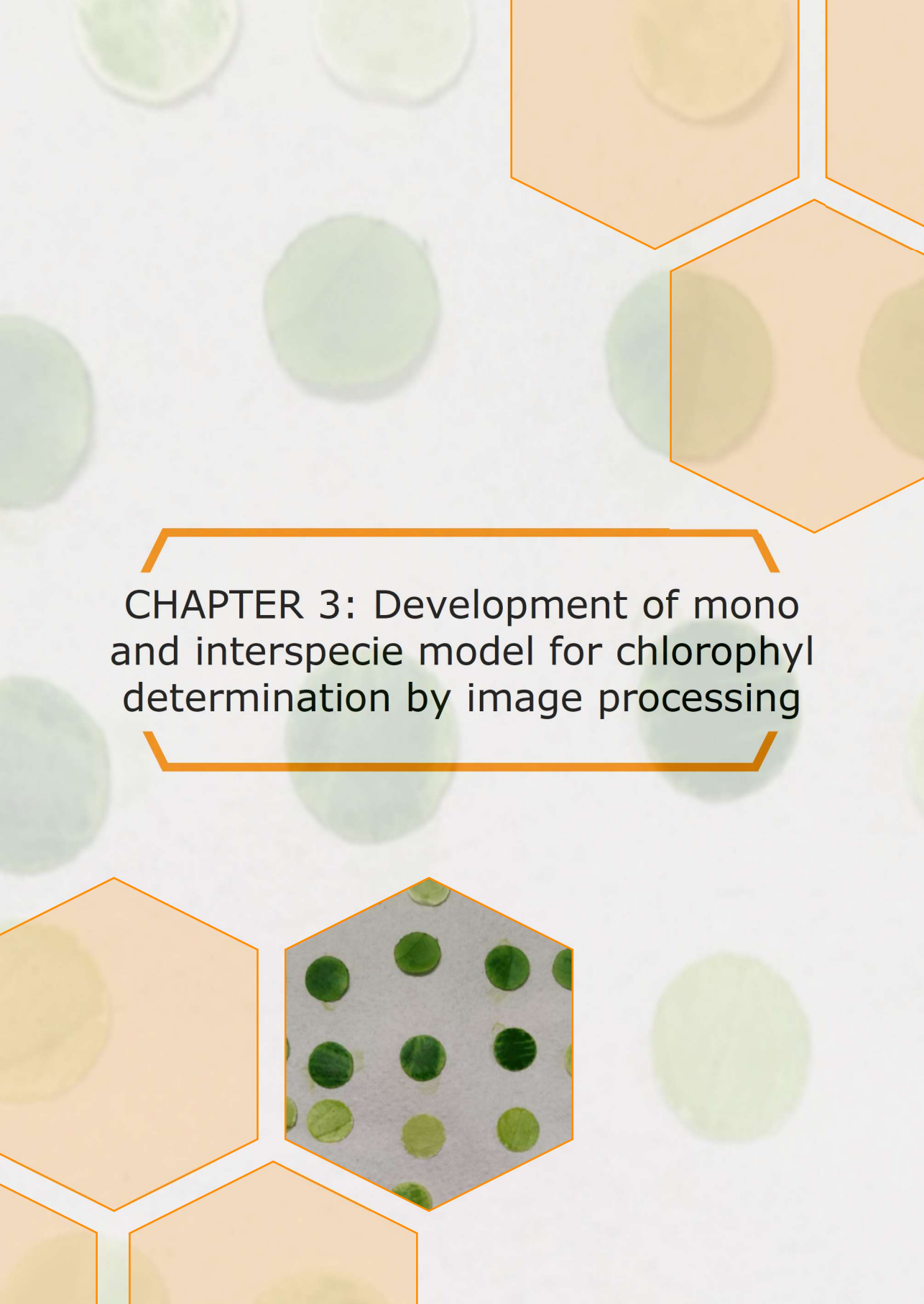
Torres, A., Héctor, E., Cué, J., & Cevallos, M. (2018). Fisiología Vegetal Volumen I: Nutrición hídrica y mineral de las plantas. Ediciones UTM-Universidad Técnica de Manabí. Ecuador.

Wang, Y., Kang, Y., Zhong, M., Zhang, L., Chai, X., Jiang, X., & Yang, X. (2022). Effects of iron deficiency stress on plant growth and quality in flowering Chinese cabbage and its adaptive response. *Agronomy*, 12(4), 875. DOI: 10.3390/agronomy12040875.

Zebec, V., Lisjak, M., Jović, J., Kujundžić, T., Rastija, D., & Lončarić, Z. (2021). Vineyard Fertilization Management for Iron Deficiency and Chlorosis Prevention on Carbonate Soil. *Horticulturae*, 7(9), 285. DOI: 10.3390/horticulturae7090285.

CHAPTER 3: Development of mono and interspecie model for chlorophyl determination by image processing

ABSTRACT

In the present work, predictive models to correlate the colour of the leaves with the chlorophyll content have been elaborated. For this, chlorophyll measurements have been made using a solvent extraction reference method and using a chlorophyll content meter (CCM). Chlorophyll data, expressed as µg in leaf area or mass and in CCM units, have been correlated with the leaf colour data, expressed in RGB, CIEL*a*b* and CIEL*h*C* colour spaces, to check which of them provides the best predictive models. This study has been carried out with 4 leaves species: peach, apricot, persimmon, and loquat. The results show that the best prediction is achieved using the model obtained with the RGB colour space and the chlorophyll concentration expressed with respect to sample area (µg cm^{-2}). Once the individual models for each leaf species were found, the development of a joint model for all the species was studied. This was done with the use of the SPSS program, using the species of tree as a categorical variable. The best joint model found was obtained using the B and R parameters of the leaf colour when the chlorophyll content is expressed by sample mass. In this developed model, both the leaves species and the G parameter are irrelevant when making the prediction of the chlorophyll content. The created model presents an R^2=0.835.

Keywords: Chlorophyll, Colour Spaces, Matlab, Smartphone, SPSS.

1.   Introduction

Photosynthetic organism such as plants, algae or bacteria are very important for life. These organisms perform photosynthesis releasing O_2 necessary for life and capturing atmospheric CO while allowing the greenhouse effect to be controlled naturally. Moreover, plants carry out the photosynthesis to transform light energy into food.

From them, plants are the most common in our terrestrial ecosystem, contain photosynthetic pigments in their leaves that are responsible for capturing the light that allows the photosynthesis process. Among the different types of pigments, the carotenoids and chlorophyll should be highlighted. Carotenoids (yellow or orange) are responsible for protecting the photosensitive apparatus, and chlorophyll (green) directly takes part in the absorption and conversion process of light energy (Azcon-Bieto & Talón, 2000).

There are several types of chlorophyll, but all are characterized by having a cyclic tetrapyrrolic ring with a magnesium cation in the centre linked inside the ring, and they also contain a long hydrophobic chain of phytol. Figure 3.1 shows the general molecular structure of chlorophyll indicating the substituents R1 to R4 which are modified depending on the type of chlorophyll in question (Azcon-Bieto & Talón, 2000). Despite having different types of chlorophylls, the main types in vascular plants are *chlorophyll a* and *chlorophyll b*, and therefore, the green colour of the plant indicates a healthy state of this (Baresel et al., 2017; Chung et al., 2018; Cortazar et al., 2015; Dey et al., 2016; López et al. 2004; Ortuño et al., 2017; Saputro & Imawan, 2017; Sookchalearn & Abdullakasim, 2017; Treder et al., 2016; Vesali, 2015). Traditional leaf chlorophyll extraction procedures use organic solvents, but due the rapid degradation of the chlorophyll after its extraction and to reduce environmental impact of the use of solvents in extraction methods, it is advisable to use direct measurement methods, which allow us to quantify the chlorophyll content in situ, on the leaves themselves.
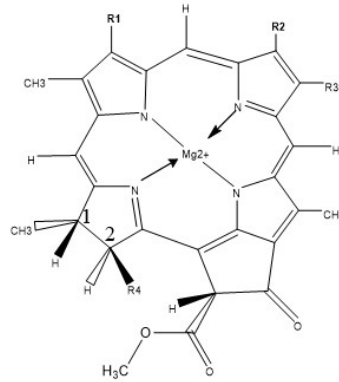
Chlorop. Type	R₁	R₂	R₃	R₄	Double bond generated between C₁ and C₂
a	-CH=CH₂	-CH₃	-CH₂CH₃	X	No
b	-CH=CH₂	-CHO	-CH₂CH₃	X	No
c₁	-CH=CH₂	-CH₃	-CH₂CH₃	-CH=CH-COOH	Yes
c₂	-CH=CH₂	-CH₃	-CH=CH₂	-CH=CH-COOH	Yes
d	-CHO	-CH₃	-CH₂CH₃	x	No
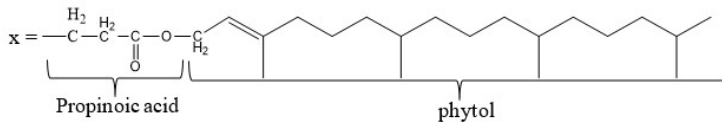
Figure 3.1: Molecular structure of chlorophyll types.

1.1. Smartphone and colour spaces

Nowadays the use of Smartphones for this type of research is increasing since almost everyone has one, so it is an inexpensive way to facilitate universal access to this type of analysis. Previous investigations have been found that, with proper treatment, it is possible obtaining the chlorophyll content from a photograph. In some cases, a photograph of the leaf is taken, and a treatment of the image's colour parameters is made (Rigon et al., 2016), or the colour parameters are taken through transmitted light (Gaviria-Palacio et al., 2017; Vesali et al., 2017), or recorded the fluorescence emitted by the algae when are excited (Friedrichs et al., 2017). There are works about the correlation between the colour and the chlorophyll content in soybean leaves (Hassanijalilian et al., 2020), in rice leaves (Mohan & Gupta, 2019) and in corn plants (Vesali et al., 2017). Moreover, there are works in which Neural network architecture is used for this purpose (Barman & Choudhury, 2022; Tang et al., 2023). In all cases the model obtained is only for one specie. Other works

employs the use of spectral reflectance reconstruction from RGB images obtained by Smartphone to determine the content of chlorophyll (Gong et al., 2023).

"A colour space can be described as a method to express the colour of an object using some type of annotation such as numbers" (Konica Minolta, 2014). In this chapter, three colour spaces, adobe RGB (RGB), CIEL*a*b* and CIEL*h*C* has been used.

The RGB colour space works in a similar way to human vision. From this colour space is possible to access to other spaces. The RGB colour space has been widely used in the quantification of coloured solutions or immobilized substances through digital image processing by specific software that allows the extraction of colorimetric information by selecting the areas of interest from an image (Capitan-Vallvey et al., 2015).

The CIEL*a*b* colour space is one of the most widely used colour spaces today. It was modelled on an opponent colour theory that states that two colours cannot be red and green at the same time or yellow and blue. As can be seen in Figure R.5, the L* coordinate indicates luminosity and the a* and b* parameters indicate the chromatic coordinates red/green and yellow/blue, respectively (Konica Minolta, 2014).

The CIEL*h*C* colour space is preferred by some industry professionals. As can be seen in Figure R.6, the L* coordinate indicates luminosity, the h* coordinate is the hue or hue angle and the C* coordinate indicates the chroma or saturation. The value of C* is the distance from the axis of luminosity (L*) and starts at 0 in the centre. The hue angle begins on the +a* axis and is expressed in degrees (Konica Minolta, 2014).

The aim of this work is the quantification of chlorophyll in leaves by a smartphone. The first is take a photo of the leaf, the second is measure the chlorophyll content by CCM-200 (Chlorophyll content meter), that is a portable instrument to measure chlorophyll and, the third is the determination of chlorophyll content by solvent extraction and UV-Vis spectrometry detection. Later, models for the determination of chlorophyll in the leaves of different species will be done to correlate the colour obtained of the image taken by smartphone with the content of chlorophyll and the CCM measurements. Finally, when the individual models would be obtained, interspecies model will be studied to try make a universal model for all species studied.

2. Materials and Methods

2.1. Samples

130 leaf samples from different fruit species were used in order to find a model capable of predicting the chlorophyll content. The samples come from leaves of 4 different species: 40 from peach trees, 30 from apricot tree, 30 from kaki and 30 from loquat. The making of the different models consists of two stages, the first stage is the development of the model for which 75% of the samples are used and, the second stage is the model validation with the remaining 25% of the samples.

2.2. Sample preparation

The leaves are carefully washed, rinsed with deionized water, and dried between two filter paper. Once dry, circles of 0.95 cm^2 are cut with the help of a punch, avoiding the nerves as far as possible, and they are introduced into previously labelled topaz vials and stored at 4°C until the following measurements and the chlorophyll extraction are carried out.

2.3. Direct measurement of chlorophyll

An Opti-Sciences CCM-200 was used for direct measurements of chlorophyll (Figure 3.2). Calibration of the instrument is required every time the unit is turned on. The calibration or "zero" equipment is adjusted closing the empty measurement chamber (without any material). Subsequently, the sample is introduced into the measurement chamber and the measure is carried out. This equipment measures the transmittance through the leaf at two wavelengths (653 nm and 931 nm) to estimate the chlorophyll content providing an average data (arbitrary units, a.u.) corresponding to 71 mm^2 of leave surface.

Figure 3.2: CCM-200 instrument.

2.4.   Smartphone characterization and image acquisition

The smartphone used, a Samsung S7 with a 12-megapixel camera with image stabilization, was previously characterised by taking pictures, under the same lighting conditions, of 514 chips of the atlas of the Munsell Colour System, sheets from the 1.35GY to 10YR plus the grey samples, which cover the chromaticity range for photographing the leaf samples.

A 5-degree polynomial model was used to relate the RGB camera responses to the L*a*b* values of the chips under standard D65 lighting, by least squares, using a training set of 268 chips evenly distributed in the Munsell colour space. Model performance, evaluated with the remaining chips, was reasonably good, with average prediction errors of 3±2 CIEL*a*b* units. This procedure is a modification of the method described by Hong to derive XYZ tristimulus values from RGB responses (Hong et al., 2000).

The photographs obtained by smartphone are all taken under the same controlled lighting conditions. As shown in Figure 3.3, a methacrylate structure that allows place a white semi-sphere of polystyrene, black painted on the outside, containing inside some led strips of white lighting at 5600 K was used. Inside the semi sphere there is a support where the sample is placed to take a photo. The semi-sphere is covered with a flat white cap perforated in the centre, thus avoiding interference produced by external light. The smartphone is placed on top of the methacrylate structure 16 cm away from the sample. Figure 3.4 shows the experimental scheme for acquiring images and obtaining the colour descriptors.
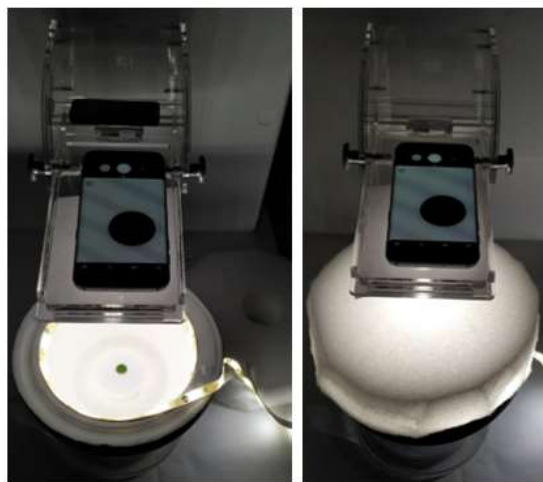
Figure 3.3: Methacrylate assembly in which the image of the leaf is made.
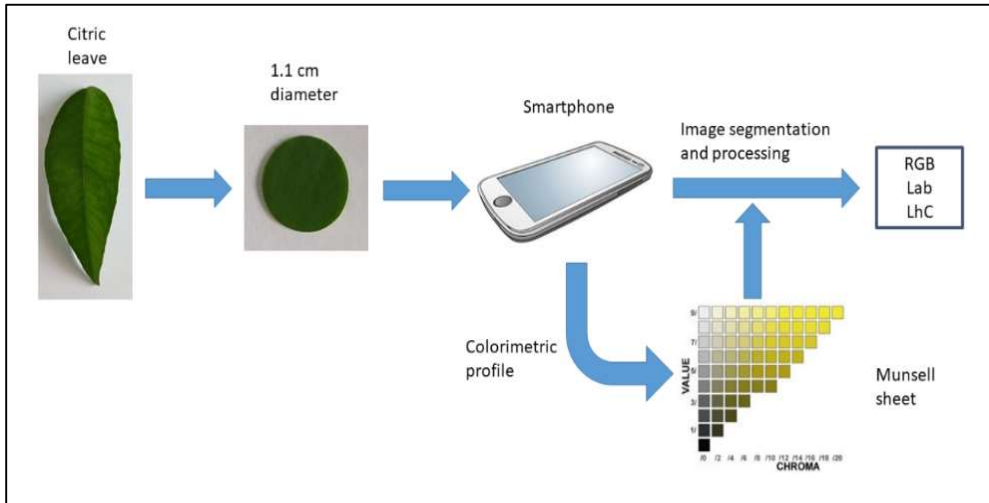
Figure 3.4: Scheme of image acquisition and obtaining colour descriptors.

2.5. Chlorophyll extraction and quantification by UV-Vis spectrophotometry

Once the direct measurements (photography and CCM) have been made on the circular sections of the leaves, they are crushed with a little amount of cold acetone in a mortar placed in an ice bath. The crushed sample is transferred using a funnel to a 10 mL volumetric flask and made up to the mark with cold acetone. Next, the sample is homogenized and with the help of a 1 mL syringe and a syringe filter, the solution is filtered introducing the resulting extract into a quartz cuvette. Finally, the spectrum of the solution is recorded by the Hewlett Packard 8452-A UV-Vis Diode-Array spectrophotometer. The chlorophyll content in the solution and in the leaf is calculated employing some theoretical equations (Lichtenhaler, 1987) provided by the department of plant physiology from the University of Valencia for acetone 100% as solvent (equations 1, 2 and 3) and data from the spectrum.

$$[\textit{Chlorophyll a}] \ (\mu g \ mL^{-1}) = 11.24 \cdot A_{662} - 2.04 \cdot A_{645} \qquad \text{(Equation 1)}$$

$$[\textit{Chlorophyll b}] \ (\mu g \ mL^{-1}) = 20.13 \cdot A_{645} - 4.19 \cdot A_{662} \qquad \text{(Equation 2)}$$

$$[\textit{Chlorophyll a+b}] \ (\mu g \ mL^{-1}) = 7.05 \cdot A_{662} + 18.08 \cdot A_{645} \qquad \text{(Equation 3)}$$

2.6. Making of the prediction models

The chemometric models are made with the CCM values, the chlorophyll content ($\mu g \ cm^{-2}$ and $\mu g \ g^{-1}$) and the photographs obtained by the smartphone. Before

starting to make the models, the pixels of the photograph must be converted to their corresponding RGB, CIEL*a*b* and CIEL*h*C* values. The models are made by relating the parameters of the different colour spaces obtained from the image with the CCM values and the chlorophyll content and, employing the "*regression learner*" app of Matlab R2017b program from Mathworks (Natick, MA, USA). For the creation of models with categorical variables SPSS program (Statistical Product and Service Solutions Ibérica, S.L.) was used.

3.   Results and discussion

3.1 Mono-species model

In order to create mono-species models, different colour spaces (RGB, L*a*b* and L*h*C*) and chlorophyll content expressions ($\mu g\ g^{-1}$, $\mu g\ cm^{-2}$ and CCM) were tested in order to find the best prediction model. As can be seen in the Table 3.1. for each colour space (in this case RGB), different combinations of the colour parameters are tried and the best model (lower root mean square error (RMSE) and higher R^2) are selected. This study is made for each colour space and plant species (Tables 3.A.1 to 3.A.11). The best models for each one is collected in Tables 3.2 to 3.5. As can be seen in these tables, the more suitable colour space is RGB for most of the fruit tree species.

Additional to the parameters of the calibration model, for the selection of the best prediction models these must be tested with the validation group of samples (25% for each species). Figures 3.5 to 3.8 provide Passing-Bablok regression diagrams of the best models (selected in Tables 3.2 to 3.5) for each chlorophyll content and each colour space. As it can be seen in the figures, the x=y line is included inside the 95% confidence interval of the adjust between predicted value and real chlorophyll content for the different units considered.

Although the best model was obtained using the training group with the RGB parameters for its creation, there are two cases in which the application of this model is worse than the application of the others. First case is the content of chlorophyll per mass in peach leaves (Figure 3.5A), where x=y line is near to the 95% confidence interval of the adjust but not inside, and the second case is the chlorophyll content per area in persimmon leaves (Figure 3.7B), where the last point could be an outlier value, but it is not assured. In both cases, the employment of the model obtained using the CIEL*h*C* colour space allows obtaining a better validation (Passing-Bablok of Figures 3.5D and 3.7D).

Table 3.1. RMSE and coefficients of determination obtained for the different models calculated for the RGB colour space in peach leaves.

Variables	[Chlorophyll] (µg g^{-1})		[Chlorophyll] (µg cm^{-2})		CCM (a.u.)	
	RMSE	r^2	RMSE	r^2	RMSE	r^2
RGB	416.36	0.72	**3.96**	**0.92**	**2.31**	**0.95**
RG	519.48	0.56	8.57	0.67	4.13	0.82
GB	420.54	0.71	4.18	0.91	2.59	0.93
RB	**410.51**	**0.72**	4.69	0.90	2.97	0.91
R	518.94	0.56	9.56	0.59	5.69	0.66
G	586.93	0.44	8.84	0.65	4.35	0.80
B	416.98	0.71	4.92	0.89	3.56	0.87

Table 3.2. Summary of the best models for the chlorophyll prediction in peach leaves according to the chlorophyll content units and the colour space. The table specify the colour parameters combination that provides the best prediction model, the lower RMSE and the higher R^2.

	[Chlorophyll] (µg g^{-1})			[Chlorophyll] (µg cm^{-2})			CCM (a.u.)		
	Parameters	RMSE	R^2	Parameters	RMSE	R^2	Parameters	RMSE	R^2
RGB	**RB**	**410.51**	**0.72**	**RGB**	**3.96**	**0.92**	**RGB**	**2.31**	**0.95**
*L*a*b**	b*	464.82	0.67	L*a*b*	7.25	0.73	L*a*	5.12	0.72
*L*h*C**	h*	447.37	0.66	h*C*	7.00	0.75	L*C*	5.58	0.67
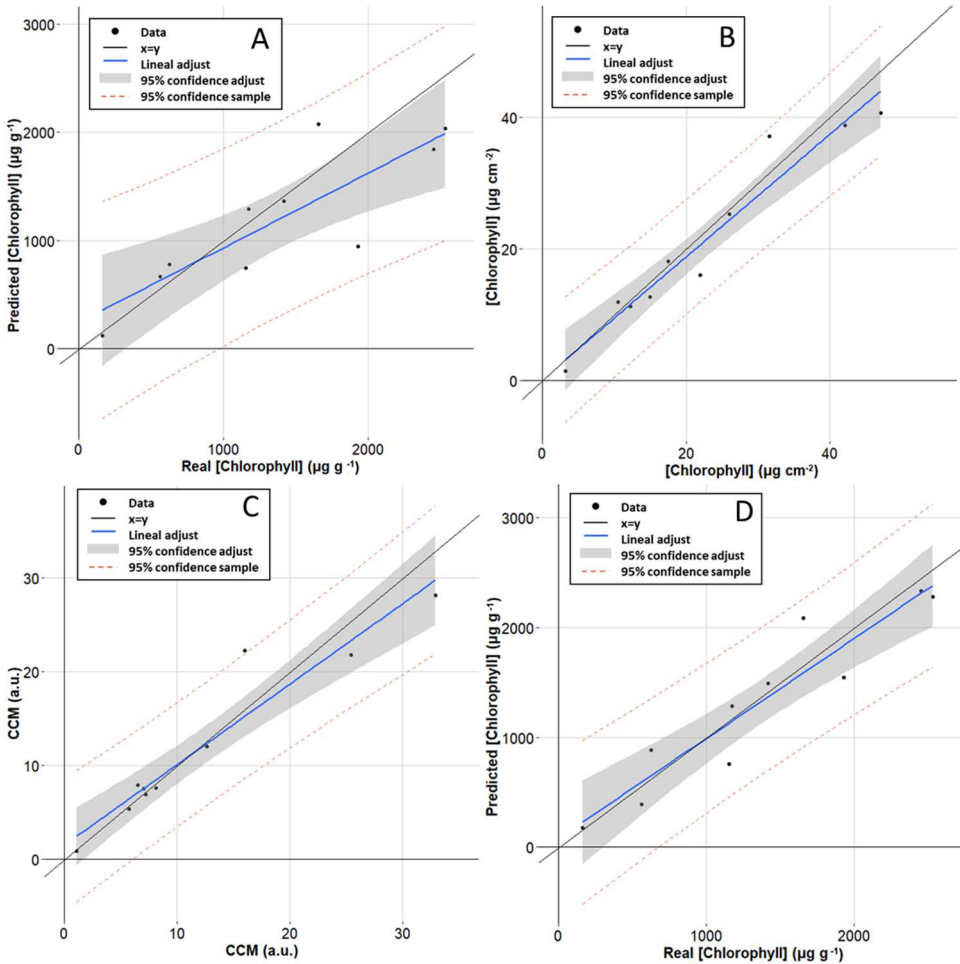
Figure 3.5: Passing-Bablok regression diagrams obtained for peach leaves for the best prediction model for A) Chlorophyll content as a function of mass (using RGB colour space), B) Chlorophyll content in area (using RGB colour space), C) CCM value (using RGB colour space) and D) Chlorophyll content as a function of mass (using L*h*C* colour space).

Table 3.3. Summary of the best models for the chlorophyll prediction in apricot leaves according to the chlorophyll content units employed and the colour space. The table specify the colour parameters combination that provides the best prediction model, the lower RMSE and the higher R².

	[Chlorophyll] (µg g^{-1})			[Chlorophyll] (µg cm^{-2})			CCM(a.u.)		
	Parameters	RMSE	R^2	Parameters	RMSE	R^2	Parameters	RMSE	R^2
RGB	**RB**	**271.14**	**0.84**	**RGB**	**4.97**	**0.88**	**GB**	**3.29**	**0.83**
L*a*b*	L*a*b*	341.40	0.77	L*	7.24	0.77	**L***	**3.32**	**0.83**
L*h*C*	L*	344.95	0.71	L*C*	6.06	0.83	L*	3.51	0.82
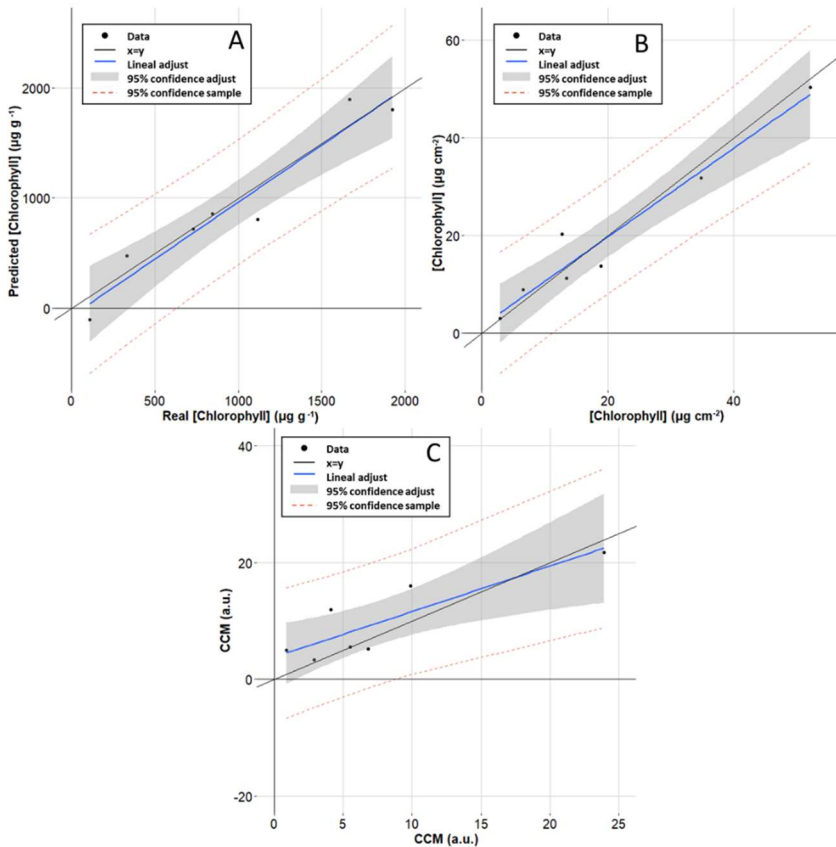
Figure 3.6: Passing-Bablok regression diagrams obtained for apricot leaves for the best prediction model for A) Chlorophyll content as a function of mass (using RGB colour space), B) Chlorophyll content in area (using RGB colour space) and C) CCM value (using RGB colour space).

Table 3.4. Summary of the best models for the chlorophyll prediction in persimmon leaves according to the chlorophyll content units employed and the colour space. The table specify the colour parameters combination that provides the best prediction model, the lower RMSE and the higher R^2.

	[Chlorophyll] (μg g^{-1})			[Chlorophyll] (μg cm^{-2})			CCM (a.u.)		
	Parameters	RMSE	R^2	Parameters	RMSE	R^2	Parameters	RMSE	R^2
RGB	**RB**	**149.37**	**0.97**	**GB**	**2.89**	**0.99**	**GB**	**2.75**	**0.98**
L*a*b*	L*b*	145.95	0.96	L*b*	4.92	0.97	L*b*	3.62	0.96
L*h*C*	**L*h***	**136.98**	**0.97**	h*	3.59	0.98	L*h*C*	2.83	0.97
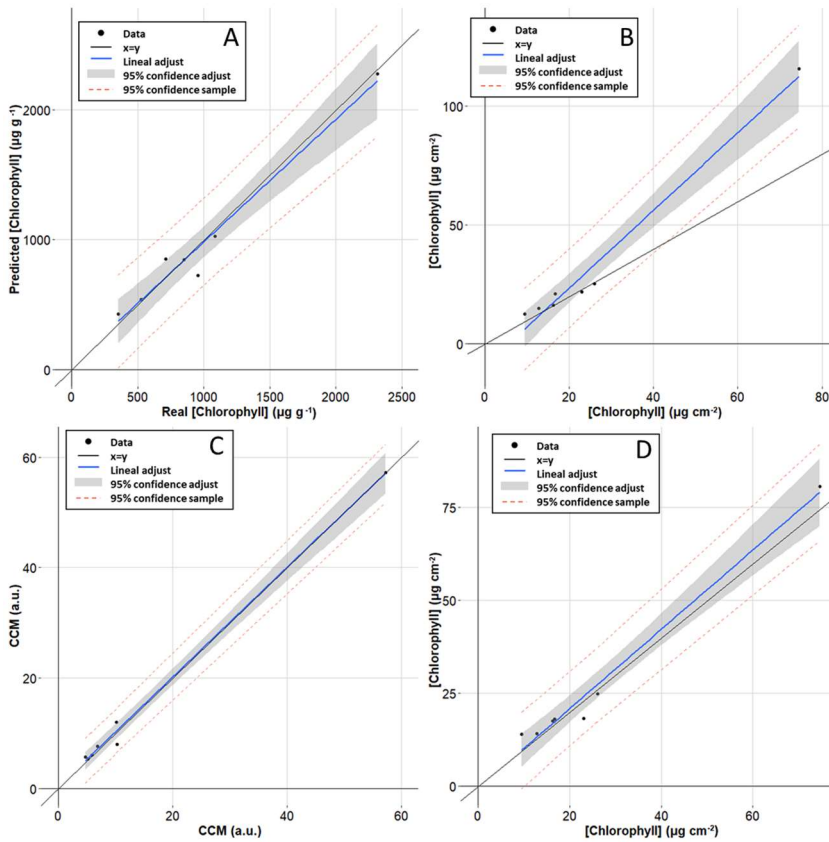
Figure 3.7: Passing-Bablok regression diagrams obtained for persimmon leaves for the best prediction model for A) Chlorophyll content as a function of mass (using RGB colour space), B) Chlorophyll content in area (using RGB colour space), C) CCM value (using RGB colour space) and D) Chlorophyll content in area (using L*h*C* colour space).

Table 3.5. Summary of the best models for the chlorophyll prediction in loquat leaves according to the chlorophyll content units employed and the colour space. The table specify the colour parameters combination that provides the best prediction model, the lower RMSE and the higher R^2.

	[Chlorophyll] (μg g^{-1})			[Chlorophyll] (μg cm^{-2})			CCM(a.u.)		
	Parameters	RMSE	R^2	Parameters	RMSE	R^2	Parameters	RMSE	R^2
RGB	**RB**	**114.89**	**>0.99**	**RGB**	**2.28**	**>0.99**	**RGB**	**5.34**	**0.92**
L*a*b*	b*	242.68	0.96	L*a*b*	7.85	0.95	a*b*	6.96	0.87
L*h*C*	h*	184.35	0.98	C*	6.93	0.96	L*C*	5.77	0.91
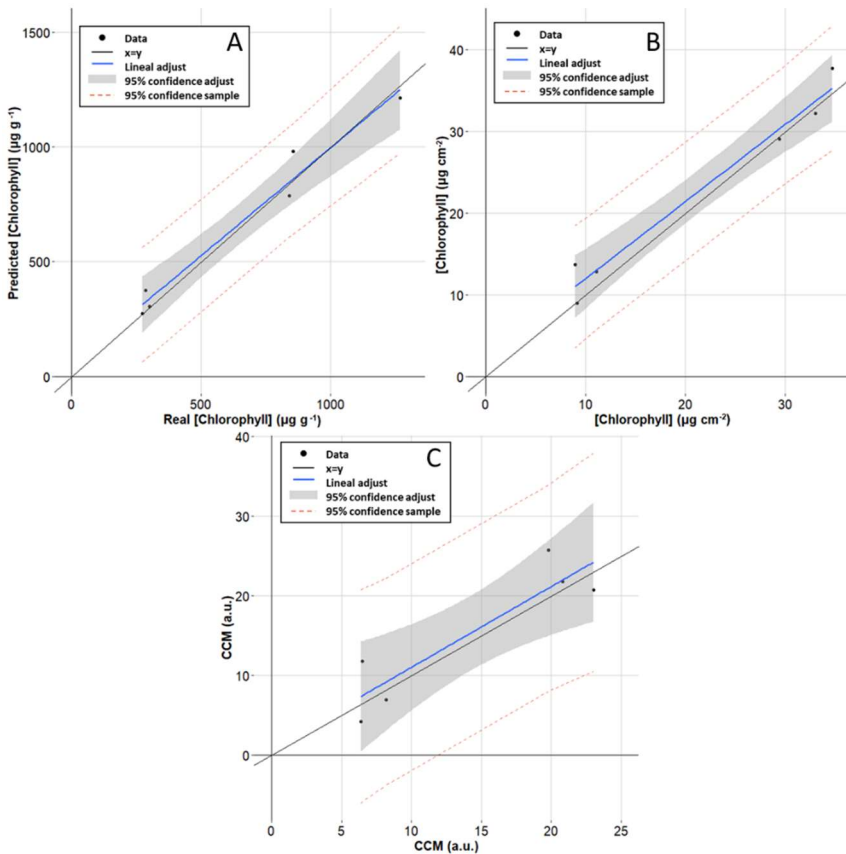
Figure 3.8: Passing-Bablok regression diagrams obtained for loquat leaves for the best prediction model for A) Chlorophyll content as a function of mass (using RGB colour space), B) Chlorophyll content in area (using RGB colour space) and C) CCM value (using RGB colour space).

It is possible to check that is necessary to test the models with the test data group in order to check the effectiveness of the model created. The table 3.6 shows the models of each colour space of each species that include the x=y line in the confidence interval of adjust and could be possible to use it for chlorophyll content predictions. As can be seen, depending on the expression of the chlorophyll content and the species a different colour space could be more suitable for the prediction model creation. Then it is necessary to study each colour space for each species to find the best parameter combination for the creation of the prediction model.

Table 3.6. Summary of the developed models, the combination of parameters employed for each colour space, and estimation of the appropriate prediction: Green - suitable; Orange- not suitable; Yellow- suitable but the 95% confidence interval adjust is too wide. Pea.: Peach; Apr.: Apricot; Per.: Persimmon; Loq.: Loquat.

	[Chlorophyll] (µg g⁻¹)				[Chlorophyll] (µg cm⁻²)				CCM(a.u.)			
	Pea.	Apr.	Per.	Loq.	Pea.	Apr.	Per.	Loq.	Pea.	Apr.	Per.	Loq.
RGB	RB	RB	RB	RB	RGB	RGB	GB	RGB	RGB	GB	GB	RGB
L*a*b*	b*	L*a*b*	L*b*	b*	L*a*b*	L*	L*b*	L*a*b*	L*a*	L*	L*b*	a*b*
L*h*C*	h*	L*	L*h*	h*C*	h*C*	L*C*	h*	C*	L*C*	L*	L*h*C*	C*

3.2.   Multispecies models

Until now, models for a single species have been developed and attempts have been made to check if these models, made with one species, are suitable for the chlorophyll content prediction in other species, which represents many possible combinations. Moreover, these studies don´t provide good results about chlorophyll content prediction. However, another way to study the data is by creating joint models in which the data of different species is considered to develop a single model valid for all species, or the maximum possible of them. This can be made using a categorical variable.

To create these join models SPSS program is used. This software allows carry out linear regressions in which the variables can be considered categories. This allow use the species as a categorical variable in order to create only one model that takes in count this parameter. This join model study is developed using each colour spaces (RGB, CIELab and CIELhC). The models are created for the different chlorophyll content units. The application of a categorical variable (species) to the regression provides a general lineal model including "corrections" of it depending on the species. The base model is the same, but the prediction uses the categorical variable as a modifier of the model in function of the studied species.

When these models are made, it is necessary to consider the values of the observed power and R^2 in the inter-individuals effects test table, and the significance in the parameter estimates and the design of the general function which can estimated:

(Design: Intersection + species + R·R'+ G·G' + B·B').

Where *Intersection (I)*, *Species (S)*, *R*, *G* and *B* are the values provided by the model and the *R'*, *G'* and *B'* values are provided by the photo of the leaf. *R*, *G* and *B* can be substituted for *L*,a*,b** or *L*,h*,C** depending on the colour space studied.

For each model a table as the Table 3.7 is obtained (Tables 3.A.12 to 3.A.25). The Table 3.7 is for the model created for the chlorophyll content expressed as a function of mass using RGB colour space. The closer to 1 the observed power is, the more relevance the parameter has in the model. If the parameter has a significance greater than 0.05 this parameter does not have relevance in the model. The allocation of species has been: 1- persimmon, 2- apricot, 3- peach and 4- loquat. A species must be selected as a reference to develop the models, in this case it is species 4 -loquat. As can be seen, in this case the *G* and *species* parameters have a low *observed power* and a *significance* over 0.05, these parameters are not relevant in the present model, and it can be created again without these parameters (Table 3.8). The Table 3.9 summarises the models created for each chlorophyll content unit and for each colour space including the model design, the parameters of the model and the adjusted R^2.

Table 3.7. Parameters of the joint model of the four fruit species for chlorophyll in µg g^{-1} in the RGB colour space.

RGB colour space - chlorophyll (µg g^{-1})

Inter-individuals effects tests			Parameter estimates			
Origin	Type III of square sum	Observed power[b]	Parameter	S	Desv. Error	Sig
Corrected model	65313150[a]	1.00	**Intersection**	1778.81	225.22	0.00
Intersection	9502882	1.00	**[species=1]**	128.43	132.70	0.34
species	636618	0.43	**[species=2]**	-41.44	124.39	0.74
R	4043757	1.00	**[species=3]**	155.99	118.09	0.19
G	19093	0.07	**[species=4]**	0[c]	-	-
B	10693117	1.00	**R**	-12.78	2.26	0.00
a. R^2 = 0.847 (Adjusted R^2 = 0.837)			**G**	-1.09	2.81	0.70
			B	38.45	4.19	0.00
b. α= 0.05			c. reference species			

Table 3.8. Parameters of the joint model of the four fruit species for chlorophyll in µg g^{-1} in the RGB colour space.

RGB colour space - chlorophyll (µg g^{-1})

Inter-individuals effects tests			Parameters estimates			
Origin	Type III square sum	Observed power[b]	Parameter	S	Desv. Error	Sig
Corrected model	64676514[a]	1.000	**Intersection**	1851.93	150.26	0.00
Intersection	19469537	1.000	**R**	-14.01	1.20	0.00
R	17492788	1.000	**B**	37.97	3.65	0.00
B	13867659	1.000				
a. R^2 = 0.839 (Adjusted R^2 = 0.835)						
b. α= 0.05						

Table 3.9. Summary of the functions for the chlorophyll content prediction of the join models and the values of the parameters in the function.

Colour space	Chlorophyll content unit	General function design	Intersection	R/L*	G/a*/h*	B/b*/C*	Species 1	Species 2	Species 3	Species 4	R² adjusted
RGB	(µg g⁻¹)	I+R·R'+B·B'	1852	-14.01	-	37.97	-	-	-	-	0.835
RGB	(µg cm⁻²)	I+S+R·R'+G·G'+B·B'	56.40	-0.24	-0.18	1.03	3.13	-9.88	12.95	0	0.808
RGB	CCM	I+S+R·R'+G·G'+B·B'	32.27	0.09	0.15	0.66	0.28	9.20	7.24	0	0.802
L*a*b*	(µg g⁻¹)	I+a*·a*'+b*·b*'	1487	-	-22.69	-31.27	-	-	-	-	0.509
L*a*b*	(µg cm⁻²)	I+S+ a*·a*'+b*·b*'	47.94	-	-0.86	-0.79	-9.69	-21.93	-25.65	0	0.446
L*a*b*	CCM	I+S+ L*·L*'+b*·b*'	44.84	-0.35	-	-0.36	-2.01	-10.18	-8.73	0	0.460
L*h*C*	(µg g⁻¹)	I+S+h*·h*'+C*·C*	389	-	718	-25.40	-319	-454	-280	0	0.668
L*h*C*	(µg cm⁻²)	I+S+h*·h*'+C*·C*	12.14	-	20.26	-0.58	-13.74	-25.61	-29.98	0	0.627
L*h*C*	CCM	I+S+h*·h*'+C*·C*	8.06	-	11.86	-0.31	-11.85	-20.16	-18.81	0	0.614

As can be seen in Table 3.9, the best joint model obtained is for RGB colour space and the chlorophyll content expressed as function of the mass. This model provides the higher R^2 using the smaller number of parameters (R and B alone, plus intersection). The models developed in the RGB space for chlorophyll content in area and in CCM units provide also higher adjusted R^2 than CIELab and CIELhC ones.

The *species* parameter can be omitted only in the models for chlorophyll content expressed as function of the mass created using the RGB or the CIELab colour spaces. In the models created using the CIELhC colour space the L* parameter doesn´t have any relevance in the function.

Figure 3.9 shows the Passing-Bablok regression diagrams obtained for the application of the join model (chlorophyll content in mass and RGB colour space) to the validation group of the samples from the four fruit species. It can be seen in the figure that the lineal adjust is very near the x=y line, and that all the samples with exception of three are included in the 95 % confidence interval of the samples, which confirm the suitability of the model.
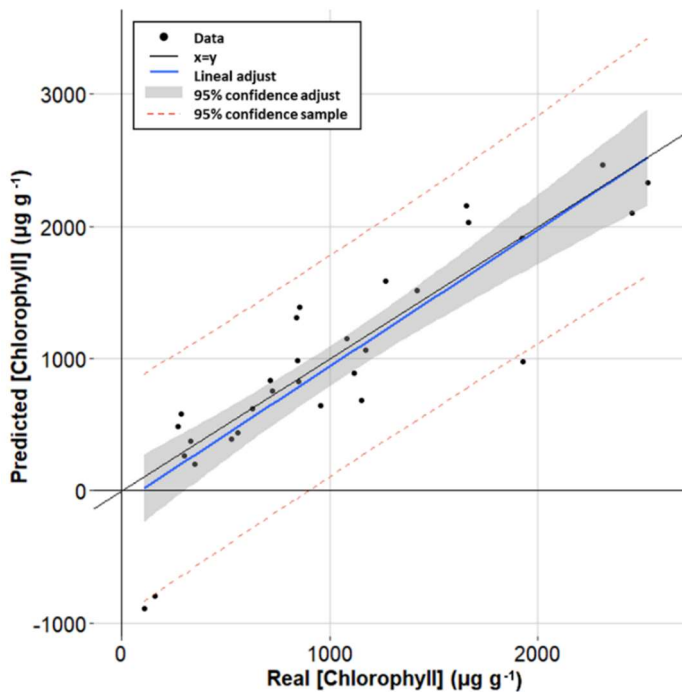
Figure 3.9: Passing-Bablok regression diagrams obtained for the application of the join model to the test group of the samples. The model is created for chlorophyll content expressed as function of mass using the RGB colour space.

4.   Conclusions

In this chapter different types of chlorophyll content in leaves prediction models have been developed, employing three different colour spaces (RGB, CIELab and CIELhC) and different chlorophyll content units ($\mu g\ g^{-1}$, $\mu g\ cm^{-2}$ and CCM units). The study was carried out for leaves of four different fruit species (peach, apricot, persimmon, and loquat). The development of prediction models for only one species (mono-species) require to study all the parameters of each colour space and select the different chlorophyll content units. In general, the best models are obtained employing the RGB colour space and chlorophyll content expressed as a function of the mass or area, being usually a little better in area because the presence of nerves could modify the mass but not the area. For each species the best prediction model is obtained using a different combination of colour parameters and chlorophyll content unit.

Joint models for the four species are created for each colour space and for each chlorophyll content unit. In this case, the best result is obtained using the chlorophyll content as a function of mass and the RGB colour space. This could be explained due the different characteristics of the leaves, as tissue thickness, because a function of the mass could reduce this effect.

5.   References

Azcon-Bieto, J., & Talón, M. (2000). Fundamentos de fisiología vegetal. Segunda edición. McGraw-Hill. Madrid.

Baresel, J. P., Rischbeck, P., Hu, Y., Kipp, S., Barmeier, G., Mistele, B., & Schmidhalter, U. (2017). Use of a digital camera as alternative method for non-destructive detection of the leaf chlorophyll content and the nitrogen nutrition status in wheat. *Computers and Electronics in Agriculture*, 140, 25-33. DOI: 10.1016/j.compag.2017.05.032.

Barman, U., & Choudhury, R. D. (2022). Smartphone image based digital chlorophyll meter to estimate the value of citrus leaves chlorophyll using Linear Regression, LMBP-ANN and SCGBP-ANN. *Journal of King Saud University-Computer and Information Sciences*, *34*(6), 2938-2950. DOI:10.1016/j.jksuci.2020.01.005

Capitán-Vallvey, L. F., Lopez-Ruiz, N., Martinez-Olmos, A., Erenas, M. M., & Palma, A. J. (2015). Recent developments in computer vision-based analytical chemistry: A tutorial review. *Analytica Chimica Acta*, 899, 23-56. DOI: 10.1016/j.aca.2015.10.009.

Chung, S., Breshears, L. E., & Yoon, J. Y. (2018). Smartphone near infrared monitoring of plant stress. *Computers and Electronics in Agriculture*, 154, 93-98. DOI: 10.1016/j.compag.2018.08.046.

Cortazar, B., Koydemir, H. C., Tseng, D., Feng, S., & Ozcan, A. (2015). Quantification of plant chlorophyll content using Google Glass. *Lab on a Chip*, 15(7), 1708-1716. DOI: 10.1039/C4LC01279H.

Dey, A. K., Sharma, M., & Meshram, M. R. (2016). An analysis of leaf chlorophyll measurement method using chlorophyll meter and image processing technique. *Procedia Computer Science*, 85, 286-292. DOI: 10.1016/j.procs.2016.05.235.

Friedrichs, A., Busch, J. A., Van der Woerd, H. J., & Zielinski, O. (2017). SmartFluo: A method and affordable adapter to measure *chlorophyll a* fluorescence with smartphones. *Sensors*, 17(4), 678. DOI: 10.3390/s17040678.

Gaviria-Palacio, D., Guáqueta-Restrepo, J. J., Pineda-Tobón, D. M., & Pérez, J. C. (2017). Fast estimation of chlorophyll content on plant leaves using the light sensor of a smartphone. *Dyna*, 84(203), 234-239. DOI: 10.15446/dyna.v84n203.64316.

Gong, L., Zhu, C., Luo, Y., & Fu, X. (2023). Spectral Reflectance Reconstruction from Red-Green-Blue (RGB) Images for Chlorophyll Content Detection. *Applied Spectroscopy*, *77*(2), 200-209. DOI: 10.1177/00037028221139871

Hassanijalilian, O., Igathinathane, C., Doetkott, C., Bajwa, S., Nowatzki, J., & Esmaeili, S. A. H. (2020). Chlorophyll estimation in soybean leaves infield with smartphone digital imaging and machine learning. *Computers and Electronics in Agriculture*, *174*, 105433. DOI: 10.1016/j.compag.2020.105433

Hong, G., Luo, M. R., & Rhodes, P. A. (2000). A study of digital camera colorimetric characterization based on polynomial modelling. *Color Research & Application*, 26, 76-84. DOI: 10.1002/1520-6378(200102)26:1<76::AID-COL8>3.0.CO;2-3.

Lichtenthaler, H.K. (1987). Chlorophylls and carotenoids: Pigments of photosynthetic biomembranes. *Methods in Enzymology*, 148, 350-382. DOI:10.1016/0076-6879(87)48036-1

López, J. M., Lucena, R. E., Mogollón, N., Rivas, R., & Anzalone, A. (2004). Design of a flow injection method for chlorophyll determination in in vitro plants. *Talanta*, 64(5), 1304-1308. DOI: 10.1016/j.talanta.2004.06.002.

Minolta, K. (2014). Entendiendo el espacio de colour CIE L* A* B*. http://sensing. konicaminolta. com. mx/2014/09/entendiendo-el-espacio-de-colour-cie-lab/.

Mohan, P. J., & Gupta, S. D. (2019). Intelligent image analysis for retrieval of leaf chlorophyll content of rice from digital images of smartphone under natural light. *Photosynthetica*, *57*(2), 388-398. DOI: 10.32615/ps.2019.046

Muñoz-Ortuño, M., Serra-Mora, P., Herráez-Hernández, R., Verdú-Andrés, J., & Campíns-Falcó, P. (2017). A new tool for direct non-invasive evaluation of *chlorophyll a* content from diffuse reflectance measurements. *Science of The Total Environment*, 609, 370-376. DOI: 10.1016/j.scitotenv.2017.07.140.

Rigon, J. P. G., Capuani, S., Fernandes, D. M., & Guimarães, T. M. (2016). A novel method for the estimation of soybean chlorophyll content using a smartphone and image analysis. *Photosynthetica*, 54(4), 559-566. DOI: 10.1007/s11099-016-0214-x.

Saputro, A. H., & Imawan, C. (2017). Chlorophylls content prediction of green amaranth (*Amaranthus tricolour* L.) leaves based on Vis-NIR image. In International Conference on Electrical Engineering and Informatics (ICELTICs). IEEE.

Sookchalearn, T., & Abdullakasim, W. (2017). A low-cost sensor for measuring and mapping chlorophyll content in cassava leaves. *Chiang Mai University Journal of Natural Sciences*, 16(3), 183-190. DOI: 10.12982/CMUJNS.2017.0015.

Tang, D. Y. Y., Chew, K. W., Ting, H. Y., Sia, Y. H., Gentili, F. G., Park, Y. K., Banat, F., Culaba, A.B., Ma, Z., & Show, P. L. (2023). Application of regression and artificial neural network analysis of Red-Green-Blue image components in prediction of chlorophyll content in microalgae. *Bioresource Technology*, *370*, 128503. DOI: 10.1016/j.biortech.2022.128503

Treder, W., Klamkowski, K., Kowalczyk, W., Sas, D., & Wójcik, K. (2016). Possibilities of using image analysis to estimate the nitrogen nutrition status of apple trees. *Zemdirbyste-Agriculture*, 103(3), 319-326. DOI: DOI:10.13080/z-a.2016.103.041.

Vesali, F., Omid, M., Kaleita, A., & Mobli, H. (2015). Development of an android app to estimate chlorophyll content of corn leaves based on contact imaging. *Computers and Electronics in Agriculture*, 116, 211-220. DOI: 10.1016/j.compag.2015.06.012.

Vesali, F., Omid, M., Mobli, H., & Kaleita, A. (2017). Feasibility of using smart phones to estimate chlorophyll content in corn plants. *Photosynthetica*, 55(4), 603-610. DOI: 10.1007/s11099-016-0677-9.

Annexes

Table 3.A.1. RMSE and coefficients of determination obtained for the different models calculated for the CIELab colour space in peach leaves.

Variables	[Chlorophyll] (µg g^{-1})		[Chlorophyll] (µg cm^{-2})		CCM (a.u.)	
	RMSE	r^2	RMSE	r^2	RMSE	r^2
L*a*b*	540.75	0.52	**7.25**	**0.73**	5.92	0.70
L*a*	621.34	0.36	7.72	0.71	**5.12**	**0.72**
L*b*	510.05	0.57	7.30	0.73	6.79	0.61
a*b*	483.04	0.61	7.59	0.72	6.43	0.65
L*	724.51	0.13	11.89	0.32	8.63	0.31
a*	669.43	0.26	11.67	0.35	8.66	0.37
b*	**464.82**	**0.67**	7.26	0.73	7.60	0.51

Table 3.A.2. RMSE and coefficients of determination obtained for the different models calculated for the CIELhC colour space in peach leaves.

Variables	[Chlorophyll] (µg g^{-1})		[Chlorophyll] (µg cm^{-2})		CCM (a.u.)	
	RMSE	r^2	RMSE	r^2	RMSE	r^2
L*h*C*	479.26	0.63	7.48	0.72	6.74	0.58
L*h*	495.71	0.61	8.03	0.68	6.72	0.58
L*C*	500.17	0.60	7.41	0.73	**5.58**	**0.67**
h*C*	469.65	0.65	**7.00**	**0.75**	6.70	0.58
L*	686.73	0.25	11.87	0.30	7.93	0.41
h*	**447.37**	**0.66**	8.10	0.68	7.25	0.51
C*	576.10	0.47	10.73	0.43	7.94	0.41

Table 3.A.3. RMSE and coefficients of determination obtained for the different models calculated for the RGB colour space in apricot leaves.

	[Chlorophyll] (μg g^{-1})		[Chlorophyll] (μg cm^{-2})		CCM (a.u.)	
Variables	RMSE	r^2	RMSE	r^2	RMSE	r^2
RGB	324.17	0.77	**4.97**	**0.88**	3.75	0.78
RG	433.76	0.60	5.32	0.88	3.35	0.79
GB	331.47	0.77	5.79	0.84	**3.29**	**0.83**
RB	**271.14**	**0.84**	6.48	0.80	4.01	0.75
R	400.96	0.66	7.27	0.78	4.13	0.73
G	436.04	0.60	7.25	0.78	4.26	0.72
B	446.72	0.58	10.76	0.51	5.52	0.43

Table 3.A.4. RMSE and coefficients of determination obtained for the different models calculated for the CIELab colour space in apricot leaves.

	[Chlorophyll] (μg g^{-1})		[Chlorophyll] (μg cm^{-2})		CCM (a.u.)	
Variables	RMSE	r^2	RMSE	r^2	RMSE	r^2
L*a*b*	**341.40**	**0.77**	7.95	0.73	3.84	0.77
L*a*	512.68	0.48	8.24	0.71	3.51	0.81
L*b*	359.83	0.70	7.68	0.74	4.30	0.71
a*b*	399.60	0.63	9.18	0.63	3.78	0.78
L*	501.10	0.50	**7.24**	**0.77**	**3.32**	**0.83**
a*	696.55	0.04	15.58	<0.005	7.50	0.05
b*	382.19	0.66	9.50	0.61	4.94	0.62

Table 3.A.5. RMSE and coefficients of determination obtained for the different models calculated for the CIELhC colour space in apricot leaves.

Variables	[Chlorophyll] (µg g⁻¹)		[Chlorophyll] (µg cm⁻²)		CCM (a.u.)	
	RMSE	r^2	RMSE	r^2	RMSE	r^2
L*h*C*	365.03	0.70	7.50	0.74	3.70	0.80
L*h*	363.02	0.68	8.10	0.69	3.84	0.78
L*C*	414.96	0.61	**6.06**	**0.83**	3.86	0.78
h*C*	364.04	0.68	7.85	0.71	3.58	0.81
L*	**344.95**	**0.71**	7.62	0.73	**3.51**	**0.82**
h*	404.42	0.60	9.55	0.57	4.85	0.66
C*	438.42	0.52	11.05	0.50	5.90	0.36

Table 3.A.6. RMSE and coefficients of determination obtained for the different models calculated for the RGB colour space in persimmon leaves.

Variables	[Chlorophyll] (µg g⁻¹)		[Chlorophyll] (µg cm⁻²)		CCM (a.u.)	
	RMSE	r^2	RMSE	r^2	RMSE	r^2
RGB	168.05	0.96	3.28	0.99	3.49	0.96
RG	235.52	0.92	5.57	0.96	7.86	0.81
GB	191.45	0.95	**2.89**	**0.99**	**2.75**	**0.98**
RB	**149.37**	**0.97**	3.34	0.98	2.95	0.97
R	221.99	0.93	5.57	0.96	7.65	0.82
G	253.76	0.91	5.57	0.96	7.74	0.82
B	408.11	0.77	13.59	0.74	6.43	0.88

Table 3.A.7. RMSE and coefficients of determination obtained for the different models calculated for the CIELab colour space in persimmon leaves.

Variables	[Chlorophyll] (µg g⁻¹)		[Chlorophyll] (µg cm⁻²)		CCM (a.u.)	
	RMSE	r^2	RMSE	r^2	RMSE	r^2
L*a*b*	199.07	0.93	5.17	0.97	3.76	0.95
L*a*	301.18	0.85	9.30	0.89	5.39	0.90
L*b*	**145.95**	**0.96**	**4.92**	**0.97**	**3.62**	**0.96**
a*b*	196.47	0.94	7.34	0.93	6.22	0.87
L*	319.82	0.83	9.84	0.88	4.95	0.92
a*	526.75	0.54	17.51	0.61	13.48	0.40
b*	195.69	0.94	5.97	0.95	4.19	0.94

Table 3.A.8. RMSE and coefficients of determination obtained for the different models calculated for the CIELhC colour space in persimmon leaves.

Variables	[Chlorophyll] (µg g⁻¹)		[Chlorophyll] (µg cm⁻²)		CCM (a.u.)	
	RMSE	r^2	RMSE	r^2	RMSE	r^2
L*h*C*	150.70	0.96	4.57	0.97	**2.83**	**0.97**
L*h*	**136.98**	**0.97**	4.13	0.98	2.83	0.97
L*C*	219.19	0.92	10.78	0.86	7.40	0.83
h*C*	170.38	0.95	4.34	0.98	3.77	0.95
L*	298.44	0.85	8.89	0.9	6.46	0.87
h*	144.23	0.96	**3.59**	**0.98**	5.32	0.91
C*	403.35	0.72	15.07	0.72	11.71	0.56

Table 3.A.9. RMSE and coefficients of determination obtained for the different models calculated for the RGB colour space in loquat leaves.

Variables	[Chlorophyll] (µg g^{-1})		[Chlorophyll] (µg cm^{-2})		CCM (a.u.)	
	RMSE	r^2	RMSE	r^2	RMSE	r^2
RGB	122.19	0.99	**2.28**	**>0.99**	**5.34**	**0.92**
RG	154.08	0.98	5.44	0.98	5.54	0.92
GB	195.69	0.97	6.91	0.96	5.65	0.91
RB	**114.89**	**>0.99**	4.38	0.99	5.45	0.92
R	120.28	0.99	5.82	0.97	5.47	0.91
G	293.24	0.94	13.04	0.87	7.91	0.82
B	249.34	0.96	9.62	0.93	7.38	0.84

Table 3.A.10. RMSE and coefficients of determination obtained for the different models calculated for the CIELab colour space in loquat leaves.

Variables	[Chlorophyll] (µg g^{-1})		[Chlorophyll] (µg cm^{-2})		CCM (a.u.)	
	RMSE	r^2	RMSE	r^2	RMSE	r^2
L*a*b*	330.74	0.93	**7.85**	**0.95**	7.41	0.86
L*a*	808.59	0.56	20.99	0.63	11.88	0.64
L*b*	359.95	0.91	8.92	0.93	7.37	0.86
a*b*	330.46	0.93	7.85	0.95	**6.96**	**0.87**
L*	1187.60	<0.005	34.36	<0.005	19.79	<0.005
a*	676.76	0.69	20.99	0.63	11.33	0.67
b*	**242.68**	**0.96**	8.56	0.94	7.37	0.86

Table 3.A.11. RMSE and coefficients of determination obtained for the different models calculated for the CIELhC colour space in loquat leaves.

Variables	[Chlorophyll] (µg g⁻¹)		[Chlorophyll] (µg cm⁻²)		CCM (a.u.)	
	RMSE	r^2	RMSE	r^2	RMSE	r^2
Lhc	202.61	0.97	8.26	0.95	5.93	0.90
Lh	344.94	0.92	12.76	0.87	8.54	0.79
Lc	208.80	0.97	8.17	0.95	5.78	0.90
hc	**184.35**	**0.98**	8.27	0.94	5.93	0.90
L	1190.90	<0.005	35.55	<0.005	18.63	<0.005
h	528.44	0.80	17.86	0.75	8.27	0.80
c	185.32	0.98	**6.93**	**0.96**	**5.77**	**0.91**

Table 3.A.12. Parameters of the joint model of the four species for µg cm⁻² in the RGB colour space.

RGB colour space - chlorophyll (µg cm⁻²)

Inter-individuals effects tests			Parameter estimates			
Origin	Type III of square sum	Observed power[b]	Parameter	B	Desv. Error	Sig
Corrected model	45299[a]	1.00	**Intersection**	56.40	6.55	0.00
Intersection	7440	1.00	**[species=1]**	3.13	3.86	0.42
species	3755	1.00	**[species=2]**	-9.88	3.62	0.01
R	1440	0.95	**[species=3]**	12.95	3.43	0.00
G	499	0.57	**[species=4]**	0[c]	-	-
B	7614	1.00	**R**	-0.24	0.07	0.00
a. R² = 0.820(Adjusted R² = 0.808)			**G**	-0.18	0.08	0.03
			B	1.03	0.12	0.00
b. α= 0.05			c. reference species			

Table 3.A.13. Parameters of the joint model of the four species for CCM values in the RGB colour space.

RGB colour space – CCM values

Inter-individuals effects tests			Parameter estimates			
Origin	**Type III of square sum**	**Observed power[b]**	**Parameter**	**B**	**Desv. Error**	**Sig**
Corrected model	16455[a]	1.00	**Intersection**	32.27	4.02	0.00
Intersection	2237	1.00	**[species=1]**	0.28	2.37	0.91
species	1441	1.00	**[species=2]**	-9.20	2.22	0.00
R	184	0.56	**[species=3]**	-7.24	2.11	0.00
G	372	0.85	**[species=4]**	0[c]	-	-
B	3139	1.00	**R**	-0.09	0.04	0.04
a. R^2 = 0.814 (Adjusted R^2 = 0.802)			**G**	-0.15	0.05	0.00
			B	0.66	0.08	0.00
b. α= 0.05			c. reference species			

Table 3.A.14. Parameters of the joint model of the four species for µg g^{-1} in the CIELab colour space.

CIELab colour space - chlorophyll (µg g^{-1})

Inter-individuals effects tests			Parameter estimates			
Origin	**Type III of square sum**	**Observed power[b]**	**Parameter**	**B**	**Desv. Error**	**Sig**
Corrected model	41344497[a]	1.00	**Intersection**	1821	409	0.00
Intersection	5031777	0.95	**[species=1]**	-323	271	0.23
species	1084572	0.25	**[species=2]**	-415	242	0.09
*L**	97163	0.08	**[species=3]**	-250	232	0.28
*a**	2842655	0.77	**[species=4]**	0[c]	-	-
*b**	14013997	1.00	**L**	-4.26	8.17	0.60
a. R^2 = 0.536(Adjusted R^2 = 0.506)			**a**	-37.54	13.32	0.01
			b	-28.66	4.58	0.00
b. α= 0.05			c. reference species			

Table 3.A.15. Parameters of the joint model of the four species for µg g⁻¹ in the CIELab colour space.

CIELab colour space - chlorophyll (µg g⁻¹)

Inter-individuals effects tests			Parameters estimates			
Origin	**Type III square sum**	**Observed power[b]**	**Parameter**	**B**	**Desv. Error**	**Sig**
Corrected model	40037665 [a]	1.00	**Intersection**	1487	98.66	0.00
Intersection	84255839	1.00	**a***	-22.69	8.35	0.01
a*	2740227	0.76	**b***	-31.27	3.31	0.00
b*	33163216	1.00				

a. $R^2 = 0.519$ (Adjusted $R^2 = 0.509$)
b. $\alpha = 0.05$

Table 3.A.16. Parameters of the joint model of the four species for µg cm⁻² in the CIELab colour space.

CIELab colour space - chlorophyll (µg cm⁻²)

Inter-individuals effects tests			Parameter estimates			
Origin	**Type III of square sum**	**Observed power[b]**	**Parameter**	**B**	**Desv. Error**	**Sig**
Corrected model	27172[a]	1.00	**Intersection**	68.11	11.46	0.00
Intersection	6023	0.99	**[species=1]**	-10.40	7.59	0.17
species	5446	0.95	**[species=2]**	-20.13	6.77	0.00
L*	974	0.43	**[species=3]**	-24.01	6.50	0.00
a*	1514	0.60	**[species=4]**	0[c]	-	-
b*	6892	1.00	**L***	-0.43	0.23	0.06
a. $R^2 = 0.492$(Adjusted $R^2 = 0.459$)			**a***	-0.87	0.37	0.02
			b*	0.64	0.13	0.00
b. $\alpha = 0.05$			c. reference species			

Table 3.A.17. Parameters of the joint model of the four species for µg cm⁻² in the CIELab colour space.

CIELab colour space - chlorophyll (µg cm⁻²)

Inter-individuals effects tests			Parameter estimates			
Origin	Type III of square sum	Observed power[b]	Parameter	B	Desv. Error	Sig
Corrected model	26198[a]	1.00	Intersection	47.94	3.83	0.00
Intersection	24340	1.00	[species=1]	-9.69	7.71	0.21
species	7324	0.99	[species=2]	-21.93	6.82	0.00
a*	1504	0.59	[species=3]	-25.65	6.55	0.00
b*	18500	1.00	[species=4]	0[c]	-	-
			a*	-0.86	0.38	0.02
a. R² = 0.474(Adjusted R² = 0.446)			b*	-0.79	0.10	0.00
b. α= 0.05			c. reference species			

Table 3.A.18. Parameters of the joint model of the four species for CCM values in the CIELab colour space.

CIELab colour space - CCM values

Inter-individuals effects tests			Parameter estimates			
Origin	Type III of square sum	Observed power[b]	Parameter	B	Desv. Error	Sig
Corrected model	10180[a]	1.00	Intersection	45.69	6.85	0.00
Intersection	2694	1.00	[species=1]	-8.33	4.53	0.07
species	1921	0.95	[species=2]	-15.18	4.05	0.00
L*	657	0.69	[species=3]	-13.52	3.89	0.00
a*	335	0.42	[species=4]	0[c]	-	-
b*	1896	0.99	L*	-0.35	0.14	0.01
a. R² = 0.504(Adjusted R² = 0.472)			a*	-0.41	0.22	0.07
			b*	-0.33	0.08	0.00
b. α= 0.05			c. reference species			

Table 3.A.19. Parameters of the joint model of the four species for CCM values in the CIELab colour space.

CIELab colour space - CCM values

Inter-individuals effects tests			Parameter estimates			
Origin	Type III of square sum	Observed power[b]	Parameter	B	Desv. Error	Sig
Corrected model	9844[a]	1.00	**Intersection**	44.84	6.95	0.00
Intersection	3390	1.00	**[species=1]**	-2.01	2.99	0.50
species	1620	0.90	**[species=2]**	-10.18	3.03	0.00
L*	653	0.67	**[species=3]**	-8.73	2.91	0.00
b*	2272	0.99	**[species=4]**	0[c]	-	-
			L*	-0.35	0.14	0.01
a. R^2 = 0.487(Adjusted R^2 = 0.460)			**b***	-0.36	0.08	0.00
b. α= 0.05			c. reference species			

Table 3.A.20. Parameters of the joint model of the four species for µg g^{-1} in the CIELhC colour space.

CIELhC colour space - chlorophyll (µg g^{-1})

Inter-individuals effects tests			Parameter estimates			
Origin	Type III of square sum	Observed power[b]	Parameter	B	Desv. Error	Sig
Corrected model	53342901[a]	1.00	**Intersection**	-355	530	0.50
Intersection	322252	0.20	**[species=1]**	-419	192	0.03
species	2392517	0.71	**[species=2]**	-593	189	0.00
L*	571322	0.32	**[species=3]**	-425	209	0.04
h*	13755660	1.00	**[species=4]**	0[c]	-	-
C*	5499014	1.00	**L***	10.92	7.04	0.12
a. R^2 = 0.692(Adjusted R^2 = 0.672)			**h***	826	109	0.00
			C*	-25.43	5.29	0.00
b. α= 0.05			c. reference species			

Table 3.A.21. Parameters of the joint model of the four species for µg g⁻¹ in the CIELhC colour space.

CIELhC colour space - chlorophyll (µg g^{-1})

Inter-individuals effects tests			Parameter estimates			
Origin	**Type III of square sum**	**Observed power[b]**	**Parameter**	**B**	**Desv. Error**	**Sig**
Corrected model	52771580[a]	1.00	**Intersection**	389	227	0.09
Intersection	45509	0.07	**[species=1]**	-319	183	0.08
species	1828385	0.57	**[species=2]**	-454	169	0.01
h*	17602576	1.00	**[species=3]**	-282	189	0.14
C*	5484003	1.00	**[species=4]**	0[c]	-	-
			h*	717.99	84.42	0.00
a. R² = 0.684(Adjusted R² = 0.668)			**C***	-25.40	5.35	0.00
b. α= 0.05			c. reference species			

Table 3.A.22. Parameters of the joint model of the four species for µg cm⁻² in the CIELhC colour space.

CIELhC colour space - chlorophyll (µg cm^{-2})

Inter-individuals effects tests			Parameter estimates			
Origin	**Type III of square sum**	**Observed power[b]**	**Parameter**	**B**	**Desv. Error**	**Sig**
Corrected model	35693[a]	1.00	**Intersection**	10.72	15.21	0.48
Intersection	29.20	0.07	**[species=1]**	-13.93	5.52	0.01
species	6711	1.00	**[species=2]**	-25.88	5.44	0.00
L*	2.09	0.05	**[species=3]**	-30.25	5.98	0.00
h*	8450	1.00	**[species=4]**	0[c]	-	-
C*	2831	0.95	**L***	0.02	0.20	0.92
a. R² = 0.646(Adjusted R² = 0.623)			**h***	20.46	3.11	0.00
			C*	-0.58	0.15	0.00
b. α= 0.05			c. reference species			

Table 3.A.23. Parameters of the joint model of the four species for µg cm^{-2} in the CIELhC colour space.

CIELhC colour space - chlorophyll (µg cm^{-2})

	Inter-individuals effects tests		Parameter estimates			
Origin	Type III of square sum	Observed power[b]	Parameter	B	Desv. Error	Sig
Corrected model	35691[a]	1.00	Intersection	12.14	6.45	0.06
Intersection	77.50	0.09	[species=1]	-13.74	5.20	0.01
species	8468	1.00	[species=2]	-25.61	4.79	0.00
h*	14010	1.00	[species=3]	-29.98	5.27	0.00
C*	2830	0.95	[species=4]	0[c]	-	-
			h*	20.26	2.39	0.00
a. R^2 = 0.646(Adjusted R^2 = 0.627)			C*	-0.58	0.15	0.00
b. α= 0.05			c. reference species			

Table 3.A.24. Parameters of the joint model of the four species for CCM values in the CIELhC colour space.

CIELhC colour space - CCM values

	Inter-individuals effects tests		Parameter estimates			
Origin	Type III of square sum	Observed power[b]	Parameter	B	Desv. Error	Sig
Corrected model	12847[a]	1.00	Intersection	14.94	9.33	0.11
Intersection	6.14	0.06	[species=1]	-10.92	3.39	0.00
species	2601	1.00	[species=2]	-18.88	3.34	0.00
L*	48.86	0.12	[species=3]	-17.49	3.67	0.00
h*	2382	1.00	[species=4]	0[c]	-	-
C*	836	0.90	L*	-0.10	0.12	0.42
a. R^2 = 0.636(Adjusted R^2 = 0.612)			h*	10.86	1.91	0.00
			C*	-0.31	0.09	0.00
b. α= 0.05			c. reference species			

Table 3.A.25. Parameters of the joint model of the four species for CCM values in the CIELhC colour space.

CIELhC colour space - CCM values

Inter-individuals effects tests			Parameter estimates			
Origin	**Type III of square sum**	**Observed power[b]**	**Parameter**	**B**	**Desv. Error**	**Sig**
Corrected model	12798[a]	1.00	**Intersection**	8.06	3.97	0.04
Intersection	62.17	0.14	**[species=1]**	-11.85	3.20	0.00
species	3883	1.00	**[species=2]**	-20.16	2.95	0.00
h*	4802	1.00	**[species=3]**	-18.81	3.30	0.00
C*	838	0.90	**[species=4]**	0[c]	-	-
			h*	11.86	1.47	0.00
			C*	-0.31	0.09	0.00
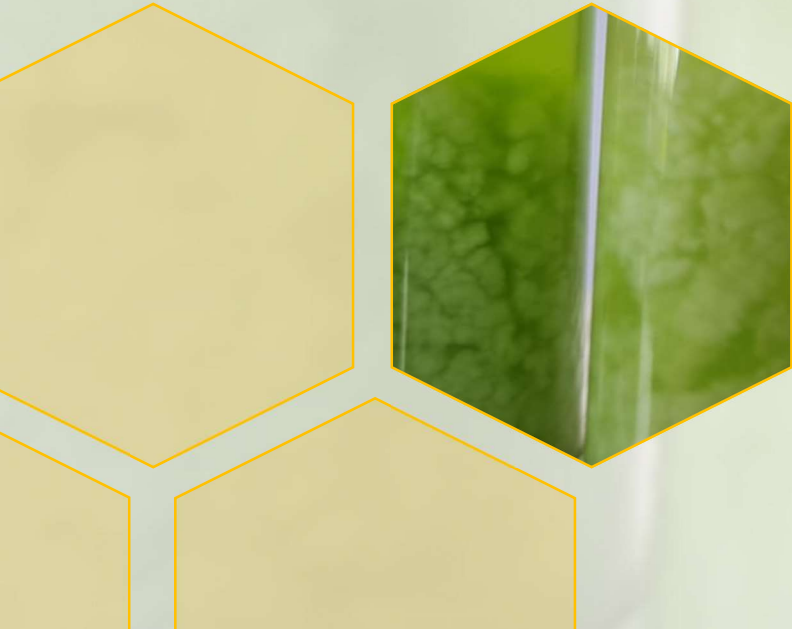
a. R^2 = 0.633(Adjusted R^2 = 0.614)

b. α= 0.05

c. reference species

CHAPTER 4: Chlorophyll determination in waters by using solid support and image processing
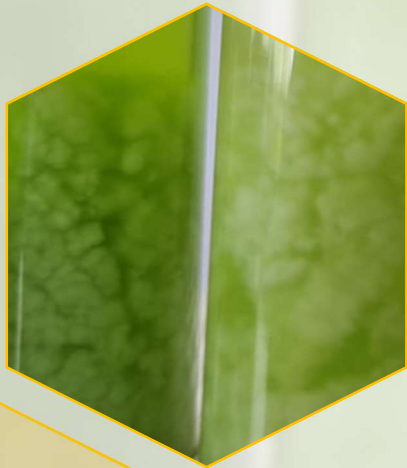
ABSTRACT

In order to quantify the degree of eutrophication of the water, one of the parameters used is the concentration of *chlorophyll a*, since it is proportional to the concentration of algae. In this study, different direct methods have been used to quantify the concentration of chlorophyll in the water from the algae retained in the filter. On the one hand, a CCM-200, that generates an arbitrary signal proportional to the concentration of chlorophyll, has been used. On the other hand, spectroscopic instruments (colourimeter and spectroradiometer) have been used to obtain colour parameters and correlate them with chlorophyll content. As a reference method for chlorophyll concentration it has been used official APHA protocol (This method is based on the measurement of chlorophyll by Spectrophotometry UV-vis after being extracted in acetone:water mixture).

In addition, image analysis has been employed to develop a model that could be able to correlate one of the colour parameters with the content of *chlorophyll a* in the water. This have been carried out by using an smartphone with subsequent image processing by using Matlab program. The waters are filtered on a filter paper so that the algae remain on it. Subsequently, the filters are photographed to try to correlate the green colour of the filter with the *chlorophyll a* concentration. The images have been obtained with a smartphone and treated with the use of the Matlab ColorLab library. The model obtained correlates the parameter L* from the CIEL*h*C* colour space with the mass of *chlorophyll a* in the filter. The model provides a correlation of 0.8123 between the colour and the amount of *chlorophyll a*.

1.   Introduction

Chlorophyll a is the most widely used parameter to control the state of aquatic ecosystems, due to its abundance in all phytoplankton species. This can be observed in the large number of articles that refer to water quality control through its determination (Aeriyanie et al., 2021; Aminot & Rey, 2014; Ayeni & Adeslau, 2018; Coria-Monter et al., 2019; Gallagher & Chuan, 2018; Gashaye et al., 2019; Gregor & Mar, 2004; Luomin et al., 2016; Ouma et al., 2018; Pápista et al., 2002; Qiu et al., 2018; Schagerl & Künzl, 2007; Trent et al., 2017). Since the concentration of *chlorophyll a* is proportional to the content of algae in the water, it is mainly used to quantify the degree of eutrophication in freshwater bodies (Peng et al., 2013).

The determination of chlorophyll is complex because it must be extracted from the cells. For this reason, it is necessary to filter the water samples and extract the chlorophyll from the filter with the appropriate solvent. This is time-consuming and involves significant sample handling, as well as the use of solvents (Aminot & Rey, 2014). On the other hand, chlorophyll degrades fast under light conditions, therefore chlorophyll extraction must be performed under dark conditions (Lee et al., 2014).

There are direct methods for the quantification of chlorophyll. The CCM-200 plus is an instrument used for the estimation of chlorophyll in leaves (Agarwal et al., 2021; Andrianto et al., 2018; Dong et al., 2019; Hutomo et al., 2016; Lazarević et al., 2016; Nikolaou et al., 2021; Sever et al., 2016), and it has also been used to quantify it in water (Trent et al., 2017). On the other hand, methods for determining chlorophyll in leaves have been developed using a smartphone (Hutomo et al., 2016). It is a direct method that requires less time and less investment than traditional methods. For the analysis of chlorophyll in water, applications such as Eye On Water and HydroColour have been created that calculate its concentration taking a photo of the body of water and some reference photographs (Gallagher & Chuan, 2018; Leeuw & Boss, 2018; Malthus et al., 2020; Ouma et al., 2018).

The objective of this work is to quantify the content of chlorophyll in water using a photograph obtained with a smartphone. For this purpose, the extraction method is optimized to obtain a known chlorophyll value and the different colours parameters obtained from the image are studied to find a correlation with the amount of *chlorophyll a*.

2.   Material and methods

2.1.   Instruments and reagents

For the measure of the content of Chlorophyll a by using the reference method, a Spectrophotometer UV-vis Hewlett Packard 8452A (Germany) was used. To take the data about the colour parameters of the filter a Spectroradiometer SpectraScan PR655 Photo Research (North Syracuse NY, EE.UU) and a colourimeter CM-26d Konica Minolta (Tokyo, Japan) were employed. A CCM-200, Opti-Sciences Inc. (Hudson, EE.UU) was used to take the direct measure of chlorophyll in the filter. To take the photo of the filters a smartphone Samsung Galaxy S7 Edge, Samsung (Seoul, South Korea) was employed.

To prepare the sample solution to make the UV-vis measure a crusher T18 Basic Ultra-Turrax IKA (Staufen, Germany), a vacuum pump KNF N86 KN 18 Biotech (Barcelona, Spain), a thermostatic ultrasound water bath IT-200 PRO Tierratech (Guarnizo, Spain), a vortex mixer VELP Scientifica (Usmate, Italy) and a centrifuge Heraeus American Scientific 1215 Medifuge (Hanau, Germany) were employed. To filter the sample, glass fibre filters Whatman GF/F 47 mm and syringe PTFE filter of 0.22 μm pore Scharlau (Barcelona, Spain) were used.

As reagents, acetone synthesis grade AnalaR Normapur VWR chemicals (Barcelona, Spain) and solid magnesium carbonate Probus (Barcelona, Spain) were used.

2.2.   Samples

Most of the assays were carried out using slightly eutrophic fresh water, from a pool, that was cultivated in the laboratory. The cultivation of the algae was performed adding fertilizer periodically and bubbling air in the water in order to dissolve oxygen and exposing it to sunlight. Samples from other origins were employed in this study: from Albufera Natural Parc, Valencia Botanical Garden and algae cultivated in the Microbiology and Ecology department of the University of Valencia.

2.3.   Chlorophyll extraction and UV-vis quantification

To avoid the chlorophyll degradation due to light exposition, all the process is performed under darkness conditions (0.15 lux). Firstly, a certain set volume of water is filtered using the system showed in the Figure 4.1. When all the volume is filtered, let it until dryness for 1 minute. Three replicates are filtered from each sample.

Figure 4.1: Set up to filter the water.

Each filter is chopped in small pieces and is put in a 13 mL centrifuge tube. 6 mL of a 90:10 (acetone:dechlorinated water) solution is added with a very little amount of magnesium carbonate, to avoid chlorophyll degradation. The chopped filter is ground with the Ultra-Turrax for 3 minutes at speed 4 (17500 rpm). This procedure is performed introducing the tube in an ice bath to avoid solvent evaporation. After that, the tube is incubated in the ultrasound bath for 30 minutes and left at least 2 hours at 4 °C in the dark, and finally the sample is mixed with the vortex mixer for 1 minute. To make the UV-vis measure the tube is centrifuged at 3500 rpm for 20 minutes. The supernatant is filtered by using a PTFE syringe filter of 0.22 µm pore and the solution is measured in a quartz cell. The three chlorophyll concentration are calculated using the equations 1, 2 and 3 reported in the APHA method (APHA, 2017).

$$C_{chl\ a} = 11.85 \cdot (A_{664} - A_{750}) - 1.54 \cdot (A_{647} - A_{750}) - 0.08 \cdot (A_{630} - A_{750}) \quad (1)$$

$$C_{chl\ b} = 21.03 \cdot (A_{647} - A_{750}) - 5.43 \cdot (A_{664} - A_{750}) - 2.66 \cdot (A_{630} - A_{750}) \quad (2)$$

$$C_{chl\ c} = 24.52 \cdot (A_{630} - A_{750}) - 7.60 \cdot (A_{647} - A_{750}) - 1.67 \cdot (A_{664} - A_{750}) \quad (3)$$

2.4. Colorimetric determination of chlorophyll in water samples

2.4.1. Smartphone measure

After filtration of samples, the photo of every filter is obtained employing the lighting box showed in Figure 4.2. A photo of a non-used filter is employed as a blank of the measure. The structure is made with methacrylate and the smartphone is placed at 15 cm over the filter, which is inside of a polystyrene hemisphere (14.5

cm inside and 20 cm outside diameter) externally black painted. As light source LED lights of 5600 K are used.
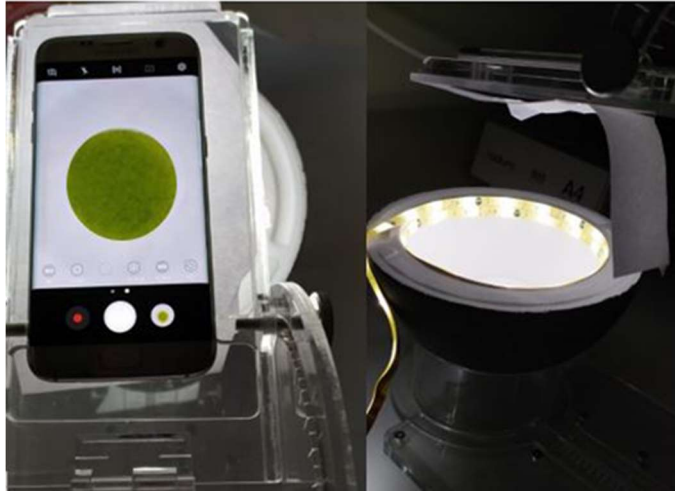
Figure 4.2: Set up to make the photo of the filters.

The photos are taken using the pro-mode of the smartphone with the parameters: ISO = 50; 1/f = 1/500; colour temperature of 5500 K and a zoom of x 2.0. The RGB parameters of the photos are obtained and processed using Matlab and the library ColorLab (Malo & Luque, 2002) for transforming the parameters in other colour spaces.

2.4.2. CCM-200 measure

To take the chlorophyll measure using the CCM-200 the filter is placed in the measurement chamber and the chlorophyll content index (CCI) value is obtained. As a blank a non-used filter is used. Previously, the instrument is adjusted "zero" closing the measurement chamber empty, without any material inside.

2.4.3. Colourimeter CM-26d measure

To take the colour measure with the colourimeter, the device is placed over the filter and the measure button is pressed. The colour parameters are obtained in the CIEL*a*b* colour space. A non-used filter is employed as reference white for image processing.

2.4.4. Spectroradiometer SpectraScan PR655 measure

The filters are placed inside of a polystyrene box (33 x 40 x 40 cm) that is used as photo booth (Figure 4.3). Over the box, a polystyrene layer is placed as diffusor of the light and over it a methacrylate plate with a grid of LED lights. Both have a

circular hole that is used to obtain the colour measure. The spectroradiometer is placed over the filter sample at 103 cm and the colour data is obtained in the XYZ colour space. Using Matlab and the ColorLab library the colour parameters in other colour spaces can be obtained.

Figure 4.3: Set up for take the colour parameters of the filter by the spectroradiometer.

3.   Results and discussion

3.1.   Optimization of the chlorophyll extraction

Following the APHA method, to completely extract the chlorophyll disrupt the cells mechanically is needed. For that different parameters are studies, as the size of the pieces in which filters are cut, ULTRA-TURRAX speed and time of crushing. Using the UV-vis spectrum and the equations of the APHA method the concentration of each type of chlorophyll is calculated. Table 4.1 shows the parameters of each extraction procedure and the chlorophyll content found. In this type of water only *chlorophyll a* and *b* are found, being similar for all the procedures, for that the procedure 7 is selected because it requires less extraction time.

For the extraction of chlorophyll from cells solution of acetone (aq) 90 % (Aeriyanie et al., 2021; Almomani & Örmcei, 2018; Ayeni & Adesalu, 2018; Gashaye et al., 2019; Luomin et al., 2016; Moberg et al., 2001), and acetone 100 % (Chung et al., 2018; Hu et al., 2013; López et al., 2004) have been employed. APHA method recommended incubate at least of 2 h at 4°C. Table 4.1 also shows the type of solvent and incubation time studied. As it can be seen for the 100 % acetone the chlorophyll extraction decreases when the incubation time increases, whereas the concentrations do not change for acetone (aq) 90 %, choosing this solvent and 2 hours as time.

Table 4.1: Parameters for each procedure of crushing of filter and for the incubation assays.

Procedure for wet crushing of filter

Procedure	Size	speed	Time (min)	[chl a]	[chl b]	[chl total]
1	Big	2 (8750 rpm)	15	0.89	1.31	2.20
2	Big	3 (13125 rpm)	12	0.78	0.77	1.55
3	Small	5.5 (24000 rpm)	5	0.70	0.89	1.59
4	Small	5 (22000 rpm)	3	0.62	0.63	1.25
5	Small	4.5 (20000 rpm)	4	0.63	0.63	1.26
6	Small	3 (13000 rpm)	4	0.89	0.97	1.86
7	Small	4 (17500 rpm)	3	0.90	0.96	1.86

Chlorophyll incubation solvent and time

Procedure	Time (hours)	solvent	[chl a]	[chl b]	[chl total]
1	2	Acetone 100 %	0.67 ± 0.01	0.37 ± 0.03	1.04 ± 0.04
2	2	Acetone 90 %	0.75 ± 0.05	0.53 ± 0.01	1.28 ± 0.05
3	4	Acetone 100 %	0.46 ± 0.01	0.36± 0.05	0.81 ± 0.17
4	4	Acetone 90 %	0.74 ± 0.02	0.44 ± 0.03	1.20 ± 0.40
5	6	Acetone 100 %	0.42 ± 0.03	0.30 ± 0.03	0.72 ± 0.06
6	6	Acetone 90 %	0.73 ± 0.01	0.44 ± 0.04	1.16 ± 0.04
7	15	Acetone 100 %	0.25 ± 0.01	0.13 ± 0.06	0.37 ± 0.05
8	15	Acetone 90 %	0.72 ± 0.01	0.50 ± 0.01	1.22 ± 0.02

It is recommended the addition of saturated $MgCO_3$ solution, $MgCO_3$ acts as pH buffer avoiding chlorophyll degradation. Three filters of the same water are crushed containing a little amount of solid $MgCO_3$ and other three without it, the results are showed in the Table 4.2. It can be observed that the addition of solid $MgCO_3$ reduces the variation in the measure. It is not possible adding the magnesium carbonate before filtration because is retained in the filter modifying the colour of that.

Table 4.2: Results obtained for the content of the different types of chlorophyll for each experiment.

Effect of the MgCO₃			
MgCO₃ (s)	[chl a]	[chl b]	[chl total]
yes	0.83 ± 0.03	0.40 ± 0.05	1.25 ± 0.02
No	1.00 ± 0.15	0.50 ± 0.10	1.50 ± 0.30
Sonication effect in the extraction			
Extraction procedure	[chl a]	[chl b]	[chl total]
ULTRA-TURRAX	0.55 ± 0.11	0.22 ± 0.05	0.785 ± 0.005
Sonication	0.07 ± 0.01	0.040 ± 0.001	0.118 ± 0.004
ULTRA-TURRAX + Sonication	0.83 ± 0.03	0.39 ± 0.02	1.247 ± 0.002
Effect of the light			
Light conditions	[chl a]	[chl b]	[chl total]
Dark	1.13 ± 0.02	0.32 ± 0.01	1.50 ± 0.03
Normal	1.03 ± 0.20	0.28 ± 0.01	1.31 ± 0.04

Other reported procedures use and ultrasonic bath to replace the use of ULTRA-TURRAX (Schagerl & Künzl, 2007, Aeriyanie et al., 2021). To check if there was an improvement in the extraction of chlorophyll, a study in which the same sample of water is extracted only employing ULTRA-TURRAX, sonification or both was performed. Each extraction was carried out three times. The sonication was performed by 30 minutes. The results of this study are showed in the Table 4.2. This study provides that the use of sonification and ULTRA-TURRAX increase the amount of chlorophyll extracted. For this reason, both extraction procedures were employed sequentially.

The light is a factor that contribute to the chlorophyll degradation. To verify how this parameter affects the extraction of chlorophyll, a study was carried out in which the extraction of chlorophyll from the same water in dark conditions was compared with the extraction carried out in normal lighting conditions. The concentration obtained for each procedure using the UV-vis spectrum and the equations of the APHA method are also shown in the Table 4.2. The concentration

obtained is very similar for both extractions, but under dark conditions there is a lower variability. Therefore, the extraction procedure finally used is carried out in the dark.

3.2.   Comparison between colour parameters obtained with the devices and the chlorophyll concentration

Once the best chlorophyll extraction conditions from the filters were known, the correlation between the colour of the filters and the chlorophyll content extracted with the solvent was studied. To obtain the colour parameters of the filters a spectroradiometer, a colourimeter, a CCM-200 and a Smartphone were employed. To carry out this study 32 different samples of water were used. Employing the extraction procedure proposed in the previous section the contents of chlorophyll obtained for each sample are shown in the Table 4.3.

The 32 water samples were filtered, and the respective photos of the filters were taken under the lighting conditions indicated previously. The colour parameters of each image were transformed, by using the Matlab program, to XYZ coordinates, from which it was possible to obtain the colour parameters expressed in the RGB, CIEL*a*b* and CIEL*h*C* colour spaces. A correlation between the data of the chlorophyll mass in each filter and the colour of each filter was tried to find.

The mass of chlorophyll per area of the processed image has been employed as the unit of measurement instead of the usual units of concentration, due to the green colour of the filter is caused by the total amount of *chlorophyll a* on it. We can find a greener filter when we filter a larger volume of water with little chlorophyll content, than when we filter a small volume of water that contains a high concentration of chlorophyll. Also, on some occasions the green colour of the filter is not homogeneous over the entire surface. This implies that a greater deposition of chlorophyll in the darker green areas does not provide the same increase in colour as in the lighter green areas. For this reason, it is not advisable to average the green colour of the entire filter, as an error would be obtained when processing the lighter colours. Since the outer edge of the filter had a very light green colour, its contribution was considered negligible for the correlation. Therefore, the mass of *chlorophyll a* on the filter was correlated with the colour per area by removing the contribution from the outer edge of the filter. The mass of *chlorophyll a* can be obtained from the concentration in the water sample and the volume filtered. When different colour parameters were studied, the best correlation was obtained with the luminance of the colour, the parameter L* from CIEL*a*b* colour space (Figure 4.4).

Table 4.3: Percentage of each type of chlorophyll obtained and total mass of chlorophyll.

Sample	% chl a	% chl b	% chl c	M chl total
M1	48.5	21.7	29.8	79.0
M2	48.1	21.9	30.0	27.7
M3	32.6	44.0	23.4	14.8
M4	51.9	21.5	26.5	79.5
M5	50.0	24.1	25.9	48.7
M6	46.1	29.8	24.1	19.0
M7	20.0	80.0	0.0	3.8
M8	11.3	88.7	0.0	4.3
M9	35.1	34.3	30.6	72.0
M10	35.1	34.3	30.6	44.9
M11	38.8	36.5	24.7	5.2
M12	37.3	35.6	27.1	14.8
M13	42.0	34.7	23.3	5.1
M14	39.5	33.8	26.7	5.7
M15	34.7	34.0	31.3	63.5
M16	35.6	34.8	29.7	59.6
M17	36.4	35.2	28.4	9.4
M18	34.9	34.6	30.5	47.6
M19	30.4	36.3	33.2	26.4
M20	37.5	32.7	29.7	8.9
M21	36.6	33.7	29.7	45.3
M22	35.5	33.8	30.7	27.0
M23	39.8	36.0	24.2	3.8
M24	34.6	33.9	31.5	59.5
M25	34.8	34.6	31.6	20.4
M26	34.4	34.0	31.6	21.3
M27	34.8	34.2	31.0	96.4
M28	34.9	34.3	30.8	48.7
M29	35.0	34.2	30.8	27.8
M30	35.3	34.2	30.5	168.1
M31	35.5	33.8	30.7	78.9
M32	36.7	33.3	30.0	31.1

$$y=-1.13 \cdot 10^{6}x + 92$$
$$R^2=0.8123$$
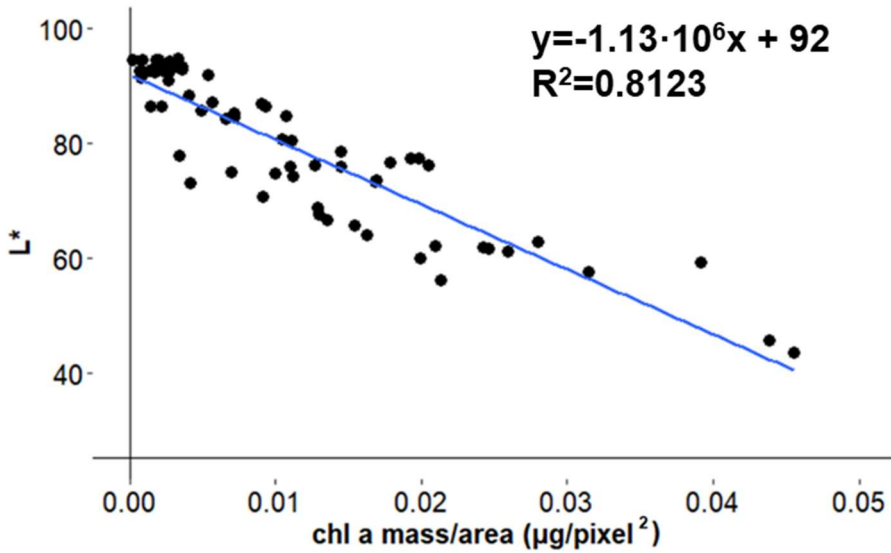
Figure 4.4: Correlation obtained between the L colour parameter from the CIEL*h*C* colour space and the amount of chlorophyll a expressed as µg/pixel². This area is obtained using the area of image that is processed in Matlab.*

The luminance of the colour obtained by the Smartphone was correlated with the L* parameter obtained using the reference devices. The Figures 4.5, 4.6 and 4.7 show that the measure of the colour by the Smartphone has a good correlation with the colour measure obtained by the direct methods.

$$y=1.181x-8.15$$
$$R^2=0.96$$
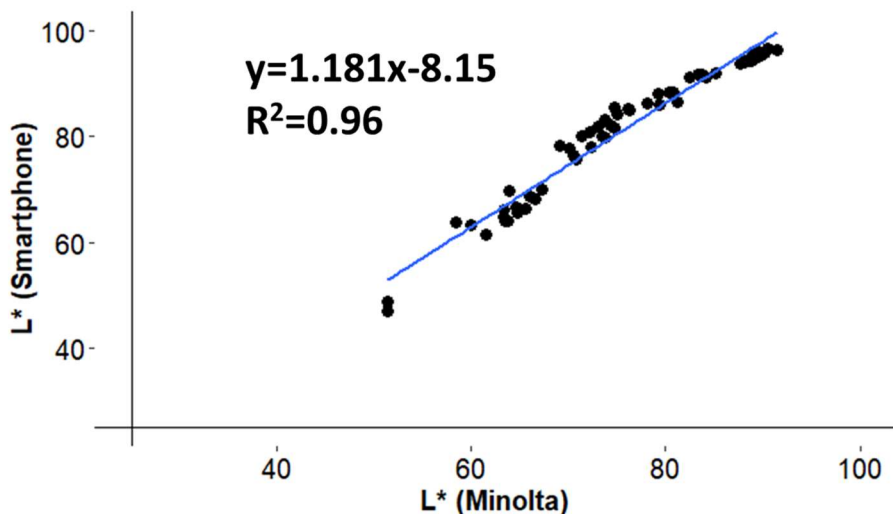
Figure 4.5: Correlation obtained between the L colour parameter from the L*h*C* colour space obtained by Smartphone and the L* parameter obtained by the colorimeter.*

153
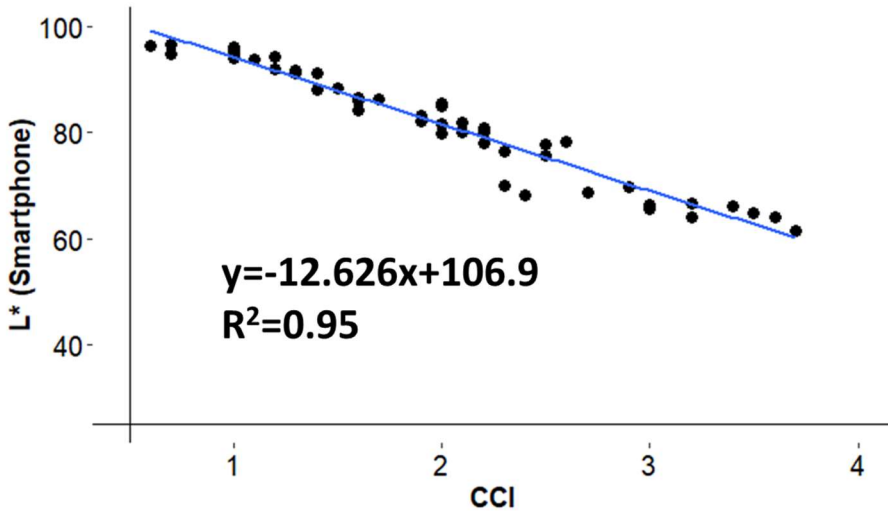
Figure 4.6: Correlation obtained between the L* colour parameter from the CIEL*h*C* colour space obtained by Smartphone and CCI obtained by the CCM-200.
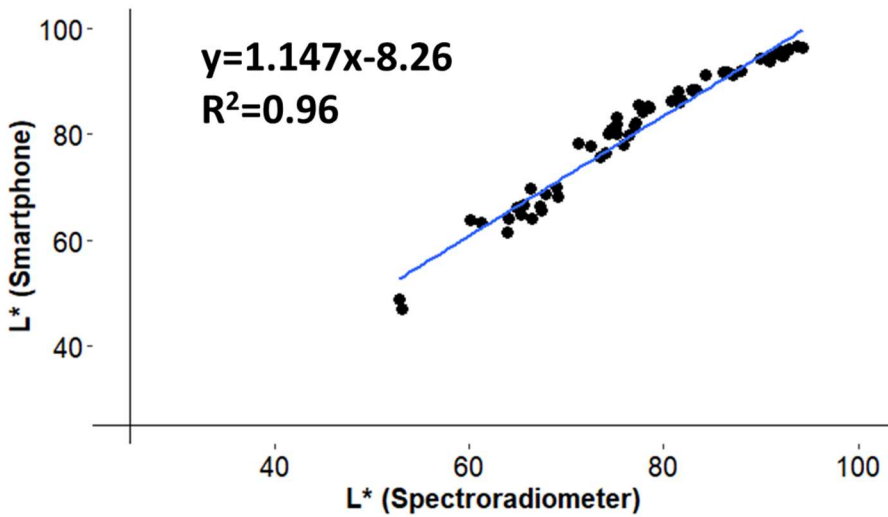
Figure 4.7: Correlation obtained between the L* colour parameter from the CIEL*h*C* colour space obtained by Smartphone and the L* parameter obtained by the Spectroradiometer.

By last, it's possible to find the correlation between the mass of *chlorophyll a* and the colour of the filter using the L* parameter and the CCI parameter (Figures 4.8, 4.9 and 4.10).
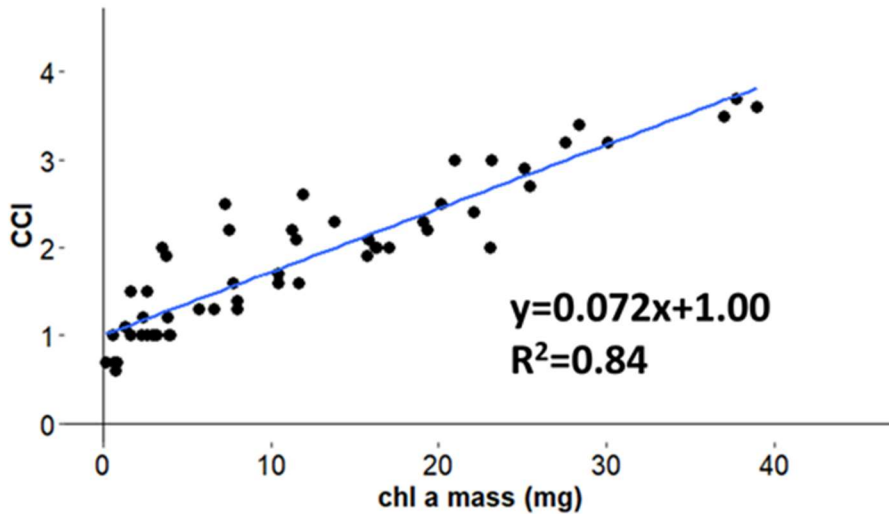
Figure 4.8: Correlation obtained between the CCI obtained by the CCM-200 and the amount of chlorophyll a in the filter (mg).
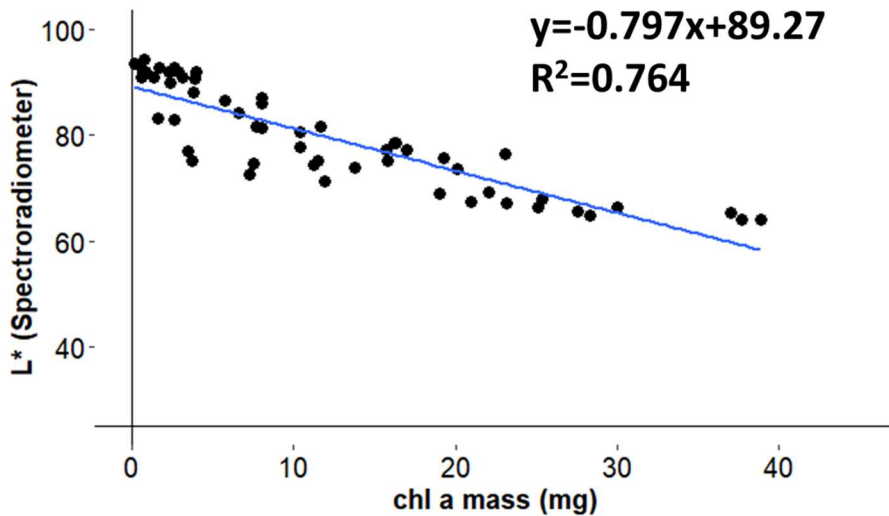
Figure 4.9: Correlation obtained between the L colour parameter from the CIEL*h*C* colour space obtained by the spectroradiometer and the amount of chlorophyll a in the filter (mg).*

$$y=-0.773x+86.57$$
$$R^2=0.76$$
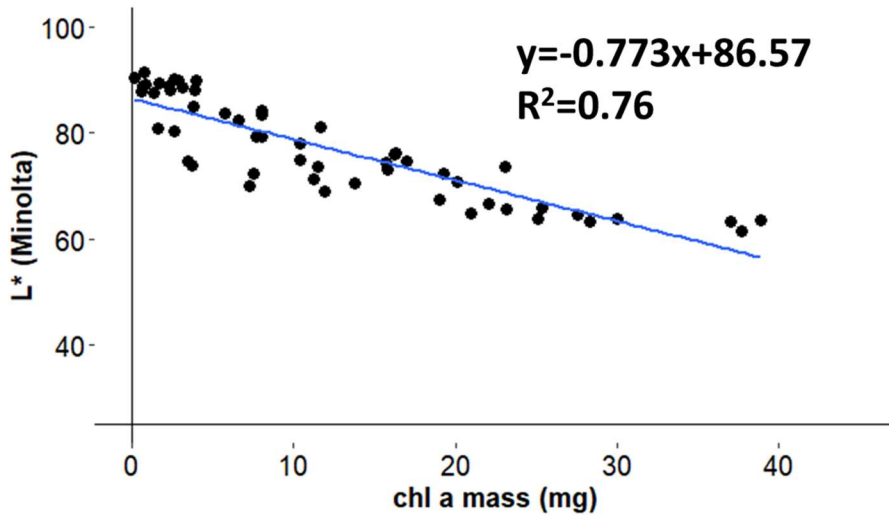
Figure 4.10: Correlation obtained between the L* colour parameter from the CIEL*h*C* colour space obtained by the colorimeter Minolta and the amount of chlorophyll a in the filter (mg).

4.   Conclusions

The best conditions to carry out the extraction of chlorophyll deposited on the filter paper were selected: darkness, 10 mL of acetone 90 % (aq) as extractant solvent, add a little amount of $MgCO_3$ (s), shredded for 3 minutes at 17500 rpm (velocity 4 of the instrument), sonicate for 30 minutes and, finally, an incubation process at 4 °C during 2 h.

A good correlation between the L* parameter of the colour of the filter obtained from the photo by the Smartphone and the amount of *chlorophyll a* (mg/pixel^2) has been found, with a $R^2=0.8123$. Moreover, the L* parameter obtained by the smartphone has a good correlation with this colour parameters provided by Minolta colourimeter and by SpectraScan PR655 spectroradiometer, and also with the CCI value obtained with the CCM-200 (R^2= 0.96, 0.96 and 0.95, respectively). It has been proved that the direct measurement of the green colour of filter by CCM-200, by the colourimeter and by the spectroradiometer also provides a good estimation of the mass of *chlorophyll a* (mg) retained on it, avoiding the extraction step.

5. References

APHA (2017). Standard Methods for the Examination of Water and Wastewater. 23rd edition. Washington DC: American Public Health Association.

Aeriyanie, A. R., Sinang, S. C., Nayan, N., & Song, H. (2021). Comparison of Water Level and Eutrophication Indicators during the Wet and Dry Period in a Eutrophic Urban Lake. *Acta Ecologica Sinica,* 41 (2), 73–78. DOI: 10.1016/J.CHNAES.2020.03.003.

Agarwal, A., Dongre, P. K., & Dutta Gupta, S. (2021). Smartphone-Assisted Real-Time Estimation of Chlorophyll and Carotenoid Concentrations and Ratio Using the Inverse of Red and Green Digital Colour Features. *Theoretical and Experimental Plant Physiology*, 33(3), 293-302. DOI: 10.1007/s40626-021-00210-4.

Almomani, F. A., & Örmeci, B. (2018). Monitoring and Measurement of Microalgae Using the First Derivative of Absorbance and Comparison with Chlorophyll Extraction Method. *Environmental Monitoring and Assessment,* 190, 1-19. DOI: 10.1007/s10661-018-6468-y.

Aminot, A., & Rey, F. (2000). Standard Procedure for the Determination of *Chlorophyll a* by Spectroscopic Methods. *ICES Techniques in Marine Environmental Sciences,* 112, 25.

Andrianto, H., & Faizal, A. (2018) Detection of Chlorophyll Content Based on Spectral Properties at Leaf Level: A Meta-Analysis. In International Conference on Information Technology Systems and Innovation (ICITSI). IEEE.

Ayeni, A. O., & Adesalu, T. A. (2018). Validating *Chlorophyll-a* Concentrations in the Lagos Lagoon Using Remote Sensing Extraction and Laboratory Fluorometric Methods*. MethodsX,* 5, 1204–1212. DOI: 10.1016/j.mex.2018.09.014.

Chung, S., Breshears, L. E., & Yoon, J. Y. (2018). Smartphone near Infrared Monitoring of Plant Stress. *Computers and Electronics in Agriculture*, 154, 93-98. DOI: 10.1016/j.compag.2018.08.046.

Coria-Monter, E., Monreal-Gómez, M. A., Salas de León, D. A., & Durán-Campos, E. (2019). Water Masses and Chlorophyll-a Distribution in a Semi-Enclosed Bay of the Southern Gulf of California, Mexico, after the "Godzilla El Niño." *Arabian Journal of Geosciences*, 12, 1-8*.* DOI: 10.1007/s12517-019-4636-1.

Dong, T., Shang, J., Chen, J. M., Liu, J., Quian, B., Ma, B., Morrison, M. J., Zhang, C., Liu, Y., Shi, Y., Pan, H., & Zhou, G. (2019). Measuring Crop Leaf Chlorophyll Concentration. *Remote Sensing*. 11, 2706.

Gallagher, J. B., & Chuan, C. H. (2018). *Chlorophyll a* and Turbidity Distributions: Applicability of Using a Smartphone "App" across Two Contrasting Bays. *Journal of Coastal Research,* 34 (5), 1236–1243. DOI: 10.2112/JCOASTRES-D-16-00221.1.

Gashaye, D., Goshu, G., & Abraha, B. (2019). Temporal and Spatial Phytoplankton Biomass Dynamics in Southern Gulf of Lake Tana, Northwestern Ethiopia. *International Journal of Aquatic Biology,* 7 (1), 1–8. DOI: 10.22034/ijab.v7i1.488.

Gregor, J., & Mar, B. (2004). Freshwater Phytoplankton Quantification by *Chlorophyll a*: A Comparative Study of in Vitro, *in Vivo* and *in Situ* Methods. *Water research*, 38, 517–522.

Hu, X., Tanaka, A., & Tanaka, R. (2013). Simple Extraction Methods That Prevent the Artifactual Conversion of Chlorophyll to Chlorophyllide during Pigment Isolation from Leaf Samples. *Plant Methods,* 9 (1), 1–13. DOI: 10.1186/1746-4811-9-19.

Hutomo E. P., E., Adibawa, M. A. S., Prilianti, K. R., Heriyanto, H., & Brotosudarmo, T. H. P. (2016). Low-Cost Chlorophyll Meter (LCCM): Portable Measuring Device for Leaf Chlorophyll. *In Second International Seminar on Photonics, Optics, and Its Applications (ISPhOA 2016). SPIE*. DOI: 10.1117/12.2243607.

Lazarević, B., Jurkić, V., Mušić, M., & Poljak, M. (2016). Effect of Aluminium Toxicity on Concentration of Photosynthetic Pigments in Two Potato Cultivars with Different Aluminium Sensitivity. In VI Balkan Symposium on Vegetables and Potatoes. DOI: 10.17660/ActaHortic.2016.1142.10.

Lee, E., Ahn, H., & Choe, E. (2014). Effects of Light and Lipids on Chlorophyll Degradation. *Food Science and Biotechnology*, 23, 1061-1065. DOI: 10.1007/s10068-014-0145-x.

Leeuw, T., & Boss, E. (2018). The HydroColour App: Above Water Measurements of Remote Sensing Reflectance and Turbidity Using a Smartphone Camera. *Sensors,* 18 (1), 256. DOI: 10.3390/s18010256.

López, J. M., Lucena, R. E., Marcó P., L. M., Mogollón, N., Rivas, R., & Anzalone G., A. (2004). Design of a Flow Injection Method for Chlorophyll Determination in in Vitro Plants. *Talanta,* 64(5), 1304–1308. DOI: 10.1016/j.talanta.2004.06.002.

Luomin, L., Quehui, T., Liang, P., Guifeng, W., Shuzhong, L., Xiangjiao, L., & Haowen, Y. (2016). Microwave-Assisted Method for Extracting *Chlorophyll-a* in Phytoplankton and Its Comparison with Freezing-Thawing Extraction Method. *Journal of Lake Sci*ences, 28 (5), 1148–1152. DOI: 10.18307/2016.0526.

Malo, J., & Luque, M. J. (2002). ColourLab: the Matlab toolbox for Colourimetry and Colour Vision. Univ. Valencia. http://isp.uv.es/code/visioncolour/colourlab.html.

Malthus, T. J., Ohmsen, R., & van der Woerd, H. J. (2020). An Evaluation of Citizen Science Smartphone Apps for Inland Water Quality Assessment. *Remote Sensing,* 12 (10), 1578. DOI: 10.3390/rs12101578.

Moberg, L., Robertsson, G., & Karlberg, B. (2001). Spectrofluorimetric Determination of Chlorophylls and Pheopigments Using Parallel Factor Analysis. *Talanta,* 54 (1), 161–170. DOI: 10.1016/S0039-9140(00)00650-0.

Nikolaou, K. E., Chatzistathis, T., Theocharis, S., Argiriou, A., Koundouras, S., & Zioziou, E. (2021). Effects of Salinity and Rootstock on Nutrient Element Concentrations and Physiology in Own-Rooted or Grafted to 1103 p and 101-14 Mgt Rootstocks of Merlot and Cabernet Franc Grapevine Cultivars under Climate Change. *Sustainability*. 13 (5), 2477. DOI: 10.3390/su13052477.

Ouma, Y. O., Waga, J., Okech, M., Lavisa, O., & Mbuthia, D. (2018). Estimation of Reservoir Bio-Optical Water Quality Parameters Using Smartphone Sensor Apps and Landsat ETM+: Review and Comparative Experimental Results. *Journal of Sensors*, 2018, 3490757. DOI: 10.1155/2018/3490757.

Pápista, É., Ács, É., & Böddi, B. (2002). *Chlorophyll-a* Determination with Ethanol - A Critical Test. *Hydrobiologia,* 485, 191–198. DOI: 10.1023/A:1021329602685.

Peng, F., Liu, S. B., Xu, H. Y. & Li, Z. Q. (2013). A Comparative Study on the Analysis Methods for Chlorophyll-a. *Advanced Materials Research,* 726-731, 1411-1415. DOI: 10.4028/www.scientific.net/AMR.726-731.1411.

Qiu, N., Wang, X., & Zhou, F. (2018). A New Method for Fast Extraction and Determination of Chlorophylls in Natural Water. *Zeitschrift fur Naturforschung C,* 73 (1–2), 77–86. DOI: 10.1515/znc-2017-0157.

Schagerl, M., & Künzl, G. (2007). *Chlorophyll a* extraction from freshwater algae - a reevaluation. *Biologia,* 62, 270–275. DOI: 10.2478/s11756-007-0048-x.

Sever, K., Bogdan, S., Škvorc, Ž., Sever, M. Z. O., & Franjić, J. (2016). Estimation of Leaf Nitrogen Concentrations in Quercus Robur L. Using the CCM-200 Portable

Chlorophyll Meter for Different Patterns of Vegetative Growth and Acorn Production. *New Forest,* 47, 513–527. DOI: 10.1007/s11056-016-9528-6.

Trent, T., Hendrickson, J., & Harwell, M. C. (2017). A Rapid, Cost-Effective Screening Tool for Measuring Chl-a in Water Samples. *Lake and Reservoir. Management,* 33 (3), 217–222. DOI: 10.1080/10402381.2017.1335360.

CHAPTER 5: Direct chlorophyll determination in waters by image processing
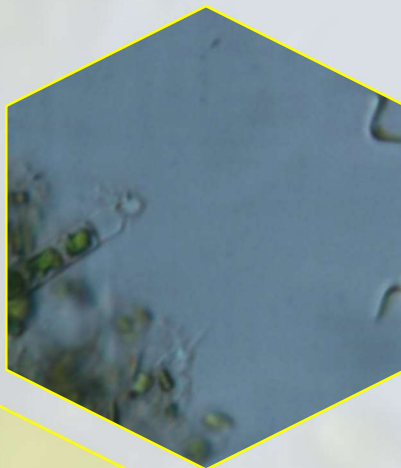
ABSTRACT

Water control is important to avoid its eutrophication. Therefore, more accessible, cheaper and direct methods requiring less time, to have a quicker procedure to analyse water for this purpose need to be developed. An example of this proposal would be the employment of Smartphones as sensors for direct analysis. Its usage is widely spreading because it is a technological daily-employed tool. This study has focused on creating direct methods to determine chlorophyll in water as an alternative to the reference method. A mathematic model has been developed for the colorimetric determination of chlorophyll by taking pictures with a Smartphone of a water column and its filter after filtration of the water column. Moreover, the colour information of the pictures has been correlated to other direct methods, like the AquaFluor handheld fluorometer AquaFluor and the colourCM-26d Konica Minolta colourimeter. The mathematical model is created using 2 equations that allows, only taking three photos of the same water at different water column height, know the content of *chlorophyll a* in the water. Furthermore, this model allows to correct the different colour of the water due the behaviour of the different algae. The correlation between the predicted content and the real content tested is $R^2= 0.964$.

Keywords: Analytical Chemistry, Chlorophyll, RGB, Smartphone.

1. Introduction

1.1. Eutrophication

Eutrophication is a natural process, which describes the biological effects of increasing the concentration of nutrients such as nitrogen or phosphorus in aquatic ecosystems (Harper, 1992). The biological changes that occur in lakes due to eutrophication can be divided into those that are a direct result of increased nutrients, such as excessive growth of phytoplankton, and those that are indirect effects, such as changes in the aquatic ecosystem as a result of reduced the concentration of dissolved oxygen in the waters (Harper, 1992).

The process of excessive accumulation of nutrients in aquatic ecosystems, the main reason for poor water quality, especially due to human activity that occurs around them (Veenashree et al., 2018), gives rise to an excessive growth of microalgae and phytoplankton. This growth produces a decrease in the transparency of the water, the sun's rays do not reach the bottom of the aquatic plants and they die due to the inability to carry out photosynthesis. At the bottom, bacteria break down dead plants along with phytoplankton that also settle to the bottom and deplete dissolved oxygen. At the top of the sheet of water, where sunlight can reach, phytoplankton generate a lot of oxygen. However, since there is no oxygen in the lower parts, it results in the disappearance of most of the living beings and the production of bad odours (Alvarez et al., 1991). As a consequence, the loss of biodiversity occurs (NOAA, 2022).

There are phytoplankton blooms that can give rise to adverse effects called HABs (Harmful algal blooms) and are mainly due to a wide variety of microscopic algae, including cyanobacteria. HABs are dangerous since they produce toxins and other bioactive substances that detrimentally affect aquatic organisms that can even cause their death or cause changes in their habitats (Burkholder, 2009). They can also produce adverse effects in humans by threatening the quality of drinking water (Xia et al., 2016). Eutrophication is causing significant impacts on ecosystems around the world (McIntryre & He, 2019) and has become a global environmental problem that requires the control of the water quality of rivers, lakes and reservoirs (Xia et al., 2016).

1.2. Direct methods for chlorophyll determination in waters

1.2.1. Smartphone

Smartphones have been a phenomenon for modern life and their use has become widespread (Rezazadeh et al., 2019). The Smartphone camera can be used as an optical detector due to its very compact high technology (Dutta et al., 2015). It can be used for colourimetry, fluorescence, chemiluminescence, bioluminescence, photoluminescence, and it is already part of analytical chemistry as one more instrument (Rezazadeh et al., 2019).

In the article by Mutlu and Kilic8 (Mutlu & Kilic, 2018), a Smartphone has been used as a sensor to determine dangerous dyes in water. In addition, articles have been found in the bibliography that have developed methods using Smartphones to control water quality, both through the determination of phosphates (Sáez-Hernández et al., 2022) and through the development of a portable fluorimeter called SmartFluo that uses a telephone for measurement and determination of chlorophyll in waters (Friedrichs et al., 2017). These methods contribute to a greater control of the quality of natural waters since they are low-cost methods and require little analysis time.

1.2.2. Remote sensing

Remote Sensing refers to the use of instruments to measure the electromagnetic radiation reflected or emitted from an object. Instruments record this radiation in ultraviolet, visible, and infrared regions. These instruments are mainly digital cameras, video systems, and radiometers found on aircraft or even satellites (Agrios, 2005). The use of Remote Sensing for water control uses the sensors found in the Landsat satellite, which determine important parameters such as the *chlorophyll a* content, the content of suspended matter and turbidity, among others. But this technique to determine the state of the water masses is not a sufficiently precise method, it must be compared with the reference methods by making measurements of that water mass, in order to be able to readjust the mathematical models to each water mass and provide values of the parameters accurately. Therefore, this method is not universal and must be adapted in each case (Ouma et al., 2018). In addition, another drawback that these techniques present is the interference that clouds can cause by changing the colour of the water masses and the change in atmospheric conditions.

Different mobile applications have also been developed that are based on Remote Sensing that use the Smartphone camera as a colorimetric sensor and the GPS that it has incorporated as a gyroscope to detect the rotation of the device in all its axes

(Gallagher & Chuan, 2018). One of the applications developed is EyeOnWater, which only requires a photography of the water surface, but needs to be compared with a digitized colour scale integrated into the app. However, the weather conditions are selected by the user, they are not the conditions that have occurred in the location where the photo is taken. The other application developed is HydroColor, which in order to carry out the measurement requires a photograph of each the water surface, a grey card and the sky. One of the drawbacks of this application is that it does not consider unfavourable weather conditions, such as wind, that can affect the colorimetric measurement, and it also requires a calibrated grey card to carry out the measurements (Ouma et al., 2018).

The main objective of this work is to create a method that can determine, from a photograph captured by means of a Smartphone, the amount of chlorophyll in water for the routine control of water masses quickly and without the need to use of organic solvents for extraction.

Among the specific objectives, it will be studied if there is a correlation of the colour parameters obtained from a photograph captured by the Smartphone of a water column with the chlorophyll signal from a portable fluorimeter, where fluorescence is measured, with the colour parameters of the filter obtained by the Minolta colourimeter and by the Smartphone and with the concentration of *chlorophyll a* obtained by UV-vis spectrometry after filtration and extraction with organic solvent.

2.   Material and methods

2.1.   Instruments and Reagents

To carry out the determination of *Chlorophyll a* by the reference method a Spectrophotometer DU 640 UV/Vis Beckman (Pasadena, California) was employed. To take the photographs a Smartphone Samsung galaxy S7 Edge (Seoul, South Korea) was used. To perform the fluorometric measure a handheld fluorimeter AquaFluor Turner Designs (San Jose, California) was employed.

As extraction solvents acetone AnalaR BDH (Dubai, United Arabian Emirates) and Dimethyl sulfoxide analytical grade EMSURE ACS Merck (Darmstadt, Germany) were employed. Moreover, filters made with glass fibre Whatman GF/F 47 mm Scharlau (Barcelona, Spain) were used to filter the water samples.

2.2.   Samples

Samples of eutrophicated water has been obtained from an irrigation ditch. The algae present in the water have been cultured by adding fertilizer and using a water oxygenator from a house aquarium to reinforce their growth. Water from the Albufera Natural Park, Valencia Botanical Garden and algae cultivated in the Microbiology and Ecology department of the University of Valencia have been analysed.

2.3.   Colorimetric determination of chlorophyll a by smartphone in the water column

The stablished volume of water sample is added to the cylindric Teflon container, and by using the assembly shown in the Figure 5.1 photos are taken from above. The light source is placed under the sample to get the colour of the sample by transmittance with the Smartphone located on the top. To obtain a homogeneous light a diffusor made with white plastic is used between the sample and the light source.

All the photos are taken by using the same conditions setting in pro-mode: ISO=125, 1/f=1/1000 and colour temperature of 5200 K. To obtain the colour parameters of the water column correctly, a blank is taken with the same volume of dechlorinated water. The images are processed using Matlab and the ColorLab library (Malo & Luque, 2002) to obtain the colour expressed in the CIEL*a*b* and CIEL*h*C* colour spaces.

Figure 5.1: Assembly employed to take photos of the water column by Smartphone.

2.4.   Fluorometric determination of *chlorophyll a*

The fluorometric measurement of *chlorophyll a* is carried out using AquaFluor device. For measure select the mode A, fill the cuvette with distilled water and press read, fill the cuvette with water sample and press read. The value of the distilled water is subtracted to the sample values.

2.5.   Spectrophotometric determination of *chlorophyll a*

The water samples are filtered through a Whatman GF/F 47 mm filter and a glass funnel under vacuum using a 1 litre Kitasato flask, as shown in Figure 5.2. Later, the filters are placed in glass tubes with 5 mL of extractant solution, dimethyl sulfoxide (DMSO):acetone 90 % (aq) in a ratio 1:1. The filters are incubated 48 h at -25 °C for chlorophyll extraction.

The tubes are centrifuged at 3500 rpm for 5 minutes and the solutions are measured in the UV-vis spectrophotometer in the range 400-800 nm. Using the Jeffrey and Humphrey equations (1, 2 and 3) (Jeffrey & Humphrey, 1975), bearing in mind the filtered volume of sample and the volume of extractant solution used, the concentration of chlorophyll is calculated.

$$C_{chl\ a} = 11.85\ A_{664}A\_664 - 1.54\ A_{647} - 0.08\ A_{630} \qquad \text{(Equation 1)}$$

$$C_{chl\ b} = -5.43\ A_{664} + 21.03\ A_{647} - 2.66\ A_{630} \qquad \text{(Equation 2)}$$

$$C_{chl\ c} = -1.67\ A_{664} - 7.60\ A_{647} + 24.52\ A_{630} \qquad \text{(Equation 3)}$$

Figure 5.2: Assembly employed for water filtration.

3.   Results and discussions

3.1.   Study of the relation of the colour parameters of the water column and chlorophyll

Firstly, increasing volumes of eutrophicated water were photographed using the Teflon container to check that there was a correlation between any colour parameter of the image and the amount of water. The results showed that for obtaining a linear correlation it was necessary to use a minimum of 30 mL of water and to avoid a colour saturation, for that the colour parameters must be G>0.25 and B>0.30, being the optical path, or water column depth, between 0.75 and 9.20 cm. If these parameters were lower than the specified ones, the colour was saturated and there was not a linear correlation.

To check if the colour parameters of the water column change using different volumes, a dilution study was carried out. In this study, 30 mL of eutrophicated water was photographed, after that 10 mL of dechlorinated water was added and a photo was taken again, performing this process until a total volume of 120 mL. As can be seen in the Figure 5.3 the colour parameters do not change, and the colour parameter values correspond to the total amount of *chlorophyll a* in the Teflon container being negligible the dilution volume.
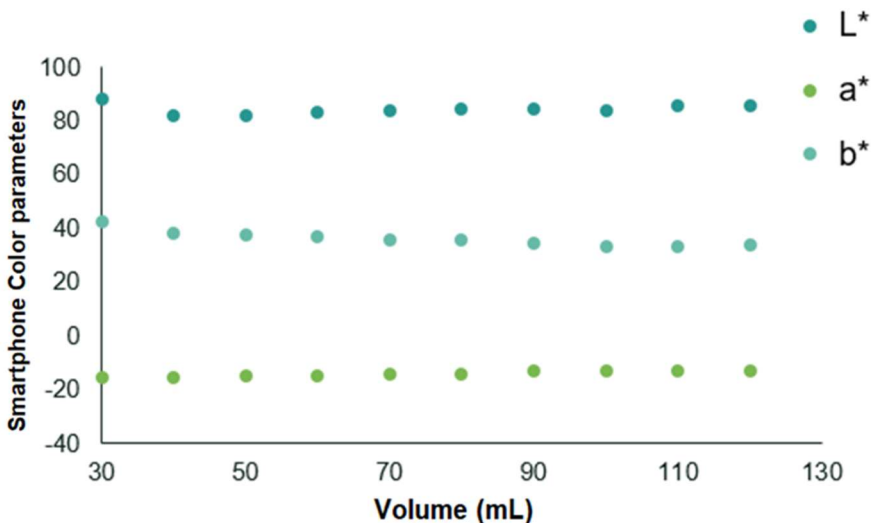
Figure 5.3: Smartphone colour parameters of the water column of the same sample diluted at different volumes.

A confirmation study with different sample concentrations was performed. In this case, one of the samples was analysed by solvent extraction spectrometric determination in order to obtain the real content of *chlorophyll a*. Later, 6 dilutions of this were prepared and photographed the water column of each one using the same volume (120 mL). The colour parameters were correlated with the content of chlorophyll, as can be seen in Figure 5.4 there is a correlation between the amount of chlorophyll and the a* and b* parameter of the water column.
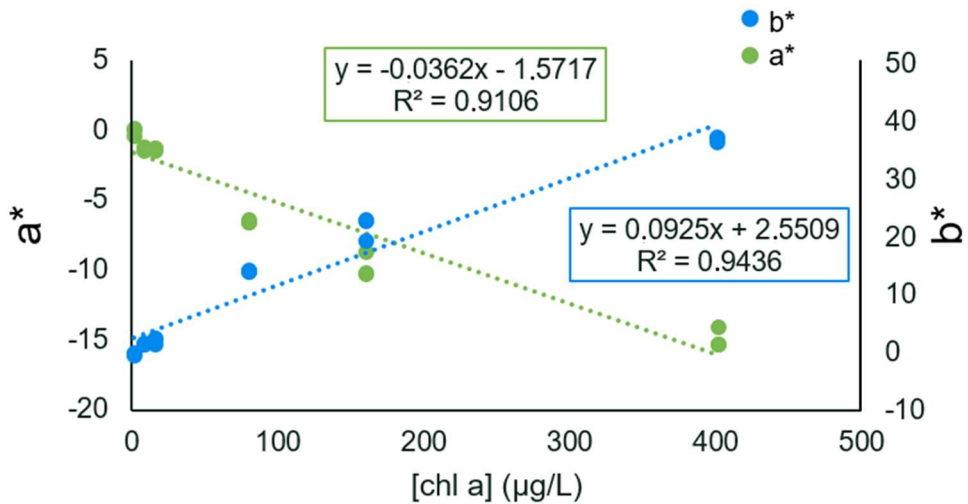
Figure 5.4: Smartphone colour parameters of the water column (120 mL) for different chlorophyll concentrations.

3.2. Develop of a model to determine the content of *chlorophyll a* using a Smartphone

To obtain the colour parameters needed to create a model, 10 different water samples were diluted at 9 different dilutions (90 solutions). The Figure 5.5 shows the scheme of the dilution process. From each sample, the dilutions D1, D5 and D8 were filtered by triplicate and analysed by the solvent extraction reference method in order to know the concentration of *chlorophyll a*, and from these concentrations calculate of the other dilution ones. All sample solutions were measured the fluorescence by AquaFluor and the colour parameters by Smartphone were carried out to. The water column volume photographed were 40, 70 and 110 mL, employing for each sample solution one, two or three volumes depends on its concentration.

The correlation between the colour parameters of the RGB, CIEL*a*b* and CIEL*h*C* colour spaces with the mass of *chlorophyll a* in the water column were studied. The best correlation was found for the b* parameter (Figure 5.6) with a R^2= 0.6374. Despite when the fluorometric values were correlated with the chlorophyll concentrations two trends were found, as can be seen in Figure 5.7, probably due to different algae species.
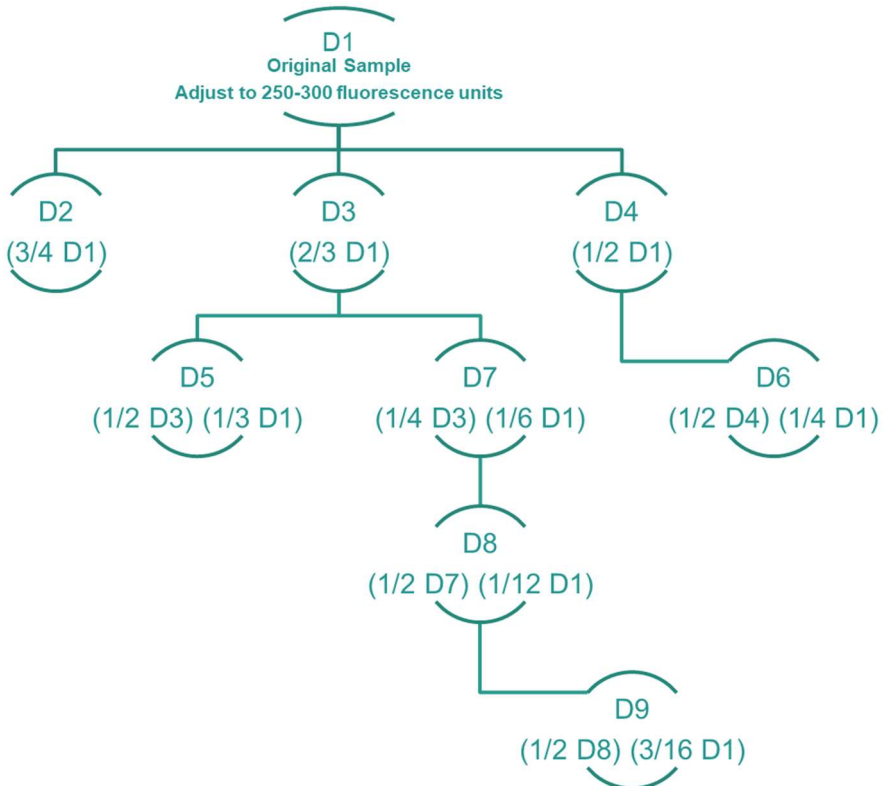
Figure 5.5: Scheme of the prepared dilutions (D1-D9) for each sample (10 water samples) indicating in brackets the proportion from the original sample D1.
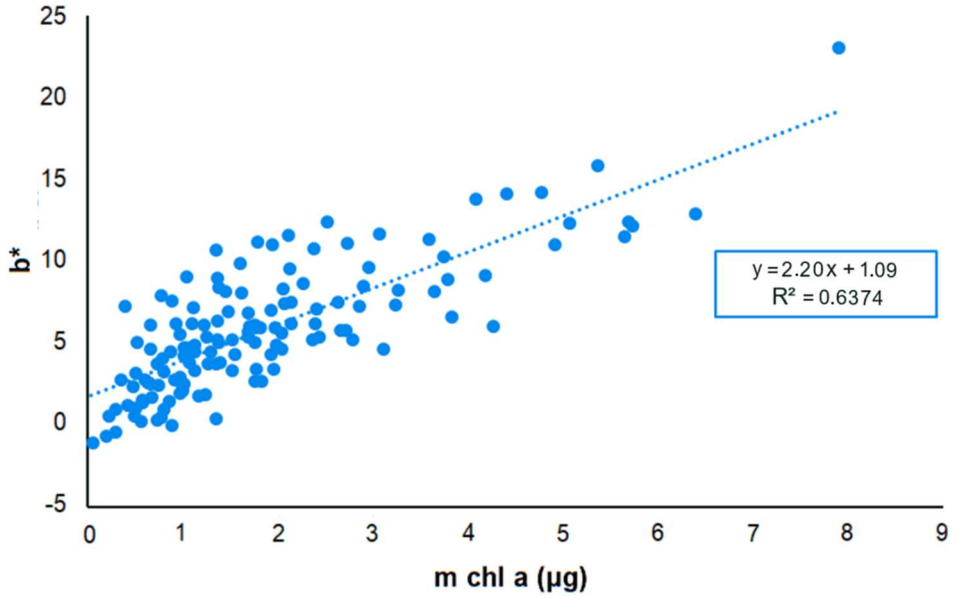
Figure 5.6: Correlation between the Smartphone b* colour parameter of the water column and the mass of chlorophyll a.
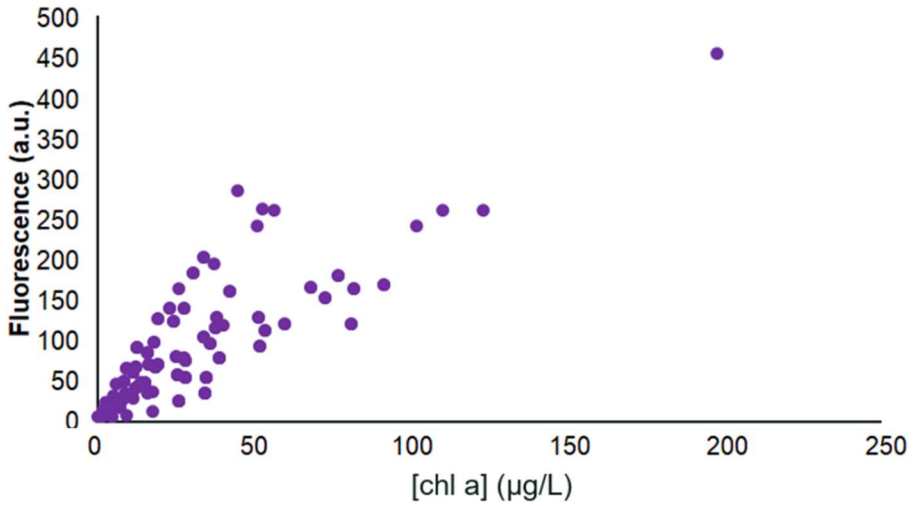
Figure 5.7: Correlation between the fluorometric measure (arbitrary units [a.u.]) and the concentration of chlorophyll a.

Some of samples were observed with an inverted microscope to check the species included. The Figure 5.8 shows that in each water sample it is possible to find different types of algae (cyanobacteria) which can explain the different behaviour in the fluorescence and in the colour of the water. Due this, it is not possible to develop a general model only using the b* parameter because the difference in colour is depending on the algae present in the water.
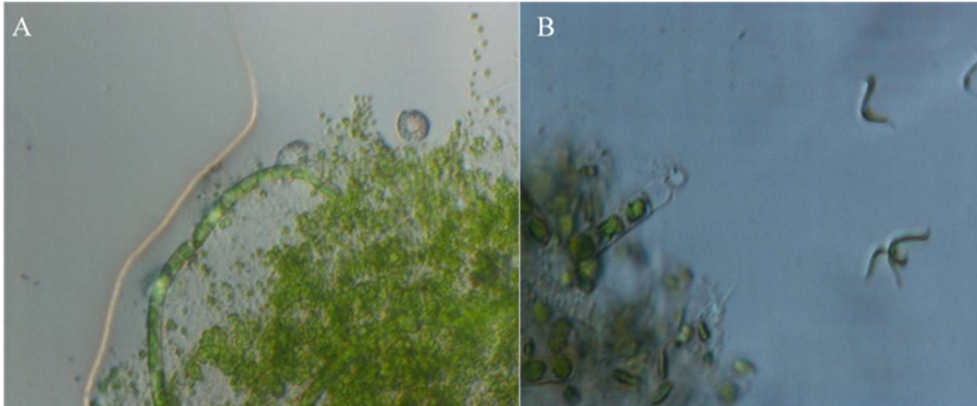
Figure 5.8: Algae species observed at microscope. A) Oscillatoria sp. B) Lyngbya sp.

Trying to solve the problem, the colour parameters of the RGB, CIEL*a*b* and CIEL*h*C* colour spaces were correlated with the mass of *chlorophyll a* in the water column for each water sample separately, including all its dilutions. In this case, the best correlation was found with the parameter C*. This correlation, depending on the original sample, presents a different slope, from 2.11 to 7.41 as can be seen in Table 5.1.

Table 5.1: Parameters of the correlation equation between C colour parameter of the water column and the mass of chlorophyll a.*

Sample	slope	R^2	Sample	slope	R^2
1	2.88	0.9359	6	7.41	0.8217
2	2.76	0.8718	7	4.96	0.7458
3	3.61	0.8704	8	3.78	0.8096
4	2.11	0.8957	9	3.19	0.8822
5	5.98	0.7806	10	2.57	0.6746

This change in slope could be indicative of the different species of algae present in the water column. It is possible to determine the chlorophyll content If we know the slope employing equation 4.

$$m_{chl\ a} = C^*/m \qquad\qquad \text{(Equation 4)}$$

However, this slope (m) varies depending on the type of water.

The slope was established taking photographs to different dilution of the same sample, which could be supplied by taking photographs to different volumes of the sample in the water column (40, 70 and 110 mL). As dilution D6 of all samples were photographed employing 40, 70 and 110 mL in the water column, we can correlate the colour parameters with the water volume. In this later case, the slope of the variation of the parameter a* between 40 and 110 mL (n1) and the variation of the parameter a* between 70 and 110 mL (n2) were calculated, since 110 is the most reliable volume at low concentrations of *chlorophyll a*. Table 5.2 shows the results for both slopes for each sample.

Table 5.2: Slopes of the correlation between the parameter a of the water column with the volume of water employed. Slope 1 for 40-110 mL and slope 2 for 70-110 mL.*

Sample	Slope 1	Slope 2	Sample	Slope 1	Slope 2
1	-0.0234	-0.0143	6	-0.0338	-0.0301
2	-0.0252	-0.0373	7	-0.0231	-0.0242
3	-0.0199	0.0071	8	-0.0050	-0.0043
4	-0.0152	0.0120	9	-0.0135	-0.0062
5	-0.0320	-0.0093	10	-0.0130	0.0132

On the other hand, a correlation has been found between the value of m obtained for each type of algae and the slope (n) obtained by correlating the value of the parameter a* with the volumes used (40-110 or 70-110, slope 1 and 2, respectively). However, depending on the volumes used, this slope varies (n1[40-110], n2[70-110]), obtaining two values of m (m1[40-110], m2[70-110]) (equations 5 and 6). So, the value of m is obtained by averaging m1 and m2. When applying these equations to calculate the concentration of the chlorophyll a in the water sample, a correlation of 0.9634 is found (Figure 5.9) between predicted value and provided by the reference method. Therefore, the use of these equations could serve to suppress the effect of different species of algae in the determination of the chlorophyll a content in water using a Smartphone.

$$n_1 = -0.0039 \cdot m_1 - 0.006 \qquad\qquad \text{(Equation 5)}$$

$$n_2 = -0.0068 \cdot m_2 + 0.0213 \qquad\qquad \text{(Equation 6)}$$
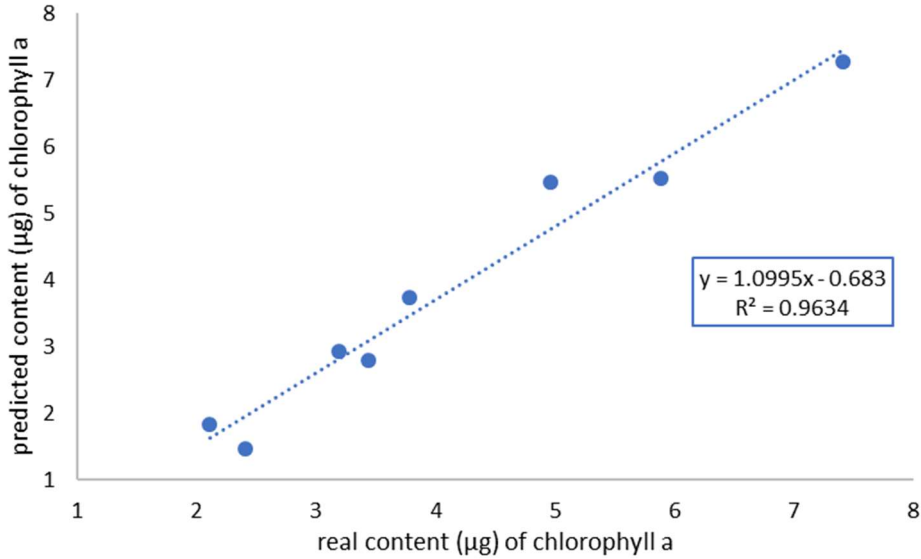
Figure 5.9: Correlation between the real content of chlorophyll a and the predicted content by using the equations before described.

4.   conclusions

This study shows that there is a correlation between the colour parameters obtained by the Smartphone and the content of *chlorophyll a* in the water column. In spite of that, the specie of algae in the water modifies the colour parameters and the fluorometric response. To solve that problem a mathematical calculation is proposed which seems solve that problem.

This new proposed method allows to determine the content of *chlorophyll a* taking only 3 photos of the water with volumes of 40 mL, 70 mL and 110 mL. Moreover, the correlation between the predicted amount of *chlorophyll a* and the real content is $R^2 = 0.9634$.

The present work shows that it is possible the direct determination of the amount of *chlorophyll a* in water using a Smartphone achieving the objective of this study.

5.   References

Agrios, G. N. (2005). Plant disease. In Plant Pathology. Fifth edition. Elsevier. London.

Álvarez Cobelas, M., Muñoz Ruiz, P. & Rubio Olmo, A. (1991). *La eutrofización de las aguas continentales españolas*. Madrid: Centro de Investigaciones del Agua, C.S.I.C.

Burkholder, J. M. (2009). Harmful Algal Blooms. In *Encyclopaedia of Inland Waters*; Likens, G. E., Ed.; Academic Press: Oxford, pp 264–285.

Dutta, S., Sarma, D., & Nath, P. (2015). Ground and river water quality monitoring using a smartphone-based pH sensor. *Aip Advances*, 5(5), 057151. DOI: 10.1063/1.4921835.

Friedrichs, A., Busch, J. A., Van der Woerd, H. J., & Zielinski, O. (2017). SmartFluo: A method and affordable adapter to measure *chlorophyll a* fluorescence with smartphones. *Sensors,* 17(4), 678. DOI: 10.3390/s17040678.

Gallagher, J. B., & Chuan, C. H. (2018). *Chlorophyll a* and Turbidity Distributions: Applicability of Using a Smartphone "App" Across Two Contrasting Bays. *Journal of Coastal Research*, 34(5), 1236-1243. DOI: 10.2112/JCOASTRES-D-16-00221.1.

Harper, D. (1992). Eutrophication of freshwaters. Principles, problems and restoration. First edition reprint. Chapman and Hall. London.

Jeffrey, S. W. & Humphrey, G. F. (1975) New spectrophotometric equations for determining chlorophylls a, b, c1 and c2 in higher plants, algae and natural phytoplankton. *Biochemie und Physiologie der Pflanzen*, *167* (2), 191–194. DOI: 10.1016/S0015-3796(17)30778-3

Malo, J., & Luque, M. J. (2002). ColourLab: the Matlab toolbox for Colourimetry and Colour Vision. Univ. Valencia. http://isp.uv.es/code/visioncolour/colourlab.html.

Mclntyre, A., & He, X. (2019). Global Marine Pollution—A Brief History. In Kirk Cochran, J., Bokuniewicz, H., & Yager P. (Eds.) Encyclopedia of Ocean Sciences. Third edition. Elsevier.

Mutlu, A. Y., & Kılıç, V. (2018). Machine learning based smartphone spectrometer for harmful dyes detection in water. In 26th Signal Processing and Communications Applications Conference (SIU).IEEE.

NOAA-National Oceanic and Atmospheric Administration. Hypoxia: Low or depleted oxygen in a water body often leads to 'dead zones '— regions where life cannot be sustained. National Ocean Service website. https://oceanservice.noaa.gov/hazards/hypoxia/, 8/03/22 (accessed April 25, 2022).

Ouma, Y. O., Waga, J., Okech, M., Lavisa, O., & Mbuthia, D. (2018). Estimation of Reservoir Bio-Optical Water Quality Parameters Using Smartphone Sensor Apps and Landsat ETM+: Review and Comparative Experimental Results. *Journal of Sensors*, 2018, 1–32. DOI: 10.1155/2018/3490757.

Rezazadeh, M., Seidi, S., Lid, M., Pedersen-Bjergaard, S., & Yamini, Y. (2019). The Modern Role of Smartphones in Analytical Chemistry. *TrAC Trends in Analytical Chemistry*, 118, 548–555. DOI: 10.1016/j.trac.2019.06.019.

Sáez-Hernández, R., Mauri-Aucejo, A. R., Morales-Rubio, A., Pastor, A., & Cervera, M. L. (2022). Phosphate Determination in Environmental, Biological and Industrial Samples Using a Smartphone as a Capture Device. *New Journal of Chemistry.* 46 (3), 1286–1294. DOI: 10.1039/D1NJ05425B.

Veenashree, Nandini, N. & Kumar, M. (2018). Nutrients Load and Eutrophication: An Overview of Bengaluru Urban Lakes*, International Journal of Research in Advent Technology*, Vol. 6(11), 2942-2945.

Xia, R., Zhang, Y., Critto, A., Wu, J., Fan, J., Zheng, Z., & Zhang, Y. (2016). The potential impacts of climate change factors on freshwater eutrophication: implications for research and countermeasures of water management in China. *Sustainability*, 8(3), 229. DOI: 10.3390/su8030229.

CHAPTER 6: Food dyes characterization in sweets by using a Smartphone

ABSTRACT

Food dyes can be toxic if the legislated maximum established concentration limits are exceeded, because of that it is necessary their control in foods to prevent them from reaching these limits. In this chapter a method to allow a fast screening of the food dyes content in sweet based on image analysis obtained by smartphone is proposed. The method only involves the use of water as reagent, a white LED lamp as lighting source and a smartphone to take the solutions photographs and could reduce the employment of more expensive and polluting methods. To validate the proposed smartphone-image method, an UV-Vis diode array spectrophotometer as reference instrumental technique has been employed. Even if the highest error of the method is considered, the maximum established legal limits are not exceeded, and up to 95% of the samples analysed could be screened, thus avoiding the use of more expensive procedures.

Keywords: Analytical Chemistry, CIELab, Food dyes, Smartphone.

1. Introduction

Food dyes are used to provide, intensify, or restore the colour of a product to make up for the colour loss related to the processing or storing, or the natural modifications of the raw material. The objective of their use is improving the final visual appealing that has the product in order to be more striking to the consumer. The applicability of the food dyes has spread widely, especially in confectionery products as sweets or ice creams, which are the ones in which this study has been focused.

Even though food dyes are widely used in the food industry, the differences between regulation laws in different countries are very remarkable. For example, in UK some of them can be employed but, in most of the EU countries are forbidden and in the north of Europe their use is not allowed. Moreover, between US and EU there are even bigger differences. Consequently, the international commercialization of food containing food dyes as additives remains an issue of global interest (Calvo, 2021).

The use of different food dyes in Europe has to be firstly authorized by the European Food Safety Authority (EFSA). These additives are controlled by a security evaluation based on the data review of human exposure and toxicity from available scientific studies. Moreover, when one of them is authorized, it must appear in the list of food additives allowed by the EU, that is included in the Regulation (CE) No.1333/2008 in which is specified their use conditions. Furthermore, the EFSA is the responsible of establishing the acceptable daily intake (ADI) for each substance, expressed as mass/kg of body weight per day. This parameter provides an amount estimation of these products that people can consume daily for a long of their lives, without any risk for their health. In the cases that there is not enough information to stablish the ADI, they calculate a security range to determine if the estimated exposure could be problematic (EFSA, 2021).

There is a large number of studies that related the presence of some food dyes with allergenic reactions and behavioural disorders of attention deficit and hyperactivity (ADHD) in children(McCann et al., 2007; Weiss, 2012). For these possible disorders, food dyes must be controlled to avoid that their content exceed the recommended maximum dose which are in the Regulation (EU) No.1129/2011 (EUR-Lex, 2022).

Accordingly, to guarantee the security is necessary to use reliable and accurate methods to determine these food dyes, and are numerous the analytical techniques that have been used to the identification and determination of synthetic food dyes. Thin layer chromatography (de Andrade et al., 2014; Vlajković et al.,

2013), differential pulse polarography (Combeau, 2002; Fogg & Yoo, 1979), capillary electrophoresis (Huang et al., 1998; Kuo et al. 1998), and techniques of high performance, such as ionic chromatography (HPIC) (Chen et al., 1998) or the ionic par liquid chromatography (IPC) (Fuh & Chia, 2002) have been widely employed. However, the high performance liquid chromatography (HPLC) coupled to different detectors, UV-Vis or mass spectrometer (MS), are the most used for the determination of food dyes (de Souza Santos Cheibub et al., 2020; Minioti et al., 2007; Khanavi et al., 2012; Yoshioka & Ichihashi, 2008; Zou et al., 2013). Because of all of these techniques require high-cost instrumentation, highly qualified operators and high analysis time, and since the molecules of interest provide coloured solutions, the spectrophotometric methods, which have advantages that are faster, cheaper and simpler, have been proposed (Soylak et al., 2011; Unsal et al., 2012).

Nowadays is necessary the employment of analytical methods that are direct, simple and economically affordable. In this sense, the smartphones, since they have cameras, can take photos from which are possible to employ the colour parameters as analytical measurement. The main advantage is their readily availability and accessibility, since most of the population can afford one of them. There are a lot of studies where the smartphone have been used to determinate substances in different samples. For example, to determine ethanol (Marinho et al., 2019), sulphites (Pires dos Santos Benedetti et al., 2015), methanol (de Oliveira Krambeck Franco et al., 2017) or furfural (de Oliveira Krambeck Franco et al., 2017) in drinks, tetracycline in milk (Masawat et al., 2015), the hardness of the water (Lopez-Molinero et al., 2013) or speciation of iron(II/III) in white wine. In all them, one of the RGB channels has been used as analytical parameter.

The most known colour space is the RGB model (Red, Green and Blue) in which each colour is characterized by their primary spectral components of red, green and blue. This model is an additive colour space, in which one colour can be represented as the addition of the three primary colours and is possible to obtain the colorimetric information from each pixel of the image (Capitán-Vallvey et al., 2015).

There are others interesting space colour, the CIEL*a*b* and the CIEL*h*C*, stablished by the l'éclaire International commission (CIE), an organization considered as the authority in the light and colour science. In the CIEL*a*b* space, the colour is defined by the L*, a* and b* coordinates, where L* is the luminance, a* is the difference of the light colour between red and green, and the b* is the difference of the light colour between blue and yellow. The second colour space is

similar to this one but in this case polar coordinates are used. The coordinate h* stands for the hue of the colour and the C* for the chrome of the colour (Capitán-Vallvey et al., 2015).

The aim of this study is to develop a smartphone method able to estimate the content of dyes used in the food industry, and to propose it as a quality control.

2.   Materials and Methods

2.1.   Reagents and Instrumentation

Stock solution of dyes from Tartrazine 85 % (Sigma Aldrich, Steinheim, Germany), Allura Red AC 80 % (Sigma Aldrich) and Brilliant Blue FCF 65 % (Sigma Aldrich) were prepared dissolving 31.9, 28.1 and 9.8 mg of each one in 1 L of water, respectively. The standards for the calibration lines were prepared by appropriate dilution of stocks ones.

To determine the spectra of food dyes in the standard and sample solutions a diode array spectrophotometer, Hewlett Packard model 8452A (Germany), has been employed. On the other hand, to obtain the photos, a Samsung (Seoul, South Korea) galaxy S/ edge model SM-G935F smartphone with a 12.2 MP camera, with the professional mode options of the camera, ISO 50, 1/2000 focal aperture, 5900 K colour temperature and zoom of 1.2 has been used. In each of the 16-wells of the 3D plate printed, 2 mL of the solutions, blanks, samples or standards were added, as indicated in figure 6.1, and the colour parameters of the images obtained were processed by Matlab® program.
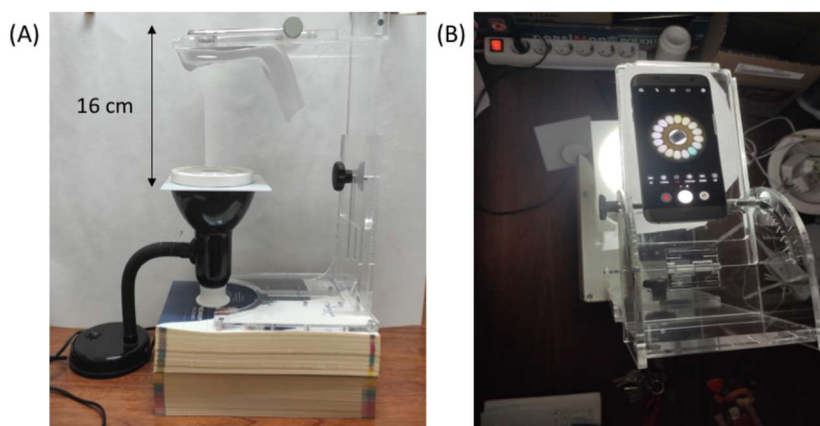
Figure 6.1: Setup of the light source, samples and standards carousel, and smartphone to take the photos.

2.2. Sample preparation

The samples employed in the study, sweets, ice cream water-based and flavoured drinks, were acquired in local supermarkets. Table 6.1 shows some characteristics of the samples, and all of them contain one or two of the food dyes under study; Tartrazine (E-102), Allura Red AC (E-129) and Brilliant Blue FCF (E-133). The typical spectra and structures of dyes are shown in the figure 6.2.

Table 6.1: Characteristics of the samples used in the study.

Sample identification	Type	Dye	Description
G01	Sweet	E-129	Uncovered; Opaque
G02	Sweet	E-129	Sugar Cover; Translucent
G03	Sweet	E-129	Uncovered; Translucent
G04	Sweet	E-129	Sugar Cover; Translucent
G05	Sweet	E-129	Uncovered; Translucent
G06	Sweet	E-133	Uncovered; Opaque
G07	Sweet	E-133	Uncovered; Translucent
G08	Sweet	E-133	Sugar Cover; Translucent
G09	Sweet	E-133	Liquid Sample
B01	Sweet	E-133	Liquid Sample
G10	Sweet	E-102	Uncovered; Opaque
H01	Ice-Cream	E-102	Liquid Sample
G11	Sweet	E-102+E-129	Uncovered; Opaque
G12	Sweet	E-102+E-129	Sugar Cover; Translucent
G13	Sweet	E-102+E-129	Sugar Cover; Translucent
G14	Sweet	E-102+E-129	Sugar Cover; Opaque
G15	Sweet	E-102+E-133	Sugar Cover; Translucent
G16	Sweet	E-102+E-133	Sugar Cover; Translucent
G17	Sweet	E-102+E-133	Sugar Cover; Translucent
G18	Sweet	E-102+E-133	Uncovered; Opaque
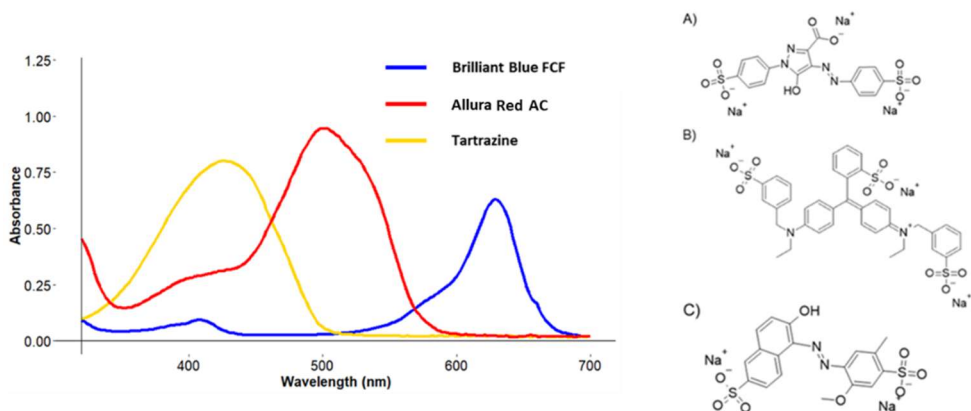
Figure 6.2: Absorbance spectra and chemical structures of the Tartrazine (A), Brilliant Blue FCF (B) and Allura Red AC (C).

To carry out the measurements, both by the reference method and by the smartphone method, the samples are weighed (± 0. 1 mg) in beakers, 30 mL of water are added to them, and they are heated until completely dissolved. The solutions are transferred to falcon tubes and water is added until 50 mL of total solution. Subsequently, the solutions are filtered and are ready to be measured; and If the colour is too intense, they are diluted appropriately.

2.3.   Dyes determination by UV-Vis

The absorbance spectra were run between the 300-700 nm range for the standards and the samples, the calibration lines were obtained at the characteristic wavelength of each food dye; at 402, 502 and 630 nm for Tartrazine, Allura Red AC and Brilliant Blue FCF, respectively. In the case of the binary mixtures, each food dye was analysed separately, using the absorbance and the first derivate of the spectrum at their wavelengths associated.

2.4.   Dyes determination by smartphone

The diluted samples and standards were photographed with the smartphone at the fixed illumination conditions that are described in the 2.1. section.

To analyse samples containing only one food dye, the plate wells were filled with a blank and 5 standards for calibration line, and the rest of the wells were filled with different samples containing the dye to be studied. On the other hand, to analyse samples with two food dyes, the wells were filled with the blank, 3 individual dye standards calibration for each food dye, 3 calibration standards for mixtures of the two dyes and the rest of wells were filled with the corresponding samples. With all the wells filled with the appropriate solutions, the photograph was taken with the smartphone as indicated above. Secondly, the image processing was carried out by using a script of Matlab®, using the ColorLab library (Malo & Luque, 2002), software and the colour parameters of the different colour spaces (RGB, CIEL*a*b* and CIEL*h*C*) were obtained.

3.   Results

3.1.   Stability of the single colour calibrations

To check the stability of the solutions, the standards were measured freshly prepared and after 10 days using UV-Vis spectrophotometer. Table 6.2 shows the linear equation of food dyes obtained in both days, and as can be seen, the solutions are stable over time.

Table 6.2: linear equations and correlations obtained for each food dye calibration line in both days (Absorbance vs µM).

Food Dye	Day 1		Day 10	
	Equation	R^2	Equation	R^2
Allura Red AC	A=0.0825x + 0.0047	0.99990	A=0.0835x + 0.0166	0.999
Tartrazine	A=0.0575x + 0.0002	0.99999	A=0.0614x + 0.0127	0.999
Brilliant Blue FCF	A=0.1602x + 0.0028	0.99994	A=0.1602x + 0.0078	0.9994

On the other hand, colour analysis of the solutions images obtained with the smartphone illustrates that the best colour parameter to study individually the food dyes are the C* and h* parameters in the CIEL*h*C* colour space, that present a linear and polynomial equation, respectively (See Table 6.3). To obtain the calibration line, all solutions has been photographed in the same image to avoid light variations that could be a source of error.

Table 6.3: Equations and correlations obtained for each food dye calibration line (Absorbance vs µM) for C and h* colour parameters.*

Food Dye	C*		h*	
	Equation	R^2	Equation	R^2
Allura Red AC	6.2889x + 2.7227	0.989	$0.0035X^3 - 0.2172X^2 + 4.1387X + 15.418$	0.997
Tartrazine	6.4867x - 1.2011	0.96	$0.0271x^3 - 0.6349x^2 + 3.5794x + 104.39$	0.98
Brilliant blue FCF	8.8804x + 1.6976	0.9915	$1.0993x^3 - 9.7674x^2 + 28.034x + 203.91$	0.9999

3.2. Binary mixtures calibration study

3.2.1. Spectra of food dye mixtures

In this study, some tests, by mixing different individual food dye concentrations that will provide green and orange colours, were performed. Table 6.4 shown the volumes taken of each dye stock solutions (28.1, 31.9 and 9.8 mg/L of Allura Red AC, Tartrazine and Brilliant Blue FCF respectively) to prepare 25 mL of the mixture solutions. Two calibration strategies were used. In the first one (Table 6.4A), the proportion of food dyes in each solution was varied, being increasing de concentration for one dye and decreasing for the other one of the binary mixtures. In the second approach (Table 6.4B), the calibration line was prepared maintaining constant the concentration of one food dye and increasing the concentration of the other one.

Table 6.4: Volumes of food dye solution taken to prepare 25 mL orange* and green** mixtures employing water to reach 25 mL.

Strategy A							
Food Dye 1	0	2	4	5	6	8	10
Food Dye 2	10	8	6	5	4	2	0
Strategy B							
Food Dye 1	5	5	5	5	5	5	5
Food Dye 2	0	2	4	5	6	8	10

*Orange colour: Allura Red AC and Tartrazine or Tartrazine and Allura Red AC
**Green colour: Brilliant Blue FCF and Tartrazine or Tartrazine and Brilliant Blue FCF

The behaviour of one dye over the other one is different in the orange colour mixtures (Allura Red AC plus Tartrazine). As can be seen in figure 6.3, the absorption at the characteristic wavelength of a 5.6 mg/L solution of the Allura Red AC dye is not interfered with by increasing concentrations of Tartrazine (until 12.75 mg/L). However, as can be seen in the figure 6.4, if the Tartrazine concentration remains constant (6.4 mg/L), the increasing concentrations of Allura Red AC (up to 11.232 mg/L) do interfere with the Tartrazine signal, and it would be necessary to use the first derivative of the spectrum. Therefore, if the concentration of both food dyes is variable in a binary mixture, is possible to determine the concentration of Allura Red AC directly from the absorbance spectrum, but the first derivative would be necessary to determine the concentration of Tartrazine.
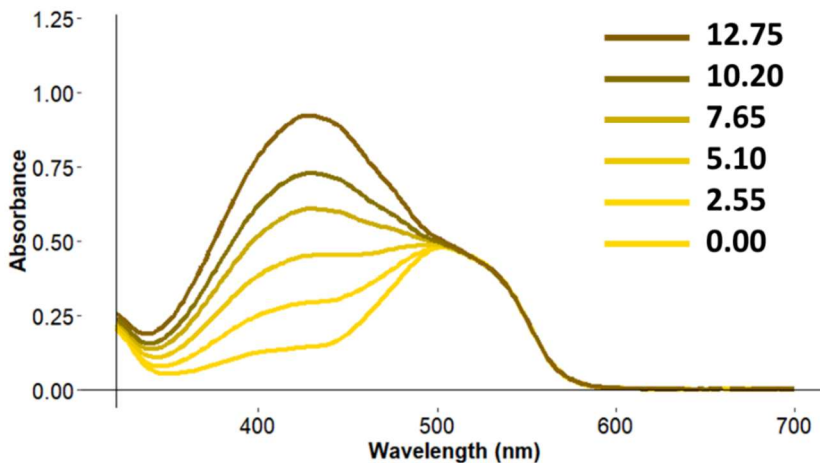
Figure 6.3: Spectra of Tartrazine and Allura Red AC mixtures with constant amount of Allura Red AC (5.6 mg/L) and increasing amounts of Tartrazine (mg/L).
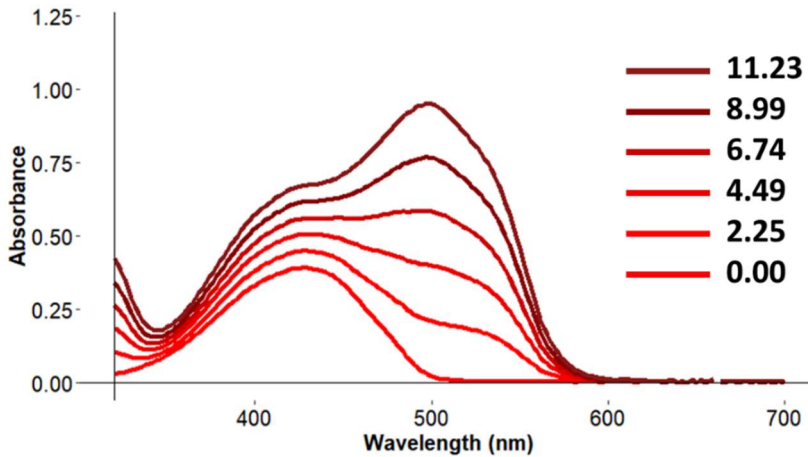
Figure 6.4: Spectra of Tartrazine and Allura Red AC mixtures with constant amount of Tartrazine (6.4 mg/L) and increasing amounts of Allura Red AC (mg/L).

In the green colour mixtures (Brilliant Blue FCF plus Tartrazine), and as can be seen in figure 6.5, Tartrazine can be determined without any problem in presence of increasing concentrations of Brilliant Blue FCF (until 12.750 mg/L). On the other hand, if the amount of Tartrazine is constant, the Brilliant Blue FCF maximum peak overlap with the maximum peak of Tartrazine (Figure 6.6). This problem could be solved using a displaced wavelength. When the calibration line of Tartrazine is studied at 444 nm, the correlation is of $R^2=0.999987$. Due to this fact, when the amount of both food dyes is variable, the tartrazine can be measured easily at this wavelength.
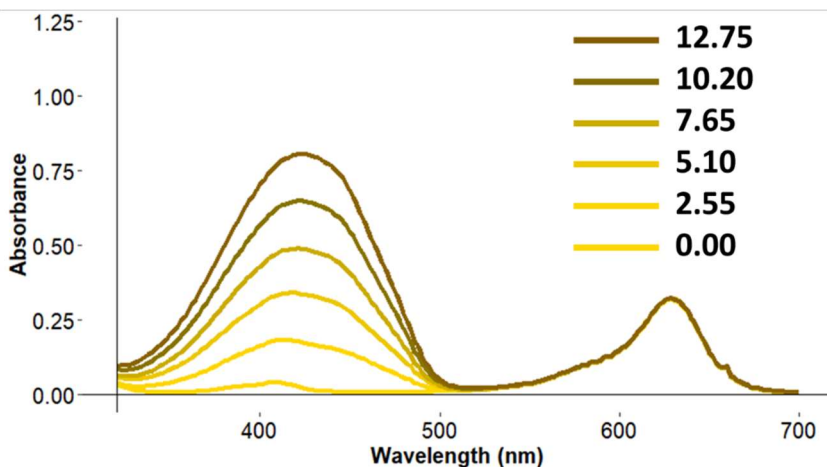
Figure 6.5: Spectra of Tartrazine and Brilliant Blue FCF mixtures with constant amount of Brilliant Blue FCF (2 mg/L) and increasing amounts of Tartrazine (mg/L).
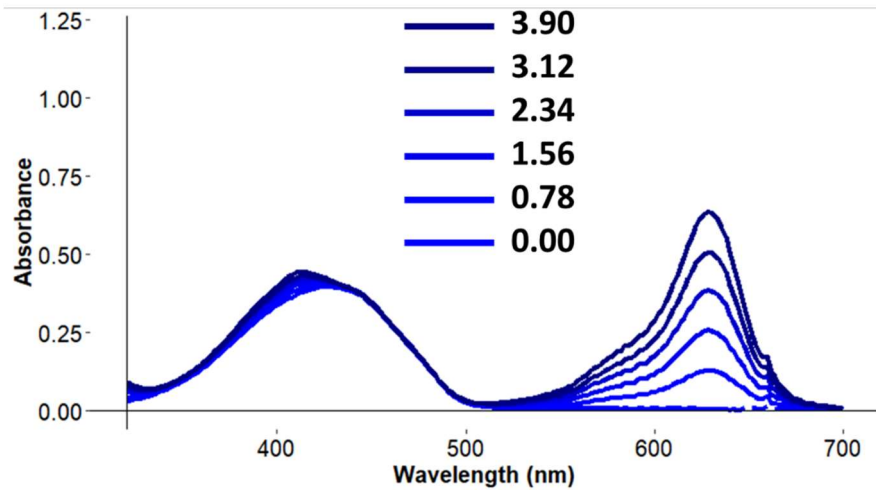
Figure 6.6: Spectra of Tartrazine and Brilliant Blue FCF mixtures with constant amount of Tartrazine (6.4 mg/L) and increasing amounts of Brilliant Blue FCF (mg/L).

As conclusions of this study, as regards the spectra, the small contribution on Tartrazine signal in green mixtures can be solved using the signal at 444 nm. On the other hand, unless the Allura Red AC interfere with the Tartrazine, as it will explain later on, only the calibration lines for solutions with a single food dye will be used, and it would not be necessary to use the first derivative of the spectrum.

3.2.2. Smartphone images study

Under controlled lighting conditions, the images of the different solutions of the food dye standard calibration were taken, and the relationships between the different parameters of the CIEL*h*C* colour space and the concentration of the dyes were studied. As can be seen in table 6.5, in the dye mixtures it is the h * parameter which presents an excellent polynomial correlation with the Tartrazine percentage. In this way, the h* parameter will be used to obtain the ratio of each food dye in the mixture, and the C* parameter will be employed to know the content of each food dyes in the sample.

Table 6.5: Equations obtained for the different calibration lines of food dye mixtures (colour parameter vs percentage of Tartrazine in the mixture).

Constant amount of Allura Red AC + different amount of Tartrazine

C*= 4.4051 x + 45.91	R^2= 0.95
h* = 0.05056 x^3- 1.30689 x^2+ 11.86375 x + 30.35715	R^2= 0.99997

Different amounts of Tartrazine and Allura Red AC

C* = -0.0943 x + 71.803	R^2= 0.19
h* = 2·10^{-5} x^3+ 0.0007 x^2- 0.8547 x + 103.1	R^2= 0.9991

Constant amount of Tartrazine + different amount of Allura Red AC

C* = 5.95 x + 34.83	R^2= 0.995
h* = -0.0662 x^3+ 1.5753 x^2- 14.617 x+ 104.71	R^2= 0.999

Constant amount of Tartrazine + different amount of Brilliant Blue FCF

C* = 0.5568 x + 45.055	R^2= 0.55
h* = -0.00992 x^3 + -0.07027 x^2+ 6.66329 x + 107.08693	R^2= 0.999990

Different amounts of Tartrazine and Brilliant Blue FCF

C* = -0.4767 x + 73.581	R^2= 0.88
h* = 0.0001 x^3- 0.0071 x^2+ 0.7643 x + 102.78	R^2= 0.99990

Constant amount of Brilliant Blue FCF + different amount of Tartrazine

C* = 7.0365 x + 13.474	R^2= 0.98
h* = -0.1925 x^3+ 4.314 x^2- 33.838 x + 222.58	R^2= 0.999

3.2.3. comparison of the methods

Both methods were compared for check the sensibility of each one applied for the measurement of the different food dyes. Table 6.6 shows that the LOD and LOQ obtained for the Allura Red and Brilliant Blue FCF are slightly higher for the smartphone than the UV-vis measure. With the Tartrazine the result is inverted. The results for both instruments for all food dyes are very similar.

Table 6.6: Comparison for the LOD and LOQ for both instruments employed for the measurement of three food dyes. Results are expressed as mg/L.

	UV-vis		Smartphone	
	LOD	LOQ	LOD	LOQ
Allura Red AC	0.65	2.17	0.86	2.87
Brilliant Blue FCF	0.11	0.37	0.25	0.83
Tartrazine	1.00	3.33	0.78	2.60

3.3.   Sample analysis

3.3.1.   Solid samples

The possibility of carrying out the image processing on the photography of the solid samples themselves, without any preparation, was studied. Nevertheless, the results obtained were not adequate because of the difficulty of taking an useful image of the different types of samples; by the coating, reflections, shadows, transparencies, or irregularities in samples with two colours, among others, as can be seen in figure 6.7.
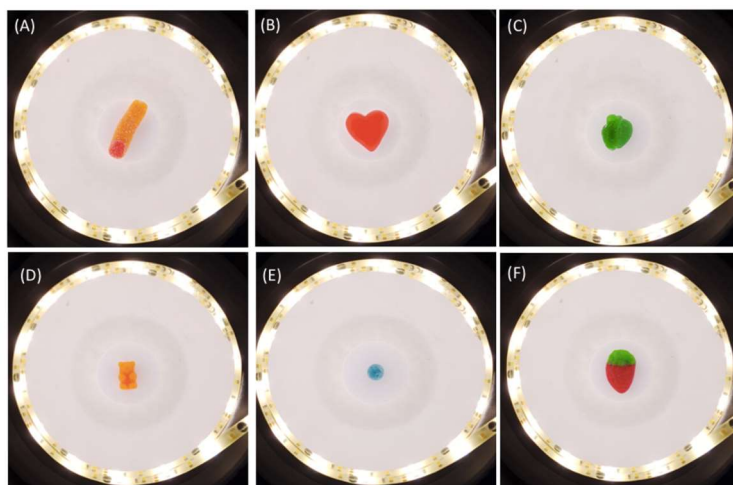
Figure 6.7: Direct photos of some samples.

3.3.2.   Dissolved samples

For the orange or green colour samples, that contain Tartrazine plus other food dye, the mixing ratio of the dyes were calculated using the h* values of the sample solutions images. Since the content of Tartrazine was very high compared to the other food dyes in a mixture, Tartrazine could be consider as the only food dye to quantify the amount of total food dyes, and therefore, the content of the Tartrazine

was calculated by interpolating the C* parameter of the images of the solutions in their calibration line, as previously indicated above.

To check the variability of the samples, the content of food dyes in three replicates of the samples G02, G09 and G13 were measured by the UV-Vis spectrophotometer and the smartphone. Table 6.7 shows the results obtained and can be concluded that the concentration and standard deviation values of the samples, obtained by both methods are comparable.

Table 6.8 shows the concentrations of the food dyes in the different samples obtained both, the UV-Vis spectrometric method and the smartphone method. As can be seen, taking as correct the concentration values of the dyes obtained with the UV-Vis spectrometer, in all the samples that contain Brilliant Blue FCF as the only dye, when using the smartphone method error of less than 10 % are obtained. In all the other samples, containing both the binary mixtures of the three dyes studied, and Tartrazine or Allura Red AC as the only dyes, the errors made by the smartphone method are between 0.4% and 17%. Even with this 17 % error, the concentrations of the dyes are still very far from the limit values established in the legislation. Because of that, this method could be used as quality control when the operator will not require the exact content of the dye but should know if it is within legal limits.

Figure 6.8 shows the concentration of the dyes in the different samples analysed, and a segment has been added, for all of them, showing the range of the hypothetical error of 17%. As can be seen, the content of food colouring in the samples is so low that there is still a very high margin left to reach the legal limits.

Table 6.7: Checking test of the variability of the results.

	UV-vis	Smartphone
Sample	**Mean ±Standard deviation (mg/kg)**	**Mean±Standard deviation (mg/kg)**
G02 ALLURA RED AC	83 ± 2	84.6 ± 0.4
G09 BRILLIANT BLUE FCF	16 ± 1	18 ± 2
G13 ALLURA RED AC + TARTRAZINE	88 ± 4	87 ± 7

Table 6.8: Food dyes in the samples analysed.

Sample	Food Dye			UV-vis Spectrometer						Smartphone						Error (%)		
	R	B	T	R(%)	B(%)	T(%)	R(mg/kg)	B(mg/kg)	T(mg/kg)	R(%)	B(%)	T(%)	R(mg/Kg)	B(mg/kg)	T(mg/kg)	R	B	T
G01	X			100			99			100			114			15		
G02	X			100			75			100			75			0.4		
G03	X			100			25			100			29			15		
G04	X			100			19			100			20			3		
G05	X			100			113			100			95			-16		
G06		X			100			44			100			47			8	
G07		X			100			113			100			112			-1	
G08		X			100			27			100			25			-9	
G09		X			100			13			100			14			4	
B01		X			100			8			100			8			-5	
G10			X			100			62			100			71			16
H01			X			100			68			100			57			-17
G11	X		X	<0.01		100	<LOD		38	<0.01		102	<LOD		44			14
G12	X		X	-		-	-		-	<0.01		106	<LOD		9			-
G13	X		X	<0.01		100	<LOD		82	<0.01		100	<LOD		78			-5
G14	X		X	<0.01		100	<LOD		146	<0.01		103	<LOD		148			2
G15		X	X		17	83		16	77		17	83		14	69		-12	-11
G16		X	X		-	-		-	-		32	68		6	13		-	-
G17		X	X		21	79		11	41		23	77		12	41		9	1
G18		X	X		12	88		16	114		11	89		13	106		-17	-7

Food Dye: R: Allura Red AC   B: Brilliant Blue FCF   T: Tartrazine
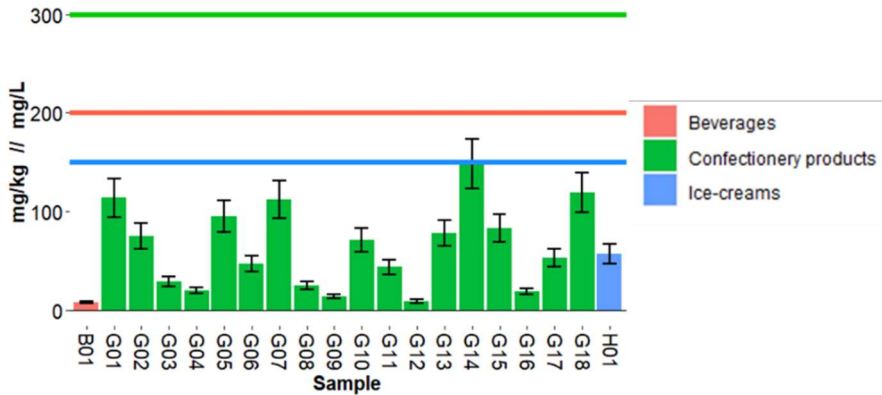
Figure 6.8: Estimated Content of food dyes with the use of a smartphone with the highest error obtained (17 %). The horizontal lines represent the maximum content allowed depending on the type of product.

4. Discussion and conclusions

One of the main objectives of the proposed method has been to avoid the use of techniques such as HPLC, since it requires longer analysis times and more specialized instrumentation. This can be check in the work of Minioti et al. (2007) in which the retention times for the food dyes Tartrazine, Allura Red AC and Brilliant blue FCF are 10.90, 19.07 and 24.68 minutes, respectively. Moreover, the time that is need to condition the instrument and the time to prepare the samples has to be considered.

The proposed smartphone method only requires the employment of water to dissolve the sample, a 3D printed wells plate and a script of Matlab® to obtain the results of the image processing by the CIEL*h*C* colour space. The method allows to estimate the food dye content in 16 samples only using 3 minutes to obtain the result. The developed method allows estimate the content of food dyes in samples when it has only one dye or a mix of two dyes. In this type of products is rarely found samples with more than two food dyes, and in this study no samples of this type were found. Although the method provides a maximum error of 17 %, it can be used as a screening method due that rarely the foods have high content of food dyes. The use of this screening would avoid the employ of expensive analysis, time consumption and waste generation that require methods like HPLC. In this way is possible to analyse a higher number of samples in a very low time, and only in doubt case, bearing in mind the error range of the proposed method, would be necessary to analyse the sample with more accurate techniques.

5.   References

Calvo, M. (accessed June 15, 2021). Colorantes Artificiales. Bioquímica de los alimentos, University of Zaragoza. http://milksci.unizar.es/bioquimica/temas/aditivos/colourartif.html.

Capitán-Vallvey, L. F., Lopez-Ruiz, N., Martinez-Olmos, A., Erenas, M. M., & Palma, A. J. (2015). Recent developments in computer vision-based analytical chemistry: A tutorial review. *Analytica Chimica Acta*, 899, 23-56. DOI: 10.1016/j.aca.2015.10.009.

Chen, Q. C., Mou, S. F., Hou, X. P., Riviello, J. M., & Ni, Z. M. (1998). Determination of eight synthetic food colorants in drinks by high-performance ion chromatography. *Journal of Chromatography A*, 827(1), 73-81. DOI: 10.1016/S0021-9673(98)00759-6.

Combeau, S., Chatelut, M., & Vittori, O. (2002). Identification and simultaneous determination of Azorubin, Allura red and Ponceau 4R by differential pulse polarography: application to soft drinks. *Talanta*, 56(1), 115-122. DOI: 10.1016/S0039-9140(01)00540-9.

de Andrade, F. I., Florindo Guedes, M. I., Pinto Vieira, Í. G., Pereira Mendes, F. N., Salmito Rodrigues, P. A., Costa Maia, C. S., Marqués Ávila, M. M., & de Matos Ribeiro, L. (2014). Determination of synthetic food dyes in commercial soft drinks by TLC and ion-pair HPLC. *Food Chemistry*, 157, 193-198. DOI: 10.1016/j.foodchem.2014.01.100.

Cheibub, A. M. D. S. S., de Lyra, E. S. B., Alves, B. J., Donagemma, R. A., & Netto, A. D. P. (2020). Development and validation of a multipurpose and multicomponent method for the simultaneous determination of six synthetic dyes in different foodstuffs by HPLC-UV-DAD. *Food Chemistry*, 323, 126811. DOI: 10.1016/j.foodchem.2020.126811.

de Oliveira Krambeck Franco, M., Suarez, W. T., Maia, M. V., & dos Santos, V. B. (2017). Smartphone application for methanol determination in sugar cane spirits employing digital image-based method. *Food Analytical Methods*, 10, 2102-2109. DOI: 10.1007/s12161-016-0777-y.

de Oliveira Krambeck Franco, M., Suarez, W. T., & Santos, V. B. D. (2017). Digital image method smartphone-based for furfural determination in sugarcane spirits. *Food Analytical Methods*, 10, 508-515. DOI: 10.1007/s12161-016-0605-4.

EUR-Lex. (Accessed July 18, 2022). Commission Regulation (EU) No 1129/2011 of November 2011 amending Annex II to Regulation (EC) No 1333/2008 of the European Parliament and of the Council by establishing a Union list of food Additives Text with EEA relevance. https://eur-lex.europa.eu/legal-content/EN/ALL/?uri=celex%3A32011R1129.

European Food Safety Authority (EFSA). (accessed June 15, 2021). Colorantes alimentarios. https://www.efsa.europa.eu/es/topics/topic/food-colours.

Fogg, A. G., & Yoo, K. S. (1979). Direct differential-pulse polarographic determination of mixtures of food colouring matters, chocolate brown HT, tartrazine and Green S. *Analyst*, 104(1244), 1087-1090. DOI: 10.1039/AN9790401087.

Fuh, M. R., & Chia, K. J. (2002). Determination of sulphonated azo dyes in food by ion-pair liquid chromatography with photodiode array and electrospray mass spectrometry detection. *Talanta*, 56(4), 663-671. DOI: 10.1016/S0039-9140(01)00625-7.

Huang, H. Y., Chiu, C. W., Sue, S. L., & Cheng, C. F. (2003). Analysis of food colorants by capillary electrophoresis with large-volume sample stacking. *Journal of chromatography A*, 995(1-2), 29-36. DOI: 10.1016/S0021-9673(03)00530-2.

Kuo, K. L., Huang, H. Y., & Hsieh, Y. Z. (1998). High-performance capillary electrophoretic analysis of synthetic food colorants. *Chromatographia*, 47, 249-256. DOI: 10.1007/BF02466528.

López-Molinero, A., Cubero, V. T., Irigoyen, R. D., & Piazuelo, D. S. (2013). Feasibility of digital image colorimetry—application for water calcium

hardness determination. *Talanta*, 103, 236-244. DOI: 10.1016/j.talanta.2012.10.038.

Malo, J., & Luque, M. J. (2002). ColourLab: the Matlab toolbox for Colourimetry and Colour Vision. Univ. Valencia. http://isp.uv.es/code/visioncolour/colourlab.html.

Marinho, O. R., Lima, M. J., Rocha, F. R., Reis, B. F., & Kamogawa, M. Y. (2019). A greener, fast, and cost-effective smartphone-based digital image procedure for quantification of ethanol in distilled beverages. *Microchemical Journal*, 147, 437-443. DOI: 10.1016/j.microc.2019.03.05444.

Masawat, P., Harfield, A., & Namwong, A. (2015). An iPhone-based digital image colorimeter for detecting tetracycline in milk. *Food Chemistry*, 184, 23-29. DOI: 10.1016/j.foodchem.2015.03.089.

McCann, D., Barrett, A., Cooper, A., Crumpler, D., Dalen, L., Grimshaw, K., Kitchin, E., Lok, K., Porteous, L., Prince, E., Sonuga-Barke, E., Warner, J. O., & Stevenson, J. (2007). Food additives and hyperactive behaviour in 3-year-old and 8/9-year-old children in the community: a randomised, double-blinded, placebo-controlled trial. *The Lancet*, 370(9598), 1560-1567. DOI: 10.1016/S0140-6736(07)61306-3.

Minioti, K. S., Sakellariou, C. F., & Thomaidis, N. S. (2007). Determination of 13 synthetic food colorants in water-soluble foods by reversed-phase high-performance liquid chromatography coupled with diode-array detector. *Analytica Chimica Acta*, 583(1), 103-110. DOI: 10.1016/j.aca.2006.10.002.

Khanavi, M., Hajimahmoodi, M., Ranjbar, A. M., Oveisi, M. R., Ardekani, M. R. S., & Mogaddam, G. (2012). Development of a green chromatographic method for simultaneous determination of food colorants. *Food Analytical Methods*, 5, 408-415. DOI: 10.1007/s12161-011-9259-443.

dos Santos Benedetti, L. P., dos Santos, V. B., Silva, T. A., Benedetti-Filho, E., Martins, V. L., & Fatibello-Filho, O. (2015). A digital image analysis method for quantification of sulfite in beverages. *Analytical Methods*, 7(18), 7568-7573. DOI: 10.1039/C5AY01372K.

Soylak, M., Unsal, Y. E., & Tuzen, M. (2011). Spectrophotometric determination of trace levels of allura red in water samples after separation and preconcentration. *Food and Chemical Toxicology*, 49(5), 1183-1187. DOI: 10.1016/j.fct.2011.02.013.

Unsal, Y. E., Soylak, M., & Tuzen, M. (2012). Column solid-phase extraction of sunset yellow and spectrophotometric determination of its use in powdered beverage and confectionery products. *International Journal of Food Science & Technology*, 47(6), 1253-1258. DOI: 10.1111/j.1365-2621.2012.02966.x.

Vlajković, J., Andrić, F., Ristivojević, P., Radoičić, A., Tešić, Ž., & Milojković-Opsenica, D. (2013). Development and validation of a TLC method for the analysis of synthetic food-stuff dyes. *Journal of Liquid Chromatography & Related Technologies*, 36(17), 2476-2488. DOI: 10.1080/10826076.2013.790771.

Weiss, B. (2012). Synthetic food colors and neurobehavioral hazards: the view from environmental health research. *Environmental Health Perspectives*, 120(1), 1-5. DOI: 10.1289/ehp.1103827.

Yoshioka, N., & Ichihashi, K. (2008). Determination of 40 synthetic food colors in drinks and candies by high-performance liquid chromatography using a short column with photodiode array detection. *Talanta*, 74(5), 1408-1413. DOI: 10.1016/j.talanta.2007.09.015.

Zou, T., He, P., Yasen, A., & Li, Z. (2013). Determination of seven synthetic dyes in animal feeds and meat by high performance liquid chromatography with diode array and tandem mass detectors. *Food chemistry*, 138(2-3), 1742-1748. DOI: 10.1016/j.foodchem.2012.11.084.

CHAPTER 7: Smartphone determination of azo dyes using Arata-Possetto extraction method
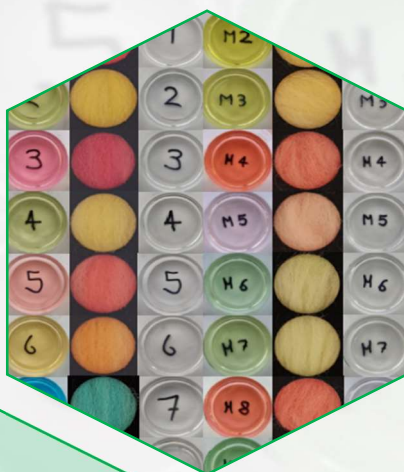
ABSTRACT

The use of all kinds of additives, including dyes, is common in the preparation of food products. The analytical control of artificial food dyes, as azo dyes, is very relevant since these have been found that can produce some kinds of cancer, and attention deficit disorders and hyperactivity in children. Consequently, the maximum permitted concentration of these azo dyes in food is regulated by current legislation. Therefore, it is of interest to find simple and fast procedures for the control of these compounds. The aim of this study has been to determine the concentration of azo dyes in food samples by using the Arata-Possetto method, that extract the azo dyes employing natural wool, but with the novelty of taking a photograph with a smartphone of the dyed wool and relating its colour to the content of the dye in the food. The study of the extraction conditions of the dyes on wool has been carried out and the calibration line between standard solutions of dyes and the colour of the dyed wool was obtained. To compare the results obtained from the dyed wool image processing, the absorbance spectra of the solutions before their extraction were measured with a diode array spectrophotometer. The spectrophotometer and the image processing were employed to obtain the calibration line of each food dye. The analysis of food samples was carried out using both methods. The data statistical treatment shows that the results of both methods are comparable.

Keywords: Analytical Chemistry, Azo dyes, RGB, Smartphone.

1. Introduction

The "Food Safety Regulation" defines food additives as "any synthetic compound or natural substance added to food to improve its quality, colour, fragrance and flavour, or to enhance the preservation, freshness, and processing" (Sun et al., 2017). A colour additive is any dye, pigment or other substance that provides colour to food, drink, or to any other non-food applications, as in the textile industry; but any chemical that reacts with another substance and causes the appearance of colour could be considered as a colour additive too (Amchova et al., 2015). Food colourants can be classified according to origin, solubility and covering, being the distinction between soluble and insoluble substances the most widely used classification. At the same time, soluble colourants can be subdivided into natural and synthetic ones. The synthetic organic azo-dyes are the most employed in food industry because they have generally more intense and permanent colour than natural substances (Amchova et al., 2015). Chemical structures determine the colours, properties, and applications of dyes, and provide a rational basis for a classification of these compounds, thus allowing the colourants to be classified in categories depending on its chemical structure (Kiernan, 2001).

The authorization to use colourants in the food industry is subjected to a wide range of toxicity tests and strict legislative provisions in all developed countries. In the last decade, the toxicity of food additives, especially azo dyes ones, has been gaining attention (Amchova et al., 2015). Azo dyes are organic compounds with an azo group, which are pairs of nitrogen atoms double-bonded to each other, R-N=N-R', where R and R' are usually aromatic rings. Due to the presence of this azo bond and the aromatic substituents these compounds are quite stable and can produce vivid colours. Azo dyes were not classified as hazardous substances for many years as their toxicity was considered quite low. However, some azo dyes can cause chronic effects and have been found to be mutagenic or carcinogenic in laboratory rodents at a dose level of 200 to 1000 mg/kg body weight (Jiang et al., 2020). The current legislation set in the Commission Regulation (EU) No 1129/2011 of 11 November 2011 regulated the use of additives for different types of food products. It should be noted that in the Commission Regulation there are two classifications for dyes, *quantum satis* dyes and dyes with a legislated maximum concentration (LMC). Azo dyes belong to the last group. Table 7.1 shows some characteristics of different additives regulated in the Commission Regulation.

Table 7.1: Characteristics of different additives regulated in the Commission Regulation (UE) No 1129/2011 of 11 November 2011.

Additive	Category	Azo dye	Additive	Category	Azo dye
Curcumin (E100)	LMC	No	Sulphite-ammonia caramel (E150d)	Quantum satis	No
Riboflavin (E101)	Quantum satis	No	Brilliant Black BN (E151)	LMC	yes
Tartrazine (E102)	LMC	yes	Vegetable carbon (E153)	Quantum satis	No
Quinoline Yellow WS (E104)	LMC	yes	Brown HT (E155)	LMC	yes
Sunset Yellow FCF (E110)	LMC	yes	Alfa-, Beta- and Gamma-Carotene (E160a)	Quantum satis	No
Carminic acid (E120)	LMC	No	Annatto, Bixin, Norbixin (E160b)	Specific of the product	No
Azorubine (E122)	LMC	yes	Paprika extract (E160c)	Quantum satis	No
Amaranth (E123)	Specific of the product	yes	Lycopene (E160d)	Specific of the product	No
Ponceau 4R (E124)	LMC	yes	Beta-apo-8'-carotenal (E160e)	LMC	No
Erythrosine (E127)	Specific of the product	No	Lutein (E161b)	LMC	No
Allura Red AC (E129)	LMC	yes	Canthaxanthin (E161g)	Specific of the product	No
Patent Blue V (E131)	LMC	yes	Beetroot extract (E162)	Quantum satis	No
Indigo carmine (E132)	Specific of the product	No	Anthocyanins (E163)	Quantum satis	No
Brilliant Blue FCF (E133)	LMC	yes	Calcium carbonate (E170)	Quantum satis	No
Chlorophylls (E140)	Quantum satis	No	Titanium dioxide (E171)	Quantum satis	No
Copper Complexes of Chlorophyll (E141)	Quantum satis	No	Iron oxides (E172)	Quantum satis	No
Acid Green 50 (E142)	LMC	No	Aluminium (E173)	LMC	No
Plain caramel (E150a)	Quantum satis	No	Silver (E174)	LMC	No
Caustic sulphite caramel (E150b)	Quantum satis	No	Gold (E175)	LMC	No
Ammonia caramel (E150c)	Quantum satis	No	Litholrubine BK (E180)	LMC	yes

Due this legislated maximum concentration limit for dyes content in food it is interesting the development of analytical techniques for their quantification. Among the methods to measure food dyes content are capillary electrophoresis (Rovina et al., 2016. Siddiquee & Shafwanah, 2020. Yamjala et al., 2016), spectrometry (Siddiquee & Shafwanah, 2020. Yamjala et al., 2016) and liquid chromatography (Hu et al., 2019. Rovina et al., 2016. Siddiquee & Shafwanah, 2020. Yamjala et al., 2016). However, it is required a previous extraction of the dyes using techniques such as solid phase extraction (Rovina et al., 2016. Siddiquee & Shafwanah, 2020. Yamjala et al., 2016), liquid-liquid extraction (Liu et al., 2019. Rovina et al., 2016. Siddiquee & Shafwanah, 2020. Yamjala et al., 2016), cloud-point extraction (Liu et al., 2019. Rovina et al., 2016. Siddiquee & Shafwanah, 2020. Yamjala et al., 2016) or ultrasound-assisted extraction (Rovina et al., 2016. Siddiquee & Shafwanah, 2020. Yamjala et al., 2016). The Arata-Possetto method is based on a dye extraction into wool and their subsequent alkaline retro-extraction and further analysis. This procedure was described by Teodoro Cromberg in 1918 (Cromberg, 1918), and it consists of introducing the sample, that potentially containing azo dyes, in a porcelain capsule together with embroidery wool and then they are boiled by adding potassium bisulphate, or HCl. This procedure has been used to extract azo dyes in wine samples. The azo-dyes are retro-extracted in an alkaline media (Martinez, 2019). However, if the colour of the dyed wool could be correlated with the concentration of azo dye in the original sample, the retro-extraction step could be avoided, thus saving time and reagents, as well as reducing waste generation.

In recent works, determinations of colorants have been carried out using image devices, such as smartphones (Botelho et al., 2017; Saadati, 2021), scanners (de Sá et al., 2020; Sorouraddin et al., 2015; Vidal et al., 2018), and webcams (Francisco da Silva Neto et al., 2021). These works have focused on the analysis two-four azo-dyes, like Brilliant Blue FCF, Quinoline Yellow FCF, Tartrazine, Amaranth, Allura Red AC, Carmoisine, and Sunset Yellow.

The aim of our study has been to develop a method to determine the content of azo dyes in food samples by image processing of the dyed wool. Moreover, the selectivity of the wool for the extraction and its absorption capacity has been evaluated. On the other hand, a prediction model based on the colour of the dyed wool for calculating dye concentration in the original liquid samples has been developed.

2. Materials and Methods

2.1. Instrumentation

For the colorimetric determination of azo dye solutions, a Hewlett Packard model 8452A diode array spectrophotometer (Waldbronn, Germany) was used. For the extraction of dyes in the wool, a laboratory heat plate was employed. The samples were photographed under controlled illumination conditions inside a lighting booth using a Smartphone Samsung Galaxy S7 edge model SM-G935F with a 12.2 MP camera. The camera was used in professional mode with fixed parameters (ISO 50, 1/90 focal aperture, standard filter, and a white balance of 3900 K). The lighting booth was an expanded polystyrene box of 27.5 x 27.5 x 27.5 cm inside illuminated by a grid of 5700 K white LED lights distributed symmetrically on top (Figure 7.1).
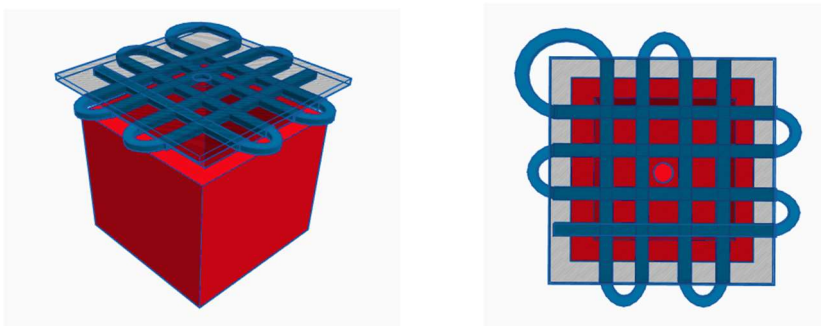
Figure 7.1: Scheme of the lighting booth. Red: expanded polystyrene box, Blue: LED lights strips illuminating inside the box, Transparent: methacrylate plate with a hole to make the photo.

2.2. Reagents

All solutions were prepared with analytical-grade chemicals and freshly distilled-deionized water. The food dyes Acid green 50, Allura Red AC (80 %), Amaranth, Brilliant Black BN, Chromotrope FB (Azorubine) (50 %), Erioglaucine (Brilliant Blue FCF), Erythrosin B, Indigo carmine, Ponceau 4R (75 %), Sunset Yellow FCF (90 %), Tartrazine (55 %), Patent Blue V sodium salt and Quinoline Yellow, were purchased from Sigma-Aldrich (Steinheim, Germany), 37 % ultratrace hydrochloric acid was obtained from Scharlau (Barcelona, Spain).

2.3. Samples

The natural wool and the different coloured food samples were obtained from haberdashery and local markets respectively. The samples analysed include confectionery products, flavoured drinks, ice creams, spirits, chewing gum, sauces, and different food dyes. The Table 7.2 collects the information about foods and the type of dye in each food sample.

Table 7.2: Samples analysed including a simple description and the food dye used in its formulation.

Sample	description	Food dye	Sample	description	Food dye
1	Red candy	Allura Red AC	14	Ice-cream	Brilliant blue FCF
2	Flavoured tonic	Allura Red AC	15	Vodka	Brilliant blue FCF
3	Flavoured tonic	Allura Red AC	16	Vodka	Allura Red AC
4	Sweet	Allura Red AC	17	Ice-cream	Azorubine
5	Sweet	Allura Red AC	18	Vodka	Azorubine
6	Sweet	Allura Red AC	19	Chewing gum	Brilliant Blue FCF
7	Sweet	Allura Red AC	20	Flavoured drink	Allura Red AC
8	Sweet	Allura Red AC	21	Food dye	Tartrazine
9	Food dye	Tartrazine	22	Flavoured drink	Brilliant Blue FCF
10	Sweet	Tartrazine	23	Ice-cream	Azorubine
11	Sweet	Tartrazine	24	Ice-cream	Tartrazine
12	Ice-cream	Tartrazine	25	Sauce	Ponceau 4R
13	vodka	Tartrazine	26	Flavoured drink	Brilliant Blue FCF

2.4.   Experimental design

2.4.1.   Dye Extraction

The proposed extraction method consists of taking 20 mL of a solution (standard or sample) containing the food dye, adding 200 µL of HCl 1 M and 0.25 g of natural lamb wool. The beaker with the solution and the wool is placed on a laboratory heat plate and stirred while heating. After boiling three minutes, the dyed wool is removed from the heated solution, washed with cold water and dried. Once the dyed wool is dry, the strands are mixed repeatedly by hand to homogenize the colour.

2.4.2.   Photograph of the dyed wool

The well-mixed strands of dyed wool are placed in a holder covered with a black velvet mask, with a circular window in the centre (Figure 7.2). This velvet mask is used to have a homogeneous black background that does not reflect the light. The holder containing the dyed wool is introduced into the lighting booth and the picture is taken, with the plane of the camera parallel to the sample, at a 30 cm height. Colour parameters of each picture were described by the RGB average values of the image inside the circular window mask and the correlations between dye concentration and the R/B, R/G and G/B ratios were used to obtain the calibration lines.

Figure 7.2: Real image of the wool in the holder.

3.   Results

3.1.   Extraction selectivity

To evaluate the extraction efficiency of the method for the different dyes, an extraction test was performed with individual standard solutions of the azo dyes containing Tartrazine (E-102), Allura Red AC (E-129) or Brilliant Blue FCF (E-133), to assess whether the wool might be able to extract all the dye from the solutions. For each dye, 30 mL of a 0.01 mM solution were prepared. 20 mL of the solutions were used to extract the dye on the wool and then obtain the spectra of the decoloured solutions. The other 10 mL was used to obtain the original UV-vis spectra of the coloured solutions. After the procedure, the original solutions were colourless and, in addition, the dyed wools did not lose colour after washing with water. Figure 7.3 shows the spectra of the three dyes used in the test and the respective solutions after extracting the dye from the wool, and as can be seen, they have been quantitatively extracted from the aqueous solution.
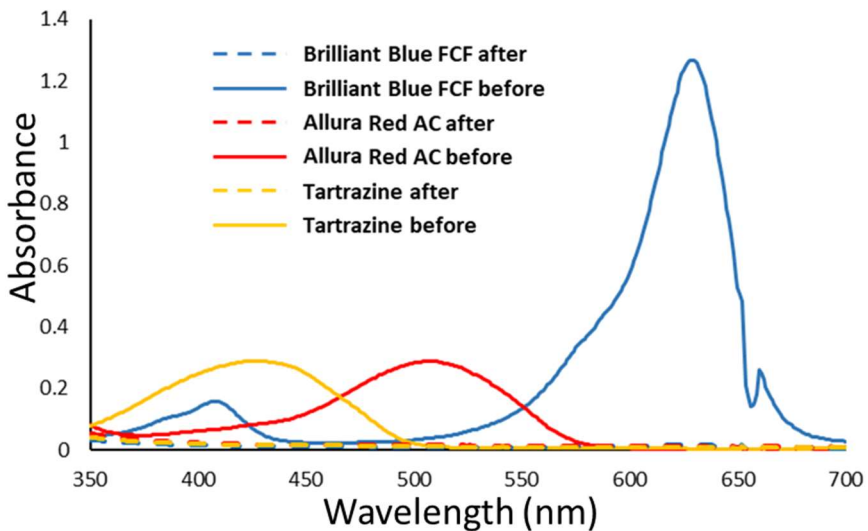
Figure 7.3: Absorbance spectra of three azo dyes standards before and after extraction by wool.

Since these three dyes were adequately extracted by the wool, the test was extended to other legislated dyes. The Figure 7.4 shows their individual absorption spectra, at a concentration of 0.01 mM, and the corresponding spectra of the solutions after the dye extraction process on the wool and, as can be seen, extractions close to 100 % are achieved in all cases.
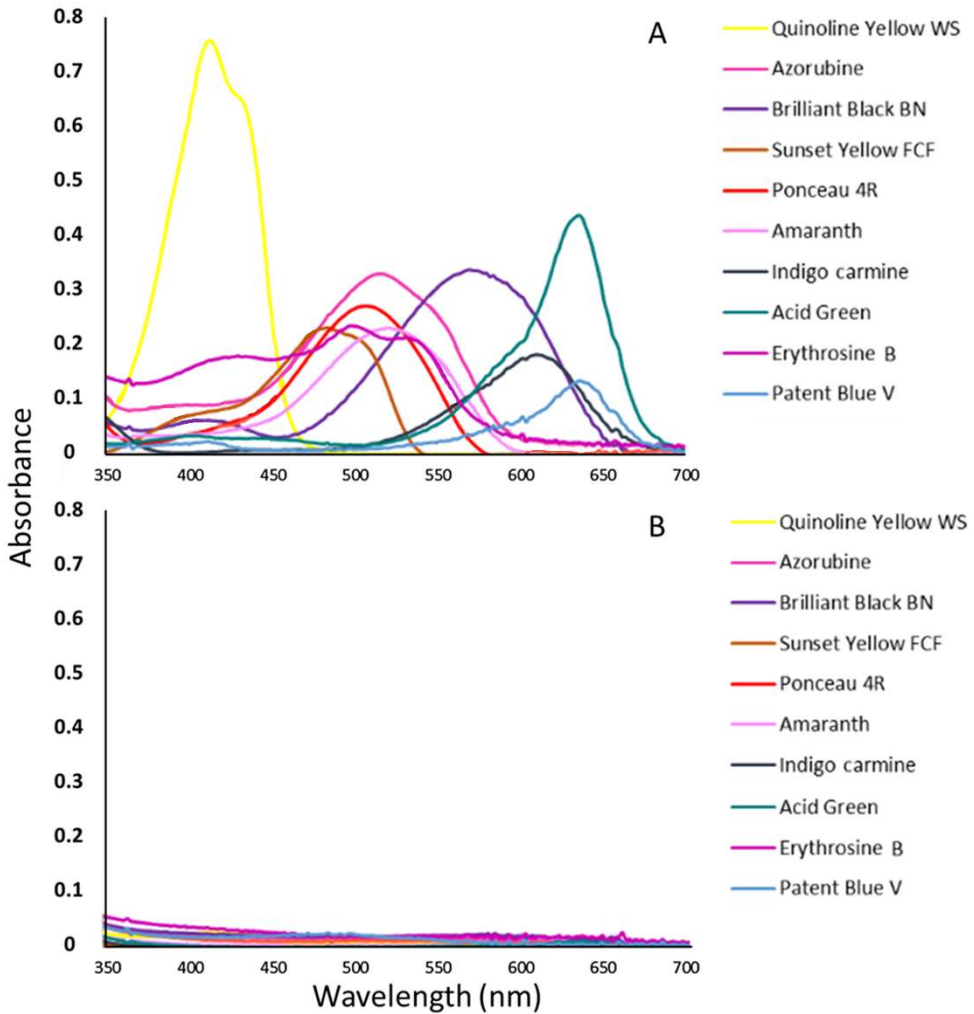
Figure 7.4: Absorbance spectra of different dyes (with a limited maximum concentration) before (A) and after extraction (B).

Although the original method (Cromberg, 1918) was proposed for the determination of azo dyes, we have observed that wool can extract other dyes, such as indigo carmine or erythrosine, and therefore, in this study the method has been extended to those dyes in which the legislation proposes a maximum concentration limit. Since wool can extract different dyes, it was tested whether would be able to extract dyes that were not limited to a maximum concentration. As it can be observed in the spectra presented in Figure 7.5, regard to foods with natural dyes, the extraction on the wool does not take place, since the spectra

before and after extraction have no significant differences, which proves that this extraction is only effective with synthetic dyes.
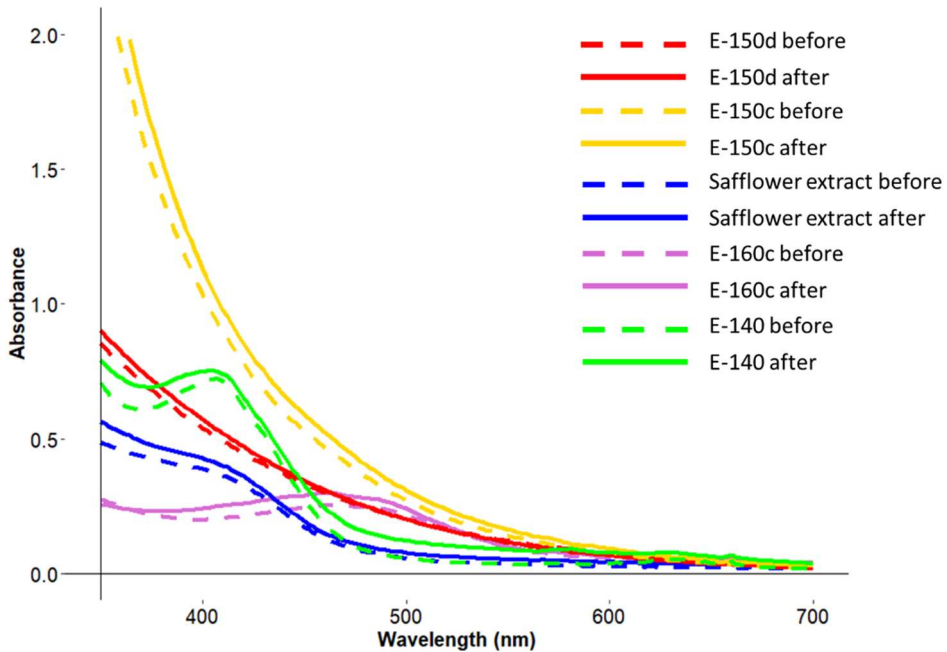
Figure 7.5: Spectra of food samples containing the specified food dye before and after extraction by wool.

3.2.   Study of extraction conditions

To evaluate the adequate conditions for the dyes extraction, the influence of three parameters were studied: the amount of lamb wool, the dye solution volume for extraction and the acid concentration employed.

3.2.1.   Effect of mass of lamb wool

In this experiment, the efficiency of dye extraction was studied using different quantities of wool (0.25. 0.50. 0.75 and 1.00 g). For each of the wool masses used, the extraction was carried out on calibration solutions of Ponceau 4R dye, with concentrations of 2, 5, 8 and 10 µM. To 20 mL of each standard solution, 0.5 mL of HCl 1 M were added, and the absorbance spectra were measured before and after the dye extraction process on the wool to check the remaining concentration of the dye in the decoloured solutions. Once the dyed wools were clean and dry, a picture of each one was taken to obtain the RGB parameters, and the correlations between R/G and R/B ratios versus the amount of dye added and versus µmol of dye per gram of wool were calculated. Ratio G/B does not provide a good correlation. The

Figures 7.6A and 7.6B show, for the same amount of dye in the original standard solution, that the R/G and R/B ratios decreases when increasing mass of wool. A greater sensitivity is obtained for smaller mass of wool, since the extracted dye does so on a smaller amount of wool. On the other hand, as can be seen in Figure 7.7, the values of the R/G and R/B ratios *versus* the amount of dye (µmol) per gram of wool are equivalent regardless the mass of wool employed. For a same amount of dye, the colour intensity is lower for a higher mass of wool meaning that the colour of this is proportional to the dye content but inversely proportional to the mass of wool.
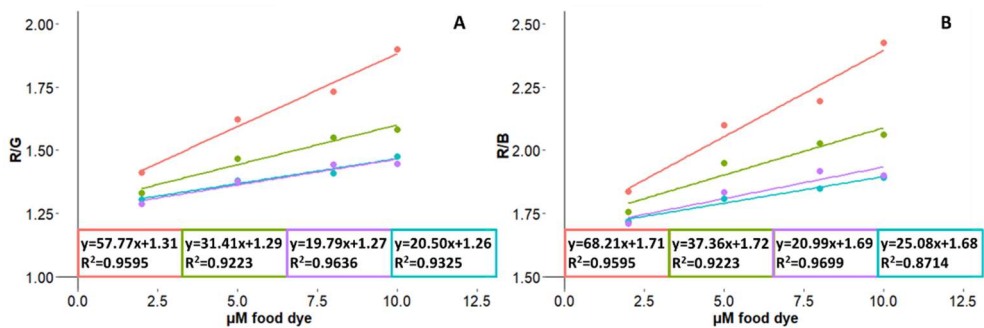
Figure 7.6: R/G and R/B values vs. concentration for different amounts of wool. Data have fitted by a linear model. 0.25 g of wool (orange); 0.50 g of wool (green); 0.75 g of wool (blue); 1.00 g of wool (purple).
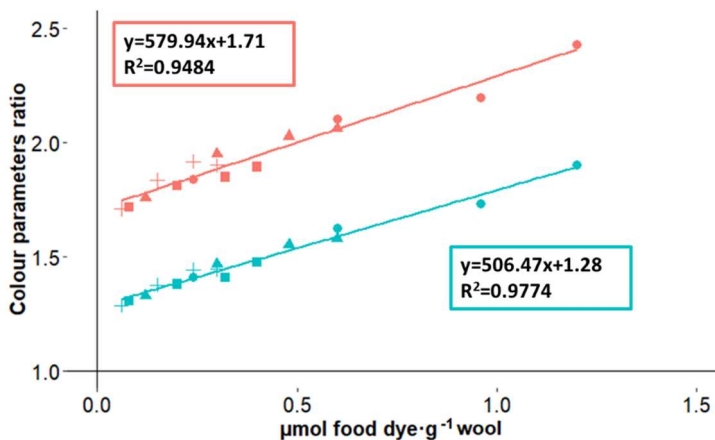
Figure 7.7: Linear relation of the average R/G (Blue) and R/B (Orange) ration versus the amount of dye per gram of wool. (●) 0.25 g; (▲) 0.50 g; (■) 0.75 g; (+) 1.00 g.

3.2.2.   Effect of dye solution volume

To carry out this study, three solutions of 20, 40 and 60 mL were prepared in triplicate from 2 mL of Ponceau 4R dye standard (0.2 mM) and 0.5 mL of HCl 1 M; and the dye was extracted by wool as procedure indicated before. In this case the same amount of dye is extracted from different volumes. Although the time required for extraction increases with the solution volume, it is easier to keep the wool submerged with a higher volume and the colour of the dyed wool is more homogeneous. However, longer extraction times give a greater dispersion of the results between the three replicates. Figure 7.8 shows that the ratios of the colour parameters are independent of the volume of the extracted solutions, which implies that the final wool colour is related with the net amount of dye (µmol) and not to the concentration of dye in the solution.
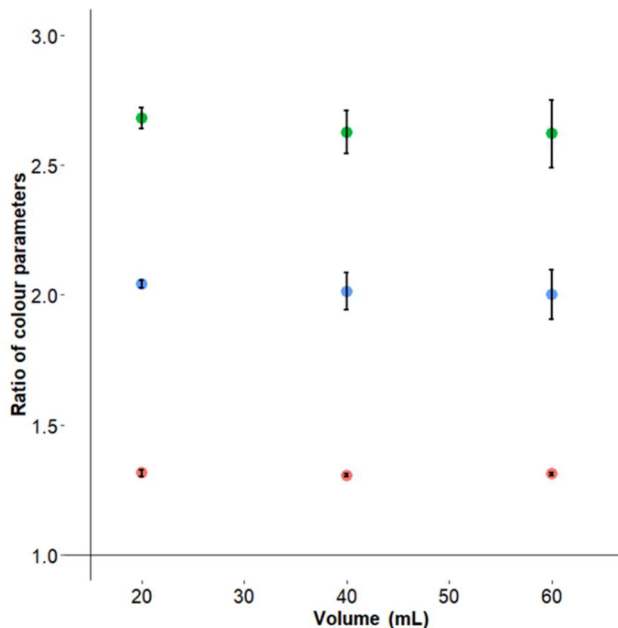
Figure 7.8: Colour parameters ratio for the different solutions and their standard deviations. Green: R/B; Blue: R/G; Orange: G/B.

3.2.3.   Effect of acid concentration

For this experiment, 5 solutions of 20 mL of a 0.02 mM Ponceau 4R dye standard were prepared. Later, different volumes of HCl 1 M (0, 0.1, 0.25, 0.5, 1 mL) were added to each solution and the dye was extracted. Figure 7.9 shows that for a successfully extraction it is necessary a slightly acidic medium. Moreover, an excess of acid does not influence on the colour of the wool.
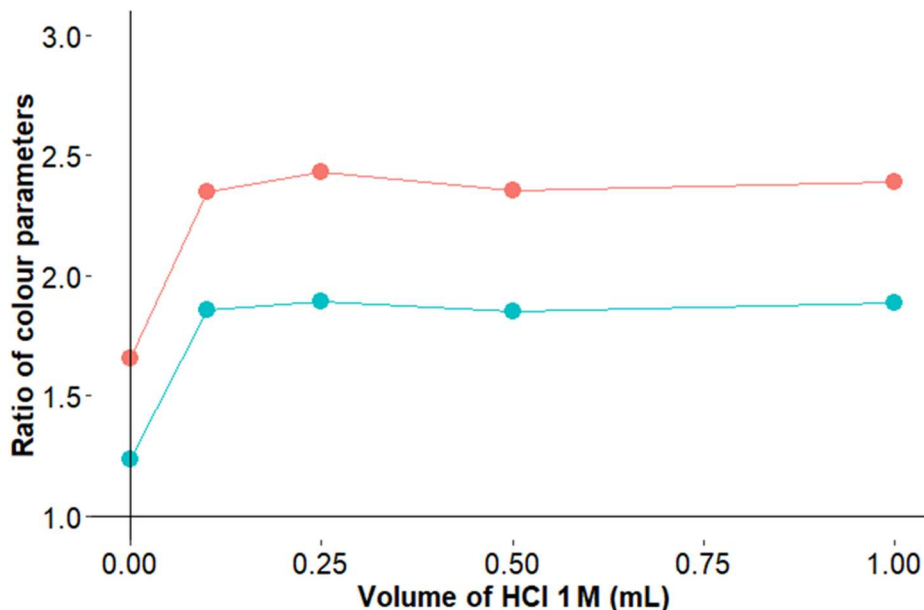
Figure 7.9: Ratio of colour parameters versus the volume of HCl 1 M used in the procedure. Orange: R/B; Blue: R/G.

After studying the effect of the different extraction process parameters, the most adequate conditions were 0.25 g of lamb wool, 20 mL of solution volume and 0.2 mL of HCl 1 M. Though changes in the first parameter do not significantly affects the results (Figure 7.7), a lower mass of wool was selected to get a more homogenous colour and higher sensitivity. The volume of HCl was selected to minimize the amount of reagent employed.

3.3. Calibration lines of dyes by UV-Vis and Smartphone

Once established the adequate extraction process, a calibration study of different dyes was made, with the final objective of knowing their concentration through the colour of a photograph taken with a smartphone of the dyed wool.

3.3.1. UV-Vis calibration line

UV-Vis spectroscopy has been employed as reference measure technique for the dyes analysis. Standard food dye solutions between 0.2 and 20 µM were prepared, their absorbance spectra were measured and the calibration lines, at the appropriates wavelengths, were established. Table 7.3 shows that there are a good R^2 for all dyes and the calibration line slopes varies from 111.92 to 788.80 (mM^{-1}).

Table 7.3: Parameters of the calibration line equation for the different dyes studied.

Dye	y-intercept	Slope (mM^{-1})	R^2	Wavelength (nm)
Acid Green 50	-0.0277	136.08	0.998	642
Allura Red AC	-0.0059	269.91	0.9990	502
Amaranth	-0.0339	232.22	0.9992	520
Azorubine	-0.0045	315.69	0.9993	515
Brilliant Black BN	-0.0115	628.61	0.98	570
Brilliant Blue FCF	0.0072	111.92	0.9998	630
Indigo carmine	-0.0201	173.33	0.998	612
Patent Blue V	-0.0418	344.23	0.9992	640
Ponceau 4R	-0.0115	286.79	0.995	506
Quinoline Yellow WS	-0.0058	788.80	0.9998	414
Sunset Yellow FCF	-0.0114	243.59	0.993	484
Tartrazine	0.0016	267.94	0.998	430

3.3.2. Smartphone calibration line

After dye extraction on the wool, the image processing of the dyed wool photo was carried out from the camera's RGB colour space information. Figures 7.10, 7.11 and 7.12 show the R/G, R/B and G/B colour parameter ratios of dyed wool photo *versus* µmol of dye per gram of wool. The figures only show the calibration line if the ratio provides a good one. Not all the ratios are suitable for all food dyes. The amount of dye that can be quantified by image processing varies with each one, as shown with the different slope of calibration lines, but all of them have a good R^2.
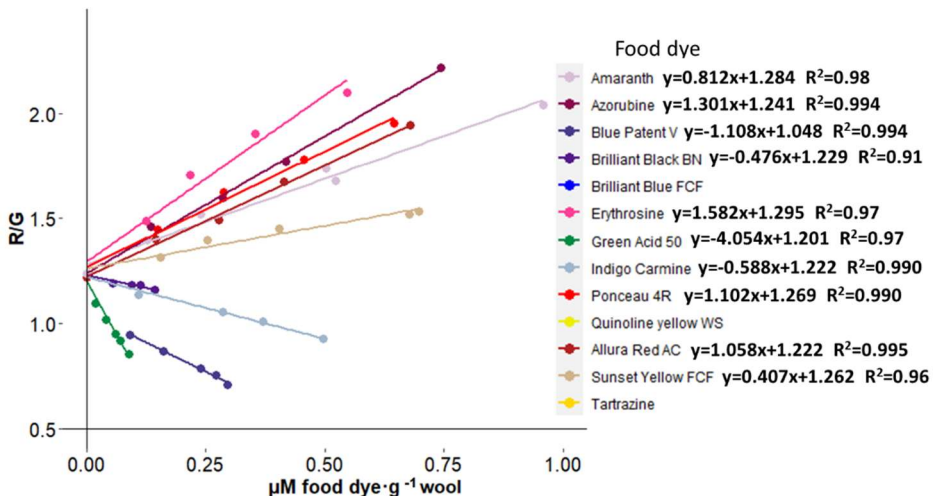
Figure 7.10: Calibration line obtained for each food dye using the R/G colour parameters ratio.
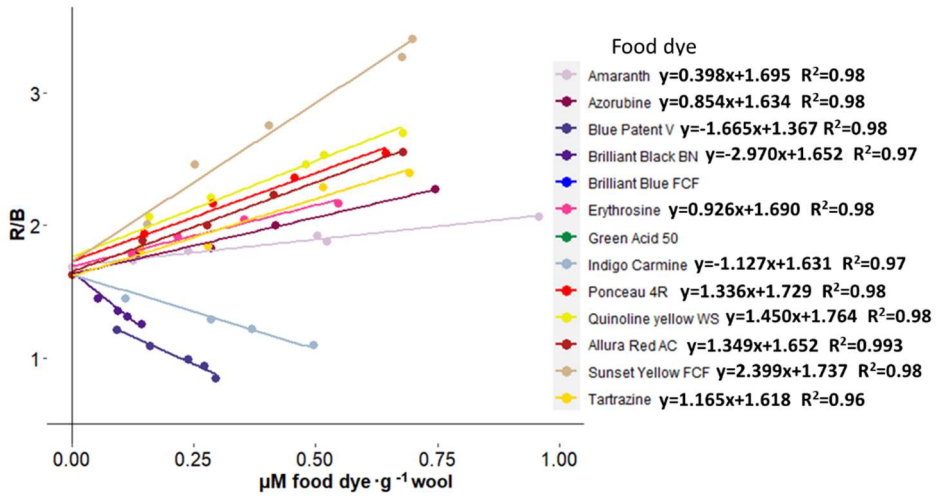
Figure 7.11: Calibration line obtained for each food dye using the R/B colour parameters ratio.
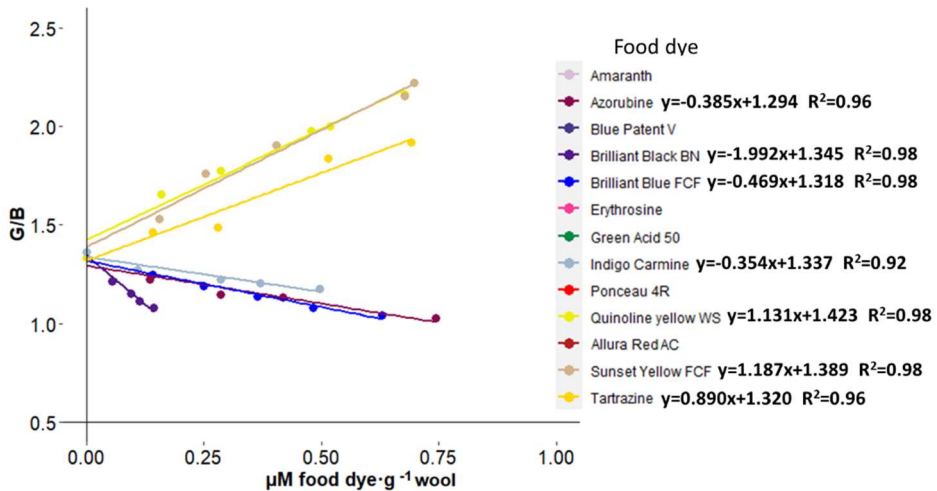
Figure 7.12: Calibration line obtained for each food dye using the G/B colour parameters ratio.

3.4.   Study of the dyed wool colour degradation

To check the colour stability of the dyed wool, a test was made to evaluate if the wool, once dyed, could be reuse in further days to avoid the preparation of new calibrations for each analysis. The dyed wool colour was measured on three different days, day = 0, day = 14 and day = 94, and the differences observed between colour parameters in these measurements were evaluated to check if there had been some change in colour with time. Table 7.4 shows the data, for Brilliant Blue FCF, Tartrazine and Allura Red AC, of the mean value of the relationships of the colour parameters, for each of the patterns measured in the three days, as well as their standard deviations and the relative standard deviations. As can be seen, the differences in all of them are less than 6.3 %, and in 93 % of the cases they are less than 5 %.

Table 7.4: Values of the mean, standard deviation, and RSD for the measure of dyed wool colour (0, 14 and 94 days).

Food Dye	Standard (µmol of dye g^{-1} of wool)	mean			Standard deviation			RSD %		
		R/G	R/B	G/B	R/G	R/B	G/B	R/G	R/B	G/B
Blank	0	1.216	1.616	1.330	0.013	0.028	0.010	1.1	1.7	0.7
	0.141	0.903	1.113	1.233	0.025	0.017	0.016	2.8	1.6	1.3
	0.250	0.740	0.881	1.191	0.007	0.006	0.004	1.0	0.7	0.3
Brilliant Blue FCF	0.365	0.586	0.663	1.133	0.028	0.028	0.005	4.7	4.3	0.4
	0.483	0.552	0.611	1.106	0.020	0.031	0.021	3.6	5.1	1.9
	0.630	0.443	0.470	1.062	0.007	0.006	0.017	1.7	1.3	1.6
	0.141	1.234	1.802	1.460	0.019	0.048	0.016	1.6	2.7	1.1
	0.279	1.243	1.952	1.570	0.007	0.091	0.071	0.5	4.7	4.5
Tartrazine	0.434	1.243	2.304	1.853	0.009	0.105	0.073	0.7	4.6	3.9
	0.514	1.237	2.234	1.805	0.015	0.075	0.040	1.2	3.4	2.2
	0.692	1.249	2.414	1.933	0.015	0.015	0.021	1.2	0.6	1.1
	0.145	1.376	1.827	1.328	0.037	0.075	0.018	2.7	4.1	1.4
	0.278	1.537	2.059	1.339	0.040	0.051	0.004	2.6	2.5	0.3
Allura Red AC	0.413	1.607	2.133	1.327	0.087	0.133	0.011	5.4	6.3	0.9
	0.528	1.710	2.243	1.311	0.012	0.039	0.015	0.7	1.7	1.1
	0.679	1.927	2.548	1.322	0.024	0.008	0.012	1.26	0.33	0.9

3.5.   Figures of merits of the proposed method

This study was carried out with three of the most used food dyes, Allura Red AC, Tartrazine and Brilliant Blue FCF. The calibration lines of each dye were carried out and the analytical parameters, like LOD and LOQ, recovery percentages and linear range of the method were evaluated. For each dye, the most appropriate relationship of the RGB parameters was selected. LOD and LOQ were obtained using LOD = 3 σ/s and LOQ = 10 σ/s where σ defined as standard deviation of the calibration line and s de slope of the this. The LOD for Allura Red AC, Tartrazine and Brilliant Blue FCF were 0.106, 0.035 and 0.048 µmol of food dye·g^{-1} of wool respectively; and the LOQ were 0.353, 0.117 and 0.160 µmol of food dye·g^{-1} of wool, respectively (for Allura Red AC the R/G ratio, for Tartrazine the R/B ratio, and for Brilliant Blue FCF the G/B ratio were employed). As can be seen in Table 7.5, the recoveries for spiked samples of sweet (Allura Red AC), food dye (Tartrazine) and flavoured drink (Brilliant Blue FCF) were quantitative, with percentages from 99 to 106 %.

Table 7.5: Recovery percentage for the food dyes.

Allura Red AC

	Amount of dye in the solution (µmol)	Mean (µmol)	Added (µmol)	Recovery (%)
Sample (sweet)	0.055			
	0.070	0.056		
	0.044			98.9
Spiked sample	0.091			
	0.107	0.096	0.040	
	0.090			

Tartrazine

	Amount of dye in the solution (µmol)	Mean (µmol)	Added (µmol)	Recovery (%)
Sample (food dye)	0.093			
	0.104	0.099		
	0.100			100.6
Spiked sample	0.134	0.139	0.040	
	0.144			

Brilliant Blue FCF

	Amount of dye in the solution (µmol)	Mean (µmol)	Added (µmol)	Recovery (%)
Sample (flavoured drink)	0.060			
	0.065	0.060		
	0.055			106.6
Spiked sample	0.101	0.102	0.042	
	0.104			

Table 7.6 collect the LOD and LOQ of each food dye using the different colour parameters ratio, and the linear range for the recommended ratio (bold face). The LOD, LOQ and linear range are expressed as µM, which belong to the concentration of food dye in the solution for extraction with wool (20 mL extracted on 0.25 g of wool according to proposed method). The LOD and LOQ could be modified if increasing/diminishing the mass of wool (larger wool mass provides lower slope increasing the LOD and LOQ values).

Table 7.7 summarises a comparison between methods where synthetic food dyes are measured by image treatment and the results obtained in the present work. As can be seen the proposed method provides lower LOD and LOQ then most of the methods, similar RSD additionally that has been tested for 12 food dyes.

Table 7.6: LOD and LOQ (µM in the solution of extraction) obtained using the proposed method.

	R/G		R/B		G/B		Linear Range
	LOD	LOQ	LOD	LOQ	LOD	LOQ	
Acid Green 50	**0.24**	**0.80**	0.44	1.45	4.16	13.88	0.80-1.25
Allura Red AC	**0.71**	**2.40**	0.84	2.80	6.95	23.15	2.40-16.67
Amaranth	**1.06**	**3.54**	0.71	2.37	1.15	3.83	3.54-6.67
Azorubine	**1.60**	**5.34**	2.93	9.76	2.34	7.79	5.34-16.67
Brilliant Black BN	0.74	2.48	**0.04**	**0.14**	0.18	0.59	0.14-1.67
Brilliant Blue FCF	2.30	7.68	2.34	7.78	**0.60**	**2.00**	2.00-16.67
Erythrosine B	**0.72**	**2.40**	0.76	2.52	2.24	7.46	2.40-5.00
Indigo carmine	**0.95**	**3.18**	1.78	5.91	2.48	8.26	3.18-6.67
Patent Blue V	**0.29**	**0.96**	0.58	1.91	2.34	7.79	0.96-3.50
Ponceau 4R	**1.08**	**3.58**	1.20	3.99	2.43	8.08	3.58-8.00
Quinoline Yellow WS	16.23	54.09	1.16	3.86	**1.09**	**3.64**	3.64-10.00
Sunset Yellow FCF	2.46	8.21	**1.48**	**4.91**	1.63	5.40	4.91-10.00
Tartrazine	7.83	26.00	**0.44**	**1.46**	1.10	3.66	1.46-16.67

Table 7.7: Comparison of analytical parameters of the proposed method with literature reported ones using image treatment for food dyes determination.

	Proposed method	Saadati (2021)	Sorouraddin et al. (2015)	Francisco da Silva Neto et al. (2021)	de Sá et al. (2020)	Vidal et al. (2018)	Botelho et al. (2017)
Instrument	SP	SP	SC	WC	SC	SC	SP
Data processing	NONE	NONE	NONE	NONE	NONE	PLS	N-PLS
Dyes Studied	12	4	4	4	1	2	1
RSD%	≤6.3	≤5.53	≤4.46	≤3.5	2.16	≤11.0	≤3.7
Linear Range (mg/L)	0.12-13.21	10-500	20-250	4-250	0.1-5.0	2.0-40	22.9-788
LOD (mg/L) (Range)	0.03-0.8	5.05-5.86	4.82-8.05	2-30	0.2	0.6-1.8	4.2
LOQ (mg/L) (Range)	0.12-2.68	15.55-17.73	16.06-26.84	NA	0.68	NA	NA

SP: Smartphone   // SC: Scanner   // WC: Webcam   // NA: Not Available

3.6.   Commercial samples

The method was applied to evaluate the content of dye in different commercial food samples with different matrix. The amount of dye predicted with the smartphone from the dyed wool photography was evaluated *versus* the concentration of dye in solutions obtained by using the spectrophotometer. As can be seen in Table 7.8 the results are comparable between both methodologies for 24 of the studied samples. The proposed method allows the quantification of food dyes even if the sample or the solution from sample are not transparent, which is not possible by spectrophotometry.

The food dye content found in all the samples is lower than the legislated maximum concentration.

Table 7.8: Concentration of dye predicted with the smartphone and measured with the spectrophotometer, specifying the food category and maximum allowed concentration of dye for this category.

Sample	Azo dye in the sample	Prediction with R/G ratio (ppm)	Prediction with R/B ratio (ppm)	Prediction with G/B ratio (ppm)	Spectrophotometer measure (ppm)	Food category[a]	Maximum allowed concentration[b]
1	Allura Red AC	132.8 ± 1.2	143.5 ± 1.4	-	135 ± 11	1 (5.2.)	300 mg/kg[8,9]
2	Allura Red AC	1.81 ± 0.11	1.8 ± 0.2	-	1.41 ± 0.04	2 (14.1.4.)	100 mg/L[9,10]
3	Allura Red AC	20.2 ± 1.5	20.1 ± 1.4	-	22.1 ± 0.4	2(14.1.4.)	100 mg/L[9,10]
4	Allura Red AC	72 ± 2	74 ± 1	-	52 ± 1	1 (5.2.)	300 mg/kg[8,9]
5	Allura Red AC	36 ± 7	35 ± 10	-	25.5 ± 0.7	1 (5.2.)	300 mg/kg[8,9]
6	Allura Red AC	147 ± 18	141 ± 21	-	-	1 (5.2.)	300 mg/kg[8,9]
7	Allura Red AC	87 ± 5	84 ± 11	-	54.8 ± 0.3	1 (5.2.)	300 mg/kg[8,9]
8	Allura Red AC	20 ± 3	16 ± 5	-	18.0 ± 0.3	1 (5.2.)	300 mg/kg[8,9]
9	Tartrazine	-	227 ± 31 ($\cdot 10^3$)	220 ± 31 ($\cdot 10^3$)	217 ± 17 ($\cdot 10^3$)	7	
10	Tartrazine	-	13.9 ± 2.2	13.6 ± 2.2	14.8 ± 0.5	1 (5.2.)	300 mg/kg[8,9]
11	Tartrazine	-	7.6 ± 2.2	7.3 ± 1.6	-	1 (5.2.)	300 mg/kg[8,9]
12	Tartrazine	-	87 ± 10	82 ± 10	79 ± 1	3 (3.)	150 mg/L[9,10]
13	Tartrazine	-	156 ± 24	152 ± 22	161 ± 1	4 (14.2.6.)	200 mg/L
14	Brilliant Blue FCF	-	-	23 ± 2	22 ± 1	3 (3.)	150 mg/L[9,10]
15	Brilliant Blue FCF	-	-	6 ± 5	6.4 ± 0.1	4 (14.2.6.)	200 mg/L
16	Allura Red AC	87 ± 2	86 ± 2	-	86 ± 1	4 (14.2.6.)	200 mg/L
17	Azorubine	36 ± 5	-	-	35.6 ± 0.7	3 (3.)	150 mg/L[9,10]
18	Azorubine	21 ± 2	-	-	19.9 ± 0.3	4 (14.2.6.)	200 mg/L
19	Brilliant Blue FCF	-	-	<LOD	0.9 ± 0.1	5 (5.3.)	300 mg/kg[9,10]
20	Allura Red AC	2.9 ± 0.4	2.8 ± 0.7	-	-	2 (14.1.4.)	100 mg/L[9,10]
21	Tartrazine	-	165 ± 10 ($\cdot 10^3$)	-	179 ± 8 ($\cdot 10^3$)	7	
22	Brilliant Blue FCF	-	-	4.2 ± 0.4	5.2 ± 0.1	2(14.1.4.)	100 mg/L[9,10]
23	Azorubine	28 ± 3	-	-	30 ± 1	3 (3.)	150 mg/L[9,10]
24	Tartrazine	-	76 ± 7	-	77 ± 1	3 (3.)	150 mg/L[9,10]
25	Ponceau 4R	25 ± 3	-	-	22 ± 1	6 (12.6.)	500 mg/L
26	Brilliant Blue FCF	-	-	4.4 ± 1.5	4.8 ± 0.1	2(14.1.4.)	100 mg/L[9,10]

[a]Food category:
In brackets the *code used in the Commission Regulation (UE) Nº1129/2011 of 11 November 2011*

1: Other confectionery products
2: Flavoured drinks
3: Ice-creams
4: Spirits
5: Chewing gum
6: Sauces
7: Food dyes

[b]Maximum allowed concentration:
8: Combined maximum limit of food dyes (except candied fruit and vegetables)
9: Amount of each dye E110, E122, E124 and E155 cannot overcome 50 mg/kg or mg/L
10: Combined maximum limit of food dyes

4.   Discussion

Nowadays, developed methods for the analysis of food dyes are based basically on HPLC. Although, the technique allows the analysis of several colourants simultaneously, food does not normally have more than two colourants, and most of them only contain one. Chromatographic methods have the disadvantage of using long times to perform the separation and analysis. In addition, they require the use of expensive equipment and relatively expensive reagents. The proposed method would only require the use of a slightly acidic medium (0.2 mL of HCl 1 M), a heating plate, natural sheep wool and water.

Given the nature of the method, several samples can be prepared simultaneously, greatly reducing the costs derived from the analysis and the time spent. The Smartphone proposed method allows the quantification of a great variety of colourants in different types of matrices. This method also allows an extraction and subsequent measurement of the dye in the sample at a very low cost, less than 10 cents for the analysis. Using the Smartphone method, we can discriminate which samples are within the legal limits, and which are not, within in a wide range of concentrations.

Only in those cases where the concentration is so close to the established limit, which is unusual for this type of food analysed and does not allow us to discriminate whether it is within the law or not, we would be forced to perform the quantification with other more accurate techniques, such as the HPLC.

5.   Conclusions

Regarding the efficacy of the Smartphone method and the conditions in which the extraction must be carried out, some aspects must be considered. The method works very well to extract synthetic colourants from food samples whereas natural colourants, are not extracted. In addition, the wool used for the calibration line can be used for long periods of time without producing colour degradation of the dyed wool.

The results show that the method has low limits of quantification, and quantitative recovery factors. There are relative standard deviations of around 10% in repeatability that increase when much lower concentrations are measured. Besides, this new simple and straightforward methodology is affordable, accurate and requires short times to analyse a vast banch of different food dyes, following the principles of Green Analytical Chemistry, and it also allows the analysis of

colourants in different types of matrices. Nevertheless, the main drawback is still the homogeneity of the dyeing of the wool which can lead to somewhat errors in the measurements. However, this disadvantage can be readily solved it out by studying the design of a wool support which allows an easy introduction into the solution and therefore a more homogeneous dyeing.

6.   References

Amchova, P., Kotolova, H., & Ruda-Kucerova, J. (2015). Health safety issues of synthetic food colorants. *Regulatory Toxicology and Pharmacology*, 73(3), 914-922. DOI: 10.1016/j.yrtph.2015.09.026.

Botelho, B. G., Dantas, K. C., & Sena, M. M. (2017). Determination of Allura red dye in hard candies by using digital images obtained with a mobile phone and N-PLS. *Chemometrics and Intelligent Laboratory Systems*, *167*, 44-49. DOI: 10.1016/j.chemolab.2017.05.004

Cromberg, T. (1918). Colorantes Artificiales en substancias alimentarias. Tesis. Facultad de ciencias Exactas y Naturales. Universidad de Buenos Aires. http://digital.bl.fcen.uba.ar/Download/Tesis/Tesis_0118_Cromberg.pdf.

da Silva Neto, G. F., de Andrade Rodrigues, M. L., & Fonseca, A. (2021). A new quantitative gel electrophoresis method with image-based detection for the determination of food dyes and metallic ions. *Talanta*, *221*, 121602. DOI: 10.1016/j.talanta.2020.121602.

de Sá, I. C., Feiteira, F. N., & Pacheco, W. F. (2020). Quantification of the food dye indigo carmine in candies using digital image analysis in a polyurethane foam support. *Food Analytical Methods*, *13*, 962-969. DOI: 10.1007/s12161-020-01715-5

EUR-Lex. (Accessed July 18, 2022). Commission Regulation (EU) No 1129/2011 of November 2011 amending Annex II to Regulation (EC) No 1333/2008 of the European Parliament and of the Council by establishing a Union list of food Additives Text with EEA relevance. https://eur-lex.europa.eu/legal-content/EN/ALL/?uri=celex%3A32011R1129.

Hu, Z., Qi, P., Wang, N., Zhou, Q. Q., Lin, Z. H., Chen, Y. Z., Mao, X. W., Jiang, J. J., & Li, C. (2020). Simultaneous determination of multiclass illegal dyes with different acidic–basic properties in foodstuffs by LC-MS/MS via polarity switching mode. *Food Chemistry*, 309, 125745. DOI: 10.1016/j.foodchem.2019.125745.

Jiang, L. L., Li, K., Yan, D. L., Yang, M. F., Ma, L., & Xie, L. Z. (2020). Toxicity assessment of 4 azo dyes in zebrafish embryos. *International Journal of Toxicology*, 39(2), 115-123. DOI: 10.1177/1091581819898396.

Kiernan, J. A. (2001). Classification and naming of dyes, stains and fluorochromes. *Biotechnic & Histochemistry*, 76(5-6), 261-278. DOI: 10.1080/bih.76.5-6.261.278.

Liu, W., Liu, J., Zhang, Y., Chen, Y., Yang, X., Duan, L., Dharmarajan, R., Wang, X., & Li, L. (2019). Simultaneous determination of 20 disperse dyes in foodstuffs by ultra high performance liquid chromatography–tandem mass spectrometry. *Food Chemistry*, 300, 125183. DOI: 10.1016/j.foodchem.2019.125183.

Martínez R. (2019). Análisis y optimización de la extracción de colorantes azoicos en vino para la detección de fraudes. Trabajo final de grado en Ciencia y Tecnología de Alimentos. Facultad de Ciencias. Universidad de Burgos. https://riubu.ubu.es/bitstream/handle/10259/5143/Mart%EDnez_Mart%EDnez.pdf;jsessionid=488AA9743CF4E03F18AA7C5C8B8B470E?sequence=1.

Rovina, K., Siddiquee, S., & Shaarani, S. M. (2016). Extraction, analytical and advanced methods for detection of Allura red AC (E129) in food and beverages products. *Frontiers in Microbiology*, 7, 798. DOI: 10.3389/fmicb.2016.00798.

Saadati, M. (2021). Smartphone-based digital image analysis for determination of some food dyes in commercial products. *Food Analytical Methods*, *14*(11), 2367-2374. DOI: 10.1007/s12161-021-02059-4

Siddiquee, S., & Shafwanah, A. M. S. (2020). Toxicology and analytical methods for the analysis of Allura red (E129) in food and beverage products: a current perspective. *Safety Issues in Beverage Production*, 18, 335-357. DOI:10.1016/b978-0-12-816679-6.00010-3.

Sorouraddin, M. H., Saadati, M., & Mirabi, F. (2015). Simultaneous determination of some common food dyes in commercial products by digital image analysis. *journal of food and drug analysis*, *23*(3), 447-452. DOI: 10.1016/j.jfda.2014.10.007

Sun, Q., Yang, L., Yang, J., Liu, S., & Hu, X. (2017). Study on the interaction between Rhodamine dyes and Allura Red based on fluorescence spectra and its analytical application in soft Drinks. *Analytical Sciences*, 33(10), 1181-1187. DOI: 10.2116/analsci.33.1181. PMID: 28993594.

Vidal, M., Garcia-Arrona, R., Bordagaray, A., Ostra, M., & Albizu, G. (2018). Simultaneous determination of color additives tartrazine and Allura red in food products by digital image analysis. *Talanta*, *184*, 58-64. DOI: 10.1016/j.talanta.2018.02.111.

Yamjala, K., Nainar, M. S., & Ramisetti, N. R. (2016). Methods for the analysis of azo dyes employed in food industry–a review. *Food Chemistry*, 192, 813-824. DOI: 10.1016/j.foodchem.2015.07.085.

Chapter 8: Quinine determination in different beverages by image treatment
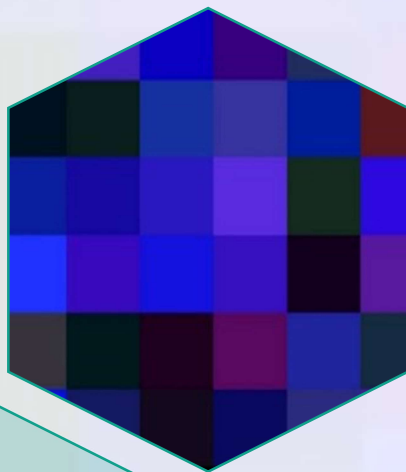
ABSTRACT

In this chapter, a method to quantify quinine in commercial samples of tonic by fluorescence with smartphone has been developed. The procedure implies only an ultraviolet flashlight (396 nm) as a light source, a polystyrene box as a booth light, a black plastic cover with an internal black velvet lining to place the measurement cell and a Smartphone. To ensure the reliability of the colorimetric measurements, the smartphone camera has been characterized using a colour chart and a spectroradiometer. The analysis of 14 samples of tonic water with different characteristics: I) normal; II) with dyes; III) with a special matrix; IV) with alcohol, have been carried out. The fluorometric measurement of the solutions with a bench instrument has been used as the reference method. The image treatment to quantify quinine has provided results comparable to those obtained with the fluorimeter. In some samples of tonic water, it is possible to observe that the measurements with smartphone did not present the matrix effect shown in the fluorimeter for samples with a special matrix (hibiscus, pink pepper, lime, lemon). The smartphone proposed method provides a LD of 0.92 and a LQ of 3.06 mg/L.

Keywords: Smartphone, Quinine, Analytical Chemistry, CIELab, Tonic, Gin Tonic, Fluorimetry.

1.   Introduction

Quinine sulphate or quinine chlorhydrate is a natural quinoline alkaloid extracted from the Cinchona bark (Semedo et al., 2022). The antimalarial properties of quinine are well recognized, but in recent years it has been used extensively by the cosmetic industry and especially as a flavouring agent in soft drinks (Lefrère et al., 2021). It is most often added to non-alcoholic carbonated beverages, commonly known as tonic water, for a characteristic bitter taste (Rudnicki et al., 2021)

Despite the variety of therapeutic benefits that this alkaloid has (analgesic, antipyretic and antimalarial), its excessive use causes health complications. A typical side effect of quinine is called cinchonism and can be mild at therapeutic doses or severe at high doses. The toxic effects of quinine involve the gastrointestinal tract and the nervous and cardiovascular systems (Freund et al., 2020). It has been linked to several cases of sudden death since it relaxes muscles such as the heart. Its toxic effects appear to be related to high plasma concentrations. As a result, some countries, mandate that soft drinks containing quinine must be declared on the food label. In United States, quinine sulphate has been removed from the market in 2006 due its adverse events including deaths (Ashley, 2018).

The European Food Safety Authority (EFSA) has established new standards that govern the labelling of quinine in beverages and food, so it is necessary to clearly indicate the presence of quinine to the consumer in the list of ingredients (EFSA, 2015). Drinks called tonic waters and non-wine bitters may contain quinine in a maximum quantity of 100 milligrams per litre. This restriction occurs both for flavourful substances (those ingredients capable of conferring characteristic flavours to the beverages that contain them), in flavoured soft drinks, extract soft drinks and in fruit disintegrated soft drinks (BOE, 1992).

There is a great variety of techniques that have been used for its determination, such as high-performance liquid chromatography (HPLC) (Kudláček et al., 2017), capillary electrophoresis with UV detection (Mikus et al., 2011), fluorimetry (Nikolaeva et al., 2019), gas chromatography (Roberson et al., 2020) and electrochemical detection (Rudnicki et al., 2021).

Molecular fluorescence is a widely used analytical method, due to the extreme analytical sensitivities achieved in many cases (Zhou et al., 2021), used in the identification and quantification of many environmentally important compounds such as polycyclic aromatic hydrocarbons. Different studies show that quinine has a fluorescence signal in a medium of 0.05M H_2SO_4, with two analytical useful

excitation wavelengths, 250 and 350 nm. Regardless of which excitation wavelength is used, the maximum fluorescence emission wavelength is 450 nm (Nikolaeva et al., 2019).

Bearing that there are countries that don´t have resources to acquire advance instrumentation, the new technologies offer intelligent and simple solutions to ensure the security of water and food (Ayala et al., 2012, Vidal et al., 2020), and recently a lot of devices have been developed, from light booths until systems coupled to smartphone through the informatics interfaces (Fan et al., 2021, Kanchi et al., 2018, Vidal et al., 2020).

The main objective of this work is the development of a method for the fluorometric determination of quinine using a characterised smartphone as a sensor. The proposed method will be applied to the analysis of samples of commercial tonic waters with different matrices and characteristics: normal tonics, tonics with dyes, tonics with a special matrix and tonics with alcohol.

2. Materials and Methods

2.1. Instrumentation

Quinine determination by reference method was carried out with a Fluorimeter (Jasco, Japan). To perform the measure by image treatment a smartphone Samsung Galaxy s/Edge model SM-g935F was employed. To standardize the measure, the pro-mode of the camera was employed with fixed conditions of ISO 125, 1/F 1/45, colour temperature of 5900 K and a zoom of 1.2. To carry out the characterization of the smartphone a spectroradiometer SpectraScan PR655 Photo Research (EEUU) was used. A flashlight with nine 396 nm LEDs were employed to perform the quinine analysis by image treatment.

2.2. Reagents

A solution of 151.7 mg/L of quinine sulphate hydrate (Guinama, Valencia, Spain) was prepared for standard calibration line. Sulfuric acid 95-97 % (Scharlau, Sentmenat, Spain) was used to provide the acid medium. Absolut ethanol (Scharlau, Sentmenat, Spain) was used to perform studies of the ethanol effect on the fluorescence measure.

2.3.   Experimental design

2.3.1.   Tonic water samples

Fourteen commercial beverages with different types of matrices were purchased and analysed. Table 8.1 collect the information of the samples. Samples were filtered and degassed in an ultrasounds bath for 15 minutes before analysis.

Table 8.1: Characteristics of the different tonic water samples studied.

Normal Tonics	Tonics with food dyes	Tonics with special matrix	Tonics with ethanol
A: Brand 1	F: Brand 2 - pink	H: Brand 2 - lime	L: Brand 5
B: Brand 2		I: Brand 2 - lemon and quinine	M: Brand 6
C: Brand 3		J: Brand 2 - pink pepper	
D: Brand 1 sugar free	G: Brand 1 - Blue		N: Brand 6 - pink
E: Brand 4		K: Brand 2 - hibiscus	

2.3.1.   Smartphone characterization

In this work a self-luminous analyte is studied, for that to ensure the reliability of the measure it is necessary to find a relation between the luminous stimulus obtained with the smartphone and the real colour of the light. When an image treatment is made to carry out an analysis it is necessary to fix the light conditions. In this case the light conditions are controlled by the analyte, for that it is not possible to fix them. To avoid variations in the measure due to the light detected from the sample by the smartphone, a characterization of the camera is performed. This characterization was carried out with a colour chart created in a computer screen with a Matlab script (Figure 8.1); being necessary that the chart be self-luminous. For the colour chart a range of colours with a R normalized values between 0-0.3, a G normalized values between 0-0.15 and a B normalized values between 0-0.8 were selected. The 162 colours created were measured by the spectroradiometer and the smartphone in a dark room. The smartphone was placed 15 cm away from the screen. The relation between the RGB values of the images and the XYZ tristimulus values obtained by the spectroradiometer were rendered to create a smartphone characterization model by using ColorLab (Malo & Luque, 2002) Matlab library. The model created is based on a 5-grade polynomial.
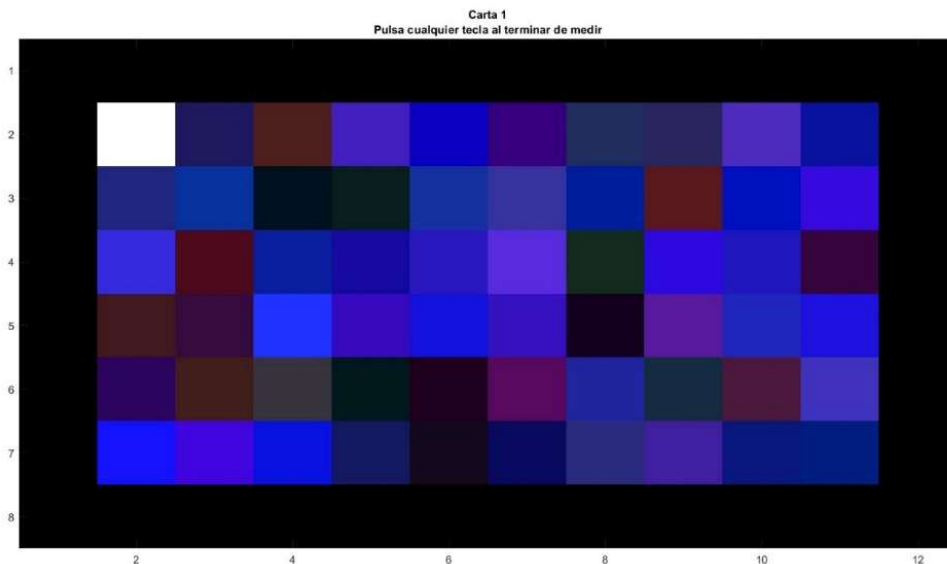
Figure 8.1: One of the colour charts used to make the Smartphone characterization.

2.3.3. Reference method.

A calibration line between 0 and 3.5 mg/L of quinine was measured by using a fluorimeter. The measure conditions were bandwidth of 5 nm for excitation and emission windows, and excitation wavelength of 350 nm and emission wavelength of 450 nm.

2.3.4. Determination by smartphone.

10 mL vials were filled with the calibration standards and the sample solutions. Solutions between 0 and 15 mg/L of quinine were employed as standards calibration. They were placed over the flashlight inside the polystyrene box in a dark room. The smartphone was placed at the same height that the vial at 15 cm away. The vial is covered with a 3D printed dull black PLA cover with an internal black velvet lining and two holes to collect the fluorescence. The Figure 8.2 shows how to perform the smartphone measure.

Figure 8.2: Set-up to take the fluorescence measure by smartphone.

3.   Results and Discussion

3.1.   Light source stability

To evaluate how much time, it is possible to work with the flashlight without light loss intensity, images of a 15 mg/L solution of quinine have been collected each minute for one hour in three consecutive days. Due it is working with fluorescence intensity, the parameter L* of CIEL*a*b* colour space has been studied. In this study the parameter L* is stable for 90 min, providing a L* value of 37 ± 3 (n = 90). Although the flashlight is stable for 90 minutes, to standardize the measurement procedure, the flashlight is going to be full charge at the beginning of each work session.

3.2.   Cover study

To avoid possible reflections inside the vial, different types of cylindrical covers for the vial has been studied. The cover is 3D printed with dull black PLA, being a cylinder with one or two facing holes. Moreover, an internal coating of black velvet that reduce the shines and reflections have been studied. Figure 8.3 shows the different cylindrical covers studied.
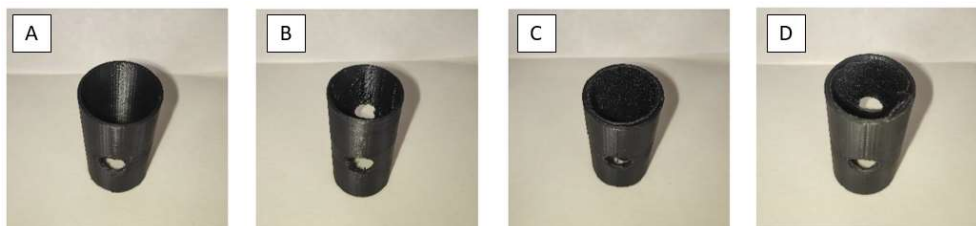
Figure 8.3: Different covers used to take the measure. A) Only one hole and without internal covering, B) Two faced holes and without internal covering, C) Only one hole and with internal velvet covering, D) Two faced holes and with internal velvet covering.

A calibration line between 0 and 15 mg/L of quinine has been measured with each cylindrical cover. The Table 8.2 summarises the data obtained for each calibration line. The best correlation is obtained when internal velvet covering is employed, selecting for that two holes.

Table 8.2: Linear regressions obtained with different cylindrical covers.

Cover	Equation	R^2
Without cover	y = 1.3607x + 3.4026	0.992
Without internal covering - 1 hole	y = 1.8474x − 3.3884	0.987
Without internal covering - 2 holes	y = 1.6298x − 2.5976	0.990
With internal covering - 1 hole	y = 1.3608x − 1.2417	0.997
With internal covering - 2 holes	y = 1.6542x − 3.3409	0.998

3.3. Method characteristics

The Table 8.3 shows the results for the LOD and the LOQ obtained for the fluorometric determination (reference method) and the smartphone measure using the cover with internal velvet and 2 holes. The LOD and LOQ are calculated using the slope deviation.

Table 8.3: Analytical parameters of the new and the reference method.

	Fluorimetry	Smartphone
slope	282.76	1.13
Interception point	-0.64	-2.24
LOD_{inst} (mg/L)	0.12	0.61
LOQ_{inst} (mg/L)	0.40	2.02
R^2	0.999	0.998

3.4. Matrix interference study

For normal tonic water samples there are not significant differences between the slopes from the external calibration and standard addition method, which are 280±3 and 278±5, respectively. A significance test for a paired experiment between the results obtained for the samples using the external and the standard addition method provides a confidence interval for the mean (95 %) of [-1.03; 0.08] (that includes 0) a p-value of 0.083 (0.083> 0.05) and a computed t statistic of -1.98 (1.98< 2.75 [$t_{0.025,8}$]), proving that there is not a matrix effect when normal tonic waters are analysed. This effect is not present in the smartphone measure either (Figure 8.4)
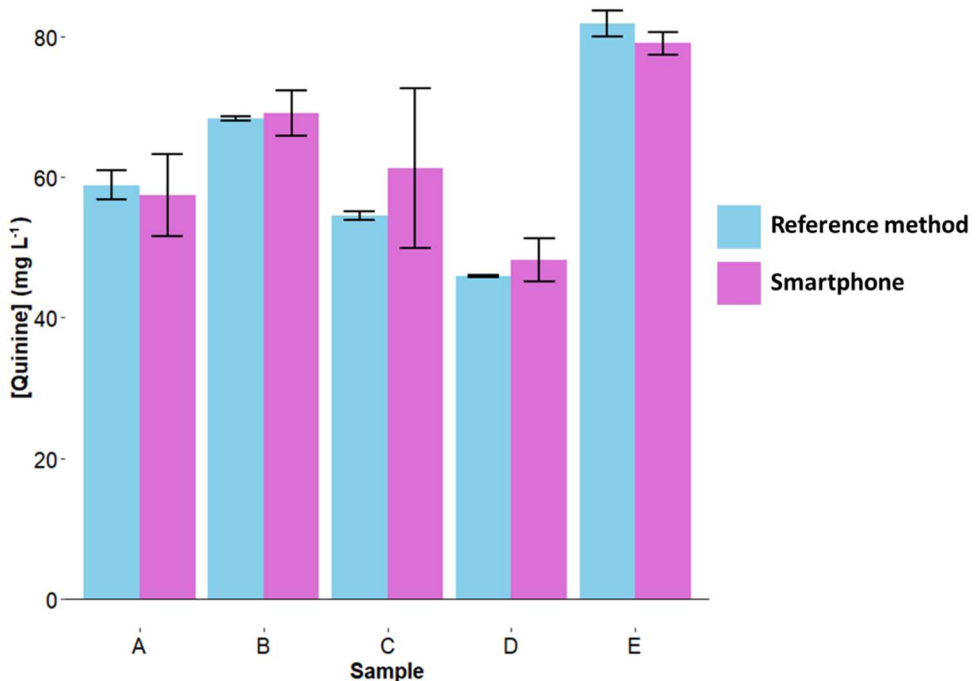
Figure 8.4: Comparison between the results obtained with the fluorometric reference method and the smartphone method for the quinine content in normal tonic waters samples.

Tonics with food dyes have a very low amount of quinine, lower the LOD of the smartphone method, being only possible to study the matrix effect employing the fluorometric reference method. The results show that the slope obtained from the standard addition method for the samples F and G are a 36 and a 76 %, respectively, respect the slope obtained with the external calibration, which makes evident that food dyes have an interference effect in the fluorometric measure and the quinine determination requires standard addition method.

Tonics with special matrix (containing lime, lemon, pink pepper or hibiscus) present a matrix effect by fluorometric reference method, obtaining slopes of standard addition method between 19-87 % of the external calibration one, interference effect that depends on the type of vegetable extract comprised in the drink. Of these samples, two of them (sample I and K) have a content of quinine lower the LOD of the smartphone method, employing the other two for the matrix effect study. Figure 8.5 shows that the smartphone provided the same concentration by external calibration than the result obtained by standard addition method using the fluorometric reference method, proving there is not matrix effect by smartphone measure.
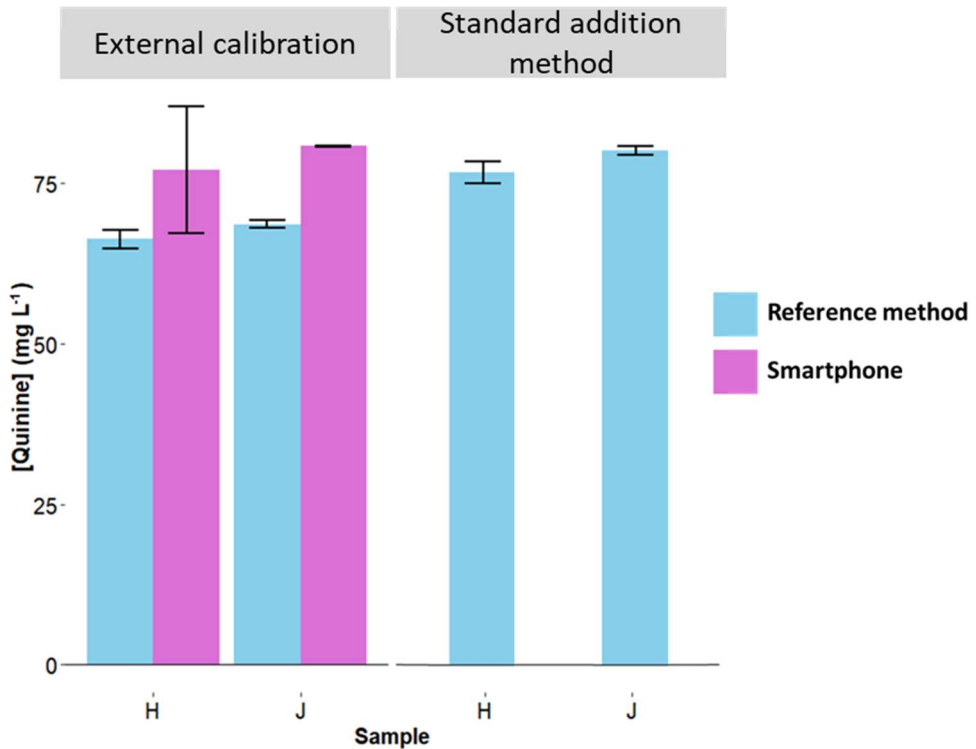
Figure 8.5: Comparison between the results obtained with the fluorometric reference method and the smartphone method for the quinine content in tonic waters samples containing vegetal extracts.

By last, the ethanol content effect in the sample was studied comparing the calibration line obtained in a medium with ethanol (at the same level as in these type of drinks) and sulfuric acid (sulphuric 0.05 M and ethanol 6.5 %) with the calibration line obtained in sulfuric medium (sulphuric 0.05 M), checking that there are not differences between them, with equations of Y = 284x + 8 (R^2= 0.9994) and Y = 285x + 8 (R^2= 0.9997), respectively. The ethanol does not have a matrix effect in both the fluorometric and smartphone measure of quinine. From the three samples of gin-tonic, one of them (sample L) has a content of quinine lower than LOD of both methodologies, and another one (sample N) additional to ethanol contains a food dye requiring the use of standard addition method due to the interference effect of the food dyes on the quinine determination for both methodologies.

3.5. Sample analysis

Table 8.4 summarises the analysis carried out with both methods, as can be seen the results are comparable between them. We can find tonic samples with the normal content of quinine (45.9 to 83 mg/L) and special drinks with low

concentrations (< 6.8 mg/L) included any drink with not detected. The type of calibration employed has been specified in the table, the fluorometric measure by the reference method requires standard addition method for drinks containing food dyes or vegetal extracts, otherwise using the smartphone the matrix effect happens only if food dyes are present in the drink.

Table 8.4: Quinine content in different samples obtained by both methods indicating the type of calibration employed, expressed as mean± standard deviation in mg/L.

	Matrix type	Reference method	Smartphone
A	Normal	59±2[a]	57±6[a]
B	Normal	68.3±0.3[a]	69±3[a]
C	Normal	54.5±0.6[a]	61±11[a]
D	Normal	45.9±0.2[a]	48±3[a]
E	Normal	82±2[a]	79±2[a]
F	Food dye	1.84±0.01[b]	<LOD
G	Food dye	0.18±0.01[b]	<LOD
H	Vegetable extract	77±2[b]	77±10[a]
I	Vegetable extract	6.81±0.03[b]	<LOD
J	Vegetable extract	82±2[b]	80.7±0.1[a]
K	Vegetable extract	1.92±0.01[b]	<LOD
L	alcohol	<LOD	<LOD
M	alcohol	54.8±0.2[a]	57±7[a]
N	Alcohol; Food dye	78±2[b]	83±9[b]

a: result obtained employing the external calibration.
b: result obtained employing the standard addition method.

4.   Conclusions

In this chapter a new method to determine quinine in tonic water samples using a smartphone have been developed. In order to work with a fixed conditions, the characterization of the smartphone is required. Due in this case the luminescence must be registered a self-luminous colour chart from the laptop screen has been employed to create a polynomial model of grade 5 for the characterization.

Using only a smartphone, a little photo booth, a flashlight, and a cylindrical cover for the vial it is possible to carry out an analysis of quinine. Smartphone method present less sensitivity, with higher LOD and LOQ as compared with fluorometric reference method, but the LOQ = 2.0 mg/L is adequate and is much lower than 100 mg/L the maximum level allowed in drinks. In addition, smartphone measure is less prone to matrix effect interference. Again, in this chapter it is shown the potential of a smartphone to perform chemical analysis due it is very simple and low-cost instrument obtaining comparable results to the reference method.

5. References

Ashley, D. D. (2018). Clarifying misconceptions about US food and drug administration unapproved drugs program. *Anesthesia & Analgesia*, 127(6), 1292-1294. DOI: 10.1213/ANE.0000000000003852

Ayala, A., Leal, L. O., Ferrer, L., & Cerdà, V. (2012). Multiparametric Automated System for Sulfate, Nitrite and Nitrate Monitoring in Drinking Water and Wastewater Based on Sequential Injection Analysis. *Microchemical Journal*, 100, 55-60. DOI: 10.1016/j.microc.2011.09.004.

BOE. (1992). «Real Decreto 15/1992, de 17 de enero, por el que se aprueba la Reglamentación Técnico-Sanitaria para la Elaboración, Circulación y Venta de Bebidas Refrescantes». 17 January, 1992. BOE-A-1992-1726.

EFSA. (2015). Panel on Food Contact Materials, Enzymes, Flavourings and Processing Aids (CEF). Scientific Opinion on Flavouring Group Evaluation 35, Revision 1 (FGE.35Rev1): Three Quinine Salts from the Priority List from Chemical Group 30. *European Food Safety Authority Journal*, 13(9), 4245-4282. DOI: 10.2903/j.efsa.2015.4245.

Fan, Y., Li, J., Guo, Y., Xie, L., & Zhang, G. (2021). Digital Image Colourimetry on Smartphone for Chemical Analysis: A Review. *Measurement*, 171, 108829. DOI: 10.1016/j.measurement.2020.108829.

Freund, P. R., Wright, T., & Margolin, E. A. (2020). Toxic optic neuropathy from quinine overdose. *Journal of Neuro-Ophthalmology*, 40(2), 258-261. DOI: 10.1097/WNO.0000000000000865

Kanchi, S., Sabela, M. I., Mdluli, P. S., Inamuddin, & Bisetty, K. (2018). Smartphone Based Bioanalytical and Diagnosis Applications: A Review. *Biosensors and Bioelectronics*, 102, 136–149. DOI: 10.1016/j.bios.2017.11.021.

Kudláček, K., Nesměrák, K., Štícha, M., Kozlík, P., & Babica, J. (2017). Historical injection solutions of quinine analyzed by HPLC/MS. *Monatshefte Für Chemie-Chemical Monthly*, 148, 1613-1618. DOI: 10.1007/s00706-017-1940-x

Lefrère, B., Barbaud, A., Bagot, M., & Bourgogne, E. (2021). Tonic water and quinine-a bicentennial booming cocktail. *Revue Francaise D'allergologie* (2009), 61(6), 425-431. DOI: 10.1016/j.reval.2021.04.002

Malo, J., & Luque, M. J. (2002). ColourLab: the Matlab toolbox for Colourimetry and Colour Vision. Univ. Valencia. http://isp.uv.es/code/visioncolour/colourlab.html.

Mikus, P., Maráková, K., Veizerová, L., & Piešťanský, J. (2011). Determination of quinine in beverages by online coupling capillary isotachophoresis to capillary zone electrophoresis with UV spectrophotometric detection. *Journal of Separation Science*, 34, 3392–3398. DOI: 10.1002/jssc.201100633

Nikolaeva, A. A., Korotkova, E. I., & Lipskikh, O. I. (2019). Determination of quinine in drugs and beverages by fluorimetric method. *Вестник Карагандинского университета. Серия: Химия*, (2), 56-61. DOI: 10.31489/2019Ch2/56-61

Roberson, Z. R., Gordon, H. C., & Goodpaster, J. V. (2020). Instrumental and chemometric analysis of opiates via gas chromatography–vacuum ultraviolet spectrophotometry (GC-VUV). *Analytical and Bioanalytical Chemistry*, 412, 1123-1128. DOI: 10.1007/s00216-019-02337-5

Rudnicki, K., Sobczak, K., Borgul, P., Skrzypek, S., & Poltorak, L. (2021). Determination of quinine in tonic water at the miniaturized and polarized liquid–liquid interface. *Food Chemistry*, 364, 130417. DOI: 10.1016/j.foodchem.2021.130417

Semedo, M. G., Pereira, A. L., & Pita, J. R. (2022). Cinchona bark and quinine in the Portuguese official pharmacopoeias (1794–2001). Die Pharmazie-An International *Journal of Pharmaceutical Sciences*, 77(7-8), 278-285. DOI: 10.1691/ph.2022.2034

Vidal, E., Lorenzetti, A. S., Aguirre, M. Á., Canals, A., & Domini, C. E. (2020). New, Inexpensive and Simple 3D Printable Device for Nephelometric and Fluorimetric Determination Based on Smartphone Sensing. *RSC Advances*, 10 (33), 19713-19719. DOI: 10.1039/D0RA02975K

Zhou, Y., Huang, X., Hu, X., Tong, W., Leng, Y., & Xiong, Y. (2021). Recent advances in colorimetry/fluorimetry-based dual-modal sensing technologies. *Biosensors and Bioelectronics*, 190, 113386. DOI: 10.1016/j.bios.2021.113386

CHAPTER 9: In situ colorimetric method for copper determination in the irrigation ditch water from Acequia Real del Júcar

ABSTRACT

In this chapter a colorimetric Kit for copper *in situ* analysis has been developed. For this, complexing reaction between copper, previously reduced by ascorbic acid, and bicinchoninic acid has been employed. Flame atomic absorption spectroscopy has been employed as reference method, and UV-vis spectrophotometry as colorimetric reference method. The copper of waters from the Acequia Real del Júcar irrigation ditch has been analysed *in situ* by a colorimetric analysis kit and by image treatment by Smartphone using the C* parameter from the CIEL*h*C* colour space. The method developed by Smartphone provides a LOD = 0.146 mg/L and a LOQ = 0.49 mg/L in front of the colorimetric method by UV-vis spectrophotometry which provides a LOD = 0.099 mg/L and a LOQ = 0.33 mg/L. The UV-vis and Smartphone methods provide a correlation of R^2 = 0.993 and 0.977 with FAAS, respectively. The colorimetric kit provides a 75 % of hits. The results show that the errors provided by the kit are not due to the method, but to the subjectivity of the user.

Keywords: Analytical Chemistry, Bicinchoninic acid, Colorimetric Kit, Copper.

1.   Introduction

Dreissena polymorpha, or zebra mussel, is a freshwater bivalve mollusc from the Caspian and Black Seas. As morphological characteristics, it has a triangular shell with light and dark zigzag stripes and it can reach 4.5 cm length size (Burlakova et al., 2000). This mollusc has become abundant in fresh water, where they are the only bivalves which attach to hard substrates and have a planktonic larval stage. In a short period of time, they can obtain biomass orders of magnitude greater than other native invertebrates. The zebra mussel is competitively dominant and has a great impact on the entire ecosystem (Confederación Hidrográfica del Ebro, 2007). The consequences of the invasion of the species include economic losses caused by incrustations of an organic nature on submerged structures in aquatic environments, and environmental losses by modifying the conditions of the habitats that they colonize. This phenomenon is called "biofoulling". In the infrastructures, the presence of adult specimens is the main problem for two situations. The first is that the incrustation of the mollusc in the pipes reduces their calibre. The second is the complete plugging of pipelines and valves (Burlakova et al., 2000).

Faced with this situation, mainly two different types of treatments to combat them are presented. Preventive treatments, whose action is aimed at preventing the settlement of colonies, and reactive treatments, whose action is aimed at eliminating the adult specimens already attached to the structures. One of the treatments is the use of non-oxidizing chemical compounds used for bacterial disinfection and algae control in water treatment systems. Among the most used non-oxidizing chemical compounds it can find $Al_2(SO_4)_3$, NH_4NO_3, Na_2SO_3, $CuSO_4$ and K^+ (Passamaneck & Pucherelli, 2018).

To fight the situation caused by the zebra mussel, the Acequia Real del Júcar periodically performs a treatment with $CuSO_4$ in the water distribution pipes. This treatment lasts 48 hours in which the copper content must maintain minimum levels of 0.2 mg/L, although they add enough to maintain the concentration around 0.5 mg/L in the distribution network. In order to ensure that the content in the network is adequate, they require an *in situ* analysis method for the determination of copper in water.

Among the copper determination in water methods, it can find some such as differential pulse anodic stripping voltammetry (DPASV) (Liu et al., 2017), X-ray fluorescence spectrometry (XRF) (Pytlakowska et al., 2019), atomic absorption spectrometry (AAS) (Huang et al., 2019; González-Alvarez et al., 2020), atomic

emission spectrometry (AES) (Yu et al., 2018), inductively coupled plasma atomic emission spectrometry (ICP-OES) (Kobylinska et al., 2020), inductively coupled plasma mass spectrometry (ICP-MS) (Fei et al., 2021). These conventional methods require expensive equipment, expert operator, special laboratory facilities, organic solvents and chemicals, and in addition to not being portable instruments.

Another widely used way to determine copper is colorimetry. There are copper detection methods that that form coloured complexes, such as the formation of a blue complex with zinc dibenzyldithiocarbamate (García et al., 1993), or the formation of a yellow complex between copper and thiocarbazone 2-carboxybenzaldehyde (López-de-alba et al., 1999). The use of hen egg white lysozyme and a Cu^{2+} specific rhodamine dye (Hu et al., 2021) or colorimetric chemosensor based on benzyl carbazate (Park et al., 2021).

On the other hand, there are colorimetric methods that use copper as reagent to determine certain substances as the determination of proteins using bicinchoninic acid (Smith et al., 1985). In this method, protein quantification is performed by adding Cu(II) that interacts with proteins reducing it to Cu(I), and finally, Cu(I) reacts with bicinchoninic acid forming a violet complex. Using the previously described reaction, Jimenez and Schosinsky (Jiménez-Díaz & Schosinsky-Nevermann, 2002) determine copper in serum. They reduce the copper present in the serum using ascorbic acid and then make it react with bicinchoninic acid. This colorimetric method is fast and simple and is a good alternative to perform copper analysis in situ.

The objective of this chapter is the development of a colorimetric kit for the determination of copper in situ. Once the kit is created, it will be tested in the field and compared with the copper values obtained in the laboratory using a reference method. The kit will be studied both semi-quantitatively by visual perception, and quantitatively by using a Smartphone as a colorimetric detector.

2.   Materials and Methods

2.1.   Instrumentation and Reagents

For total Cu determination by Flame Atomic Spectroscopy (FAAS) an S2 Series AA System AA Spectrometer Thermo Electron Corporation (Cambridge, UK) equipped with a Photron hollow cathode lamp multielement for Cu/Co/Mg/Ni/Fe (Victoria, Australia) were used. Elemental composition of samples was determined by ICP-OES using an Optima 5300 DV, from Perkin Elmer (Norwalk, CT, USA), equipped with an autosampler AS 93-plus and a cross flow nebuliser. For colorimetric

determination of the complex between Cu(I) and bicinchoninic acid a Diode-Array spectrophotometer Hewlett Packard model 8452A (Germany) was used.

For colorimetric determination of Cu by Smartphone a Samsung galaxy S/ edge model SM-G935F with a 12.2 MP camera and a 6500 K white light led lamp were employed.

A copper stock standard of 1000 mg/L for AA (Scharlau, Barcelona, Spain) was used to prepare the calibration standards by diluting the stock one in the range from 0.5 to 7.5 mg/L. For ICP-OES determination, a multi-element standard solution (100 mg/L) containing 26 elements (Al, As, Ba, Be, Bi, B, Cd, Ca, Cr, Co, Cu, Fe, K, Li, Mg, Mn, Mo, Na, Ni, Pb, Se, Sr, Ti, Tl, V and Zn) in 5 % HNO_3 (Scharlau) was used to prepare the calibration standards in the range from 0.05 to 4 mg/L. Additional calibration for Ca, Mg, and Na was carried out using 1000 mg/L standard solutions of each element (Scharlau) in a range from 10 till 200 mg/L. Scandium standard solution 1000 mg/L (Fluka, Steinheim, Germany) was used as internal standard and added to all samples, blanks and standards at a final concentration of 0.25 mg/L.

Solutions of 9.2 and 2.12 g/L of L(+)-ascorbic acid were prepared from solid reagent grade (Scharlau). The A reagent of the protein determination kit ThermoScientific™ Pierce™ BCA Protein Assay Kit (Rockford, Ill, USA) was employed. The A reagent is an aqueous solution of 1 % $BCNA-Na_2$, 2 % $Na_2CO_3 \cdot H_2O$, 0.16 % Na_2tartrate, 0.4 % NaOH, and 0.95 % $NaHCO_3$.

2.2.   Well plate design

A homemade well plate was designed and 3D printed, to put the water samples and standards and make the photograph by the Smartphone. The well plate was designed with 16 cavities of 7 mL capacity, symmetrically distributed every 22.5 degrees and with an ellipsoidal shape to avoid reflexes and shadows in the photograph. A 2.5 mm thick white polypropylene diffuser was glued to the base of the plate to diffuse homogeneously the light from the source (Figure 9.1).

Figure 9.1: 3D printed well plate.

2.3.   Samples

58 water samples from different locations of the Acequia Real del Júcar irrigation ditch was used for this study: 34 of them were employed for optimization the method and other 24 for the evaluation of colorimetric kit. The Cu in samples was determined by FAAS as reference method, and by UV-vis as colorimetric reference method and, finally, by the Smartphone as new colorimetric detector.

A colorimetric kit was prepared for the *in situ* determination of Cu by visual comparison with standard solutions. The colorimetric kit was used along 24 sampling points in the Acequia Real del Júcar and water samples were also taken for subsequent analysis in the laboratory (Figure 9.2). These samples were measured by the FAAS reference method to assess whether this kit is suitable for estimating Cu concentration *in situ*. Furthermore, all these samples were measured by the proposed Smartphone colorimetric method.
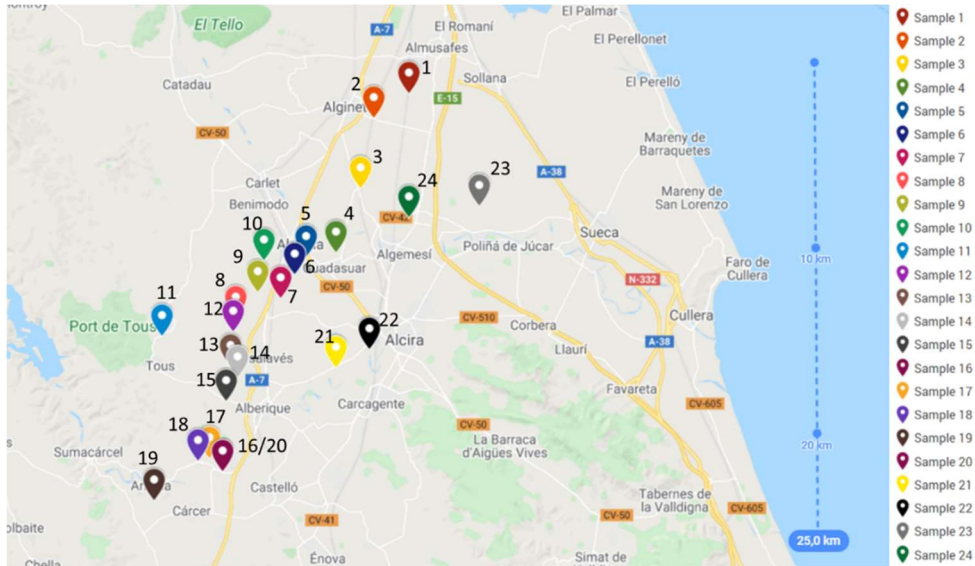
Figure 9.2: Localization of the place where the samples were taken.

2.4.   Experimental

2.4.1.   Copper determination by FAAS

For the measurement by FAAS the samples were prepared adding 0.1 mL of concentrated nitric acid to 10 mL of sample

Instrumental conditions for Cu determination by FAAS were: oxidizing air-acetylene flame, wavelength of 324.8 nm, background correction and external standard

calibration between 0 and 7.5 mg/L. Every 10 samples a standard solution was measured for checking the signals stability.

2.4.2. Colorimetric determination of copper

Following the method proposed by Jimenez and Schosinsky (Jiménez-Díaz & Schosinsky-Nevermann, 2002) for copper determination in serum employing bicinchoninic acid as complexing agent and ascorbic acid as reductant, an adapted procedure was proposed for the colorimetric copper determination in waters (UV-vis, Smartphone and *in situ* kit). The samples were prepared as follow: i) firstly 0.1 mL of ascorbic acid 9.2 g/L was added to 5 mL of each sample and homogenised; ii) 30 μL of A reagent was added and the solution was again homogenised. The presence of copper is confirmed because the solution turns deep violet after being homogenised (a couple of seconds).

To make the determination of copper in the samples by UV-vis spectroscopy, the absorbance at 558 nm corrected by the signal at 800 nm of copper standards solutions between 0 and 3 mg/L and samples were measured.

For the analysis of copper in the samples by the smartphone procedure, the well plate was situated over the lamp, with the light arranged upwards as shown in Figure 9.3. The wells of the plate were filled with 5 mL of the prepared solutions of the standards (0-3 mg/L Cu) and samples. The Smartphone was situated over methacrylate support taking the photo using the professional mode of the camera with fixed conditions (ISO:200, f/12000 and 5800 K). Later, the Matlab program and ColorLab library (Malo & Luque, 2002) was used to take the RGB colour parameters of the photo and get the colour parameters of other colour spaces. The selected parameter for Cu determination was C* from CIEL*h*C* colour space.

Figure 9.3: Methacrylate support to take the photograph.

To make the determination of copper in water samples by the *in situ* colorimetric kit, first, the reagents and materials were prepared: i) a polypropylene tube with 368 mg of ascorbic acid, ii) a polypropylene tube with 40 mL of distilled water, iii) a vial with the A reagent, iv) 10 glass vials with 5 mL of each of the copper standards between 0 and 3 mg/L, and v) 10 mL glass vials for samples (empty) and a 15 mL polypropylene tube for measure the sample volume.

Before to start the *in situ* determination, the ascorbic acid is dissolved with the 40 mL of distilled water by stirring. At each vial of the copper standard solutions, four drops of this ascorbic acid solution are added, after homogenization, a drop of A reagent is added, and the solutions are homogenised again. The water samples, 5 mL measured with the propylene tube, are prepared following the same procedure than standards. Finally, colour of samples is compared with the calibration standard solutions by visual perception.

2.4.3. Determination by ICP-OES

The elemental composition of the water samples was determined by ICP-OES with the aim of know the concentration of possible interferent elements. For the measurement, 50 µL of scandium 25 mg/L solution were added to 4950 µL of the sample solution previously prepared for FAAS determination. Instrumental conditions employed were a radiofrequency power of 1300 W, a plasma Ar flow rate of 15 L/min, an auxiliary Ar flow rate of 0.2 L/min, a nebulizer Ar flow rate of 0.8 L/min, and a sample flow rate of 1.1 mL/min. All the elements were measured in axial mode (except for Ca, Mg, Na, K, and Sr with were measured in radial mode).

The most sensitive emission line, free of spectral interferences, was selected for each element. For the background correction two points were used, and control standards were measured for every series of 10 independent sample measurements.

3. Results

3.1. Copper determination by FAAS reference method

Table 9.1 shows the copper concentration, obtained by FAAS, of the water samples taken in different points of the Acequia Real del Júcar. The experimental calibration line, A = 0.0768 C (mg/L) + 0.0037, with a determination coefficient R^2 = 0.9998, provided a LOD = 0.035 mg/L and a LOQ = 0.117 mg/L.

Table 9.1: Copper content in the water samples by FAAS (n=3).

Sample	Concentration (mg/L)	Sample	Concentration (mg/L)	Sample	Concentration (mg/L)
m1	0.797 ± 0.006	m12	0.523 ± 0.005	m23	1.213 ± 0.004
m2	0.390 ± 0.006	m13	0.557 ± 0.003	m24	1.218 ± 0.005
m3	0.360 ± 0.015	m14	0.572 ± 0.006	m25	0.937 ± 0.006
m4	0.354 ± 0.006	m15	0.561 ± 0.009	m26	0.901 ± 0.001
m5	0.363 ± 0.004	m16	0.822 ± 0.010	m27	0.954 ± 0.005
m6	0.280 ± 0.009	m17	0.788 ± 0.015	m28	0.944 ± 0.014
m7	0.283 ± 0.006	m18	0.949 ± 0.006	m29	0.915 ± 0.015
m8	0.241 ± 0.007	m19	0.970 ± 0.004	m30	0.553 ± 0.009
m9	0.240 ± 0.008	m20	1.124 ± 0.015	m31	0.249 ± 0.006
m10	0.220 ± 0.003	m21	1.164 ± 0.010	m32	ND
m11	0.207 ± 0.002	m22	1.266 ± 0.010	m33	0.107 ± 0.004
				m34	0.303 ± 0.008

3.2. Elemental composition of water by ICP-OES

The characterization of the water sample was carried out through analysis by ICP-OES to know the concentration of elements that could have an interfering effect on copper. As can be seen in the Figure 9.4, the water sample from the irrigation ditch contains very low concentrations of all the elements studied (lower than 0.050 mg/L), except for the major components Ca, Mg, Na and Sr, which are common in continental Mediterranean waters.
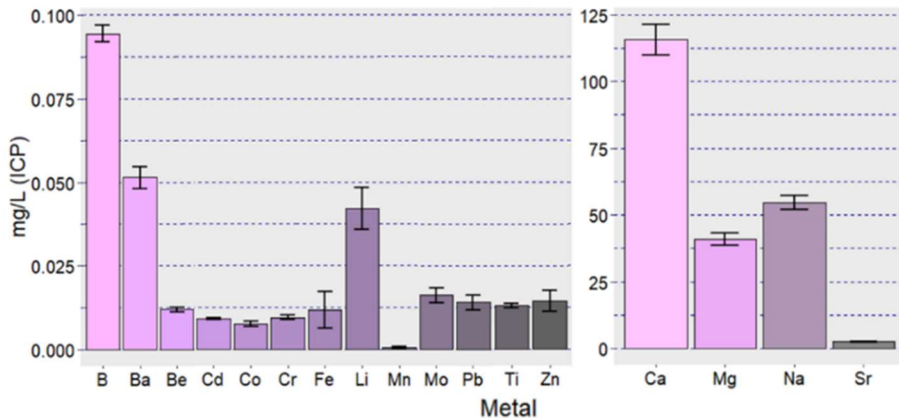
Figure 9.4: Content of elements in the water sample obtained by ICP-OES.

3.3.   Copper determination by colorimetric methods

3.3.1.   Copper determination by UV-Vis spectrophotometry

To evaluate the effect of the amount of ascorbic acid in the reaction, seven different calibration lines prepared with different concentration of ascorbic acid (0.02 to 0.24 g/L) were measured. Figure 9.5 shows that different amounts of this reductant in the solutions do not affect the results, all points are overlapped, and the copper concentration obtained in the samples, using different amounts of reductant, is not affected either. However, to avoid problems in samples with a complex matrix that could consume ascorbic acid, it was considered appropriate to use a high amount of this. On the other hand, the stability of the purple solution was evaluated, a less than the 3 % difference in the slope of the calibration curve obtained three days later from the first day was observed. Therefore, the copper complex solutions are stable for at least three days. The measure by UV-vis spectrophotometry provides a LOD = 0.085 mg/L and LOQ = 0.282 mg/L.

The 34 samples used to optimize the method, as explained above, were analyse also using the colorimetric method by UV-vis spectrophotometry. The correlation between copper content obtained by FAAS and obtained by UV-vis provides an equation Y = 0.928X + 0.011 and a R^2 = 0.993.
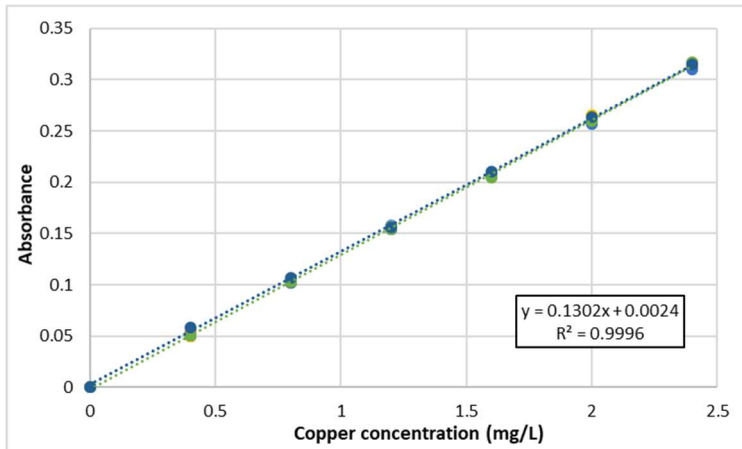
Figure 9.5: Calibration lines obtained by UV-vis spectrophotometry for standard solutions prepared with different concentrations of ascorbic acid (0.02, 0.04, 0.06, 0.08,0.11,0.18 and 0.24 g/L).

3.3.2. Smartphone

For the colorimetric measurement by smartphone, the lighting conditions and photographic parameters are critical to obtain correct results. Due the sample is a liquid, shines and reflexes can appear more easily. To avoid these problems, it was decided to illuminate the samples from below and employ a white diffuser to eliminate glares in the photograph. In this way, the colour parameters of the photography are obtained from the transmitted light that passes through the solution and not by the reflected light.

The photograph was taken zenithally with controlled lighting conditions to 5 mL of prepared solutions of standards and samples (Figure 9.6). The original RGB data of the photography was transformed to parameters of CIEL*a*b* and CIEL*h*C* colour spaces. The best correlation with copper concentration was obtained with the C* parameter, with a calibration equation of Y = 35.885 C (mg/L) + 1.3978 with a R^2=0.997. The method provides a LOD of 0.146 mg/L and a LOQ of 0.49 mg/L, with a repeatability of 0.8 % for a sample with a copper content of 1 mg/L (1.016 ± 0.008 mg/L) (n=3). The correlation between copper content obtained by Smartphone and obtained by FAAS provides an equation Y = 0.948X + 0.006 and a R^2 = 0.986.

3.3.3. Colorimetric Kit

Due that there is a correlation between the colour of the solution and the content of copper, a kit for *in situ* determination of copper was prepared. One test was made on July 17 in the afternoon in 24 sampling points of Acequia Real del Júcar. The copper concentration was estimated by visual perception in front of the

calibration solutions kit. Afterwards in the laboratory, the content of copper was determined by FAAS to check if the *in situ* determination was correct. The Table 9.2 shows the results of copper content obtained by FAAS and the visual *in situ* estimate range and if it was a hit or a miss, and as can be seen in the results there are a 75 % of hits.

To check if the errors were due the colour of the solution or to the visual perception of the user, the samples that were determined *in situ* were measured in the laboratory by Smartphone and by UV-vis spectrophotometry. In all cases, the correlation between the copper concentration obtained by Smartphone and by UV-vis spectrophotometry and the content of copper obtained by FAAS were very good. The first one provides an equation Y = 0.947X + 0.101 and a R^2= 0.977. The second one provides an equation Y = 0.954X + 0.016 and a R^2= 0.993. This indicates us that the errors of the estimation *in situ* were due to the user´s subjectivity and the light conditions of the sampling place but not due to the method.

Table 9.2: Range of in situ estimated concentration by the colorimetric kit and the real copper content (mg/L).

	Estimated content	FAAS	Success		Estimated content	FAAS	Success
m1	0.5-1	0.51	Yes	**m13**	1.5-2	1.27	No
m2	1-1.5	0.88	No	**m14**	1-1.5	1.22	Yes
m3	0	0.00	Yes	**m15**	1-1.5	1.17	Yes
m4	1-1.5	1.24	yes	**m16**	0.5-1	0.48	Yes
m5	1.5-2	1.21	No	**m17**	0-0.5	0.25	Yes
m6	1-1.5	1.07	Yes	**m18**	0.5-1	0.37	No
m7	1-1.5	1.27	Yes	**m19**	0	0.00	Yes
m8	1-1.5	1.25	Yes	**m20**	0.5-1	0.75	Yes
m9	1-1.5	1.28	Yes	**m21**	1-1.5	1.14	Yes
m10	1-1.5	0.97	Yes	**m22**	1-1.5	1.04	Yes
m11	1.5-2	1.32	No	**m23**	0-0.5	0.23	Yes
m12	1.5-2	1.29	No	**m24**	1-1.5	1.15	Yes

3.3.4. Interference study

To check if there are any interference of other elements on the bicinchoninic acid-Cu reaction, the UV-Vis absorbance signal of a solution of 1 mg/L of copper was compared whit that achieved of a solution of copper (1 mg/L) in presence of 0.1 mg/L of 25 elements (Al, As, Ba, Be, Bi, B, Cd, Ca, Cr, Co, Fe, Pb, Li, Mg, Mn, Mo, Ni, k, Se, Na, Sr, Tl, Ti, V and Zn). The difference between signals was less than 3 %, and

therefore, it can be considered that the reaction is very specific for copper and other elements do not interfere significatively with the copper signal.

4.   Discussion

The instrumental techniques (UV-vis spectrophotometry, FAAS or ICP-OES) do not allow *in situ* analysis of copper, at different points, with instantaneous results. The method developed in this work facilitates the control of copper concentration in water, allowing in a short time to check the state of the facilities and, in case of anomaly, to solve the problem.

There are situations when it is only necessary to estimate the copper content to verify, as in the present case, that the concentrations reach a necessary minimum. Although there may be situations where it is necessary to establish the exact copper content.

The colorimetry detection of copper using the complex with bicinchoninic acid is the first time applied to the determination in water samples.

The method developed in the present chapter would allow estimating the copper content in a simple and fast way, with instantaneous results even outside the laboratory. In case of needing an estimation of content in the water the visual perception kit can be used; while in the case it is needed to know their exact content, a determination by Smartphone with a suitable lighting booth of small dimensions can be carried out, being all this portable instrumentation. Considering the accuracy, precision and limits of detection and quantification, in addition to the portability advantage, it can be considered that it is an effective method to perform this type of analysis in the field.

5.   Conclusions

In this chapter, a colorimetric kit has been developed that allows the determination of the copper content *in situ*. The colour of the solution obtained with the optimized reaction correlates with the copper content obtained by the reference method. In addition, the colour allows a visual estimation of the copper content in the solution. If you need an exact copper content, you can use a photo booth and smartphone to perform copper analysis.

The method developed is simple, fast and does not generate large amounts of waste, with only 0.15 mL of reagents used. The present procedure shows an efficient and portable alternative for copper analysis.

6.   References

Burlakova, L.; Karatayev, A., & Padilla, D. (2000). The impact of *Dreissena polymorpha* (PALLAS) invasion on unionid bivalves. *International Review of Hydrobiology*, 85. 529-541. DOI: 10.1002/1522-2632(200011)85:5/6<529:AID-IROH529>3.0.CO;2-O.

Confederación Hidrográfica del Ebro. (2007). "Mejillón cebra: manual de control para instalaciones afectadas". 2ª ed. Zaragoza. 56pp.

Fei, J.J., Wu, X.H., Sun, Y.L., Zhao, L.Y., Min, H., Cui, X.B., Chen, Y.J., Liu, S., Lian, H.Z., & Li, C. (2021). Preparation of a novel amino functionalized ion-imprinted hybrid monolithic column for the selective extraction of trace copper followed by ICP-MS detection. *Analytica Chimica Acta*, 1162, 338477. DOI: 10.1016/j.aca.2021.338477.

García, M., Holst, I., Schosinsky, K., & Rodríguez, R. (1993). Optimización de un método colorimétrico para la cuantificación de cobre en suero. *Revista Costarricense de Ciencias Médicas*, 14(3/4), 33-42.

González-Álvarez, R.J., Bellido-Milla, D., Pinto, J.J., & Moreno, C. (2020). A handling-free methodology for rapid determination of Cu species in seawater based on direct solid micro-samplers analysis by high-resolution continuum source graphite furnace atomic absorption spectrometry. *Talanta*, 206, 120249. DOI: 10.1016/j.talanta.2019.120249.

Hu, J., Wang, L., Zhang, X., Yu, W., Gao, H.W., Solin, N., Hu, Z., & Uvdal, K. (2021). Selective colorimetric detection of copper (II) by a protein-based nanoprobe. *Spectrochimica Acta. Part A, Molecular and Biomolecular Spectroscopy*, 252, 119462. DOI: 10.1016/j.saa.2021.119462.

Huang, Y., Peng, J., & Huang, X. (2019). Allylthiourea functionalized magnetic adsorbent for the extraction of cadmium, copper and lead ions prior to their determination by atomic absorption spectrometry. *Microchimica Acta*, 186, 1-8. DOI: 10.1007/s00604-018-3101-2.

Jiménez-Díaz, M., & Schosinsky-Nevermann, K. (2002). Validación de la determinación de cobre en suero empleando el ácido bicinconínico: relación cobre/ceruloplasmina en pacientes con enfermedad de Wilson y pacientes sin la enfermedad. *Revista Costarricense de Ciencias Médicas*, 23, 33-43.

Kobylinska, N., Kostenko, L., Khainakov, S., & Garcia-Granda, S. (2020). Advanced core-shell EDTA-functionalized magnetite nanoparticles for rapid and efficient magnetic solid phase extraction of heavy metals from water samples prior to the multi-element determination by ICP-OES. *Microchimica Acta*, 187, 1-15. DOI: 10.1007/s00604-020-04231-9.

Liu, M., Pan, D., Pan, W., Zhu, Y., Hu, X., Han, H., Wang, C., & Shen, D. (2017). In-situ synthesis of reduced graphene oxide/gold nanoparticles modified electrode for speciation analysis of copper in seawater. *Talanta*, 174, 500-506. DOI: 10.1016/j.talanta.2017.06.054.

López-de-Alba, P.L., López-Martínez, L., & Amador-Hernández, J. (1999). Determinación espectrofotométrica de cobre en formulaciones médicas, salvado de trigo y aguas potables. *Boletín de la Sociedad Chilena de Química*, 44(4), 469-477. DOI: 10.4067/S0366-16441999000400011.

Malo J. & Luque M.J. (2002). ColorLab: the Matlab toolbox for Colorimetry and Color Vision. Univ. Valencia. https://isp.uv.es/code/visioncolor/colorlab.html

Park, S., Choe, D., Lee, J.J., & Kim, C. (2021). A benzyl carbazate-based colorimetricchemosensor for relay detection of Cu2+ and S2− in near-perfect aqueous media. *Journal of Molecular Structure*, 1240. 130576. DOI: 10.1016/j.molstruc.2021.130576.

Passamaneck, Y. & Pucherelli, S. (2018) Literature Review and Synthesis of Invasive Mussel Control. Final Report ST-2018-1868-01. Bureau of Reclamation, Technical Services Center, Hydraulic Investigations and Laboratory Services Group. https://www.usbr.gov/research/ (Accessed March 27, 2023).

Pytlakowska, K., Pilch, M., Hachuła, B., Nycz, J.E., Kornaus, K., & Pisarski, W.A. (2019). Energy dispersive X-ray fluorescence spectrometric determination of copper, zinc, lead and chromium species after preconcentration on graphene oxide chemically modified with mercapto-groups. *Journal of Analytical Atomic Spectrometry*, 34(7), 1416-1425. DOI: 10.1039/c9ja00081j.

Smith, P.K., Krohn, R.I., Hermanson, G.T., Mallia, A.K., Gartner, F., Provenzano, M.D., Fujimoto, E.K., Goeke, N.M., Olson, B.J., & Klenk, D.C. (1985). Measurement of protein using bicinchoninic acid. *Analytical Biochemistry*, 150(1), 76-85. DOI: 10.1016/0003-2697(85)90442-7.

Yu, J., Zhang, X., Lu, Q., Sun, D., Wang, X., Zhu, S., Zhang, Z., & Yang, W. (2018). Evaluation of analytical performance for the simultaneous detection of trace Cu, Co and Ni by using liquid cathode glow discharge-atomic emission spectrometry. *Spectrochimica Acta Part B: Atomic Spectroscopy*, 145, 64-70. DOI: 10.1016/j.sab.2018.04.011.

CHAPTER 10: Colour transform to optimize fruit ripeness discrimination in dichromats

ABSTRACT

The objective of this chapter is to develop a colour transformation that allows dichromats to establish visual differences in those fruits whose ripening occurs parallel to a colour change from green to red. Valencian-type tomato was used as a case study, in 4 stages of maturity, whose colour was measured with a spectrocolourimeter. The ColorLab library of functions was used to transform the measured XYZ tristimulus values to CIELAB colour space and obtain recoded palettes to take advantage of the discrimination in the blue-yellow mechanism of the red-green defectives, simulating, through the algorithm of the corresponding pair, the appearance that the original and modified palettes had for dichromats. To study the effects of image transformation, the original and recoded descriptors of the samples were represented and the geometric boundaries of each state were defined, seeking an optimal separation. The results of the classifications, in the form of a confusion matrix, show that, thanks to the new recoding of the colour palette, the red-green defectives would reduce the number of failures in the classification by at least 60 %.

Keywords: CIEL*a*b*, Dichromats, Palette optimization, Tomatoes

1.   Introduction

The tomato (*Solanum lycopersicum L.*), with a world production of 181 million tons (Faostat, 2019), is one of the most popular fruits, and is currently cultivated and consumed throughout the world.

Although varieties with other shades have emerged in recent years, studies show that consumers have a preference for red varieties (Adegbola et al., 2019), which continue to be the majority today. In these tomato varieties, as in other fruits such as strawberries, cherries, or certain apple varieties, the ripening of the fruit is accompanied by a colour change from green to red. Thus, the colour of the tomato is the visible characteristic used by consumers to assess the degree of ripeness, and it is a key factor in their choice and purchase decision. Keep in mind that other attributes such as flavour or texture are not as obvious at the point of sale. This is one of the reasons why fruit packaging is always transparent, not only to make the product more attractive, but also to allow decisions to be made based on its appearance (Oltman et al., 2014).

However, red-green defectives, that is subjects with congenital or acquired damage to the red-green colour visual mechanism, experience difficulties in using fruit colour as an indicator of ripeness (Cole, 2024). This would be the case of red-green dichromatic subjects -protanopes and deuteranopes-, for whom the absence of one type of cone (long-wavelength sensitive or L and middle-wavelength sensitive or M, respectively) disable the red-green mechanism (Neitz & Neitz, 2011). To a lesser degree, this is also the case of red-green anomalous subjects -protanomalous and deuteranomalous-, who have a red-green mechanism with reduced sensitivity to colour changes along this direction, due to the displacement of the sensitivity maximum of their L or M cones (Neitz & Neitz, 2011).

The objective of this chapter is to develop a colour transformation that allows dichromats to perceive visual differences between tomato fruits at different stages of ripeness. This transformation could serve as the basis for the development of a mobile application to help dichromatic consumers when buying not only tomatoes, but also other fruits with a similar colour evolution.

2.   Materials and methods

2.1.   Samples

The Valencian-type tomato samples were provided by the Cooperativa Valenciana-Unió Protectora d'El Perelló. The fruits were visually classified by an expert into four stages of maturity (from 1 to 4), according to the colour of their skin. Stage 1

corresponds with the colour change from green to red (when the fruit begins to show small reddish areas), and Stage 4 with the intense red colouration typical of a fully ripe tomato. The four stages of maturity selected are representative of the variability that the consumer can find at the time of purchase for this variety of tomato. Colour measurements for subsequent recoding were performed on 20 tomatoes of each stage of maturity.

2.2.   instrumentation and software

The XYZ CIE1931 tristimulus values and the CIELAB L*a*b* colour descriptors (Fairchild, 2013) of the samples were measured using a portable colourimeter (Minolta, mod. CR-300, Ramsey, N.Y., USA). The measurement was made at four points of the tomato, as shown in Figure 10.1, the measured XYZ values were subsequently averaged and transformed to CIELAB, using a white sample of tristimulus values X=77.13, Y=78.6, Z=83.9 as a reference. Although the colourimeter also provides the parameters of the CIEL*a*b* colour space, this space is non-linear, so it was decided not to average these values, but to perform the calculation in the linear CIEXYZ space.
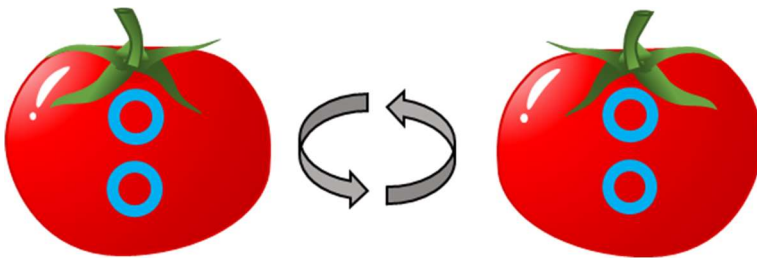
Figure 10.1: Visual representation of the colour measurement with the portable colourimeter. Two measurements were taken, one slightly above and one slightly below the equator, and the process was repeated after rotating the tomato 180˚.

The colour transformations to recode the original colour palette were carried out in a Matlab® environment, using the COLOURLAB library (Malo & Luque, 2002). Simulations of the original and recoded images were obtained by applying the corresponding pair algorithm (Capilla et al., 2004).

To carry out the tomato classification studies based on colour, the regions of the CIELAB space corresponding to the different stages of maturity were determined. The boundary between two states was defined as the bisecting line of the segment that links the centroids of said ripeness states. Since colours that are less than one CIELAB unit are not distinguishable (Fairchild, 2013), a region of colour confusion was defined around each boundary, within which the observer would not be able

to discern which group the tomato belongs to. In this way, a classification would be generated that mimics what a human observer would do, but with the limitations that this implies. The results were obtained in different 2D-projections of the colour space, looking for the projection that would provide an optimal separation. The results of the classifications are displayed in the form of a confusion matrix.

3.   Results

3.1.   Colour palette recoding

Most subjects with congenital colour vision defects have problems discriminating changes in the red-green direction (Birch, 2012). Thus, it was proposed to recode changes in this direction as changes in the blue-yellow direction, in which the discrimination capacity of these subjects would be normal (Barbur et al., 2008; Costa Marcelo et al., 2016). In CIELAB space (Figure R.5), a* corresponds to a red-green axis and b* to a blue-yellow axis, so it was thought that this recoding could be done by exchanging the value of those two coordinates. With this change, the dichromats would be able to differentiate a green tomato (not very ripe) from a red one (ripe), using colour cues, since they would be recoded as blue and yellow, respectively.

Two recoding options, based on this principle, were analysed. If we call the recoded CIELAB values L_r^*, a_r^* and b_r^*, the first option consisted in an exchange of the a* and b*values (L*b*a* recoding, Equation 1) and the second, the same exchange followed by red-green channel cancellation (L*0a* recoding, Equation 2)

$$L_{r,1}^*=L^*, \; a_{r,1}^*=b^* \; b_{r,1}^*=a^* \qquad\qquad \text{(Equation 1)}$$

$$L_{r,2}^*=L^*, \; a_{r,2}^*=0 \; b_{r,2}^*=a^* \qquad\qquad \text{(Equation 2)}$$

In both cases, the CIELAB values were transformed to CIEXYZ, after which the corresponding pair algorithm (Capilla et al., 2004) was used to simulate the dichromatic appearance, that is, to compute an image would elicit in an observer with normal colour vision the same perception as the original image seen by the dichromatic subject.

To study the effect that these transformations had on the colour of the tomatoes, the average colour of the samples was obtained for each stage of ripeness, and the appearance of the three types of dichromats of the original and recoded colours was simulated (Figure 10.2).
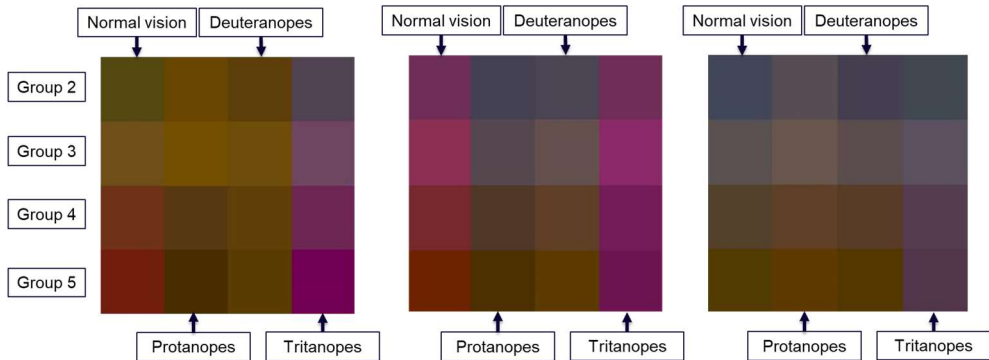
Figure 10.2: Original colour palette of the different groups of tomatoes studied (left); L*b*a* colour recoding (center) and L*0a* colour recoding (right). In each image, the rows represent the average colour of the tomatoes of a stage of maturity and the columns the perception of each type of subject.

The analysis of the Figure 10.2 shows that protanopes and deuteranopes are not able to find significant hue differences between red and green tomatoes, since both colours are perceived as yellow. The only perceived differences are related to lightness and colourfulness. If protanopes and deuteranopes are shown a variety of fruits, they may be able to pick the more mature fruit: protanopes would choose the darker and deuteranope the lighter fruits, but if the gamut does not include a large enough range of colours or if illumination is too high or too low, errors may easily occur. The tritanopes, subjects lacking the short-wavelength or S cone, who keep a normal red-green mechanism and a defective blue-yellow one (Neitz & Neitz, 2011), despite not perceiving colours with the same hues as the normal subject, are capable of differentiating red tomatoes from green ones by hue.

With the **L*b*a*** colour recoding we can observe a decrease in the differentiation capacity of a person with normal vision, since the range of colours is reduced to reds. However, the simulation shows that the protanopes and deuteranopes are now capable of differentiating the different stages by hue cues: unripe fruit is perceived as bluish and ripe fruit as yellowish. Tritanopes and, to a lesser extent, subjects with normal colour vision, reduce their ability to grade ripeness, given that all fruits appear within the range of magenta colours.

The second recoding (**L*0a***), which cancels the colour coordinate a*, whose changes would not be perceived by protanopes or deuteranopes as hue changes, would allow normal and dichromat people to distinguish the different ripeness stages by hue (bluish for state 1 and yellowish for the rest). However, although the colour differentiation capacity of tritanopes improves with respect to **L*b*a*** recoding, it is worse than when they visualize the original image. For protanopes

and deuteranopes, this modification has effects similar to those mentioned in the previous recoding, for differentiation purposes, but we can observe colour differences between both recodings.

In what follows, only the results for the two red-green defectives shall be discussed.

3.2.   L*b*a* and L*0a* colour palettes

The difficulties of red-green defectives in judging fruit ripeness and the effect of the new colour palettes on fruit ripeness classification can be seen in Figure 10.3. The corresponding pair algorithm shows that protanopes and deuteranopes can distinguish very red from very green tomatoes, using lightness cues (Figures 10.3B and 10.3C), but lightness information does not allow to distinguish intermediate degrees of maturity. The **L*b*a*** coding (Figure 10.3D) would allow discrimination between close stages, as can be seen in the corresponding simulations (Figures 10.3E and 10.3F). Figures 10.3G, 10.3H and 10.3I show the image transformed with the **L*0a*** recoding. This encoding provides results similar to those seen with the **L*b*a*** transformation.

All the plots in Figure 10.4 present the following elements: a) the samples, classified by ripeness stage (yellow, blue, magenta and black, for stages 1, 2, 3 and 4 respectively); b) the boundaries between regions corresponding to contiguous states (continuous lines, red for stages 1 and 2, green for stages 2 and 3 and blue for stages 3 and 4) and c) the region of uncertainty around each boundary (dotted lines), which includes colours at a distance of less than 1 CIELAB unit and that will be difficult to classify correctly by an observer, since visually they could be indistinctly in both states.

Figure 10.4A shows that, in the original image, a person with normal colour vision is able to differentiate tomatoes using the a* coordinate. The two red-green defectives must, however, necessarily resort to the b* coordinate (Figures 10.4B and 10.4C). When applying the new recodings (Figures 10.4D and 10.4G), subjects with normal vision must resort to the b* coordinate to be able to differentiate the tomatoes.

The success rate of the segmentation in ripeness stages with the original and recoded palettes is shown in the confusion matrices of Figure 10.5, for the subjects with normal colour vision and the two red-green defectives with the different recodings.
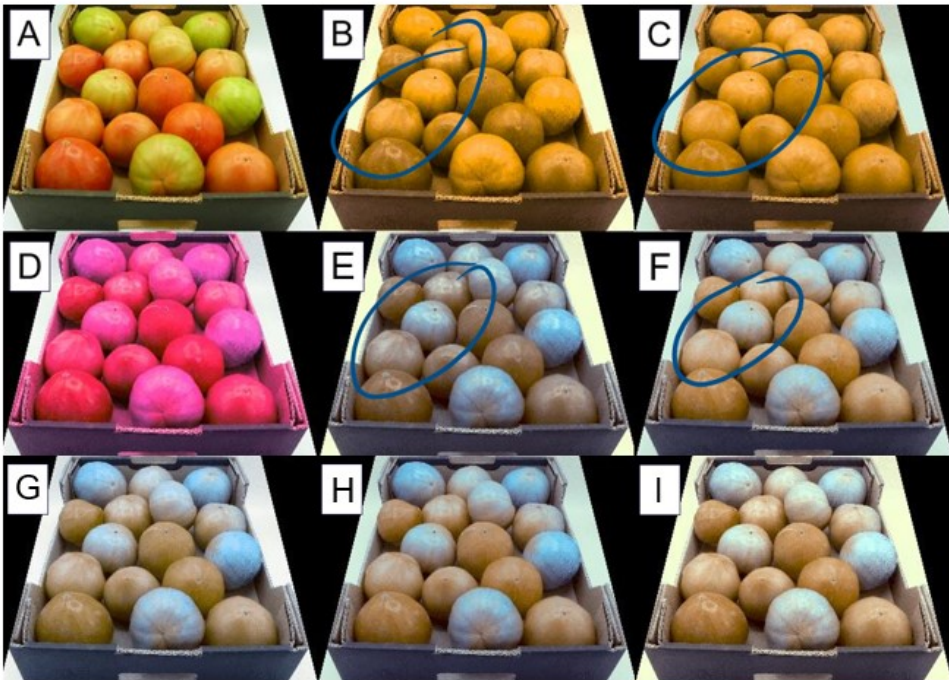
Figure 10.3: Original image (A), protanopic perception of the original image (B), deuteranopic perception of the original image (C), L*b*a* transformed image (D), protanopic perception of the L*b*a* transformed image (E), deuteranopic perception of the image transformed with L*b*a* (F), image transformed with L*0a* (G), protanopic perception of the image transformed with L*0a* (H) and deuteranopic perception of the transformed image transformed with L*0a* (H) and perception deuteranope of the transformed image with L*0a*(I).
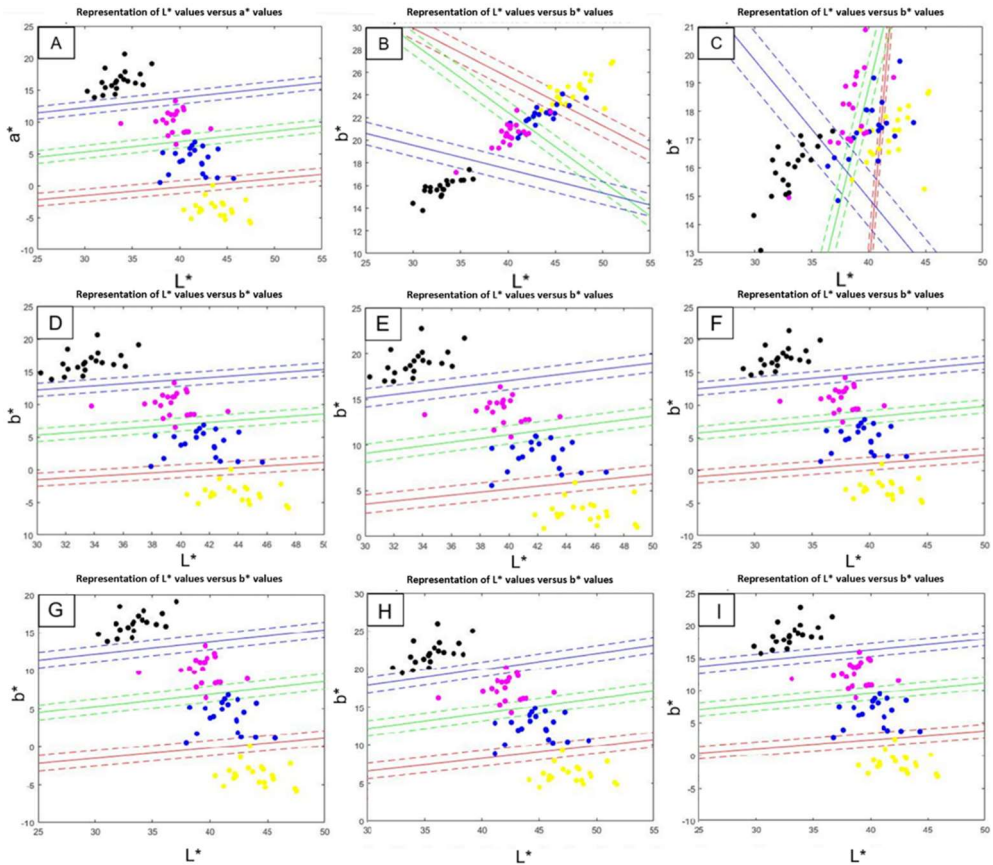
Figure 10.4: Segmentation of the colour space that would perform subjects with normal colour vision and red-green defectives for a maximum separation between tomato ripeness stages with the different colour palettes. Original image: normal vision (A), protanope (B), and deuteranope (C). L*b*a* coding: normal vision (D), a protanope (E), and a deuteranope (F). L*0a* coding: normal vision (G), protanope (H) and deuteranope (I).

In the regions of confusion mentioned above, because the values could be found indistinctly in the two border regions, it has been decided to consider that 50 % of the values located in these regions correspond to successes and 50 % to failures. This is so because an observer who would classify on chance tomatoes located in the region of confusion, getting 50 % of the classified tomatoes right.
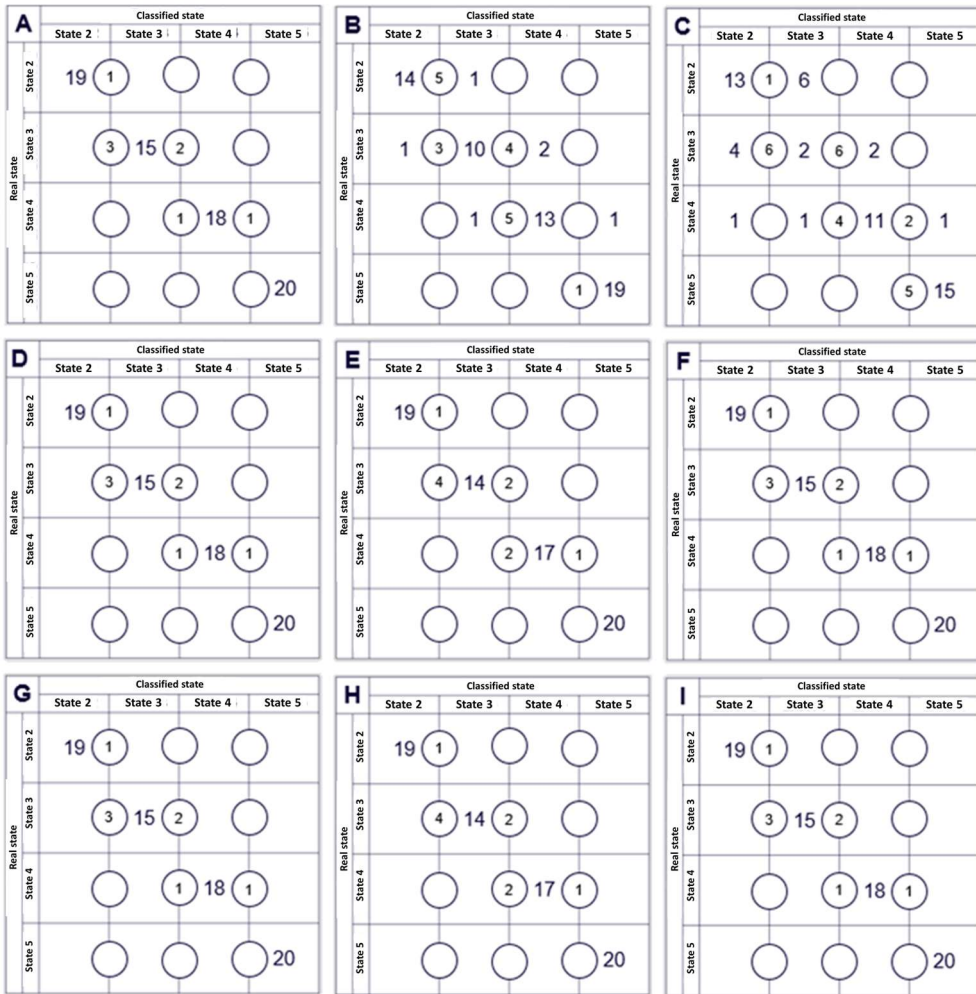
Figure 10.5: Confusion matrices of the classification of tomatoes in ripeness stages with the segmentation of Figure 10.4. Original image: normal vision (A), protanope (B) and deuteranope (C). L*b*a* coding: normal vision (D), protanope (E) and deuteranope (F). L*0a* coding: normal vision (G), protanope (H) and deuteranope (I). The circles represent tomatoes within a region of colour confusion.

3.3.   Recoded colour palettes

Figure 10.3 shows that we are able to verify visually that the transformations have significant positive effects on the capacity of red-green defectives of judging tomato ripeness by colour. With the segmentations in Figure 10.5, we can observe a significant improvement in the classification of tomatoes, which is reflected numerically in the confusion matrices. Table 10.1 shows that failures decrease, reaching a minimum reduction of 60 % (from 25 % of failures in the original image

to in the recoded image 6.7 %) and a maximum of 88 % (from 74 % of failures to 5.3 %).

Table 10.1: Failure rates (%) in the classification of tomatoes by states for the different recodings and visual perceptions.

Colour palette	Visual perception	Total success	Total errors	errors (%)
L*a*b*	Normal	76	4	5.26
	Protanope	64	16	25.00
	Deuteranope	46	34	73.91
L*b*a*	Normal	76	4	5.26
	Protanope	75	5	6.67
	Deuteranope	76	4	5.26
L*0a*	Normal	76	4	5.26
	Protanope	74	6	8.11
	Deuteranope	76	4	5.2

4.   Discussion

The easy access to electronic devices with colour screens has stimulated the development of algorithms to reduce the discrimination problems of subjects with colour vision deficiencies (Ribero & Gomes, 2019; Zhu & Mao, 2021). The objective of these algorithms is to minimize the loss of information in the image, although, in addition, they can meet other requirements, such as trying to maintain a "natural" appearance in the processed scenes (Zhu & Mao, 2021). The procedures used can be based on point-to-point transformations, as in our case, or on local transformations, which take into account the environment of each pixel in the image. The drawbacks of these transformations are usually the calculation time, the need to make "à la carte" adjustments for each image, the fact that the colour chosen by the algorithm to replace a given one cannot be generated by the device, and the appearance of artifacts, such as halos, especially in local transformation algorithms (Zhu & Mao, 2021).

In our case, the proposed algorithm is a simple, low-level calculation method that can be performed in real time with complex images without the need for a very powerful processor. However, it is dependent on the colour gamut of the image, and the principle of operation (shifting colours from the axis of low discrimination of the subject to a direction where discrimination is better) may not work equally well in scenes in which the perceptually significant differences are not on a single axis. To prevent the algorithm from providing colours outside the range of colours

generated by the device, and which would be represented by colours of the same hue at the border of the range, reducing the contrast, it would be necessary to normalize the transformation, so that the maximum and minimum of a* in the scene are represented by the maximum and minimum values of b* generated by the device (Zhu & Mao, 2021).

5.   Conclusions

Observing the different figures shown in this work, we can confirm several points. The first is that the calculations confirm the difficulties that dichromats present when visually determining characteristics associated with colour, due to their loss of discrimination in the red-green direction of the colour space.

When we propose a colour recoding within the b* coordinate of the CIEL*a*b* colour space, because this coordinate encodes colours easily discernible by dichromats, this population is capable of perceiving information that was previously impossible or very hard.

In addition, not only has it been possible to visually demonstrate the effects of the new recodings, but numerical studies with colour data have been proposed to objectively demonstrate that, effectively, these transformations have great benefits in the dichromatic population, in this case protanopes and deuteranopes.

6. References

Adegbola, Y. P., AhoyoAdjovi, N. R., Adekambi, S. A., Zossou, R., Sonehekpon, E. S., AssogbaKomlan, F., & Djossa, E. (2019). Consumer preferences for fresh tomatoes in Benin using a conjoint analysis. *Journal of International Food & Agribusiness Marketing*, 31(1), 1-21. DOI: 10.1080/08974438.2018.1469448.

Barbur, J. L., Rodriguez-Carmona, M., Harlow, J. A., Mancuso, K., Neitz, J., &Neitz, M. (2008). A study of unusual Rayleigh matches in deutan deficiency. *Visual Neuroscience*, 25(3), 507-516. DOI: 10.1017/S0952523808080619.

Birch, J. (2012). Worldwide prevalence of red-green colour deficiency. *Journal of the Optical Society of America A*, 29(3), 313-320. DOI: 10.1364/JOSAA.29.000313.

Capilla, P., Dıez-Ajenjo, M. A., Luque, M. J., & Malo, J. (2004). Corresponding-pair procedure: a new approach to simulation of dichromatic colour perception. *Journal of the Optical Society of America A*, 21(2), 176-186. DOI: 10.1364/JOSAA.21.000176.

Cole, B. L. (2004). The handicap of abnormal colour vision. *Clinical and Experimental Optometry*, 87(4-5), 258-275. DOI: DOI: 10.1111/j.1444-0938.2004.tb05056.x.

Costa, M. F., Goulart, P. R., Barboni, M. T., & Ventura, D. F. (2016). Reduced discrimination in the tritanopic confusion line for congenital colour deficiency adults.*Frontiers in Psychology*,7, 429. DOI: 10.3389/fpsyg.2016.00429.

Fairchild, M. D. (2013). Color appearance models. John Wiley & Sons.

FAOSTAT (Accessed 17 October, 2021). Food and Agriculture Organization of the United Nations. https://www.fao.org/faostat/es/#data/QCL.

Malo, J.,&Luque, M. J. ColourLab: the Matlab toolbox for Colourimetry and Colour Vision. Univ. Valencia 2002. http://isp.uv.es/code/visioncolour/colourlab.html.

Neitz, J., &Neitz, M. (2011). The genetics of normal and defective colour vision. *Vision Research*, 51(7), 633-651. DOI: 10.1016/j.visres.2010.12.002.

Oltman, A. E., Jervis, S. M., & Drake, M. A. (2014). Consumer attitudes and preferences for fresh market tomatoes. *Journal of Food Science*, 79(10), S2091-S2097. DOI: 10.1111/1750-3841.12638.

Ribeiro, M., & Gomes, A. J. (2019). Recolouring algorithms for colourblind people: A survey. *ACM Computing Surveys*, 52(4), 1-37. DOI: doi.org/10.1145/3329118.

Zhu, Z., & Mao, X. (2021). Image recolouring for colour vision deficiency compensation: a survey. *The Visual Computer*, 37(12), 2999-3018. DOI: 10.1007/s00371-021-02240-0.
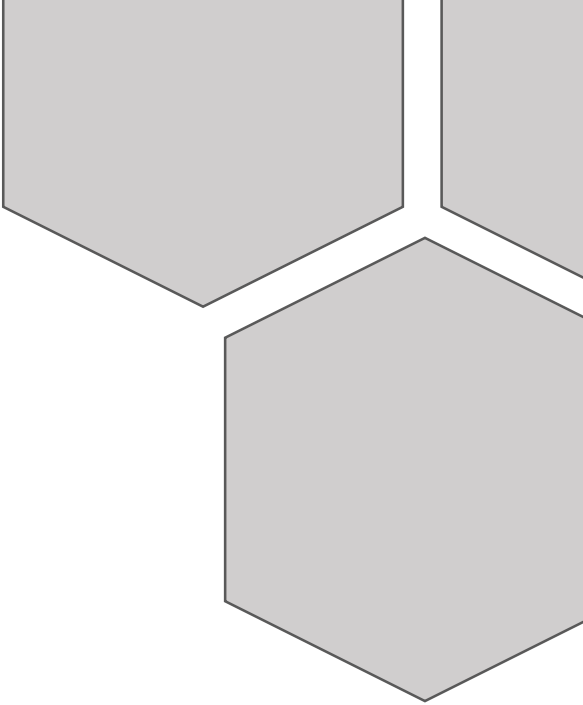
SECTION 2

ROBOTICS AND PROGRAMMING FOR ANALYSIS
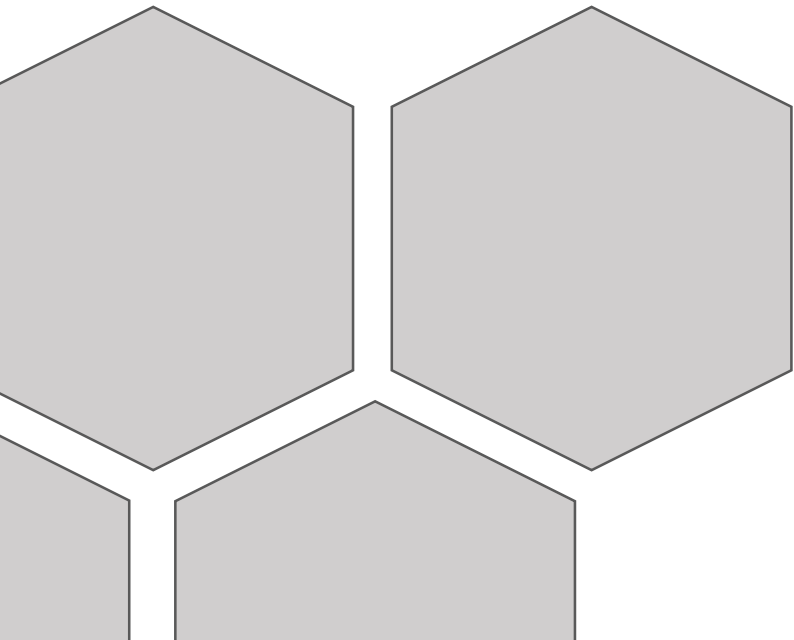
CHAPTER 11: Arduino for chemists: assembly and programming of sensors
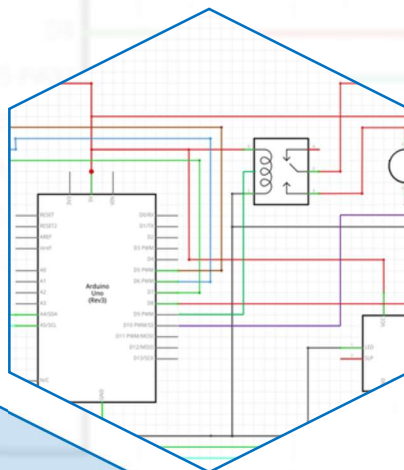
ABSTRACT

This chapter shows studies in which Arduino sensors are used for different purposes, reviewing how they are used, the different ways to connect the sensors and the codes that are required for their use. The sensors are divided in 4 types: thermal sensors, electric sensors, light sensors, and chemical sensors. Bearing in mind that all the sensors works in the way that their resistance change according a physical parameter, the first type modify their resistance due temperature changes; the second group depends on the conductivity of the medium, the third group change the response according the light detected, and the fourth group have a different response due to a specific chemical compound. The sensors are employed mainly for monitoring some process. The chemical sensors are very specific and are based in the response modification due to changes in concentration of gases that are monitored. Due that they are only useful for air quality monitoring or get a specific information of the air, their application will depend on the usuary necessities.

Keywords: Arduino, Chemistry, Programming codes, Sensors.

1.   Arduino

Electronic devices have had a transformational impact in the modern age (McClain, 2014). The advancement of technology has provided solutions that use computer applications (Demiris & Hensel, 2008) that have been used in the research environment. Among the solutions provided by the technological advance, which have begun to be used in research, the Arduino controllers can be found.

Arduino is a low-cost platform for embedded computing developed by a team of computer scientists and artists in Milan and New York (Brock et al., 2009, Banzi & Shiloh, 2022). The Arduino platform, introduced in 2005, changed the landscape of microcontrollers that existed until then (Perea, 2015). Microcontrollers are small computers contained on a single integrated circuit or computer chip, and are an excellent way to program and control electronic components (Nussey, 2013). At that time, working with microcontrollers meant paying a high price for integrated circuits in addition to all the necessary components (Perea, 2015). On the other hand, to work with them it used to be necessary to use their own languages or, in the best of cases, the assembly language, neither of which was easy to learn for non-advanced users (Perea, 2015, Banzi & Shiloh, 2022). These boards changed all those aspects (Perea, 2015).

Arduino is being used for cheap development of interactive applications (Brock et al., 2009). This device is a controller board based on the ATmega328 (Brock et al., 2009, Kubínová & Šlégr, 2015, Badamasi, 2014) microprocessor that allows the connection of different programmable components. The board is open source with the goal of developing a line of easy-to-use microcontrollers. The Arduino board is programmed using the Arduino programming language, which is C with a bit of C++ (Brock et al., 2009, Schmidt, 2015). The code written in Arduino tells the microcontroller what to do (Nussey, 2013). To design the code that the board will read the Arduino software known as the Integrated Development Environment (IDE) is used. This environment is based on the processing language, which was developed to help artists create computer art without having to be an engineer beforehand (Banzi & Shiloh, 2022).

Arduino is made up of two main parts, the hardware, which is the board with which you work to build the objects, and the IDE, which is the software that runs on the computer. IDE is used to create a sketch that is loaded onto the board. The sketch tells the board what to do (Banzi & Shiloh, 2022). In order to create devices in Arduino, the in/out pins system is used. The board has a series of black rows coded

with a number; these rows are the connectors/pins. The pins can be inputs or outputs, which read or provide information respectively, and they van be of two types, analogic and digital. The digital pins can only read two values HIGH/1 or LOW/0 (Banzi & Shiloh, 2022). The analogic pins allow reading the voltage measurement of the connected sensors, being able to measure up to 1024 voltage levels (Banzi & Shiloh, 2022). They also allow a voltage measurement to be provided by averaging pulses over time. That is, if the maximum voltage is 5V/cycle, it can turn on the voltage for half a cycle to provide a signal of 2.5V/cycle on average, a 512 level measure of voltage. The board can be powered from the computer's USB port or an external battery using an AC adapter (Banzi & Shiloh, 2022).

According to Scopus repository, there are 17753 articles related to Arduino, counting on all knowledge fields between 2000 and 2023. When the search is limited to chemistry and chemistry engineering only there is 1011, little less than 6 %. The Figure 11.1 shows the trend in the publishing of documents related to Arduino in the last 23 years.

This chapter presents some monitoring and analysis works in which different types of sensors have been used. The chapter explains how to connect the sensors to Arduino and how to program the board to use them, the codes in txt format employed and as an Arduino IDE file allows the user to easily use the sensor.
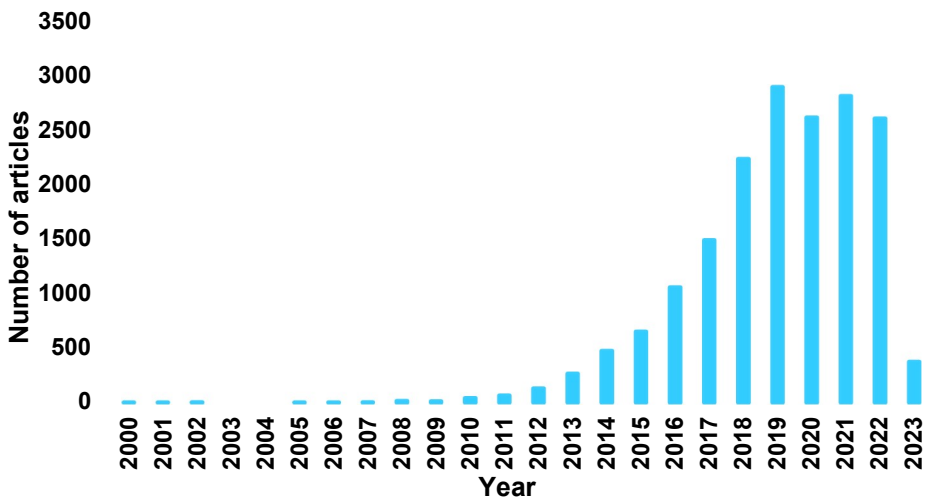
Figure 11.1: Number of articles published associated with "Arduino" according the Scopus repository.

2.   Thermal sensors

Between the sensors that can be useful to carry out laboratory experiments are thermal sensors. This type is simple, and their principle is the change of the resistivity according to the temperature (Parihar et al., 2017, Recktenwald, 2013). They are not lineal resistors, but the analogic values of the resistance are transformed into digital values of temperature (Parihar et al., 2017).

The use of this sensors is very limited. They can be employed to monitoring the temperature in closed systems (Han et al., 2018, Pundir & Singh, 2019). In this situations it is recommended the use of K-Type thermocouple. These are used as probes that can be introduced into closed systems to control the parameters inside, as in this case, the temperature. These devices have two different electric conductors that form an electric union-thermic union. The change of the temperature in the union create a low voltage difference that it is measurable and can be used to calculate the temperature (Santos, 2022). In the case of K-type thermocouple, they are formed by chromel and alumel that are chrome and nickel, and aluminium and nickel composition alloys, respectively (Lozano, 2020). Thermocouples has to be connected to other modules like MAX6675 to make the compensation and linearization of the signal.

To make the connections of the thermocouple to the MAX6675 module and to the Arduino board the scheme of the Figure 11.2 can be used. To connect the thermocouple to the MAX6675 module the red wire and the blue wire have to be connected to the (+) and (-) of the MAX6675 module. To connect the module to the Arduino board GND, VCC, SCK, CS and SO of the module have to be connected to GND, 5V and three pines of the Arduino board. To get the information of the module it is necessary to use the "max6675.h" library. The code to make the data reading is in Annex 11.1, the temperature values are showed by screen using the "monitor serie" option in the Arduino IDE program.
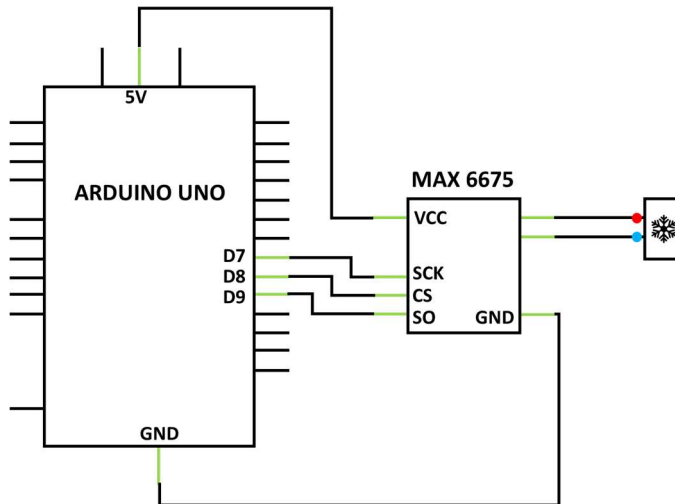
Figure 11.2: MAX6678 sensor assembly diagram.

Thermal sensors are useful for environment conditions monitoring. For example, farms require control the humidity and the temperature of the soil depending on the type of the crop (Bhadani & Vashisht, 2019). This monitoring is more important in aquaponics crops, where it is necessary to control the temperature of the water to avoid the death of the plants (Supriadi et al., 2019). The temperature of the air is important too (Hariyanto et al., 2020), this is due mainly to heat received from the sun, as for a higher radiation in a surface higher is the temperature of the air (Hariyanto et al., 2020). The thermal sensor that has been used for this problematics are the DHT11 (Bhadani & Vashisht, 2019, Hariyanto et al., 2020) and the DS18B20 (Supriadi et al., 2019).

The DHT11 sensor measure the temperature and the humidity at same time. This sensor has a capacitive humidity sensor and a thermistor (Naylamp Mechatronic, 2021). This sensor has some very low precision characteristics. On the one hand, the temperature work range is 0-50 ± 2 grades, and the humidity work range is 20-80 ± 5 % (Naylamp Mechatronic, 2021). Although this sensor is limited can be used when it is not necessary to get accurate information. If it is necessary to get more accurate information, it is possible to use DHT22 sensor being the same that the DHT11 but with better characteristics. This sensor has a temperature work range of -40-125 ± 0.5 grades and a humidity work range of 0-100 ± (2-5) % (Llamas, 2016), and allows to get more accurate information with a very low cost.

To make the connection of the DHT11/DHT22 to the Arduino board the scheme of the Figure 11.3 can be used. To make the connections between both devices the GND, VCC and I/O//DATA pins of the DHTXX must be connected to the GND, 5V and a digital pin of the Arduino board respectively. It is necessary to connect a 10KΩ resistance between VCC-5V and I/O//DATA-digital pin connections. If the DHTXX has a NC pin have not been connected. To get the information of the module it is necessary to use the "DHT.h" library. The code to make the data reading is in Annex 11.2. the temperature values are showed by screen using the "monitor serie" option in the Arduino IDE program.
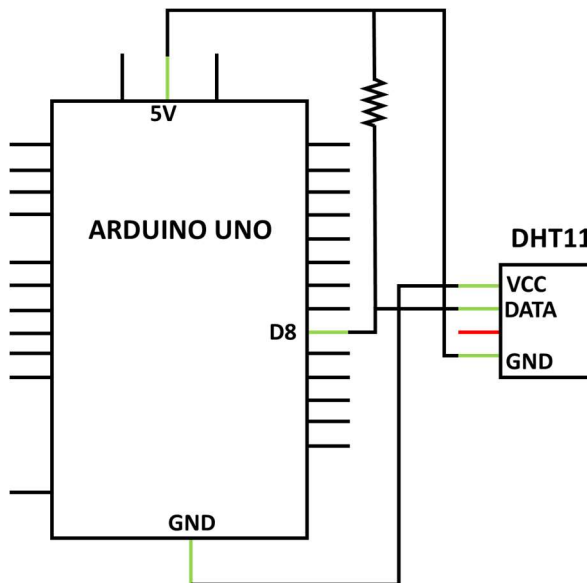
Figure 11.3: DHT11 sensor assembly diagram.

The DS18B20 sensor is a low cost device that is pretty advanced. The temperature range work is very wide from -55 until 125 grades. The accurate of the sensor depends on the temperature range. Between -10 and 85 grades the accurate is ± 0.5 grades, for the other ranges is ± 2 grades (Del Valle, 2017; Llamas, 2016). The sensor is available in 2 models, normal and waterproof.

To make the connection of the DS18B20 sensor to Arduino board the scheme of the Figure 11.4 can be used. To connect the sensor, the GND, VDD and DQ pins have to be connected to the GND, 5V and digital pin of the Arduino board respectively. It is necessary to connect a 4.7KΩ resistance between VDD-5V and DQ-digital pin connections. To get the information of the module it is necessary to use the

"OneWire.h" and "DallasTemperature.h" libraries. The code to make the data reading is in Annex 11.3. the temperature values are showed by screen using the "monitor serie" option in the Arduino IDE program.
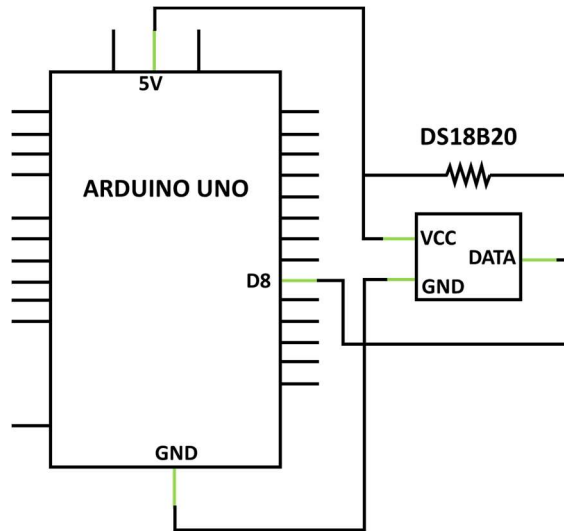
Figure 11.4: DS18B20 sensor assembly diagram.

Other sensor that can be used is the LM35, there is a work where is used to create a device to data acquisition in learning environments (Vallejo et al., 2020). Although is other type of thermal sensor it is not interesting talk about it because is very similar to the DS18B20, but the first one provides an analogic signal and the second one provides a digital signal (Santocoyo, 2019). About the connections the only difference is that is not necessary to use a resistance. The code don´t require a specific library and is simpler as can be seen in the Annex 11.4.

3.   Electric sensors

The electric sensors are based on the conductivity of the medium. These sensors are used mainly for obtain information related on liquids. For example, there is sensor that are able to measure the humidity (Koestoer et al., 2019; Susa et al., 2020; Tang et al., 2020) or the moisture soil (Taneja & Bhatia, 2017; Thakare & Bhagat, 2018). Moreover, there is sensor that can measure the water level (DFRobot, 2022) or more important for laboratory works, the pH (Kubínová & Šlégr, 2015; Thakare & Bhagat, 2018).

As it has been seen in the thermal sensors, there are sensors that can measure the humidity, as the DHT11 and the DHT22 sensors. Both type of sensors, thermal and humidity are used mainly to create automatic monitoring systems to control the crops conditions (Liu & Zhang, 2019) or storage conditions (Tang et al., 2020). As the previous one, the other type of sensor that is mostly used to monitoring crops are the moisture soil sensor, that allows get information to changes in the electrical conductivity of the land (MisterBotBreak, 2019). The sensor is formed by two electrodes connected to an intermediate plate to get the moisture readings. The resistance between both electrodes is measured. The electrodes are connected to the (+) and (-) connectors of the intermediate board. This board require connect the analogic out or digital out, the GND and the VCC GPIOS to the analogic or digital GPIO, GND and VCC GPIOS of the Arduino board respectively. When the soil moisture is low the digital read is recommended (Das, 2022). The scheme of the Figure 11.5 can be used. The sensor can be used in two ways. The first one is using the analogic GPIO. The analogic GPIO provide a value between 0 and 1023 that can be normalized to 100 to provide the percentage value of moisture. The code is provided in the Annex 11.5.
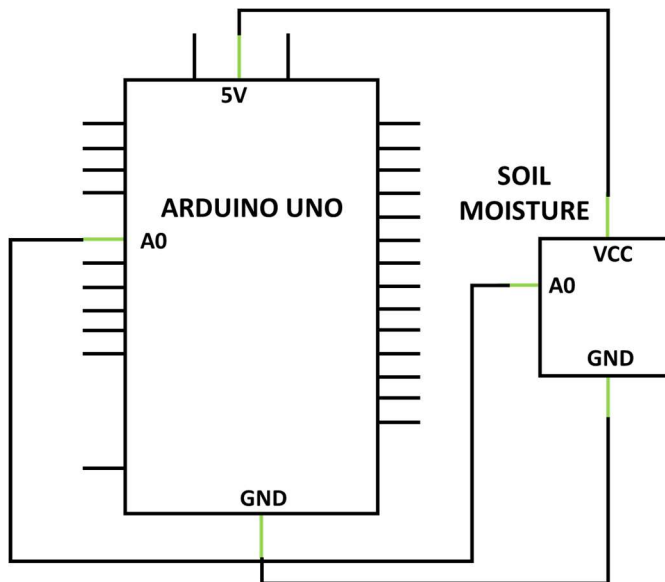
Figure 11.5: Soil moisture sensor assembly diagram.

Other sensor that uses the electrical conductivity of the medium is the water level sensor (Thakare & Bhagat, 2018). This sensor can be used to monitoring the use of liquid reagents. In this case, a work is found using this to evaluate the consumption

of water in an automatic irrigation system provided with a soil moisture sensor by comparing the use of water employing the sensor and without use this, using the water level sensor (DFRobot, 2022). The connection of this sensor is very simple, the scheme is showed in the Figure 11.6. To connect the sensor to the Arduino board, the (-), (+) and S pins of the sensor has to be connected to the GND, 5V and an analogic GPIO of the Arduino board. The code to use the sensor is in the Annex 11.6. Due the analogic pin provides a value between 0 and 1023 it is recommended to use map function (explained in the Annex 11.5) to get a data related to the water level.
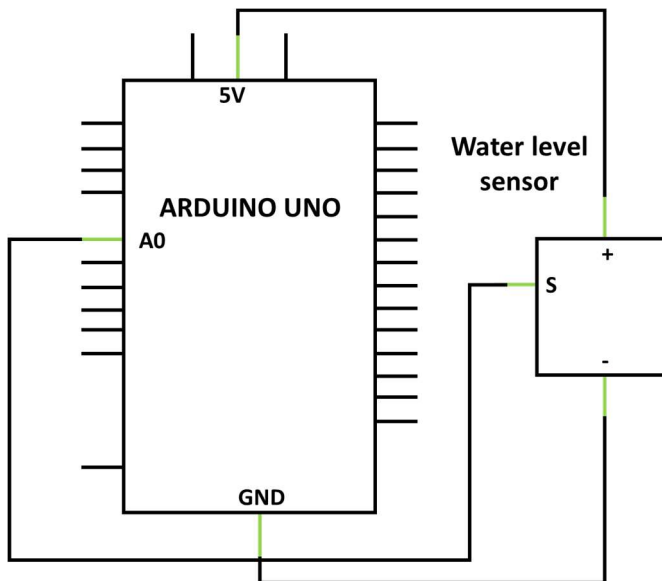
Figure 11.6: Water level sensor assembly diagram.

The last electric sensor is the pH sensor. This can be used in a temperature range of 5-60 grades and has an accuracy of ± 0.1 at 25 grades. This sensor has been used for the monitoring of crops and to develop learning devices for high school. On the one hand, this module is useful to control de pH of aquaponics crops to avoid the death of the plants. Moreover, these sensors can be connecting to WiFi modules like the ESP8266 to get the information by wireless connection (Thakare & Bhagat, 2018). On the other hand, the use of low cost sensors allows to create devices that can be used in institutions that do not have economical resources (Kubínová & Šlégr, 2015).

The connection of this type of sensor to the Arduino board is simple, is described in the Figure 11.7. The pH probe must be connected to the complementary board. This complementary board has to be connected to the Arduino with the (-)-GND, (+)-5V and A-Analogic GPIO connections (Parida, 2020). There are different pH probes of different companies and each one requires a different code. One example of the different pH probes is the gravity: analogic pH Sensor whose code is available in their web page (DFRobot, 2022). Due each brand has a different model with a different library and for that a specific code it is not possible to provide an only one code to use in all devices, it is necessary to search the code provided by the company.
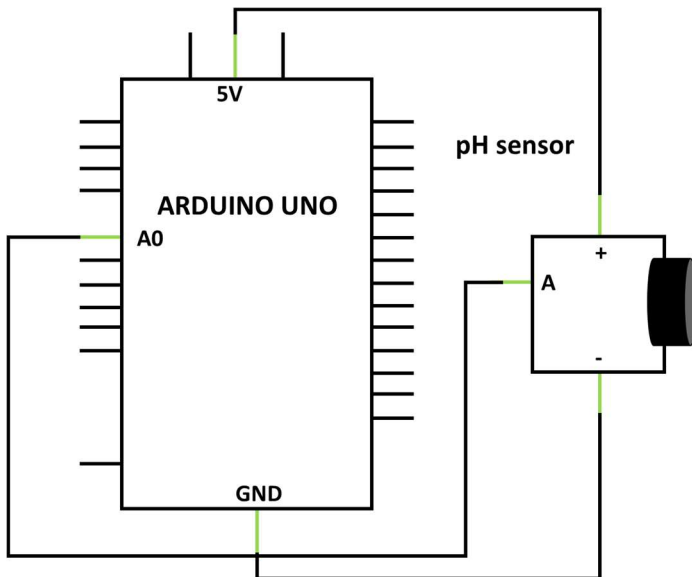
Figure 11.7: pH sensor assembly diagram.

4.   Light sensors

A photoresistor or LDR (light-dependant resistor) is a simple device that change its resistance according to the light received (Llamas, 2015). This type of devices can be used as light sensors. It is possible to use the variation of its resistance using analogic GPIOS to get a value of the measure of the light. Due this type of sensors can measure changes in the light conditions it is possible to obtain information about different parameters. For example, it is possible to get information about the turbidity of a solution. For a higher turbidity, less is the amount of light that the photoresistor receive and then the resistance of the sensor is higher (Faroqi et al., 2018). Other usefulness of this type of devices is the creation of automated analysis

instruments. If the analytical procedure involves colour changes it is possible to use LDRs. One of them is a titration with an indicator (Vijayalaxmi et al., 2020). With an evaluation of the resistance of the sensor before and after performing the titration it is possible to determine the end point of the procedure. This allows to automate the analysis with very low cost elements.

LDRs can work by itself, but it is useful to couple other elements to create instruments more complex. If a wavelength selector is coupled to an LDR it is possible to create a spectrophotometer (Adams-McNichol et al., 2019). This combination allows the sensor to only measure the resistance due to radiation of the specific wavelength. Other use of this sensor is use it as detector of the light emitted due to a chemical reaction. It is possible to create devices with materials that carry out a (bio)luminescent reaction and the radiation emitted would be measured by the LDR (Chao et al., 2021). In this case is possible to make a calibration line to be able to measure the concentration of the analyte in the surface or solution (Halima et al., 2022). This sensor is very versatile and work in different systems according to the user necessities.

The simplest photoresistors are made with a semiconductor with a high resistance like the cadmium sulphide. Normal values of resistance are from 1 MΩ in dark to 100 Ω under bright light (Llamas, 2015). To assembly this sensor it is necessary to connect one side of the LDR to the 5V GPIO and the other side to a 10 KΩ resistance and to an analogic GPIO of the Arduino board simultaneously. The other side of the resistance has to be connected to GND GPIO of the Arduino board. The scheme to connect the sensor is showed in the Figure 11.8. The code to program this sensor is very simple and is in the Annex 11.7.

Other light sensor that is more complex is the lux sensor like the BH1750. The difference between this type of sensor and the photoresistor is that this provides the lux measure (lumen/m^2) (Nylamp Mechatronic, 2021). These sensors, as the previous one, can be used to get the light measure using it as spectrophotometer (Nandiyanto et al., 2018) or to monitoring environment conditions (Sobari et al., 2021). Photoresistors and lux sensor has the same purpose, but the second one is more sensible and accurate. Photoresistors only provide a measure of the resistance in a 1024 scale, but the lux sensor provides the light measure in a range of 65536 units (2^{16} bits). This sensor is bit more complex of connect and program, because it is necessary to use the I2C protocol. The I2C (inter-integrated circuit) protocol is a way to connect 2 devices where one of them is the master and the other is the slave. This connection requires two data channels. The first one is the

SCL (Serial Clock) that is used by the master device to provide the clock signal to the slave device. The other one is the SDA (Serial Data) that is used to exchange data between both devices (Cambell, 2016).
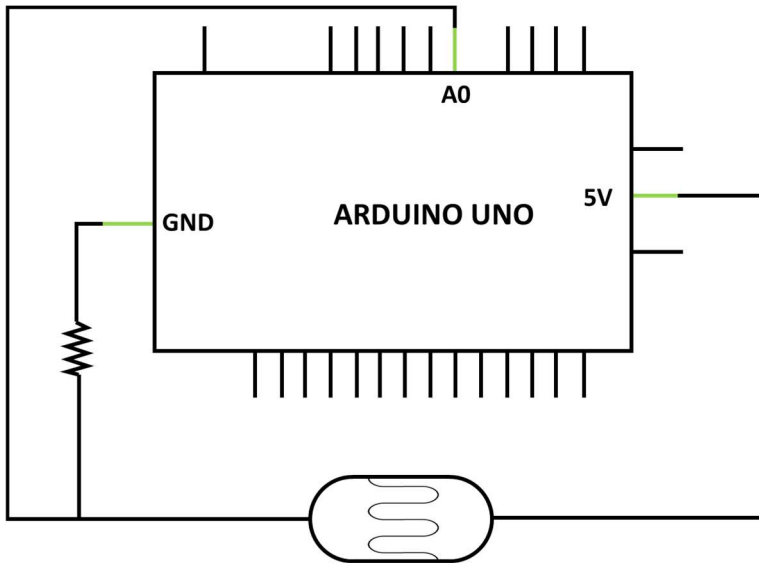
Figure 11.8: Photoresistor assembly diagram.

The scheme to connect this sensor is in the Figure 11.9. To make the connections it is necessary connect the GND, SDA, SCL and Vcc GPIOs of the Lux sensor to the GND, SDA, SCL and 5V GPIOs of the Arduino board respectively. The SDA and SCL GPIOs of the Arduino board it is different according to the board model. In Arduino Uno, Nano and Mini Pro the SDA GPIO is the A4 and the SCL is the A5. The code to use the BH1750 sensor is in the Annex 11.8. For this sensor it is necessary to include the "Wire.h" and "BH1750.h" libraries.

Previous sensors are very useful but only provide one type of information, amount of light. To solve this problematic there are colour sensors like TCS34725. This sensor has Red, Green, Blue (RGB) and Clear light sensing with IR Blocking Filter in a 4x3 matrix. This device allows to get information about the colour of the light. Sometimes the changes of the light are due to colour changes, and not due to the light amount. This can be observed in titrations with an indicator like bromothymol blue or methyl orange. TCS34725 sensor has been used as a spectrophotometer substitute to make the measure of the amount of dye in a solution (De Carvalho Oliveira et al., 2022). This sensor can be used to determine analytes by colorimetric reactions, for example monitoring of phosphorus in water to avoid algal bloom

296

using the ammonium molybdate method (De Mello, 2019). Other type of analytes that can be measured is the amount of nanoparticles in the solution by measuring the colour of the solution (Zarantonello et al., 2020).
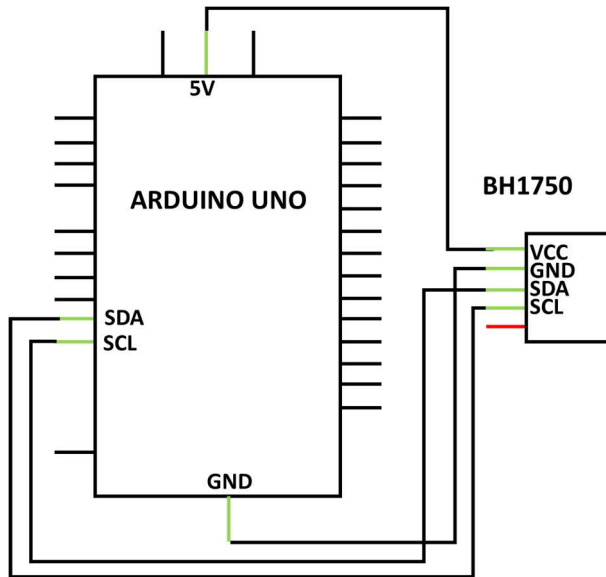
Figure 11.9: BH1750 sensor assembly diagram.

This sensor, as the BH1750 Lux sensor, require the use of the I2C protocol. The connection between the TCS34725 and the Arduino board, requires to link the SDA, SCL, GND and Vin GPIOs of the sensor with the SDA, SCL, GND and 5V GPIOs of the board respectively. Moreover, the sensor has a LED light source that turn on unless would be connected to GND GPIO of the Arduino board or the INT connection of the sensor. The mount scheme is showed in the Figure 11.10. To program this sensor, it is necessary to use the "Wire.h" and "Adafruit_TCS34725.h" libraries. The code is in the Annex 11.9.
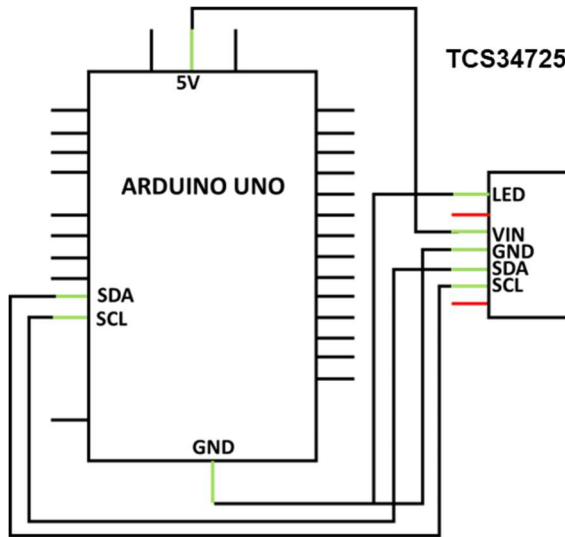
Figure 11.10: TCS34725 sensor assembly diagram.

5.   Chemical sensors

In this group the mainly sensors are the gas sensor. The sensors are sensitive to specific types of gas and then the conductivity of the material used in the different sensors increase with the increasing concentration of target gas (Pal et al., 2017). Since these types of sensors only serve to detect specific compounds, they are mainly used for the creation of air quality and safety control systems. Among the gas sensors, the most used are those of the MQ family (Abbas et al., 2020; Akpan et al., 2021; Baballe et al., 2021; Babu & Nagaraja, 2018; Colaco & Lohani, 2017; Falohum et al., 2016; Katrandzhiev & Karnobatev, 2016; Nasution et al., 2018; Nugraha, 2018; Rahmalisa et al., 2021; Rivai et al., 2019; Sakayo et al., 2019; Samaniego et al., 2016; Sanger et al., 2021; Tunggal et al., 2020). Table 11.1 lists the main sensors and what they are used for.

These sensors are made up of an Al_2O_3 ceramide tube and a gas-sensitive layer of SnO_2. These sensors have a Ni-Cr allow heater coil to provide the necessary working conditions to perform the measurement (Hanwei Electronics, 2022a-n; Winsen, 2015). These sensors have a very simple connection that can be seen in Figure 11.11. To make the connections of this sensor, you have to connect the GPIO GND, VCC and A0 of the MQ to the GPIO GND, 5V and an analogic pin of the Arduino board respectively. To obtain the sensor measurements, it is necessary to receive the signals through the analogic pin and then transform said signal into the voltage by means of a conversion factor. The programming code is found in the Annex 11.10.

Table 11.1: Main sensors used and the parameters that detect each one.

Sensor	gas	Sensor	gas
MQ-2	Methane, Butane, PLG, Smoke	MQ-131	Ozone
MQ-3	Alcohol, Ethanol, Smoke	MQ-135	Benzene, Alcohol, Smoke, Air quality
MQ-4	Methane, PLG	MQ-136	hydrogen sulphide
MQ-5	Natural gas, PLG	MQ-137	Ammonia
MQ-6	Butane, PLG	MQ-138	Benzene, Toluene, Alcohol, Acetone, Propane, Formaldehyde, Hydrogen
MQ-7	Carbon monoxide		
MQ-8	Hydrogen	MQ-214	Methane, Natural gas
MQ-9	Carbon monoxide, flammable gases	MQ-216	natural gas, coal gas

PLG: Petroleum liquid gas

These sensors can have a wide variety of uses in different environments and for different purposes. The main use of these gases is to check the quality of the air. By combining different sensors such as MQ2, MQ3, MQ5, MQ7 and MQ137, devices can be created to monitor concentrations of different compounds in the environment (Abbas et al., 2020; Akpan et al., 2021; Tunggal et al., 2020). In these cases, the sensors are not used for a specific purpose, but simply provide information on the environmental conditions. These sensors have been able to be used in specific places to verify that they presented expired conditions and thus avoid contamination (Abbas et al., 2020; Tunggal et al., 2020) such as in recycling plants (Colaco & Lohani, 2017) or the evaluation of gases released by waste (Sanger et al., 2021).
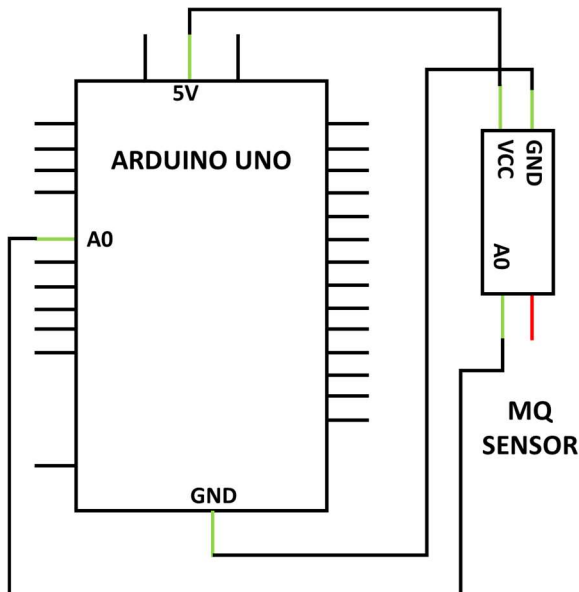
Figure 11.11: MQ type sensor assembly diagram.

Since these sensors can evaluate air quality, they have been used for risk assessment and security systems with sensors such as the MQ5, MQ6, MQ7, MQ9 or the MQ138. In these cases, the sensors have been used to control acetone breathing (Nasutio et al., 2018) or to assess leaks in conduction systems (Baballe et al., 2021; Babu & Nagaraja, 2018; Falohum et al., 2016; Katrandzhiev & Karnobatev, 2016; Rahmalisa et al., 2021). When monitoring the environment, these sensors can warn of the presence or increased concentration of gases in the environment. In this way security devices can be created. These sensors do not have to be used only in industrial or environmental environments (Samaniego et al., 2016), but can also be used in domestic environments to avoid incidents (Sakayo et al., 2019).

These sensors can not only be used to obtain information from the environment, but can also be used to interpret the information measured by them. One of these examples is the development of devices for the quantification of alcohol in drivers and in this way ensure that they are in conditions to drive the vehicle using an MQ3 (Sahu et al., 2017) sensor. As certain compounds are also found in food products, therefore, these sensors can also be used for the evaluation of the freshness of fish using the gases sensor MQ136 and MQ137 (Rivai et al., 2019). In the laboratory it could also provide information about the course of a reaction. Gas sensors placed before and after a treatment can provide information about what has happened during that procedure (Nugraha, 2018).

6. References

Abbas, F. N., Saadoon, M. I. M., Abdalrdha, Z. K., & Abud, E. N. (2020). Capable of gas sensor MQ-135 to monitor the air quality with Arduino Uno. *International Journal of Engineering Research and Technology,* 13(10), 2955-2959. DOI: 10.37624/IJERT/13.10.2020.2955-2959.

Adams-McNichol, A., L., Shiell, R. C., & Ellis, D. A. (2019). Accurate, Photoresistor-Based, Student-Built Photometer and Its Application to the Forensic Analysis of Dyes. *Journal of Chemical Education*, 96(6), 1143-1151.DOI: 10.1021/acs.jchemed.8b00862.

Akpan, V. A., Eyefia, A. S., & Adewumi, G. M. (2021).An IoT-Based Real-Time Embedded System for Gas-Smoke Detection with Automatic Electronic Alarm System. *International Journal of Electronics Engineering and Computer Science*, 6(2), 2-17.

Baballe, M. A., Magashi, U. Y., Garko, B. I., Umar, A. A., Magaji, Y. R., & Surajo, M. (2021). Automatic Gas Leakage Monitoring System Using MQ-5 Sensor. *Review of Computer Engineering Research*, 8(2), 64-75. DOI: 10.18488/journal.76.2021.82.64.75.

Babu, K. S., & Nagaraja, C. (2018). Calibration of MQ-7 and Detection of Hazardous Carbon Monoxide Concentration in Test Canister. International *Journal of Advance Research, Ideas and Innovations in Technology*, 4(1), 18-24. www.IJARIIT.com.

Badamasi, Y. A. (2014). The working principle of an Arduino. In 11th international conference on electronics, computer and computation (ICECCO), Abuja, Nigeria, pp. 1-4, DOI: 10.1109/ICECCO.2014.6997578.

Banzi, M., & Shiloh, M. (2022). Getting started with Arduino: The Open Source Electronics Prototyping Platform. 3rd Edition. Maker Media, Inc.

Bhadani, P., & Vashisht, V. (2019). Soil moisture, temperature and humidity measurement using arduino. In 9th International Conference on Cloud Computing, Data Science & Engineering (Confluence). Noida, India, pp. 567-571. DOI: 10.1109/CONFLUENCE.2019.8776973.

Brock, J. D., Bruce, R. F., & Reiser, S. L. (2009). Using Arduino for introductory programming courses. *Journal of Computing Sciences in Colleges*, 25(2), 129-130.

Cambell, S. (2016) Basic of the I2C communication protocol. https://www.circuitbasics.com/basics-of-the-i2c-communication-protocol/ [Accessed October 21, 2022]

Chao, Y. T., Prabhu, G. R. D., Yu, K. C., Syu, J. Y., & Urban, P. L. (2021). BioChemPen for a Rapid Analysis of Compounds Supported on Solid Surfaces. *ACS Sensors*, 6(10), 3744-3752. DOI: 10.1021/acssensors.1c01540.

Colaco, J., & Lohani, R. B. (2017). Health care System in recycling plants and garbage waste disposal sites. *International Research Journal of Engineering and Technology*, 4(11), 772-775.

Das, D. (2022). How Does a Soil Moisture Sensor Work and how to use it with Arduino?. https://circuitdigest.com/microcontroller-projects/interfacing-soil-moisture-sensor-with-arduino-uno. [Accessed October 19, 2022]

De Carvalho Oliveira, G., Machado, C. C. S., Inácio, D. K., da Silveira Petruci, J. F., & Silva, S. G. (2022). RGB colour sensor for colorimetric determinations: Evaluation and quantitative analysis of coloured liquid samples. *Talanta*, 241, 123244. DOI: 10.1016/j.talanta.2022.123244.

De Mello, R. V. N., dos Santos Junior, C. R., de Melo, L. A., da Silva, L. M., Cardoso, V. F., & Pelegrini, M. V. (2019). An Autonomous Microfluidic Device for Water Quality Monitoring in Continuous Flow. https://sbmicro.org.br/sforum-eventos/sforum2019/An%20Autonomous%20Microfluidic%20Device%20for%20Water%20Quality%20Monitoring%20in%20Continuous%20Flow.pdf

Del Valle, L. (2017). DS18B20 sensor de temperatura para líquidos con Arduino. https://programarfacil.com/blog/arduino-blog/ds18b20-sensor-temperatura-arduino/ [Accessed October 19, 2022]

Demiris, G., & Hensel, B. K. (2008). Technologies for an aging society: a systematic review of "smart home" applications. *Yearbook of medical informatics*, 17(01), 33-40.

DFRobot. https://www.dfrobot.com/product-1782.html. [Accessed October 19, 2022]

Falohun, A. S., Oke, A. O., Abolaji, B. M., &Oladejo, O. E. (2016). Dangerous gas detection using an integrated circuit and MQ-9. *International Journal of Computer Applications*, 135(7), 30-34. DOI: 10.5120/ijca2016908473.

Faroqi, A., Ramdhani, M. A., Kamelia, L., Hidayat, C., & Rofiq, A. (2018). Automatic water clarity monitoring and filtration system using light dependent resistor based on arduino uno. In 4th International Conference on Wireless and Telematics (ICWT) (pp. 1-4). IEEE. DOI: 10.DOI:10.1088/1742-6596/986/1/0120121109/ICWT.2018.8527786.

Halima, A. N. S. A., Keyon, A. S. A., & Nor, N. S. M. (2022). Development of a Portable Spectrophotometer Employing Arduino Microcontroller System for Pollutant Analysis. *Proceedings of Science and Mathematics,*6, 6-9.

Han, Y., Feng, Y., Lou, H., & Zhang, X. (2018). Thermocouple-based Temperature Sensing System for Chemical Cell Inside Micro UAV Device. In *Journal of Physics: Conference Series,* 986(1), 012012. DOI: 10.1088/1742-6596/986/1/012012.

Hanwei Electronics. (2022a). Technical Data MQ-2 gas sensor. https://datasheetspdf.com/pdf-file/622943/Hanwei/MQ-2/1. [Accessed October 21, 2022]

Hanwei Electronics. (2022b). Technical Data MQ-3 gas sensor. https://www.sparkfun.com/datasheets/Sensors/MQ-3.pdf. [Accessed October 21, 2022]

Hanwei Electronics. (2022c). Technical Data MQ-4 gas sensor. https://www.e-ika.com/downloads/MQ-4.pdf. [Accessed October 21, 2022]

Hanwei Electronics. (2022d). Technical Data MQ-5 gas sensor. https://files.seeedstudio.com/wiki/Grove-Gas_Sensor-MQ5/res/MQ-5.pdf. [Accessed October 21, 2022]

Hanwei Electronics. (2022e). Technical Data MQ-6 gas sensor. https://www.sparkfun.com/datasheets/Sensors/Biometric/MQ-6.pdf. [Accessed October 21, 2022]

Hanwei Electronics. (2022f). Technical Data MQ-7 gas sensor. https://www.sparkfun.com/datasheets/Sensors/Biometric/MQ-7.pdf. [Accessed October 21, 2022]

Hanwei Electronics. (2022g). Technical Data MQ-8 gas sensor. https://dlnmh9ip6v2uc.cloudfront.net/datasheets/Sensors/Biometric/MQ-8.pdf. [Accessed October 21, 2022]

Hanwei Electronics. (2022h). Technical Data MQ-9 gas sensor. https://www.electronicoscaldas.com/datasheet/MQ-9_Hanwei.pdf. [Accessed October 21, 2022]

Hanwei Electronics. (2022i). Technical Data MQ-131 gas sensor. https://cdn.sparkfun.com/assets/9/9/6/e/4/mq131-datasheet-low.pdf. [Accessed October 21, 2022]

Hanwei Electronics. (2022j). Technical Data MQ-135 gas sensor. https://www.olimex.com/Products/Components/Sensors/Gas/SNS-MQ135/resources/SNS-MQ135.pdf. [Accessed October 21, 2022]

Hanwei Electronics. (2022k). Technical Data MQ-136 gas sensor. http://www.sensorica.ru/pdf/MQ-136.pdf. [Accessed October 21, 2022]

Hanwei Electronics. (2022l). Technical Data MQ-138 gas sensor. https://www.mysensors.org/dl/57c3ebeb071cb0e34c90057a/design/MQ-138.pdf. [Accessed October 21, 2022]

Hanwei Electronics. (2022m). Technical Data MQ-214 gas sensor. https://www.mysensors.org/dl/57c3ebeb071cb0e34c90057a/design/1341.pdf. [Accessed October 21, 2022]

Hanwei Electronics. (2022n). Technical Data MQ-216 gas sensor. http://www.sensorica.ru/pdf/MQ-216.pdf. [Accessed October 21, 2022]

Hariyanto, M. W., Hendrawan, A. H., & Ritzkal, R. (2020). Monitoring the environmental temperature of the Arduino assistance engineering faculty using telegram. *Journal of Robotics and Control*, 1(3), 96-101. DOI: 10.18196/jrc.1321.

Katrandzhiev, N. T., & Karnobatev, N. N. (2016). Elaboration of a Microprocessor Unit for Gas Measurement with Sensor MQ-6. *Scientific Works of University of Food Technologies*, 63(2), 299-306.

Koestoer, R. A., Pancasaputra, N., Roihan, I., & Harinaldi. (2019). A simple calibration methods of relative humidity sensor DHT22 for tropical climates based on Arduino data acquisition system. In AIP Conference Proceedings, 2062(1), 020009. AIP Publishing LLC. DOI: 10.1063/1.5086556.

Kubínová, S., & Šlégr, J. (2015). ChemDuino: Adapting Arduino for low-cost chemical measurements in lecture and laboratory. *Journal Chemical Education*, 92(10), 1751–1753. DOI: 10.1021/ed5008102.

Liu, M., & Zhang, C. (2019). Design of hierarchical monitoring system for crop growth environment based on arduino in development platform. In 2nd International Conference on Safety Produce Informatization (IICSPI) (pp. 515-519). IEEE.

Llamas, L. (2015). Medir nivel de luz con Arduino y fotorresistencia LDR (GL55). https://www.luisllamas.es/medir-nivel-luz-con-arduino-y-fotoresistencia-ldr/ [Accessed October 21, 20022].

Llamas, L. (2016a). Medir temperatura y humedad con Arduino y sensor DHT11-DHT22. https://www.luisllamas.es/arduino-dht11-dht22/ [Accessed October 19, 20022].

Llamas, L. (2016b). Medir temperatura de líquidos y gases con Arduino y DS18B20. https://www.luisllamas.es/temperatura-liquidos-arduino-ds18b20/ [Accessed October 19, 20022].

Lozano, R. (2020). Medir temperatura con termopar tipo K y MAX6675. https://www.taloselectronics.com/blogs/tutoriales/medir-temperatura-con-termopar-tipo-k-y-max6675 [Accessed October 19, 20022].

McClain, R. L. (2014). Construction of a Photometer as an Instructional Tool for Electronics and Instrumentation. *Journal of Chemical Education*, 91(5), 747-750. DOI: 10.1021/ed400784x.

MisterBotBreak. (2019). How to use a soil moisture sensor. https://create.arduino.cc/projecthub/MisterBotBreak/how-to-use-a-soil-moisture-sensor-ce769b [Accessed October 19, 20022]

Nandiyanto, A. B. D., Zaen, R., Oktiani, R., Abdullah, A. G., & Riza, L. S. (2018). A simple, rapid analysis, portable, low-cost, and Arduino-based spectrophotometer with white LED as a light source for analyzing solution concentration. *TELKOMNIKA (Telecommunication Computing Electronics and Control)*, 16(2), 580-585. DOI: 10.12928/telkomnika.v16i2.7159.

Nasution, T. I., Asrosa, R., & Nainggolan, I. (2018, December). Application of MQ-138 Semiconductor Sensor for Breath Acetone Detection. *Journal of Physics: Conference Series,* 1116(3), 032023. DOI: 10.1088/1742-6596/1116/3/032023.

Naylamp Mechatronic. (2021). SENSOR DE TEMPERATURA Y HUMEDAD RELATIVA DHT11. https://naylampmechatronics.com/sensores-temperatura-y-humedad/57-

sensor-de-temperatura-y-humedad-relativa-dht11.html [Accessed October 19, 20022].

Nugraha, A. T. (2018). Dirty air filter using boxed equalizer MQ-8 and MQ9 wheeled robot. Journal of Electrical Engineering, Mechatronic and Computer Science, 1(1), 23-26. DOI: 10.26905/jeemecs.v1i1.2301.

Nussey, J. (2013). Arduino for dummies. John Wiley & Sons.

Parida, D. (2020). pH Meter using Arduino Uno and LCD Display. https://circuitdigest.com/microcontroller-projects/arduino-ph-meter [Accessed October 19, 20022]

Parihar, V. R., Tonge, A. Y., & Ganorkar, P. D. (2017). Heartbeat and temperature monitoring system for remote patients using Arduino. *International Journal of Advanced Engineering Research and Science*, 4(5), 237161. DOI: 10.22161/ijaers.4.5.10.

Perea, F. (2015). Arduino essentials. Packt Publishing Ltd.

Pundir, A. S., & Singh, K. (2019). Temperature control of real-time identified fixed bed reactor by adaptive sliding mode control equipped with Arduino in Matlab. *Asia-Pacific Journal of Chemical Engineering*, 14(2), e2297. DOI: 10.1002/apj.2297.

Rahmalisa, U., Febriani, A., & Irawan, Y. (2021). Detector Leakage Gas Lpg Based On Telegram Notification Using Wemos D1 and Mq-6 Sensor. *Journal of Robotics and Control*, 2(4), 287-291. DOI: 10.18196/jrc.2493.

Recktenwald, G. (2013). Temperature Measurement with a Thermistor and an Arduino. Pdx. Edu.

Rivai, M., Misbah, Attamimi, M., Firdaus, M. H., & Tukadi. (2019, November). Fish Quality Recognition using Electrochemical Gas Sensor Array and Neural Network. In International Conference on Computer Engineering, Network, and Intelligent Multimedia (CENIM), 1-5. IEEE.

Sahu, P., Dixit, S., Mishra, S., & Srivastava, S. (2017). Alcohol detection based engine locking system using MQ-3 sensor. *International Research Journal of Engineering and Technology*, 4(4), 979-981.

Sakayo, N. M., Mutuku, J. N., & Ngaruiya, J. M. (2019). Design and Calibration of a Microcontroller Based MQ-4 Gas Sensor for Domestic Cooking Gas System.

International Journal of Applied Physics, 6(2), 31-40. DOI: 10.14445/23500301/IJAP-V6I2P106.

Samaniego, J. G., Romero, F. T., Amaya, O. C., Tovar, L. M., López, G., Gonsález, J. M., & Morales, A. (2016). Sistema Computarizado de sensado de Gases Contaminantes. VII Taller Iberoamericano de Enseñanza de la Física Universitaria. La Habana, Cuba.

Sanger, J. B., Sitanayah, L., & Ahmad, I. (2021). A Sensor-based Garbage Gas Detection System. In 11th Annual Computing and Communication Workshop and Conference (CCWC), 1347-1353. IEEE. DOI: 10.1109/CCWC51732.2021.9376147.

Santocoyo. (2019). Comparison-of-sensitivity-of-temperature-sensors-LM35-and-DS18B20. https://github.com/Santocoyo/Comparison-of-sensitivity-of-temperature-sensors-LM35-and-DS18B20 [Accessed October 19, 20022].

Santos, S. (Consulted 19/10/2022). https://randomnerdtutorials.com/arduino-k-type-thermocouple-max6675/.

Schmidt, M. (2015). Arduino: a quick-start guide. Arduino: A Quick-Start Guide, 1-324.

Sobari, E., Vernanda, D., Purnawan, N. N., Apandi, T. H., & Aris, M. A. (2021). The Performances of Environmental Control Systems to Hydroponics Agriculture Based on Microcontroller. *Journal of Telecommunication, Electronic and Computer Engineering (JTEC)*, 13(1), 37-43.

Supriadi, O., Sunardi, A., Baskara, H. A., & Safei, A. (2019, July). Controlling pH and temperature aquaponics use proportional control with Arduino and Raspberry. *Conference Series: Materials Science and Engineering*, 550 (1), 012016. IOP Publishing.

Susa, J. A. B., Malbog, M. A. F., Mindoro, J. N., Casuat, C. D., & Alon, A. S. (2020). Automatic room humidifier and dehumidifier controller using Arduino Uno. *International Journal of Advanced Trends in Computer Science and Engineering*, 9(2), 2208-2212. DOI: 10.30534/ijatcse/2020/198922020.

Taneja, K., & Bhatia, S. (2017). Automatic irrigation system using Arduino UNO. In International Conference on Intelligent Computing and Control Systems (ICICCS), 132-135. IEEE. DOI: 10.1109/ICCONS.2017.8250693.

Tang, X., Tan, C., Chen, A., Li, Z., & Shuai, R. (2020). Design and implementation of temperature and humidity monitoring system for small cold storage of fruit and

vegetable based on Arduino. *Journal of Physics: Conference Series,* 1601(6), 062010. IOP Publishing. DOI: 10.1088/1742-6596/1601/6/062010.

Thakare, S., & Bhagat, P. H. (2018). Arduino-based smart irrigation using sensors and ESP8266 WiFi module. In Second International Conference on intelligent computing and control systems (ICICCS), 1-5. IEEE. DOI: 10.1109/ICCONS.2018.8663041.

Tunggal, T. P., Sanjaya, A., Widodo, H. A., Kunal, K., & Nguyen, P. T. (2020). Gas Pressure Measurement Device and Medical Vacuum Design. *Journal of Robotics and Control*, 1(2), 35-39. DOI: 10.18196/jrc.1208.

Vallejo, W., Diaz-Uribe, C., & Fajardo, C. (2020). Do-it-yourself methodology for calorimeter construction based in Arduino data acquisition device for introductory chemical laboratories. *Heliyon*, 6(3), e03591. DOI: 10.1016/j.heliyon.2020.e03591.

Vijayalaxmi, Ashwin, S. H., & Harish, S. V. (2020). Titration machine: A new approach using Arduino. In Kalam, A., Niazi, K., Soni, A., Siddiqui, S., Mundra, A. (Eds) Intelligent Computing Techniques for Smart Energy Systems. Lecture Notes in Electrical Engineering, vol 607. Springer, Singapore. DOI: 10.1007/978-981-15-0214-9_15.

Winsen. Ammonia Gas Sensor. (2015). Manual https://www.winsen-sensor.com/d/files/semiconductor/mq137.pdf [Accessed October 21, 20022]

Zarantonello, F., Mancin, F., & Bonomi, R. (2020). Working in a Team: Development of a Device for Water Hardness Sensing Based on an Arduino–Nanoparticle System. *Journal of Chemical Education*, 97(7), 2025-2032. DOI: 10.1021/acs.jchemed.9b01156.

Thermocupled with max6675 module

```
//introduce parameters of the code: libraries, constants, etc.
#Include "max6675.h"
// specify digital pins in which the pines of the module are connected
int thermoDO = 4;
int thermoCS = 5;
int thermoCLK = 6;
//Initialice the module
MAX6675 thermocouple(thermoCLK, thermoCS, thermoDO);
void setup()
{
        // Initialice the connection with the computer
        Serial.begin(9600);

}

void loop()
{
         // Reading of the temperatura values
        Serial.print("C = ");
        Serial.println(thermocouple.readCelsius());
        Serial.print("F = ");
        Serial.println(thermocouple.readFahrenheit());
         // It is neccesary to wait at least 250 ms tu updat the Reading , a wait of 1
        second is implemented
        delay(1000);
}
```

DHT11/DHT22

```
//Introduce parameters of the code: libraries, constants, etc...
#include "DHT.h"
//Define your DTH model. uncomment whtever type that you are using
#define DHTTYPE DHT11   // DHT 11
//#define DHTTYPE DHT22   // DHT 22  (AM2302), AM2321
//Digital pin of the conection with the DHTXX
const int DHTPin = 5;
//Inictialize the sensor
DHT dht(DHTPin, DHTTYPE);
void setup()
{
        Serial.begin(9600);
        dht.begin();
}

void loop()
{
        //It is necessary to wait some seconds between readings, each reading
        require 250ms
        delay(2000);
        // save the radings as variables
        float h = dht.readHumidity();
        float t = dht.readTemperature();
         //If the sensor not working correctly provide an error message
        if (isnan(h) || isnan(t))
        {
                Serial.println("ERROR");
                return;
        }
        //Print de humidity and temperature readings
        Serial.print("Humidity: ");
        Serial.print(h);
        Serial.print(" %\t");
        Serial.print("Temperature: ");
        Serial.print(t);
        Serial.print(" *C ");
}
```

DS18B20

```
#include <OneWire.h>
#include <DallasTemperature.h>
//Digital pin of the conection with the sensor
const int oneWirePin = 5;
//Inictialize the sensor
OneWire oneWireBus(oneWirePin);
DallasTemperature sensor(&oneWireBus);
void setup()
{
        Serial.begin(9600);
        sensor.begin();
}

void loop()
{
        //Print the temperature readings
        Serial.print("Temperature: ");
        Serial.print(sensor.getTempCByIndex(0));
        Serial.println(" ºC");
        delay(1000);
}
```

LM35

```
// Variables that will be used
float Cgrades;
int S = 0;  // it is necessary to connect ot an analogic GPIO
 void setup()
{
        Serial.begin(9600);
}
 void loop()
{
        // AnalogRead allow to read the sensor data (a value between 0 and
        1023)
        Cgrades = analogRead(S);
        // To calculate the temperature it is necesary to convert into
        voltage
        // The voltage provided is between 0 and 5
        // With the first equation the voltage is calculated
        // Normalization of the analogic read and voltage (mV) calculation
        float mV = (Cgrades / 1023.0) * 5000;
        // The device increase 10mV/C
        // To calculate celsius grades it is necessary to make the conversion
        float C = mV / 10;
        Serial.print(C);
        Serial.println(" C");
        // A waiting time is coded
        delay(1000);
}
```

Soil moisture sensor

```
//Analogic pin of the conection with the sensor
int pin = A0;
//Variables that will be used
//Variable X is the sensor value provided in dry soil
//Variable Y is the sensor value provided in wet soil
//Both values has to be evaluated by raw measure
int moisture ;
int X = 10;
int y = 1;
void setup()
{
        Serial.begin(9600);
  }

void loop()
{
        //The analogic measure is readed by the arduino board
        moisture= analogRead(pin);
        //To evaluate the raw data is necessary to use this part, later
        comment it
        Serial.print("Raw measure : ");
        Serial.print(moisture);
         //The map function  change the scale used into other scale.
        uncomment when the raw data is evaluated
        // moisture = map(moisture,X,Y,0,100);
        // Serial.print("Soil Mositure : ");
        // Serial.print(moisture);
        // Serial.println("%");
        delay(1000);
  }
```

Water level sensor

```
//variable that will be used
int level;
void setup ()
{
        Serial.begin (9600);
}
 void loop()
{
        // Read the input on analog pin to get the water level measure
        level = analogRead(A0);
        Serial.print(level);
 }
```

Photoresistor

```
//Introduce the GPIO that it is connected to the LDR
const int LDR= A0;
int light=0;
void setup()
{
        //Stablish the LDR as Input data GPIO
        pinMode(LDR, INPUT);
}
void loop()
{
        //Read the resistance of the sensor as a value between 0 and 1023
        light = analogRead(LDR);
        Serial.println(light);

}
```

BH1750

```
//Introduce parameters of the code: libraries, constants, etc...
#include <Wire.h>
#include <BH1750.h>
//Definte the device
BH1750 luxsensor;
//Stablish the sensor mode
//There are 3 resolution modes
//Low Resolution - 4 lux
//High Resolution - 1 lux
//High Resolution 2 - 0.5 lux
//There are 2 shot modes
//Continuous - measures all time
//One time - measures when it is requested
const byte luxM = BH1750_CONTINUOUS_HIGH_RES_MODE;
// BH1750_CONTINUOUS_HIGH_RES_MODE
// BH1750_CONTINUOUS_HIGH_RES_MODE_2
// BH1750_CONTINUOUS_LOW_RES_MODE
// BH1750_ONE_TIME_HIGH_RES_MODE
// BH1750_ONE_TIME_HIGH_RES_MODE_2
// BH1750_ONE_TIME_LOW_RES_MODE
void setup()
{
        Serial.begin(9600);
        // Initialize BH1750
        luxometro.begin(luxM);
}
void loop()
{
        // BH1750 measure reading
        uint16_t lux = luxsensor.readLightLevel();
        Serial.print(lux);
        //It is necessary to wait some time between readings
        delay(500);
}
```

TCS34725

```
//Introduce parameters of the code: libraries, constants, etc...
#include <Wire.h>
#include "Adafruit_TCS34725.h"
//The conditions of the sensor are programed
//The integration time of 700ms is used to get the higher sensibility
Adafruit_TCS34725 tcs = Adafruit_TCS34725(TCS34725_INTEGRATIONTIME
_700MS, TCS34725_GAIN_1X);
void setup(void)
{
        Serial.begin(9600);
        if (!tcs.begin())  // Check if the sensor runs correctly
        {
                Serial.println("Error");
                while (1) delay(1000);
        }
 }
 void loop(void)
{
        // stablish the variables of the parameters obtained by the sensor
        uint16_t r, g, b, c, colourT, lux;
        //obtain the value of each colour and calculate de Colour Tª and Lux
        tcs.getRawData(&r, &g, &b, &c);
        colourT = tcs.calculateColourTemperature(r, g, b);
        lux = tcs.calculateLux(r, g, b);
        Serial.println(colourT, DEC);
        Serial.println(lux, DEC);
        Serial.println(r, DEC);
        Serial.println(g, DEC);
        Serial.println(b, DEC);
        Serial.println(c, DEC);
        //It is necessary to wait 700ms to make the reading of the measures
        //Due that a 1s delay is programed between measures
        delay(1000);
}
```

MQ sensor

```
void setup()
{
        Serial.begin(9600);
}
void loop()
{
        //Read the measure with the MQ sensor
        int MQ = analogRead(A0);
        //It is neccesary to transform the measure into voltaje measure
        float v = MQ * (5.0 / 1023.0);
        //Convertimos la lectura en un valor de voltaje
        Serial.println(V);
        delay(100);
}
```

CHAPTER 12: Development of an automated colorimeter controlled by Raspberry Pi4
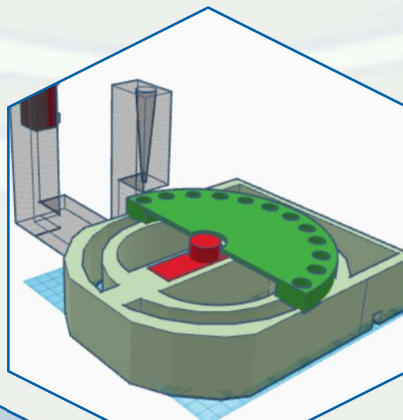
ABSTRACT

A low-cost new instrument to carry out automated colorimetric analysis has been developed. The device consists of a carousel sampler, built by a 3D-printer, and a Raspberry Pi4-controlled signal measurement module based on the RGBC (red, green, blue and clear) responses of a TCS34725 colour light-to-digital converter with IR filter. The device has been tested with calibration standards of different food dyes (Tartrazine, Red Allure AC and Brilliant Blue FCF) and three food samples containing one of each food dye. The new device provides $R^2 > 0.995$ and a LOD of 1.1, 1.4 and 0.1 mmol L^{-1} for each food dye, respectively. The results are statistically comparable to those obtained with a conventional benchtop spectrophotometer. The proposed device achieves a reduction in sample and waste volume and in analysis time, minimizes the use of energy, and allows in situ measurements, being an automated method it is safer for operators in comparison to the reference method, yielding similar analytical results and following the principles of green analytical chemistry.

Keywords: Arduino, Chemical analysis, Food dyes, RGB

1.   Introduction

The development of new technologies has caused a growth of research works in electronic devices to perform analytical procedures (Cherbuin et al., 2019; Di Nonno & Ulber, 2021; Gali, 2017; Jung et al., 2015; Leeuw et al., 2013; Otal et al., 2021; Soares et al., 2019; Wang et al., 2016). The availability and increasing quality of smartphone cameras, their portability and relative low cost have fostered their use as a colorimeter (Cherbuin et al., 2019; Jung et al., 2015; Oncescu et al., 2013; Soares et al., 2019; Wang et al., 2016). However, despite having many advantages, in order to build automated systems to carry out lab procedures, controller boards may be a simpler solution than smartphones. Nevertheless, the analytical applications that use smartphones have multiplied in recent years, and studies as varied as the determination of phosphates in environmental and industrial samples (Sáez Hernández et al., 2022[a]), studies of tuna adulteration (Sáez Hernández et al., 2022[b]) or determination of Cu^{2+} in sugar cane spirits (Maia et al., 2022) and soft drinks (Schlesner et al., 2022) can be found. The use of smartphones has advantages, but it also has some disadvantages. It is true that a mobile phone is more widely available, as everyone nowadays usually has one. However, its use as an analytical measuring device has several drawbacks that need to be considered. When performing an analysis with a smartphone photograph, the lighting conditions must be stable and reproducible (Molada-Tebar et al., 2019). Also, it is important to consider that each device captures and processes digital images in a certain way, so depending on the goal of the study, a prior characterization of the camera must be done (leal et al., 2021). After the image acquisition and treatment, colour parameters are obtained with specialized software and then data processing is carried out.

In this context, automatized procedures using colour sensors imbedded in 3D printed modules arise as alternatives, often associated to cheaper costs. Additionally, these devices present stable and reproducible lighting conditions and they do not require an image treatment step, since the raw data is readily presented to the analyst through a screen.

The use of LED photometers as a light source is not a recent development (Cantrell & Ingle, 2003), and since the beginning of the twenty-first century numerous applications have appeared with similar performances when compared with benchtop instruments. All of them have in common that they have sufficient sensitivity and linear response to provide accurate and precise information on the analytes of interest in simple, inexpensive, and small devices that make them suitable for in situ analysis. In addition, these devices, due to their small size,

require less reagents, generate less waste and perform analysis in shorter time compared to traditional instrumentation. Some of these studies are listed in Table 12.1.

Table 12.1: LED photometer applications.

Sample	Light source	Detector	Analyte	LOD	R	RSD / %	Ref.
Water	LED 470 nm	Photodiode	DBS	0.06 mg/L	0.999	0.6 (n=11)	Lavorante et al., 2007
	LED 650 nm		CPC	0.05 mg/L	0.999	0.5 (n=11)	
Water	LED 548 nm	Photodiode	Cr (VI)	2.05 µg/L	0.999	2 (n=20)	Pires et al., 2007
			Cr (Total)	1 µg/L			
Water	LED 464 nm	Photodiode	Turbidity	0.09 NTU	0.999	1.6 (n =10)	Ródenas-Torralba et al., 2007
Milk	LED 639 nm	Photodiode	Urea	0.18 mM	0.9991	<0.7 (n=10)	Suarez et al., 2018
Water	LED 590 nm	LED 590 nm	Fe	0.022 mg/L	0.998	<5.6	Place, 2019
Tonic water	Laser pen	Webcam	Quinine	-	-	0.98	Silva et al., 2021

LOD: limit of detection; RSD: relative standard deviation; DBS: Sodium dodecylbenzene sulfonate; CPC: Cetyl pyridine Chloride

The Single-Board Arduino device is a microcontroller that allows to program the functionality of different electronic components to work in a specific way. Recent literature illustrates the use of the Arduino boards in laboratory automation, including, for instance, the development of an automated peptide synthesizer (Gali, 2017), fluoride determination in drinking water (Otal et al., 2021) or measurements of phytoplankton fluorescence (Leeuw et al., 2013).

The advantage of these devices is that their design can be adapted to the needs of the user. However, they require at least a little knowledge of programming, and their lack of a screen means that a computer or LCD module are required to show the results obtained by the sensors.

An interesting alternative are single-board computers (SBC), such as Raspberry Pi (Johnston & Cox, 2017; Severance, 2013). SBCs include a full operating system and enough peripherals (memory, CPU, power regulation) to start the execution without the addition of hardware (Johnston & Cox, 2017). Raspberry was not developed to be just a low cost computer, but to be accessible to almost any user thanks the input–output (GPIO) connection pins (Johnston & Cox, 2017). They have been used to develop analytical applications, such as an UV fluorescence

spectrophotometer to classify oil spill samples (Bills et al., 2020), the development of infrared thermometric titrations to determine sodium in sauces (Tischer et al., 2020) or tequila identification using image treatment (Gómez et al., 2021).

The electronic components that can be controlled by Arduino or Raspberry include different elements, such as photoresistors and colour sensors, which may be used to obtain analytical parameters. These components can collect information about light intensity or colour, providing readings of differently spectrally tuned sensors, with maximum sensitivity peaks at the red (R), green (G) and blue (B) regions of the visible spectrum, plus an achromatic sensor (C) (Carvalho Oliviera et al., 2022). Despite these RGB readings being device-dependent and not constituting a standard colour space, it is possible to obtain general colour descriptors by a previous chromatic characterization process of the device, making it suitable for chemical analysis. Ashwin and Harish have shown the utility of Arduino as a controller device with a photoresistor sensor (Ashwin & Silva, 2022). This device is useful to study variations in light intensity, but this is not recommendable for studying colour changes. The light intensity can provide information about the light source or changes in the solution, but it is not possible to study colour changes between two colours. In this case it is possible that the light intensity does not vary, but the colour does. For this last purpose, it would be necessary to use colour sensors like TCS34725.28 If specular reflections and stray light are avoided, and distance and intensity of source are adjusted preventing the saturation of the sensor, an adequate combination of the raw RGB responses provides reliable results with a low cost.

The low-cost devices described above would take care of the data capture process, but handling the samples is also a problem that can be solved by new technologies, in this case 3D-printing. This term refers to a set of additive manufacturing techniques that create solid three-dimensional objects layer-by-layer under precise digital control (Ngo et al., 2018). This technique has been used to develop microfluidic systems (Bhattacharjee et al., 2016), soft autonomous robots (Wehner et al., 2016) or to produce vascularized cellular constructs by 3D bioprinting (Kang et al., 2016).

Nowadays, new technologies are becoming progressively more affordable, allowing users with limited resources to perform chemical analysis based on the use of a smartphone (Cherbuin et al., 2019; Jung et al., 2015; Oncescu et al., 2013; Soares et al., 2019; Wang et al., 2016) or on automated sampler and analyser devices (Leeuw et al., 2013; Otal et al., 2021). Nevertheless, this is not possible without

basic knowledge in the different fields involved in the design of these devices. For this, the creation of interdisciplinary groups is very important to the scientific progress.

Given the possibilities provided by these new systems, the aim of this work is to combine 3D printing technology and Raspberry Pi controller board to build an automated colorimeter using a TCS34725 colour sensor for colorimetric analysis using small amount of sample and short time, with low energy consumption (battery module), following the green analytical principles.

2. Materials and methods

2.1. Instrumentation and reagents

From the solid reagents of the food dyes, Tartrazine 85% (Sigma Aldrich, Steinheim, Germany), Red Allure 80% (Sigma Aldrich, Steinheim, Germany) and Brilliant Blue 65 % (Sigma Aldrich, Steinheim, Germany), stock solutions of 60 mmol L^{-1}, 57 mmol L^{-1} and 5 mmol L^{-1} were prepared, respectively. Absorption spectra of the food dye solutions were measured by an 8452A Hewlett Packard spectrophotometer (Germany).

2.2. Colorimeter development

The automated sampler module consists of a 3D printed structure and two servomotors powered by two Ky-019 relays 5 V (Figure 12.1). The more robust MG995 RC servomotor, suitable to move greater weights, was employed in the carrousel sample holder module, and a Sg90 servomotor was employed to place a capillary tube inside the sample solution. The measurement cell (Figure 12.2) relied on a TCS34725 RGBC (DollaTek, model CJMCU-34725) to acquire the RGB values of the solutions under the illumination provided by a 6000 K white 3.4 V LED chip. To transfer the sample to the 178.710-Os (Hellma) flow cell, where the solution is measured, a Thenki 12V peristaltic pump was used.

Both modules were coupled by a Raspberry Pi4 board model B (Bqeel) to make up a single device. This board was coupled to a 12.7cm LCD Touch Screen (Neiple, ASIN: B085NHLX4H) to display the results. The device provides a datasheet document and exports this one to another device by internet. Although both modules are coupled, they can be used separately. Figure 12.3 shows the final set-up.
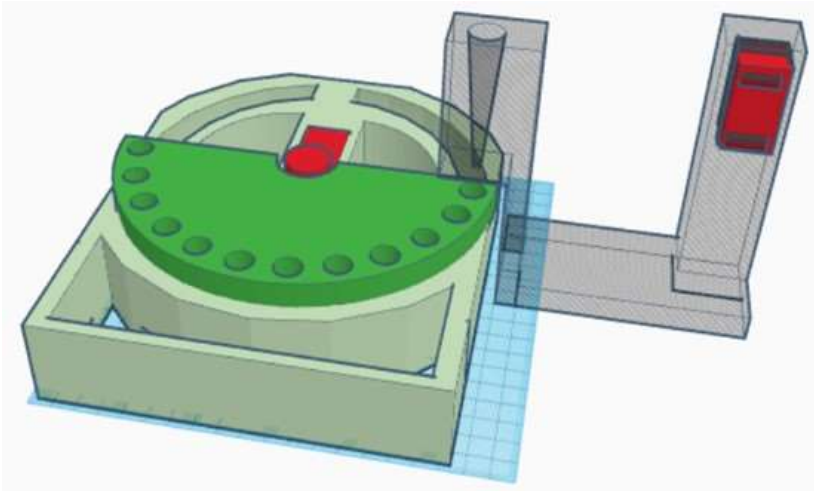
Figure 12.1: 3D design of the sampler module. The red cubes represent the servos' position. Created with www.tinkercad.com.
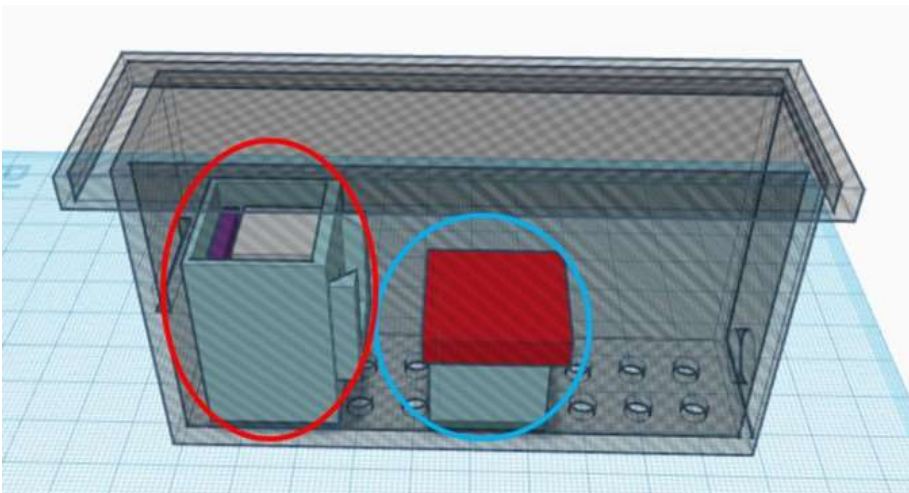
Figure 12.2: 3D design of the measurement module. The blue circle shows the light source box. The Red circle shows the box where the cell and the sensor are placed. Created with www.tinkercad.com.
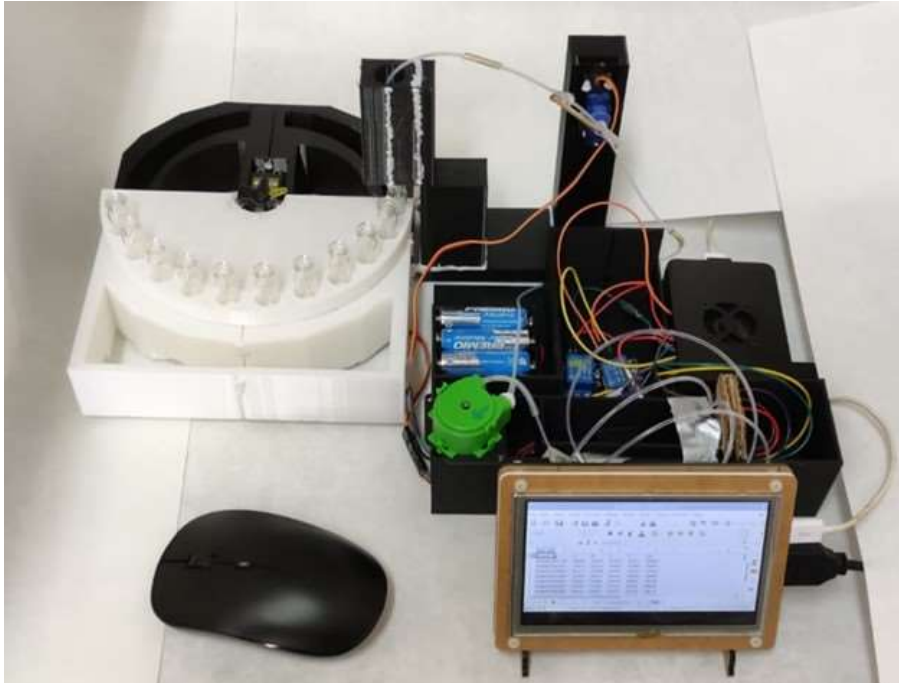
Figure 12.3: The final 3D printed device with all electronic components, the pump and the LCD screen.

2.3.   TCS34725 colour light-to-digital converter with IR filter

The TCS34725 sensor provides a digital return of red, green, blue (RGB), and clear (C) light sensing values. An IR blocking filter, integrated on-chip and placed on the colour sensing photodiodes, minimizes the IR spectral component of the incoming light, and allows colour measurements to be made accurately (Color Sensor, 2022). The sensor has been characterized by the manufacturer, the "TCS34725 Datasheet v1-04" (Color Sensor, 2022) provides the photodiode spectral responsivity RGBC and these ones as a function of angular displacement.

2.4.   Device development

2.4.1.   Control code

The code requires the time, *Adafruit_Phyton_TCS34725*, *smbus* and *xlswriter* libraries. The device is programmed using Thonny Phyton IDE program.

2.4.2.   Sampler module

Figure 12.4 shows the connections between the three components in this module: (1) the plastic shell of the module that gives stability to the structure, (2) the rotating sample selector, where samples are placed into 2 mL vials, which is

connected to one servomotor and (3) the sample capture section, driven by the other servo, to place the capillary tube inside the solution.
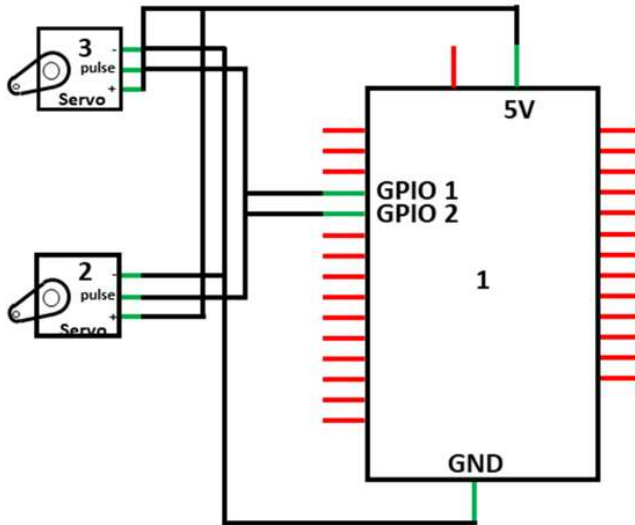
Reference	Value	Description
1	Raspberry Pi4	Microcontroller
2	MG995 RC	Servo motor
3	Sg90	Servo motor

Figure 12.4: Connection between the sampler module components.

2.4.3. Measurement module

In the signal measurement module, the lighting conditions are fixed to avoid changes in RGB responses due to the light source. The sensor is placed to measure transmitted light instead of reflected light in order to minimize the influence of the specular component. Maximum light intensity and the distance between the source and the sensor (4 cm) were adjusted avoiding saturation of this. To prevent stray light entering the sensor, the structure was 3D printed using mate black plastic. This module requires two relays to provide the energy for the pump and the light source, by a 12 V battery. Figure 12.5 shows the connection between the components of this module. The flow system uses a commercial flow cell, and the designed device allows three measures by using less than 2 mL of sample.

Reference	Value	Description
1	Raspberry Pi4	Microcontroller
2	TCS34725 RGBC	Color sensor
3	12V	Battery
4	YD-GSGJZJCHAO20100	Peristaltic Pump
5	B07DPRWVRF	LED
6	Ky-019	Relay
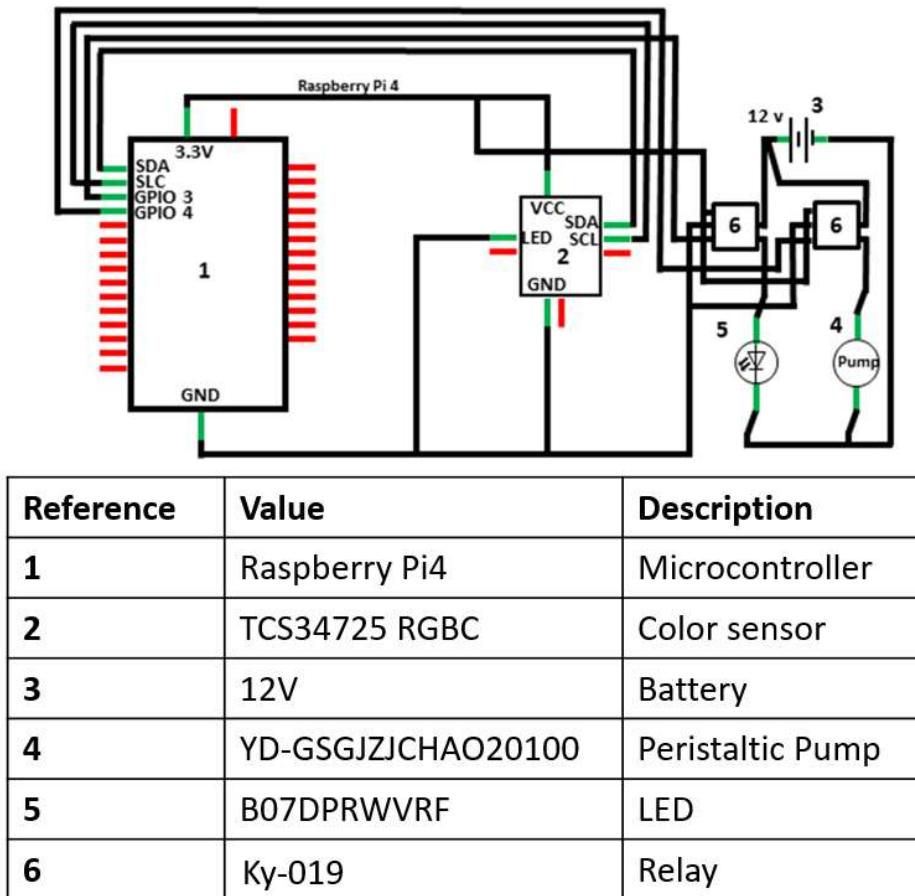
Figure 12.5: Connection between the different components in the measurement module.

2.5.   Spectrophotometric measurements

Reference measurements by the UV-vis spectrophotometer were carried out in a 10 mm path length quartz cell recording the spectrum between 190 and 800 nm. The maximum absorbance measurement for Tartrazine, Red Allure AC and Brilliant Blue FCF compounds were at wavelengths 424 nm, 505 nm and 630 nm, respectively.

2.6.   Raspberry Pi device measurements

The measurements with the Raspberry Pi-based device were performed by filling the 2 mL vials with the solutions and placing them into the sampling carousel, and after that, the device is initiated using Thonny Phyton IDE program. During the analysis process, the device transfers the solutions to the measurement cell and

three RGBC readings per solution are registered. For each measurement, the colour sensor responses are written in the OpenOffice datasheet. Finally, the user processes the data obtaining the concentration of food dyes in the sample.

2.7.   Testing samples

To evaluate the accuracy of the device, three samples with different food dyes were analysed: an isotonic drink, an ice-cream and a candy. The isotonic drink containing Brilliant Blue FCF and the ice-cream containing Tartrazine were filtered and diluted before the analysis, and a red solid candy containing Red Allure AC was weighted, dissolved in hot water and filtered before the analysis.

3.   Results and discussion

3.1.   Evaluation of the content of food dyes by Raspberry Pi device

The relationship between RGBC sensor responses and dye concentration was analysed by measurements of calibration solutions for the three food dyes.

Due to the resolution of the detector (the device works with 2 bytes data, 65536 a.u.), the variability of its measurements is large. To reduce its variability, the behaviour of the R/G, G/B and R/B ratios has also been studied. Figure 12.6A–C show the calibration curves obtained with the sensor's raw RGB data, while in Figure 12.6D the R/G, R/B and G/B ratios have been used. The response of the sensor according to the amount of food dye can be adjusted in a linear way. The response of the device depends on the type of food dye: Tartrazine is more sensible in the blue channel, Red Allure AC is more sensible in the green channel and Brilliant Blue FCF is more sensible in the red channel. It can be seen in Figure 12.7 that the most appropriate colour of the sensor, R, G or B, to analyse each dye will be the one with the greatest overlap with the corresponding absorption spectrum. Although it is possible to obtain calibration curves with the raw data, the ratios between colour parameters provide more stable readings, with lower coefficient of variation and larger linear calibration range. In order to evaluate the linear range, higher calibration standard solutions were measured for each food dye as can be seen in the Figure 12.8. Since the response of the sensor depends on the colour that is measured, each food dye requires the employment of a different colour parameter ratio. In the case of the Red Allure AC (Figure 12.6B), the R response is stable, and the higher variation is due to the G and B channels, for that it is possible to use both ratios R/G or R/B. In this work the second ratio has been selected.

The white colour in the RGB space is represented by the values 255/255/255, with 255 being the maximum value of each parameter. In order to obtain red from white,

the R component must not change. Therefore, it is G and B which decrease their value. This implies that, when measuring the change in red, the most sensitive parameters are G and B. Therefore, to evaluate how much redder something becomes, if red parameter is used, no variation of the signal will be observed. However, the values of the green and blue parameters will decrease and there will be a signal change which can be evaluated. The case of the Tartrazine is different (Figure 12.6A), the R channel is stable, and the G channel has a very low slope, the yellow in the RGB colour space is obtained with a mixture of R and G channels, for that this ratio does not provide enough information. In this case, since G channel has the higher values, the G/B ratio has been used. For the calibration equation of Brilliant Blue FCF the same procedure the Red Allure AC has been employed, the G and B channels have a similar slope, for that it is necessary to use R value for the ratio, due to the blue colour is measuring the B channel is used, being selected B/R ratio.
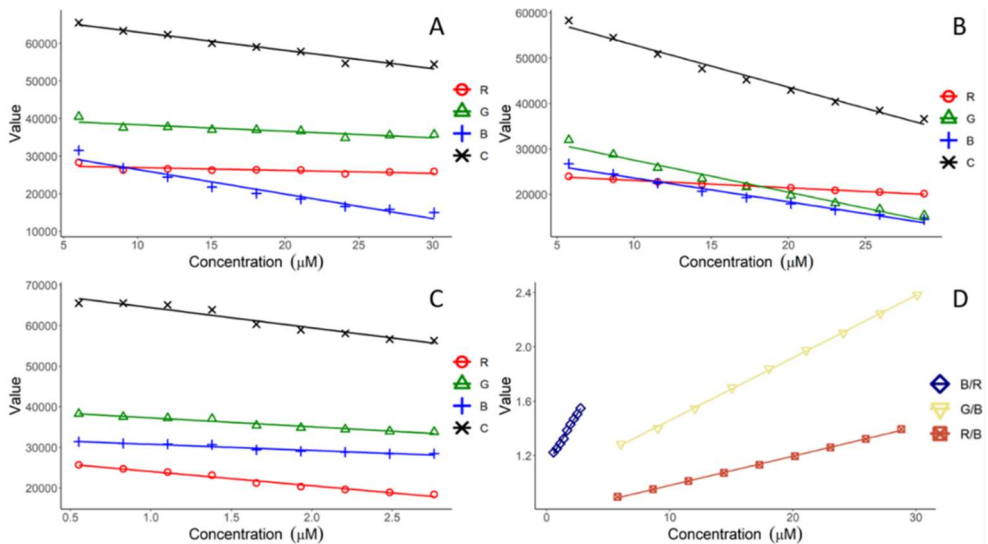
Figure 12.6: RGBC raw data obtained with the Tartrazine (A), Red Allure AC (B) and Brilliant Blue FCF (C) standard solutions. Curve calibration for the R/B ratio of Red Allure AC (■), G/B ratio of Tartrazine (▲) and B/R ratio of Brilliant Blue FCF (●) food dyes (D).
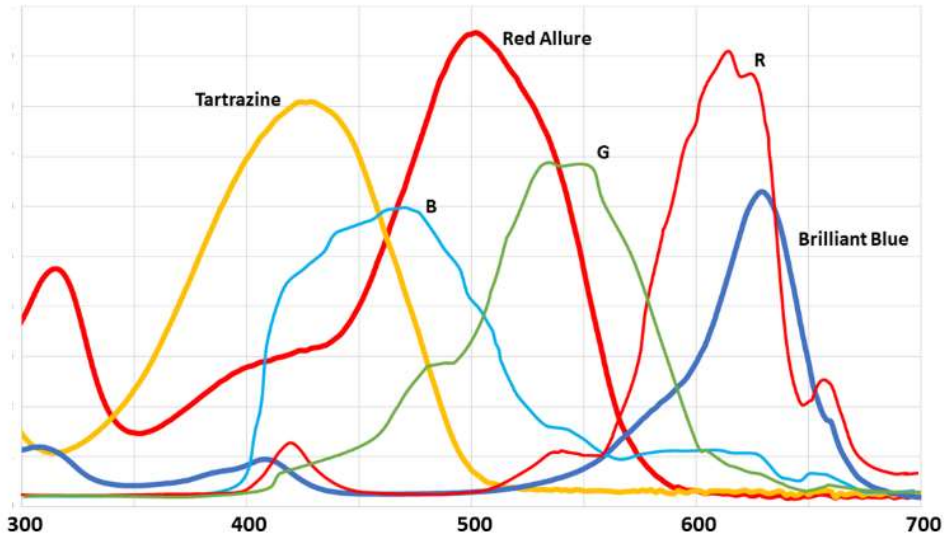
Figure 12.7: Overlapping of the food dyes spectrums and signal response for each colour channel of the sensor.
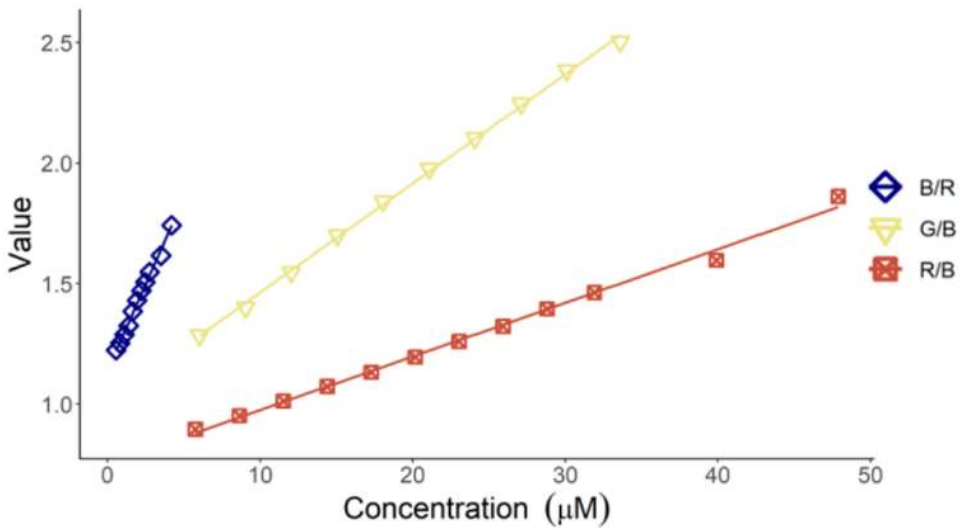
Figure 12.8: Curve calibration for the R/B ratio of Red Allure AC (■), G/B ratio of Tartrazine (▲) and B/R ratio of Brilliant Blue FCF (●) food dyes.

3.2. Comparison between Raspberry Pi colour detector and Spectrophotometer

Table 12.2 shows the analytical parameters of both methods, the new device provides higher sensitivity than the reference instrument for two of the food dyes and a smaller CV, being LOD, LOQ (limit of quantitation), linear range and R^2 very similar. The analyses with the new device requires less time (20 seconds) and generates less waste than the conventional colorimetric method (needing 2 mL versus 6–8 mL). This device has the advantage that the user does not manipulate the solutions because all analysis procedure is automated, being greener. For all of this, the instrument developed in this work provides a way to carry out automated colorimetric analysis reducing measurement time and sample volume without losing sensitivity. Moreover, this device is homemade and can be tailored according to the user's necessities with small cost. The RGB sensor provides very good precision with coloured solutions, as it can be seen in Table 12.2 obtained from the standard solutions. Regarding the blanks, which only contain water, small variation in the signal gave higher standard deviation values. The LOD in both cases was obtained using the standard deviation of the blanks, providing very similar results.

Table 12.2: Analytical parameters of the spectrophotometric method and the new device one for determination of different food dyes (T: Tartrazine; R: Red Allure AC; B: Brilliant Blue FCF).

	UV-vis			New Device		
Food Dye	T	R	B	T	R	B
Slope (L/µmol)	0.031	0.032	0.139	0.043	0.023	0.161
intercept	0.01	0.02	0.01	1.13	0.73	1.06
R^2	0.9997	0.996	0.9993	0.9992	0.996	0.998
Linear Range (µM)	LOQ-34	LOQ -32	LOQ -4.9	LOQ -34	LOQ -48	LOQ -4.2
CV (%)	[0.3-4.1]	[0.03-1.9]	[0.7-3.6]	[0.009-0.18]	[$2 \cdot 10^{-4}$-0.08]	[0.012-0.2]
LOD (µM)	1.0	1.4	0.1	1.1	1.4	0.1
LOQ (µM)	3.2	4.7	0.2	3.6	4.6	0.5

3.3. Application of the TCS34725 in sample analysis

The device was used to determine the content of food dyes in different samples. The selected samples (two liquids and a solid sample) have different matrices and were prepared as indicated in the "Testing samples" section. To carry out the analysis, standard solutions and sample solutions were measured by the spectrophotometer and the Raspberry Pi device. Table 12.3 shows the results obtained by each method. The statistical study of the results shows that for all cases the p-value of the comparison of mean values for the new device and the reference instrument is greater than 0.05, the t_{exp} lower than the theoretical value for 95%

probability and the confidence intervals of the difference between both mean values includes zero. On the other hand, for standard deviation comparison, the confidence interval for the ratio of both variance values includes 1 and the p-values are greater than 0.05. It is therefore concluded that there are no significant differences between the results obtained by the two procedures. Additionally, the analysis by the homemade device was carried out in different days to check the interday reproducibility, obtaining yielded CV of 2.6, 2.0 and 1.8% for the Tartrazine, Red Allure AC and Brilliant Blue FCF, respectively.

Table 12.3: Content of food dye obtained by both methods (n=3).

	Ice-cream (mg/L Tartrazine)	Isotonic drink (mg/L Brilliant Blue FCF)	Candy (mg/kg Red Allure AC)
Spectrophotometer	56±4	3.38±0.13	153±2
Raspberry Pi	57±1	3.28±0.02	154±3
p-value ($\bar{x}$)	0.470	0.359	0.758
t exp. ($\bar{x}$)	0.825	1.082	0.337
p-value ($\bar{s}$)	0.376	0.236	0.599

3.4.   Comparison of the TCS34725 sensor with other models

In the market, additionally to the TCS34725 it is possible to find other sensors such as the ASS7341 or the AS7262. These last sensors have 10 and 6 measurement channels, respectively, which allow to measure at discrete wavelengths, including near-infrared in the case of the 10-channel sensor. In this work, the TCS34725 sensor has been used, which only has 4 channels, as in other papers found in recent literature, providing adequate results (de Carvalho Oliveira et al., 2022; Husein & Kayahan, 2020), considering the price difference (the 6 and 10 channel sensors are 5 times more expensive). For these reasons the TCS34725 sensor was selected. In the present work, the use of a cheaper and simpler sensor has served for performing colorimetric analyses of coloured solutions and obtaining results comparable to those obtained with a UV-vis, meeting the proposed aims.

4.   Conclusions

In the present work, an automated colorimeter composed of two independent modules has been developed. A sampler module has been built using 3D-printer and a Raspberry Pi as controller. A measurement module has been developed using a peristaltic pump and a TCS34725 sensor, both controlled by Raspberry Pi. The device obtains the RGB sensor responses to the light transmitted by the sample and correlates them to the analytical parameter of interest (dye concentration in the solution). The results show R^2 values higher than 0.993 in the three dyes and

provide a LOQ of 0.5, 3.6 and 4.6 mmol L^{-1} for the Brilliant Blue FCF, Tartrazine and Red Allure AC, respectively. The comparison between the reference method, (measurement by UV-vis spectrophotometer) and the new device shows that the employment of this device provides a reduction of generated waste and of consumed time at 25%. The device allows the user to perform colorimetric analysis without the need of using a spectrophotometer, which will be employed only for measurements in UV-range or when interferents' presence requires to measure at a specific wavelength. No differences were found between the analytical parameters obtained in both procedures. Therefore, the new homemade device can be used to carry out analysis only requiring a very low investment. In summary, the prototype integrates different steps, like the sample loading and measuring, rinsing between samples, capturing colour data and direct viewing of the data from the screen, all controlled only with an Arduino board.

5.   References

Ashwin, S. H., & Harish, S. V. (2020). Titration machine: A new approach using Arduino. In Kalam, A., Niazi, K. R., Soni, A., Siddiqui, S. A., & Mundra, A. (Eds.), Intelligent Computing Techniques for Smart Energy Systems: Proceedings of ICTSES. Springer Singapore.

Bhattacharjee, N., Urrios, A., Kang, S., & Folch, A. (2016). The upcoming 3D-printing revolution in microfluidics. *Lab on a Chip*, 16(10), 1720-1742. DOI: g/10.1039/C6LC00163G.

Bills, M. V., Loh, A., Sosnowski, K., Nguyen, B. T., Ha, S. Y., Yim, U. H., & Yoon, J. Y. (2020). Handheld UV fluorescence spectrophotometer device for the classification and analysis of petroleum oil samples. *Biosensors and Bioelectronics*, 159, 112193. DOI: 10.1016/j.bios.2020.112193.

Cantrell, K. M., & Ingle, J. D. (2003). The SLIM spectrometer. Analytical Chemistry, 75(1), 27-35. DOI: 10.1021/ac026015s.

Cherbuin, M., Zelder, F., & Karlen, W. (2019). Quantifying cyanide in water and foodstuff using corrin-based CyanoKit technologies and a smartphone. *Analyst*, 144(1), 130-136. DOI: /10.1039/C8AN01059E.

Color Sensor – Color Light-To-Digital Converter – TCS34725 ams | ams, (n.d.). (accessed april 16, 2022). https://ams.com/tcs34725#tab/description.

de Carvalho Oliveira, G., Machado, C. C. S., Inácio, D. K., da Silveira Petruci, J. F., & Silva, S. G. (2022). RGB color sensor for colorimetric determinations: Evaluation and quantitative analysis of colored liquid samples. *Talanta*, 241, 123244. DOI: 10.1016/j.talanta.2022.123244.

Di Nonno, S., & Ulber, R. (2021). Smartphone-based optical analysis systems. *Analyst*, 146(9), 2749-2768. DOI: /10.1039/D1AN00025J.

Gali, H. (2017). An open-source automated peptide synthesizer based on arduino and Python. *SLAS Technology: Translating Life Sciences Innovation*, 22(5), 493-499. DOI: 10.1177/2472630316685844.

Gómez, A., Bueno, D., & Gutiérrez, J. M. (2021). Electronic eye based on RGB analysis for the identification of tequilas. *Biosensors*, 11(3), 68. DOI: /10.3390/bios11030068.

Hussein, S., & Kayahan, E. (2020). Low cost portable urine analysis system design based on color measurement. In International Marmara Sciences Congress IMASCON.

Johnston, S. J., & Cox, S. J. (2017). The raspberry Pi: A technology disrupter, and the enabler of dreams. *Electronics*, 6(3), 51. DOI: 10.3390/electronics6030051.

Jung, Y., Kim, J., Awofeso, O., Kim, H., Regnier, F., & Bae, E. (2015). Smartphone-based colorimetric analysis for detection of saliva alcohol concentration. *Applied Optics*, 54(31), 9183-9189. DOI: 10.1364/AO.54.009183.

Kang, H. W., Lee, S. J., Ko, I. K., Kengla, C., Yoo, J. J., & Atala, A. (2016). A 3D bioprinting system to produce human-scale tissue constructs with structural integrity. *Nature Biotechnology*, 34(3), 312-319. DOI: oi.org/10.1038/nbt.3413.

Lavorante, A. F., Morales-Rubio, A., de la Guardia, M., & Reis, B. F. (2007). A multicommuted stop-flow system employing LEDs-based photometer for the sequential determination of anionic and cationic surfactants in water. *Analytica Chimica Acta*, 600(1-2), 58-65. DOI: 10.1016/j.aca.2006.12.035.

Leal, V. G., Batista, A. D., & da Silveira Petruci, J. F. (2021). 3D-printed and fully portable fluorescent-based platform for sulfide determination in waters combining vapor generation extraction and digital images treatment. *Talanta*, 222, 121558. DOI: 10.1016/j.talanta.2020.121558.

Leeuw, T., Boss, E. S., & Wright, D. L. (2013). In situ measurements of phytoplankton fluorescence using low cost electronics. *Sensors*, 13(6), 7872-7883. DOI: 10.3390/s130607872.

Maia, M. V., Suarez, W. T., dos Santos, V. B., & de Almeida, J. P. B. (2022). Carbon dots on paper for determination of Cu^{2+} in sugar cane spirits samples for fluorescence digital image-based method. *Microchemical Journal*, 179, 107500. DOI: 10.1016/j.microc.2022.107500.

Molada-Tebar, A., Riutort-Mayol, G., Marqués-Mateu, Á., & Lerma, J. L. (2019). A Gaussian Process Model for Color Camera Characterization: Assessment in Outdoor Levantine Rock Art Scenes. *Sensors*, 19(21), 4610. DOI: 10.3390/s19214610.

Ngo, T. D., Kashani, A., Imbalzano, G., Nguyen, K. T., & Hui, D. (2018). Additive manufacturing (3D printing): A review of materials, methods, applications and challenges. *Composites Part B: Engineeri*ng, 143, 172-196. DOI: /10.1016/j.compositesb.2018.02.012.

Oncescu, V., O'Dell, D., & Erickson, D. (2013). Smartphone based health accessory for colorimetric detection of biomarkers in sweat and saliva. *Lab on a Chip*, 13(16), 3232-3238. DOI: 10.1039/C3LC50431J.

Otal, E. H., Kim, M. L., Dietrich, S., Takada, R., Nakaya, S., & Kimura, M. (2021). Open-source portable device for the determination of fluoride in drinking water. *ACS Sensors*, 6(1), 259-266. DOI: 10.1021/acssensors.0c02273.

Pires, C. K., Reis, B. F., Morales-Rubio, A., & de la Guardia, M. (2007). Speciation of chromium in natural waters by micropumping multicommutated light emitting diode photometry. *Talanta*, 72(4), 1370-1377. DOI: 10.1016/j.talanta.2007.01.044.

Place, B. J. (2019). Activity analysis of iron in water using a simple LED spectrophotometer. *Journal of Chemical Education*, 96(4), 714-719. DOI: 10.1021/acs.jchemed.8b00515.

Ródenas-Torralba, E., Morales-Rubio, Á., Lavorante, A. F., Dos Reis, B. F., & de la Guardia, M. (2007). Micropumping multicommutation turbidimetric analysis of waters. *Talanta*, 73(4), 742-747. DOI: 10.1016/j.talanta.2007.04.060.

[a]Sáez-Hernández, R., Mauri-Aucejo, A. R., Morales-Rubio, A., Pastor, A., & Cervera, M. L. (2022). Phosphate determination in environmental, biological and industrial samples using a smartphone as a capture device. *New Journal of Chemistry*, 46(3), 1286-1294. DOI: /10.1039/D1NJ05425B.

[b]Sáez-Hernández, R., Antela, K. U., Mauri-Aucejo, A. R., Morales-Rubio, A., & Cervera, M. L. (2022). Smartphone-based colorimetric study of adulterated tuna samples. *Food Chemistry*, 389, 133063. DOI: 10.1016/j.foodchem.2022.133063.

Schlesner, S. K., Voss, M., Helfer, G. A., Costa, A. B., Cichoski, A. J., Wagner, R., & Barin, J. S. (2022). Smartphone-based miniaturized, green and rapid methods for the colorimetric determination of sugar in soft drinks. *Green Analytical Chemistry*, 1, 100003. DOI: /10.1016/j.greeac.2022.100003.

Severance, C. R. (2013). Eben Upton: Raspberry pi. *Computer*, 46(10), 14-16. DOI: 10.1109/MC.2013.349.

Silva, W. R., Suarez, W. T., Reis, C., dos Santos, V. B., Carvalho, F. A., Reis, E. L., & Vicentini, F. C. (2021). Multifunctional webcam spectrophotometer for performing analytical determination and measurements of emission, absorption, and fluorescence spectra. *Journal of Chemical Education*, 98(4), 1442-1447. DOI: /10.1021/acs.jchemed.0c01085.

Soares, S., Torres, K. G., Pimentel, E. L., Martelli, P. B., & Rocha, F. R. (2019). A novel spot test based on digital images for determination of methanol in biodiesel. *Talanta*, 195, 229-235. DOI: 10.1016/j.talanta.2018.11.028.

Suarez, W. T., de Alvarenga Junior, B. R., de Oliveira Krambeck Franco, M., Gabriel, W. L., de Oliveira, D. M., & dos Santos, V. B. (2018). In situ determination of urea in milk employing a portable and low-cost LED photometer. *Food Analytical Methods*, 11, 1149-1154. DOI: 10.1007/s12161-017-1087-8.

Tischer, B., Teixeira, I. D., Filoda, P. F., Alessio, K. O., Barin, J. S., Duarte, F. A., Kipper, L. M., Helfer, G. A., & da Costa, A. B. (2020). Infrared enthalpymetric methods: A new, fast and simple alternative for sodium determination in food sauces. *Food Chemistry*, 305, 125456.DOI: 10.1016/j.foodchem.2019.125456.

Wang, Y., Liu, X., Chen, P., Tran, N. T., Zhang, J., Chia, W. S.,Boujday, S., & Liedberg, B. (2016). Smartphone spectrometer for colorimetric biosensing. *Analyst*, 141(11), 3233-3238. DOI: /10.1039/C5AN02508G.

Wehner, M., Truby, R. L., Fitzgerald, D. J., Mosadegh, B., Whitesides, G. M., Lewis, J. A., & Wood, R. J. (2016). An integrated design and fabrication strategy for entirely soft, autonomous robots. *Nature*, 536(7617), 451-455. DOI: 10.1038/nature19100.

CHAPTER 13: Development of an automated laboratory for carrying out colorimetric analysis
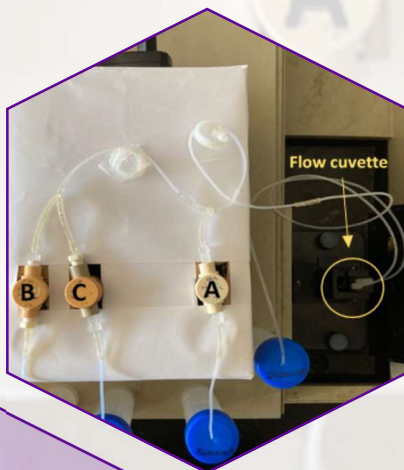
ABSTRACT

The objective of this chapter is the development of a robotic device to carry out the mixtures between samples and reagents in the colorimetric analysis. The device has been built employing an Arduino board as main element and low-cost components. The robot has been created employing a TCS34725 colour sensor, a white LED and a LCD display to show the RGB values obtained by the colour sensor. With all these elements have been possible to create a robot to make *in situ* analysis. To check the efficiency of the robot, and if it is possible to use this in a real analysis, a copper colorimetric reaction was studied employing the new device. Finally, irrigation water samples were measured with the robot and the results were compared with a reference method. The studied samples were collected along the *Acequia Real del Júcar*. A 0.984 correlation between the concentration of copper obtained by the robot and obtained by the reference method has been achieved.

Keywords: Analytical Chemistry, Arduino, copper, RGB.

1.   Introduction

1.1.   System automation

Nowadays, process automation and the use of robots in various industries is globally trending, with a reported increase in the demand for robots of 9 % per year on average between 2015 and 2020 according to the International Federation of Robotics (IFR). In 2020, the main growth driver was the electronics industry, with the automotive, metals and machinery, chemicals and food industries also making notable contributions to the overall statistics (International Federation of Robotics, 2021).

The chemical field is no exception, and over the last few years, the use of automated systems has also become widespread. Through automation, it is possible to achieve precise control over complex synthetic reactions that require careful regulation of parameters such as pH, temperature, pressure, or addition of reagents (Lindsey, 1992). According to *Sarkozi et al*. in a retrospective analysis carried out in 2002 of the last 36 years in their clinical chemistry department, the pre- and post-analytical automation of the tests conducted led to an increase in the quality of the service provided, reducing the workload and operational cost, while reporting a notable increase in productivity (Sarkozi, 2003). Modern automation trends focus on the development of automated systems whose elements are low-cost, miniaturised and have greater accessibility, with simple mechanics and easy assembly.

It should also be noted that the automation, robotisation and miniaturisation of systems allows for a closer approach to the 12 principles of green chemistry. By mechanising a process, human-induced errors are reduced, operator safety is increased due to the absence or reduction of reagents manipulation, and in some cases, even *in situ* measurements can be conducted. Moreover, by eliminating the dependence on high-cost equipment and its great energy consumption, it helps to achieve greater sustainable development (Armenta et al., 2008; Galuszka et al., 2013).

1.2.   Arduino

Arduino is an open-access computing platform based on a board designed to control various electronic components such as sensors, LEDs, and motors (Galadima, 2014; Ruiz, 2021). The initial project, promoted by Massimo Banzi at the Interactive Design Institute in Ivrea (Italy) in 2005, was aiming to develop a device that would allow him to carry out computer and electronic experiments, but at a low cost, due to the high price of microcontrollers at the time. Thus, the board was

developed and, after Fernando Barragán joined the team sometime later, C programming language was integrated, which enabled the first Arduino boards to be controlled by computers (Ruiz, 2021). Many different versions of Arduino boards exist nowadays, the Arduino Uno board being one of the most used.

Recently, the use of Arduino in microcontroller programming has become widespread since it is user friendly and easy to use having a basic knowledge of C++ programming. By connecting the board to a computer, it can be programmed to conduct a multitude of tasks, sending the information from the computer to the board and finally to the connected electronic component (Badamasi, 2014). Thus, it is possible to control the board with the Arduino IDE program (or other programs with programming languages such as python) with basic knowledge of programming and electronics.

Therefore, the use of platforms such as Arduino have proven to be extremely useful for automating, miniaturising and robotising systems. Nowadays, analytical chemistry is beginning to present this evolution, showing analyses carried out using Arduino UNO boards that allow different electronic components to be controlled using different programming languages. One of the ways in which is possible to use Arduino is with the employment of colour sensors such as TCS34725 which can be controlled by Arduino, and which generates data from the RGBC space, with C being clear light sensing values.

The main objective of this chapter is to develop a robot that allows precise and accurate mixing of reagents. The aim is that this robot can be developed with cheap components and can be used for colorimetric determination of molecules in different matrices. Moreover, is going to be attached a white LED, a colorimetric sensor and a display to the robot so that it could conduct not only continuous measurements, but also *in situ* measurements so as not to depend on high-cost equipment and to be able to conduct measurements at the location of the samples collection. To check the use of this robot to carry out analysis, the colorimetric reaction between copper and bicinchoninic acid will be employed.

2.   Materials and methods

2.1.   Reagents

To study the behaviour of the robot making solution mixtures, Quinoline Yellow, Brilliant Blue FCF 65 %, Allura Red AC 80 % and Erythrosine B by Sigma Aldrich (Steinheim, Germany) were employed to make coloured solutions. To carry out the

copper determination were employed a solution of 1000 mg/L of copper (Scharlab, Sentmenat, Spain), ascorbic acid (Scharlab) and the A reagent of the protein determination kit Thermo ScientificTM PierceTM BCA Protein Assay Kit (Rockford, Ill, USA). The A reagent is an aqueous solution of 1 % BCNA-Na$_2$, 2 % Na$_2$CO$_3$·H$_2$O, 0.16 % Na$_2$tartrate, 0.4 % NaOH, and 0.95 % NaHCO$_3$. Finally, to acidify the solution to perform the Flame atomic absorption spectroscopy (FAAS) analysis of the copper, nitric acid 69 % Ultratrace (Scharlab) was used.

2.2.   Instrumentation

For the analyses that required a UV-vis absorbance spectrophotometric method, a single beam HP-8252A spectrophotometer (Germany) with diode array detector was used, whose range in the UV-visible spectrum is from 190 to 820 nm with a resolution of 2 nm. This spectrophotometer was coupled to a computer that allowed the data obtained to be extracted and calculations to be performed. Regarding the instrument used to measure in flame atomic absorption spectroscopy, a S2 Series AA System AA Spectrometer Thermo Electron Corporation (Cambridge, UK) equipped with a Photron hollow cathode lamp multielement for Cu/Co/Mg/Ni/Fe (Victoria, Australia) were used.

2.3.   Material and software

The electronic assembly of the robot consisted of the Arduino UNO board, a USB A/B MM connection cable, relays, a prototyping board, and DUPONT connection cables from Elegoo (Shenzhen, China). When employing colorimetric measures in the RGB space, a 10 kohms trimmer, an HD44780 1602 16x2 serial LCD display board from AZ-delivery (Deggendorf, Germany), and a TCS34725 sensor from ICQUANZX were used. The mixing system consisted of three mini-pumps from Arcmed Bio-Chem Fluidics (New Jersey, USA), various tygon tubes and Y-shaped interconnections. Finally, a continuous flow cell from Hellma (Müllheim, Germany) was used for the continuous spectrophotometric analyses. The different analyses were performed using a 10 mm quartz cuvette with lid from Labbox (Barcelona, Spain). To program the board, Arduino IDE open source program was employed.

2.4.   Samples

The copper determination was conducted on water samples collected along the *Acequia Real del Júcar* after one of the copper sulphate treatments of the pipes employed for agricultural purposes. A total of 24 water samples were gathered along the canal, whose locations can be seen in Figure 13.1.
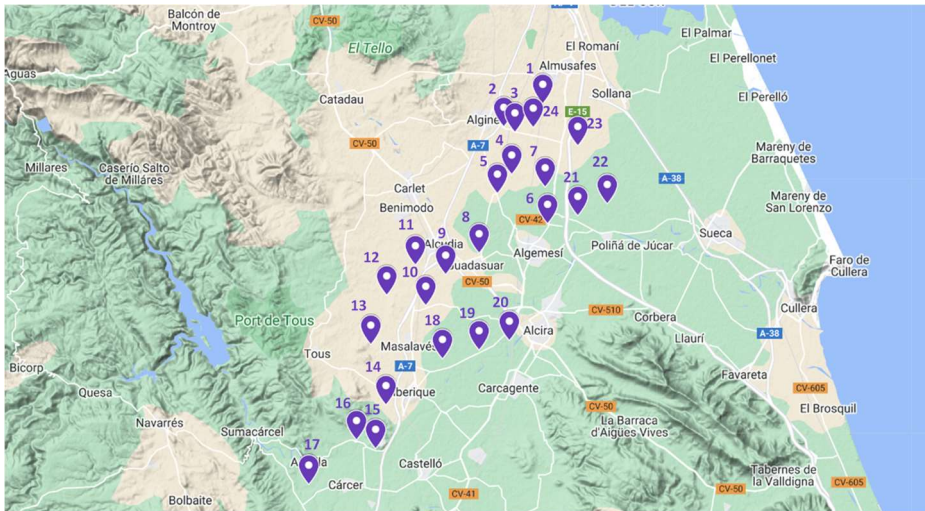
Figure 13.1: Locations of the different water samples collected along the Acequia Real del Júcar.

2.5. Experimental procedure

2.5.1. Robot developing

First, in order to visually show the robot's mixing system, a diagram can be observed in Figure 13.2. The first step was to attach a Y-shaped intersection, which allowed the tubes of mini-pumps B and C to be joined. This was followed by a first loop system that allowed a volume of 150 µL to be mixed. A second loop system was then attached to a tube, connecting to a new intersection (Y-shaped) that linked the mixing tube of mini-pumps B and C with the tube of mini-pump A. A second loop system was then positioned to mix a volume of 160 µL until the final homogenised solution was collected. In Figure 13.3, the prototype of the robot employed for study of the effectiveness of the mixture can be observed.

Next, a white LED and a TCS sensor on a 3D printed light booth were attached to the system. These were introduced and set in the light booth to fix all the conditions and avoid variability of the RGB measurements. Moreover, an LCD display was additionally attached to provide the corresponding colour values as can be seen in Figure 13.3. Finally, when it is necessary to measure spectrophotometrically the solution obtained by the robot it is only necessary to put the cell in the spectrophotometer instead of in the light booth.

For assembly the electronic part an Arduino UNO board with different electronic components was used to construct the robot. Three relays were incorporated in the main assembly, each one being connected to a mini-pump from the mixing

system. By associating each relay to a pin (inputs or outputs that can be either digital or analogue), it is possible to control the mini-pumps through programming. Figure 13.4 shows the main electronic assembly of the robot. Electrical supply is provided to the pumps through a 12V battery.

To the basic electronic assembly, the LCD display was first connected with a trimmer, which allowed the contrast of the display to be controlled. The electronic coupling of the display to the board can be seen in Figure 13.5. Finally, the TCS34725 sensor was also coupled to the Arduino UNO board, following the connections shown in Figure 13.6.
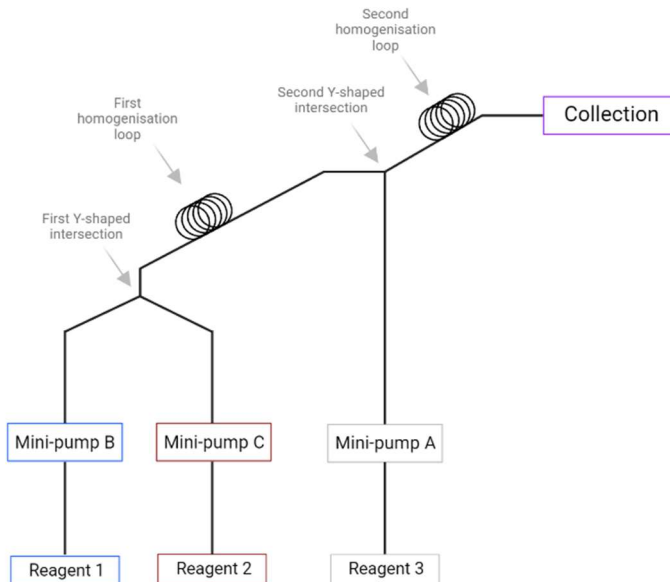
Figure 13.2: Diagram of the robot´s mixing system.
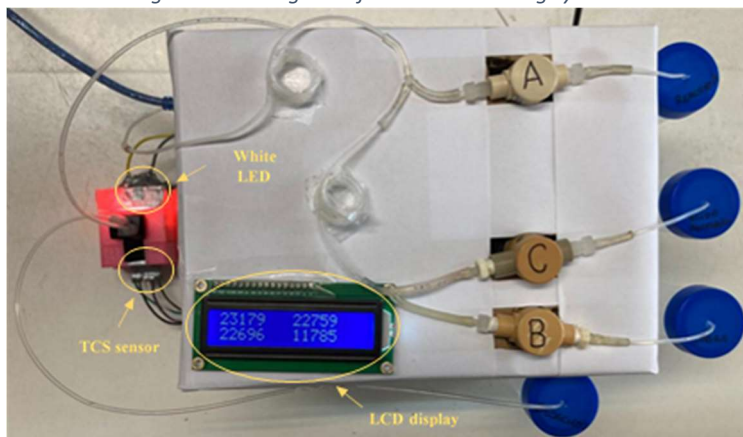
Figure 13.3: Final version of the device.

Figure 13.4: Connection of the main electronic assembly of the mixing robot.
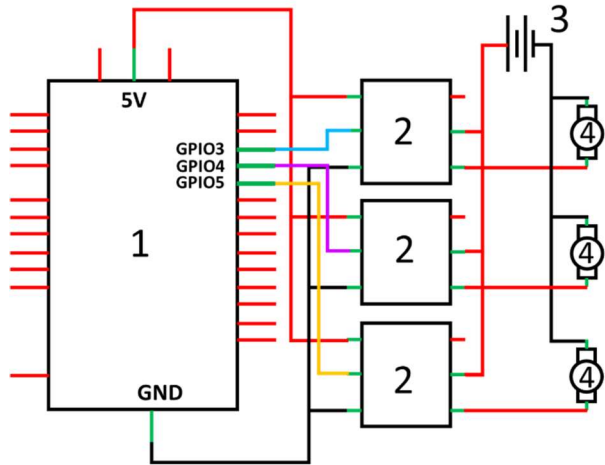
Reference	Value	Description
1	Arduino UNO	Microcontroller
2	Ky-019	Relay
3	12V	Battery
4	Bio-Chem Fluidics 7μL valve	Mini Pump

Figure 13.5: Electronic connection of the LCD display to the Arduino UNO board of the mixing robot.
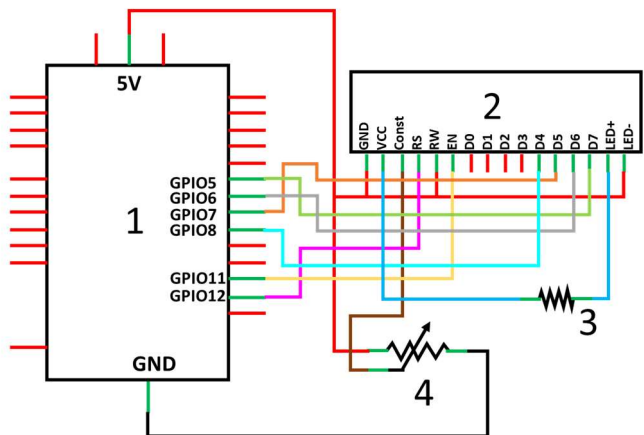
Reference	Value	Description
1	Arduino UNO	Microcontroller
2	LCD1602	LCD Screen
3	220Ω	Resistor
4	10KΩ	Trimmer
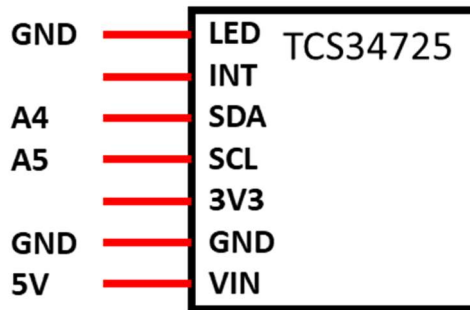
Figure 13.6: TCS34725 sensor with the connections to the Arduino UNO board.

2.5.2. Script for carry out the colorimetric reaction

In the script for control the device the variables associated with the different pins and functions to be carried out were established, being able to control the pulses generated by the mini-pumps of the mixing robot at all times. The script was written with the different tasks that the robot has to perform. In the main body of the code only it is necessary to call the tasks (clean, mixing, measure…). The total pulses of the mini-pumps needed to fill each tube section was determined. The robot was programmed to generate iterative pulses using mini-pumps B and C, up to a total equal to the number of pulses needed to fill and clean the first 150 µL mixing loop (tube between the first and second Y-intersection). The same procedure was repeated for the second 160 µL mixing loop by iterative pulses between the three mini-pumps. This last process was again carried out after the tube cleansing, as the robot was programmed to generate the necessary pulses to fill the flow cuvette section to measure the sample. For carry out the colorimetric measures the libraries *Adafruit_TCS34725.h and LiquidCrystal* were employed to collect the colour data of the solution and control the LCD screen to show the RGBC collect by the sensor respectively.

2.5.3. Copper determination

For the determination of copper in water samples collected along the *Acequia Real del Júcar*, two spectroscopic methods were carried out: FAAS and UV-vis absorption spectroscopy. In addition, a copper determination was also conducted using a white LED and a TCS sensor.

The sample treatment followed for the FAAS analysis consisted of taking a 10 mL aliquot of sample and adding 100 µL of concentrated nitric acid to it. An air/acetylene gas mixture was used for the flame and its absorbance was measured

at a wavelength of 324.28 nm. A deuterium lamp was used for background absorption correction.

The UV-vis absorption spectrophotometric analysis was conducted through two different procedures. First, a batch procedure was carried out, determining the copper concentration using equal volumes of 0.21 g/L ascorbic acid, reagent A (diluted in a 1:50 ratio) and sample. Using a 10 mm quartz cuvette, the coloured solutions (generated by the copper complexation) were measured spectrophotometrically at a wavelength of 558 nm, subtracting the absorbance of the baseline at 800 nm. Then, the mixing robot was used to conduct the reaction in an automated way, coupling it to a flow cell that allowed continuous spectrophotometric measurements at the same wavelengths.

Finally, the spectrophotometer was replaced with a white LED and a TCS sensor, which collected RGB colour data of the violet solution generated by the colorimetric reaction.

3.   Results and discussion

3.1.   Determination of the mini-pumps pulse volumes

In order to determine the driven volume by each mini-pump, three tubes with ultrapure water were weighed on an analytical balance. After connecting each tube to a mini-pump, the robot was controlled by an Arduino script that conducted iterative pulses up to 500 pulses per mini-pump. Using the difference of the water masses and assuming that the density of the water used is 997 kg/m^3 at 25°C, the data shown in Table 13.1 was obtained.

Table 13.1: Volumes per pulse (in μL/pulse) driven by each mini-pump of the mixing robot.

	Boosted volume (μL/pulse)	CV (%)	IC$_\mu$ (μL/pulse)
Mini-pump A	5.9 ± 0.3	4.5	[5.2, 6.5]
Mini-pump B	7.18 ± 0.07	1.0	[7.0, 7.4]
Mini-pump C	5.70 ± 0.15	2.7	[5.3, 6.1]

3.2.   Determination of the mini-pumps pulse volumes

3.2.1.   Mixing of two food dyes

In order to test if the robots mix correctly the coloured solutions, an Arduino script was programmed to conduct pulses alternately of two food dyes and water, driving

the mixed solution along the tubes. The ratios used to conduct each of the reagent mixtures are shown in Table 13.2, also indicating the Blue:Red ratio cycles needed to perform the first stage of mixing (generating the dye mixture) before diluting the mixture with water in the second stage of mixing.

The mixtures were collected in vials, conducting a first series of mixtures (from M1.1 to M3.3, as shown in Figure 13.7) and then repeating the process two more times, thus generating a triplicate for each mixture, which were measured in the UV-vis spectrophotometer. The separate prepared solutions of Allura Red and Brilliant Blue were also measured spectrophotometrically, thus obtaining the graph shown in Figure 13.8.

Table 13.2: Number and ratios between the pulses generated by the mini-pumps for the generation of solutions of Allura Red and Brilliant Blue at different ratios, for various dilutions of water. In brackets is the total number of pulses.

	First mixing step (Dyes)				Second mixing step (Dilution)			
	B	**R**	*B:R proportion*	*Number of cycles Dyes*	*Number of total pulses Dyes*	**W**	*D:W proportion*	*Number of cycles Dilution*
	Pulses	*Pulses*				*Pulses*		
M1.1	1	1	**1:1** (2)	5	10	2	**5:1** (12)	36
M1.2	1	1	**1:1** (2)	1	2	2	**1:1** (4)	108
M1.3	1	1	**1:1** (2)	1	2	10	**1:5** (12)	36
M2.1	1	2	**1:2** (3)	5	15	3	**5:1** (18)	24
M2.2	1	2	**1:2** (3)	3	9	9	**1:1** (18)	24
M2.3	1	2	**1:2** (3)	1	3	15	**1:5** (18)	24
M3.1	2	1	**2:1** (3)	5	15	3	**5:1** (18)	24
M3.2	2	1	**2:1** (3)	3	3	9	**1:1** (18)	24
M3.3	2	1	**2:1** (3)	1	3	15	**1:5** (18)	24

*B: Blue / R: Red / D: Dyes / W: Water
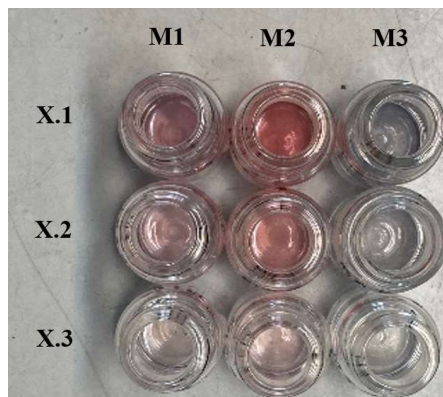
Figure 13.7: Solutions generated from the mixture of the different proportions of the food dyes.
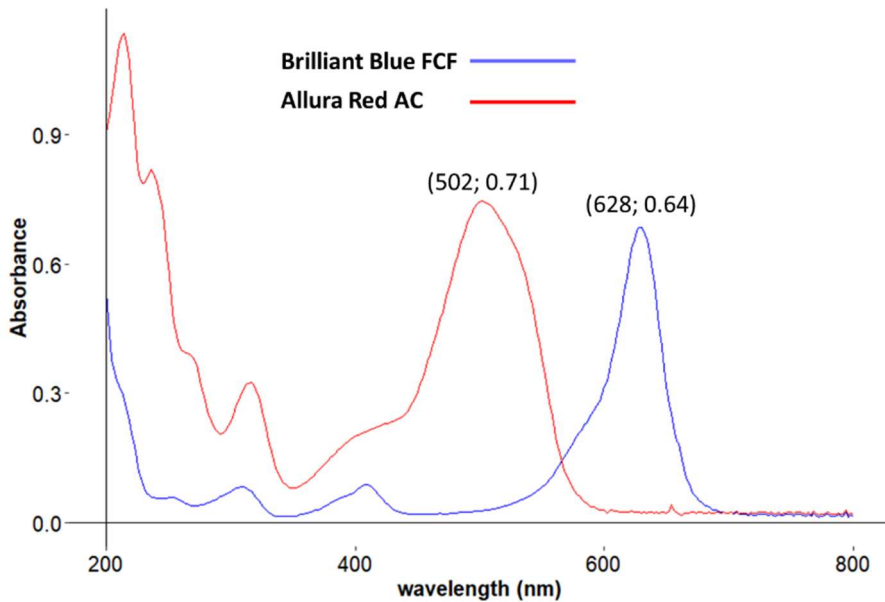
Figure 13.8: Absorbance spectra of the dyes Allura Red AC and Brilliant Blue FCF, plotting absorbance versus wavelength in nm.

For each mixture obtained, an absorbance spectrum was measured whose results are shown in Figure 13.9. As can be seen in the graphs, three groups of mixtures can be distinguished in the three figures (9.A, 9.B and 9.C), which correspond to the different dilutions with water within the same proportion of blue and red dyes. Additionally, the absorbance signals obtained were plotted against the theoretical concentrations of the dyes (knowing the concentrations of the stock solutions, the pulse volumes of each mini-pump and the pulses generated by each one of them), obtaining Figure 13.10. It can be seen that the replicates are very stables. For this reason, is possible to say that the pumps provide pulse volumes that are stable. With this robot is possible to obtain accurate mixtures.
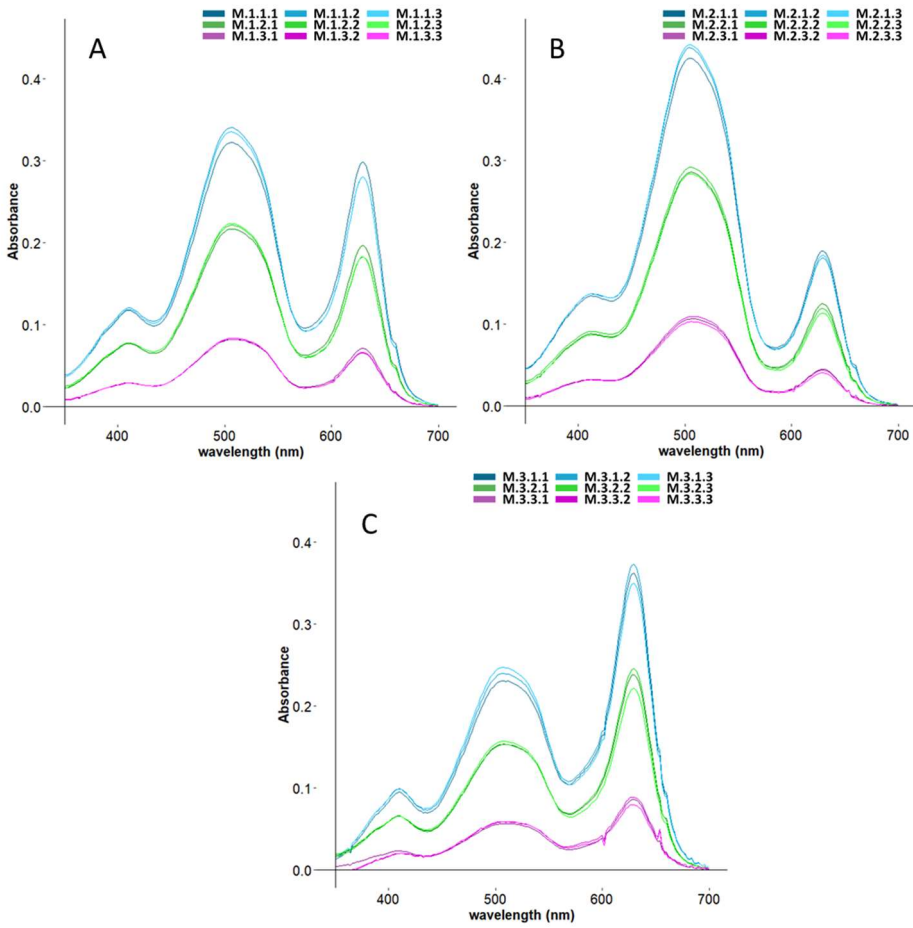
Figure 13.9: Absorbance spectra of mixtures at different ratios of Brilliant Blue and Allura Red dyes B. A) Ratio 1:1 B) Ratio 1:2 C) Ratio 2:1.
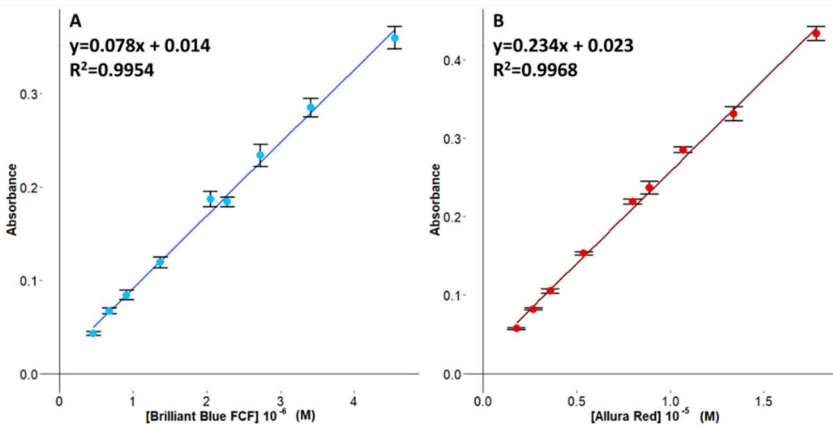
Figure 13.10: Plot of the absorbance signals versus the theoretical concentration of the different mixtures of the A) Brilliant Blue B) Allura Red food dyes.

3.2.2. Mixing of three food dyes

To determine whether the mixing robot correctly conducted the processes programmed with the Arduino script, the mixing robot and the Arduino script were tested with food dye solutions of known concentration (Quinoline Yellow, Erythrosine B and Brilliant Blue FCF). To this end, the separate solutions were first spectrophotometrically measured (between 180 and 780 nm) in order to visualise if there was a signal contribution at the maximum peak of absorbance of each dye (Figure 13.11).
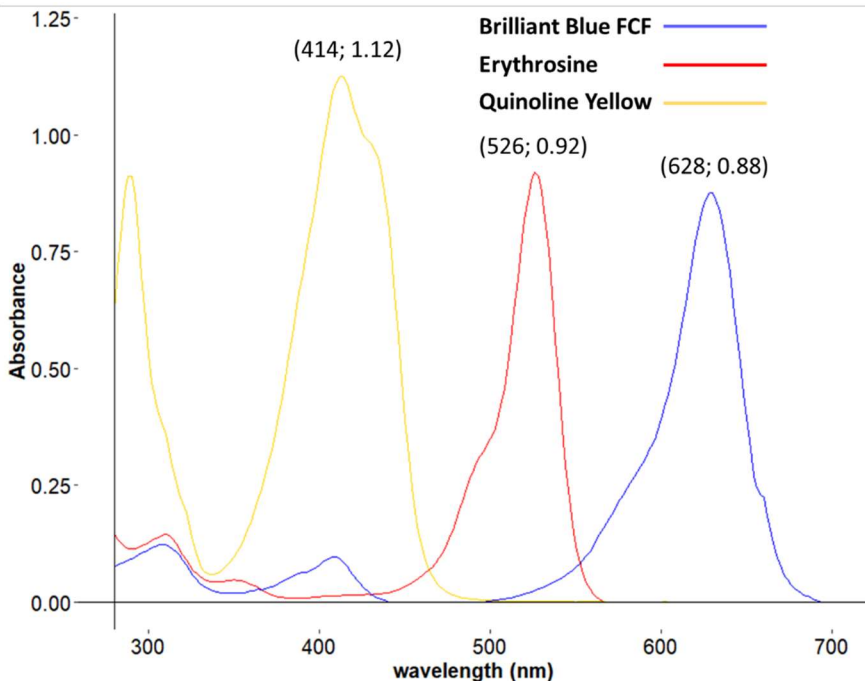
Figure 13.11: Absorbance spectra of the dyes Quinoline Yellow, Erythrosine and Brilliant Blue FCF, plotting absorbance versus wavelength in nm.

As can be appreciated in the graph, there is a slight overlap of the blue dye spectrum at the absorbance maximum peak of Erythrosine B, and a small peak of the same spectrum at the absorbance maximum of Quinoline Yellow. This does not have an important effect to study if the robot carries out correctly the mixture process.

The mixing robot was then employed to mix the dyes and, its coupling with the flow cuvette allowed to conduct continuous and simultaneous spectrophotometric measurements at the three different wavelengths. The programmed script consisted of different blocks. A first block of tube filling, starting with the tube of

mini-pump B (used for the blue dye), followed by the tube belonging to mini-pump C (used for the red dye) and finally the tube of mini-pump A (used for the yellow dye).

A second block then controlled the robot to conduct alternating and proportional pulses between mini-pumps B and C to clean the first homogenisation loop. The third block conducted the same task on the second homogenisation loop with alternating and proportional pulses between mini-pumps B, C and A. Next, the fourth block generated pulses in the same way as the previous block so that the solution would flow through the tube and would reach the cuvette for spectrophotometric measurement. Finally, a last loop was programmed to clean the system with water, only doing so from the tube of mini-pump B (cleaning the tubes of the other mini-pumps would entail a greater expenditure of reagents between measurements).

Thus, the pertinent food dye solutions were placed in the tubes of the mini-pumps and the tubes were filled up to the intersections, subsequently starting the programme and initiating, at the same time, the continuous measurement at the three wavelengths of maximum absorbance. Figure 13.12 shows the absorbance measurements of the food dyes versus time, having normalised these measurements with the maximum absorbance corresponding to each dye.

Figure 13.12: Plot of the absorbance measured at three different wavelengths simultaneously (414, 526 and 628 nm versus time).

As can be seen in the figure, an absorbance peak corresponding to the blue dye is observed, which indicates that the mini-pump B tube has been filled. The same behaviour is then observed with the Erythrosine peak (corresponding to the filling of the tube of mini-pump C) and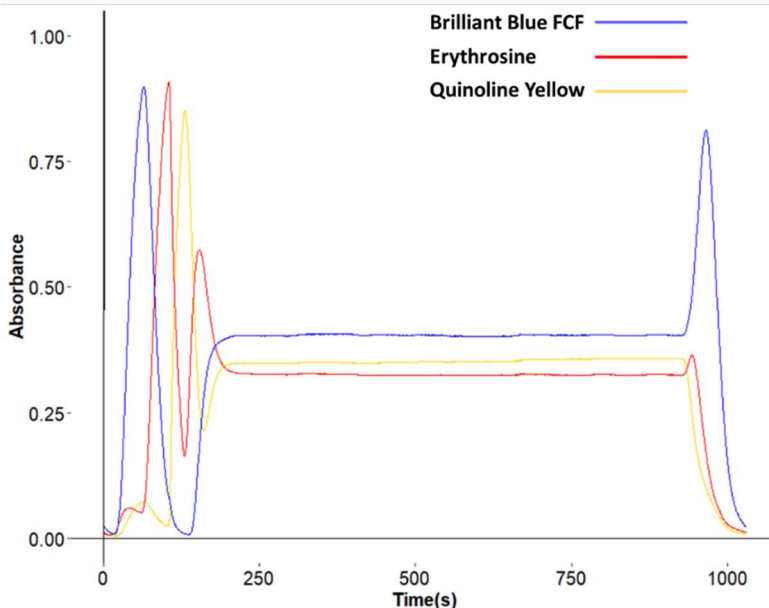, finally, the yellow dye peak (associated with the filling of the tube of mini-pump A). The three dyes' signals then stabilise, indicating that a stable and proportional mixture is being generated. Finally, a last peak of blue dye is observed at about 1000 seconds, indicating that the cleaning process is being conducted correctly from the tube connected to mini-pump B (containing the blue food dye).

Regarding the stabilisation of the signals, one would expect that, if the spectrum is normalised (by dividing the absorbance obtained by the maximum absorbance of the respective dye), an overlapping of the signals would occur instead of the observed separation. This is due to two main reasons. Firstly, as previously studied, the mixing robot generates a larger pulse volume in mini-pump B than the rest (7 µL compared to 6 µL for the other two mini-pumps). This means that, in a mixture of proportional pulses (1 pulse generated alternately by each mini-pump), the solution generated contains a higher percentage of blue dye (40% compared to 30% for the other two dyes), justifying a higher Brilliant Blue signal. Consequently, and considering that the blue dye has a contribution of around a 10% on the maximum absorbance peak of Quinoline Yellow, the signal of the yellow dye is affected, slightly exceeding the signal of the Erythrosine B.

3.3.   Copper determination

The determination of copper(II) in water samples collected along the *Acequia Real del Júcar* was carried out by two different spectroscopic methods: flame atomic absorption spectroscopy (FAAS) and UV-vis absorption spectroscopy (the last having been employed for the solutions firstly mixed by hand or in batch, and then having the robot mix the reagents and measuring them). Additionally, the copper samples were measured with the colorimetric sensor. All the different developed methods were compared to the reference one to study their analytical parameters.

A calibration curve was prepared between 0 and 2 mg/L (with increments of 0.4 mg/L) and the 24 samples collected along the *Acequia Real del Júcar*, whose copper(II) concentrations are shown in Table 13.3, were determined. From these 24 samples, a group of 10 was selected to have a representative range of concentration in the samples collected (the chosen samples were M1, M3, M5, M10, M14, M16, M17, M18 and M23).

Table 13.3: Copper(II) concentrations obtained by flame atomic absorption spectroscopy in the water samples collected along the Acequia Real del Júcar (n=3).

	$[Cu^{2+}] \pm s$ (mg/L)	CV (%)		$[Cu^{2+}] \pm s$ (mg/L)	CV (%)
M1	0.575 ± 0.004	0.7	M13	0.945 ± 0.002	0.2
M2	0.771 ± 0.004	0.5	M14	0.803 ± 0.003	0.4
M3	0.758 ± 0.002	0.2	M15	0.750 ± 0.003	0.4
M4	0.800 ± 0.003	0.4	M16	0.687 ± 0.004	0.6
M5	0.1510 ± 0.0011	0.7	M17	0.494 ± 0.003	0.6
M6	0.856 ± 0.002	0.3	M18	0.936 ± 0.011	1.2
M7	0.781 ± 0.004	0.5	M19	0.865 ± 0.006	0.7
M8	0.922 ± 0.003	0.4	M20	0.738 ± 0.002	0.3
M9	0.843 ± 0.004	0.5	M21	0.0635 ± 0.0010	1.5
M10	1.053 ± 0.004	0.4	M22	0.0175 ± 0.0015	8.4
M11	0.962 ± 0.005	0.5	M23	0.308 ± 0.003	1.1
M12	0.965 ± 0.008	0.8	M24	0.631 ± 0.006	1.0

As can be seen in the results obtained, the copper concentrations range from 0.0175 to 1.053 mg/L in the sample water locations, all of them being below the limit established by the BOE (2 mg/L) (BOE 45, 2003). Although this water is not destined for human consumption, it is still below the maximum allowed levels.

Afterwards, the batch colorimetric procedure was conducted, mixing the colorimetric reagents manually for the standards and samples. This procedure was carried out to ensure that the conditions of the reaction would not affect the determination of copper in the samples. To check the accuracy of the copper concentrations obtained by the batch spectrophotometric method, these concentrations were plotted against the reference method concentrations (FAAS), as shown in Figure 13.13A.

As can be observed, comparable data were obtained between the two methods, showing a great correlation between the data sets with a slope and interject near 1 and 0 respectively. Afterwards, the same colorimetric reaction was carried out, but using the robot coupled to the flow cell. These concentrations were also compared to the reference method, obtaining Figure 13.13B. Can be observed that, in addition to obtaining a higher dispersion in the concentration values by mixing the reagents with the robot, a notable difference was registered in the parameters of the curve. A decrease in the slope and a slight increase in the interject can be appreciated when comparing the curve parameters between Figures 13.13A and 13.13B.
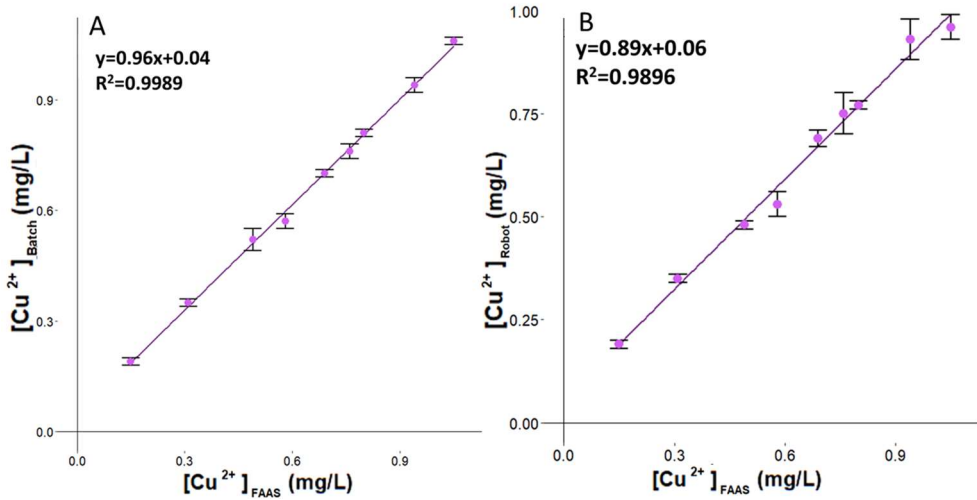
Figure 13.13: Plot of the copper concentrations obtained by the colorimetric method conducted by A) in batch and B) the robot, compared to those obtained by the reference method (FAAS).

To ensure that the measure with the cell does not produce error, the mixed solutions made with the robot were collected in vials and then were measured spectrophotometrically. When the measure made manually was compared with the FAAS measure the equation y= 0.87x + 0.03 and a R^2 = 0.994 are obtained. This equation is very similar to the obtained doing the measure with the flow cell. Due this the measure does not have any problem. It is therefore assumed that there are no significant differences between the two tests and that there is indeed a correction factor that needs to be applied when using the mixing robot to conduct the copper determination and thus, to obtain its true concentration value (equation 1).

$$[Cu^{2+}]_{Real} = \frac{[Cu^{2+}]_{Obtained\ by\ the\ mixing\ robot} - 0.06}{0.89} \tag{1}$$

Applying the corrector factor to the samples analysed by the robot and comparing these concentrations with those ones obtained by the reference method, the new obtained correlation equation was y = 0.98x + 0.02, showing that this difference could be resolved.

A final analysis was then carried out after connecting a white LED and a TCS sensor in series with the cuvette that allowed colour data to be obtained in the RGB space (third prototype). By studying the different combinations between the R, G, B and Clear parameters (collected from the LCD display) through the calibration curve and

the copper concentrations obtained in the samples, it was concluded that the Clear/G ratio would be used. These copper concentrations, after applying the correction factor, were then plotted against the concentrations obtained by the reference method, resulting in Figure 13.14. Using a low cost RGB colour sensor for Arduino and applying the correction factor due to the mixture is made with the robot it is possible to carry out an automated colorimetric reaction with a high accurate.
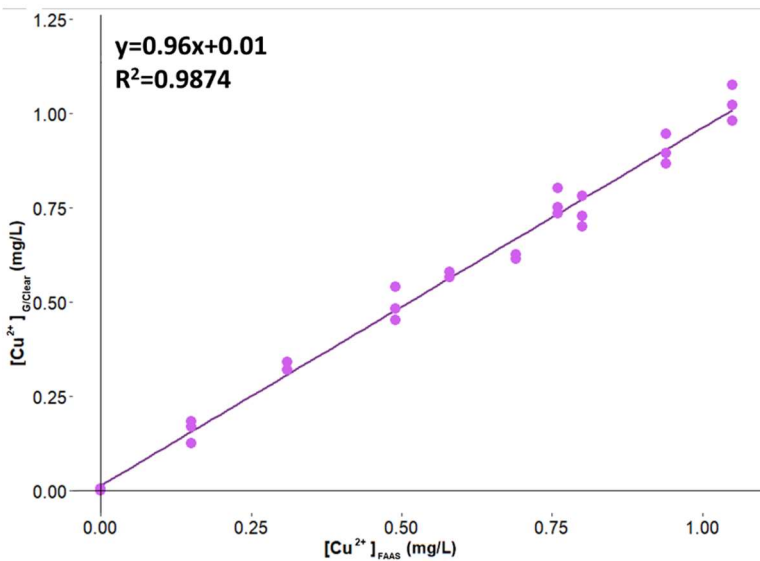
Figure 13.14: Plot of the copper concentrations obtained using the RGB sensor before applying the correction factor versus those obtained using the reference method (FAAS).

3.4.   Comparison of the methods

As mentioned above, copper(II) standards between 0 and 2 mg/L were prepared and measured by the different methods employed throughout this project to determinate copper in water samples. Table 13.4 shows the parameters corresponding to these calibration lines, together with the instrumental and method limits of detection and quantification. It should be noted that for the calculation of the detection and quantification limits, the deviation of the signal of 10 blanks was used, except for the detection method using the RGB colour space, in which the deviation of the curve calibration is used. In the case of the RGB colour sensor, low variations in the light provide a high deviation in the sensor response due a ratio between two parameters is used. For coloured solution the ratio reduces the variation in the signal, for the blank the ratio could provide a high dispersion.

Table 13.4: Analytical parameters of the different methods used for the determination of copper(II) in water.

	FAAS	UV-vis *batch*	UV-vis robot	RGB
Slope (mg/L)$^{-1}$	0.105	0.125	0.126	-0.130
Intercept	$8 \cdot 10^{-4}$	$3 \cdot 10^{-3}$	$2 \cdot 10^{-3}$	$524 \cdot 10^{-3}$
Coefficient of determination	0.9996	0.9999	0.9999	0.994
LOD$_{method}$ (µg/L)	31	33	33	52
LOQ$_{method}$ (µg/L)	103	110	110	172

At first glance, it can be observed how the values for the sensitivity of the four methods are quite similar, with very similar slope values between them. At the same time, the coefficients of determination of the spectrometric methods show a clear and very good correlation between the analytical signal obtained and their respective copper(II) concentrations. When discussing the method that used an RGB sensor, it shows a lower correlation in the data obtained. Despite this small difference, it still shows a very acceptable coefficient of determination, especially having only coupled tools which, unlike analytical instruments that usually require a large amount of funds, are easily accessible and are of a much lower cost.

Regarding the detection and quantification limits obtained, the method that showed lower values was the reference method (FAAS). As for the colorimetric methods measured by UV-vis spectrophotometry, they showed very similar values, both conducted in batch, and by generating the reagent mixtures developed with the mixing robot, showing quantification levels of around 100 µg/L. Finally, the data that stand out the most in the table are the values for the limits of detection and quantification of the RGB method. This one showed slightly higher values than the others.

Summarising and conducting a general comparison of the methods used, it can be highlighted that the method that stands out for its precision and accuracy for the determination of copper in water is the FAAS, that is the reference method. However, it is also true that it is the least green method of all those used, using very hazardous reagents (such as concentrated nitric acid or acetylene), which not only put the operator at risk, but also contaminate the environment to a greater extent. In addition, it uses equipment that is not very accessible due to its high cost and energy consume, contrasting with the principles of green chemistry.

The colorimetric method with UV-vis detection uses reagents that are not as hazardous as those used by FAAS, greatly reducing operator risk and environmental

contamination. The only drawback is the fact that it still uses equipment which is still an instrument whose access is more difficult due to its high cost. On the other hand, by using the mixing robot, the operator handles less reagents (reducing exposure to chemical reagents) and reduces random errors, narrowing the gap to a greener method. It is also worth mentioning that while instruments such as FAAS or spectrophotometry require approximately 3 mL to conduct a measurement, the mixing robot requires only 1.5 mL, reducing the expense of reagents and samples by half and, consequently, the waste generation also by half (which is also a principle of green chemistry). Therefore, by attaching to the robot lower-cost devices as the colour sensor allowing continuous and *in situ* measurements to be performed, the required analyses and their cost can be greatly reduced.

4.   Conclusions

The chapter conducted has enabled the development of a mixing robot programmed and controlled by Arduino that correctly mixes the reagents using iterative pulses from its mini-pumps, making it possible to determine compounds through a colorimetric reaction, such as the present case (copper in water).

In the study of efficiency of the system using food dyes, the results obtained show that, if the system has mini-pumps with pulse volumes that do not vary significantly, mixtures of different proportions of reagents are obtained with high accuracy, also reducing the variability between replicates. The robot's cleaning system has also been checked to avoid cross-contamination between standards and samples. At the same time, the script and that the robot executes the orders correctly have been verified by a continuous spectrophotometric measurement of food dyes.

A copper determination method has been developed which uses the robot to conduct the reagent mixtures coupled to a colour detection system in the RGB space, which provides results comparable to the reference method, using a correction factor that allows the real copper concentration to be obtained. In addition, the developed method reduces operator contact with reagents, reduces the reagent consumption by half and developing a model that does not require expensive equipment or high budgets.

Finally, having been able to develop and create a robot mixer with inexpensive components that can, not only control the mixing pattern but also allow continuous and *in situ* of a colorimetric determination of copper in irrigation water, demonstrates that automation and robotics are the future in the green analytical chemistry.

5.   References

Armenta, S., Garrigues, S. & de la Guardia, M. (2008). Green Analytical Chemistry. *TrAC-Trends in Analytical Chemistry*, 27 (6), 497–511. DOI: 10.1016/j.trac.2008.05.003.

Badamasi, Y. A. (2014). The Working Principle of an Arduino. In *11th International Conference on Electronics, Computer and Computation (ICECCO)*; IEEE: Abuja, Nigeria. DOI: 10.1109/ICECCO.2014.6997578.

Galadima, A. A. (2014). Arduino as a Learning Tool. In *11th International Conference on Electronics, Computer and Computation (ICECCO)*; IEEE: Abuja, Nigeria. DOI: 10.1109/ICECCO.2014.6997577.

Gałuszka, A., Migaszewski, Z. & Namieśnik, J. (2013). The 12 Principles of Green Analytical Chemistry and the SIGNIFICANCE Mnemonic of Green Analytical Practices. *TrAC-Trends in Analytical Chemistry*, 50, 78–84. DOI: 10.1016/j.trac.2013.04.010.

International Federation of Robotics. (2021). Executive Summary World Robotics 2021 Industrial Robots. https://ifr.org/img/worldrobotics/Executive_Summary_WR_Industrial_Robots_2021.pdf. [Accessed October 22, 2022]

Lindsey, J. S. (1992). A Retrospective on the Automation of Laboratory Synthetic Chemistry. *Chemometrics and Intelligent Laboratory Systems*, *17* (1), 15–45.

BOE 45, 21/02/2003. REAL DECRETO 140/2003, de 7 de febrero, por el que se establecen los criterios sanitarios de la calidad del agua de consumo humano.

Ruiz, V.M. (2021). Arduino, Programación y Robótica; Anaya Multimedia: Madrid.

Sarkozi, L., Simson, E. & Ramanathan, L. (2003). The Effects of Total Laboratory Automation on the Management of a Clinical Chemistry Laboratory. Retrospective Analysis of 36 Years. *Clinica Chimica Acta*, *329* (1–2), 89–94. DOI: 10.1016/s0009-8981(03)00020-2.

CHAPTER 14: Development of an automated device for monitoring photo-Fenton reactions.
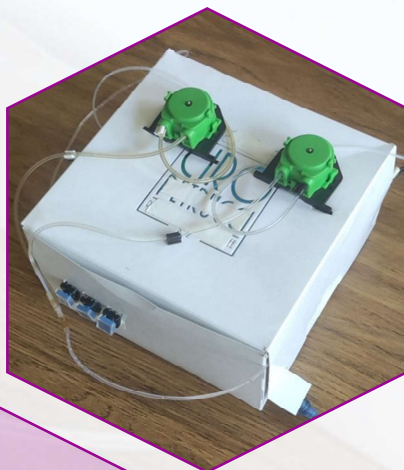
ABSTRACT

In this study, the photo-Fenton process was used to degrade caffeine, selected as model target compound, and the experimental setup was automated using a Arduino controlled robot. The robot allowed to measure the hydrogen peroxide concentration in the reaction cell through a colorimetric reaction and to take samples of the solution for HPLC analysis minimizing the operator manual intervention and exposure to UV radiation. The robot's ability to control flow rates and the reproducibility of peristaltic pumps were also evaluated. Additionally, H_2O_2 measurements were also performed manually using a classic laboratory UV-Vis spectrophotometry to measure the colour and the results were compared with the ones obtained using the robot. The results showed that the robot's LOD and LOQ were 0.032 mM and 0.106 mM, respectively, which were lower than those obtained through UV-Vis spectrophotometry, which were 0.064 mM and 0.213 mM, respectively. To evaluate the photo-Fenton reaction's behaviour under varying starting conditions, a Design of Experiments (DoE) was employed. The results showed that the robot was able to effectively monitor the reaction according to the desired requirements. The use of a robot for such monitoring provides several advantages, including automation, precision, and reduced experimental workload. Overall, this study demonstrates the potential of using robots for process monitoring, especially in cases where the process requires continuous and precise measurements.

Keywords: Arduino, Caffeine, Design of experiments, Hydrogen peroxide, Photo-Fenton

1.   Introduction

1.1.   Arduino and automatized devices

Automatized systems in chemistry refer to the use of technology to control and monitor chemical process automatically. These systems employ electronic devices such as sensors or actuator to collect information or allow control the chemical process in an accurate and reproducible way. One of the most widely employed electronic devices in homemade automatic systems are the Arduino boards (Abdulraheem et al., 2020; Asadullah & Raza, 2016; Gunge & Yalagi, 2016).

Arduino is a hardware platform featuring an open-source software that allows users to create their own electronic devices in an easy and fast way. Arduino is made up of impress circuit cards, a microcontroller, and a software develop environment. This allows users to program and control the electronic devices without advanced knowledge in programming (Badamasi, 2014; Goon et al., 2019; Wu et al., 2021).

There are different advantages in using automatized devices in chemistry. Firstly, this type of systems can improve the accurateness and repeatability of the chemical process. This allows to obtain more consistent results in experiment also in the perspective of the scale-up at industrial level. Another advantage is that these systems can improve the efficiency and productivity in chemistry labs. Arduino systems can perform tasks in a fast and automated way allowing to save time and resources when experiments are carried out, therefore reducing also wastes. Moreover, such automated systems can be safer for the user when in case the experimental procedures involve dangerous reagents (Antela et al., 2019).

1.2.   Advance oxidative process

Advance Oxidation Processes (AOPs) are chemical reactions in which free radicals (mainly hydroxyl radicals), that are very reactive, are formed. These radicals can be very effective for the oxidative degradation of many organic contaminants in water (Garrido-Cardenas et al., 2020). That reactions are employed in a variety of water treatment process (Boczkaj & Fernandes, 2017; Ma et al., 2021). Some of these techniques are assisted by UV(-VIS) radiation and/or include the use of catalysts. Once the radicals are generated, they reacts with the contaminants, breaking them down into simpler and (hopefully) less harmful compounds (Boczkaj & Fernandes, 2017; Deng & Zhao, 2015; Ma et al., 2021; Miklos et al., 2018). One of the advantages of the use of AOPs is that are highly efficient in the degradation of a wide variety of contaminants. Moreover, that reactions are usually performed at

room T and pressure, avoiding extreme conditions and making them a valid and useful tool in water treatment processes (Kumar et al., 2021; Wang & Wang, 2021).

Photo-Fenton reaction is an advanced oxidation process in which free radicals of oxygen are formed from hydrogen peroxide and iron (Equation 1) (Liu et al., 2018). In this process, iron is a catalyst that reacts with hydrogen peroxide in order to obtain hydroxyl radicals (Equation 2) (Liu et al., 2018). In this process, light has been proven to accelerate the reaction, by regenerating Fe(II) ions (Equation 3) (Liu et al., 2018), the principal specie responsible for H_2O_2 decomposition yielding OH radicals formation (Palma et al., 2018; Palma et al., 2021).

$$Fe^{2+} + H_2O_2 \rightarrow Fe^{3+} + OH^- + \cdot OH \qquad \text{(Equation 1)}$$

$$Fe^{3+} + H_2O_2 \rightarrow Fe^{2+} + H^+ + HO_2^\cdot \qquad \text{(Equation 2)}$$

$$Fe^{3+} + H_2O + h\upsilon \rightarrow Fe^{2+} + H^+ + \cdot OH \qquad \text{(Equation 3)}$$
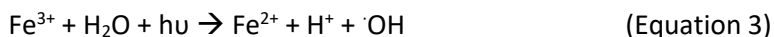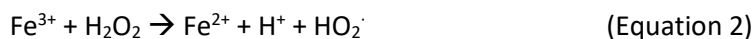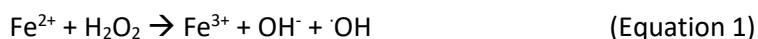
The aim of this work was the development of an automatic device employing an Arduino board allowing to automatize the measurement of the concentration of hydrogen peroxide during the photo-Fenton treatment. It has indeed been discussed in the literature the way of adding hydrogen peroxide to the system (either in several aliquots or only once at the beginning of the process) At the same time, the robot also allowed to withdraw samples of the treated solution to perform HPLC measurements of caffeine residual concentration. To carry out the colorimetric reaction for the determination of H_2O_2 concentration, the procedure described by Minella et al. has been used (Minella et al., 2016). Combining the design of experiments (DoE) with this device, it was possible to obtain a high amount of information with a reduced number of experiments. This automatized approach allowed to reduce the wastes by reducing the number of experiments and the amount of reagents and to obtain the results with a more accurate procedure.

2.   Materials and methods

2.1.   Reagents and instrumentation

Photodegradation experiments were carried out by irradiating, under continuous stirring, 100 mL of aqueous samples in a closed Pyrex® cell with a Xenon (1500 W) lamp (Solarbox, CO.FO.ME.GRA S.r.l., Milan, Italy) paired with a 340 nm cut-off filter. The irradiance of the lamp, measured with a UV-Multimeter system, was 26.7 W m^{-2}.

Caffeine was monitored by HPLC, employing a Merck-Hitachi instrument, equipped with Lichrospher RP-C18 (125 mm × 4 mm i.d., particle diameter = 5 µm, from Merck, Darmstadt, Germany), l-6200 pumps and UV/Vis l-4200 detector using a measurement wavelength of 210 nm. The employed eluent was a 0.1 % H_3PO_4 in 50/50 (vol %) methanol/water mixture at 0.8 mL min^{-1} constant flow.

Caffeine solutions were employed in a concentration between 5 and 35 mg/L. H_2O_2 was used in a concentration between 0.1-1.5 mM. $FeSO_4 \cdot 7H_2O$ was used as iron(II) source to obtain iron concentrations between 0.1 and 0.9 mg/L.

2.2.   Electronic components

For the development of the robot, an Arduino ONE board has been employed. The components of the robot included a Bluetooth module (DSD TECH HM-10, 25 m), two peristaltic pumps (Hyudio, ASIN: B07Q1WNHHT), a colour sensor TCS34725 (TECNOIOT, ASIN: B07YXDZVJN), a white high intensity LED, two relay KY-019 5V (WINGONEER, ASIN:B06XHJ2PBJ) and simple elements as buttons, resistors, and wires. To carry out the colorimetric measure, a 178.710-Os (Hellma) flow cell was employed.

2.3.   Robot development

To perform the colorimetric measure a support for colorimetric cell was 3D-printed; the Figure 14.A.1 shows a scheme of the structure with the disposition of the different elements. the robot was turned on 15 minutes before the beginning of the experiment to allow LED emission to get stable. The buttons have been configured to perform the following actions: "Take sample", "colour measure" and "colorimetric reaction".

The first instruction, "Take sample", turned on the peristaltic pump connected to the irradiated solution. In this way, the pump allowed to obtain samples from the irradiation cell without manual intervention from the operator. This instruction was performed 3 times, the first 2 to clean the system, the last one is to obtain the sample. The function "colour measure" was used to obtain information from the TCS34725 sensor. This sensor provides information about the Colour temperature, Lux, red (R), green (G), blue (B) and white light (clear). The last instruction, "colorimetric reaction", turns on both pumps, connected to the sample and the colorimetric reagent, to mix both solutions inside the system. This mixture filled the measuring cell irradiated with LED source. After 6 minutes, the reading from the colour sensor was obtained providing the same information explained in the "colour measure" function.

These three instructions could be controlled both from the robot itself using the dedicated buttons and remotely using the Bluetooth module. For that, these works if the device receives the text characters "a", "b" or "c" respectively through the Bluetooth module from a connected device. To carry out this connection, the "Arduino Bluetooth Controller" app, available in the play store, has been employed (Figure 14.A.2). The electronic scheme and the physic system of the are showed in the Figure 14.1. The final prototype of the robot is shown in the Figure 14.2.
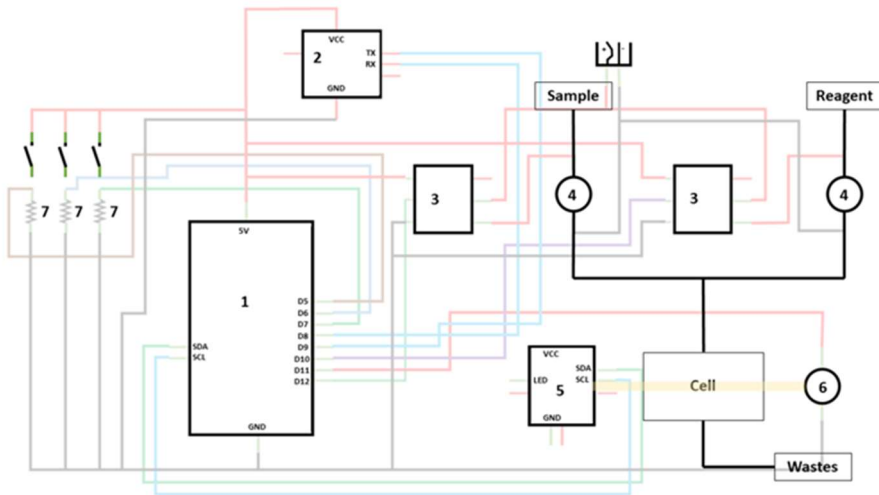
Reference	Value	Description
1	Arduino ONE	Microcontroller
2	B06WGZB2N4	Bluetooth module
3	Ky-019	relay
4	YD-GSGJZJCHAO20100	Peristaltic pump
5	TCS34725 RGBC	Color sensor
6	B07DPRWVRF	LED
7	220Ω	Resistor

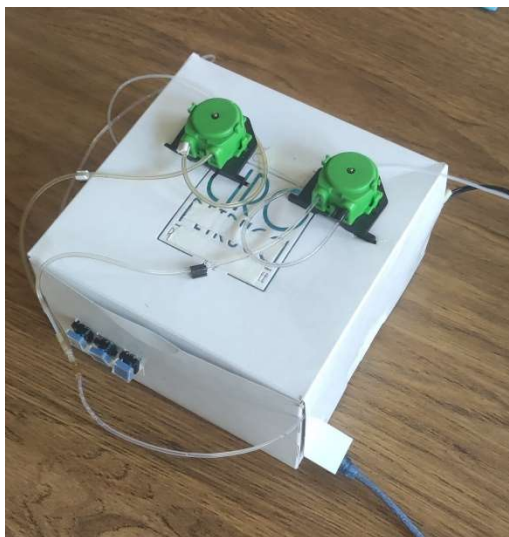*Figure 14.1: overlap of the Physic and electronic scheme of the developed device.*

Figure 14.2: Device developed for monitoring the photo-Fenton reaction.

2.4.   Photo-Fenton reaction

Different iron concentrations have been tested (0.1, 0.5 and 0.9 mg/L). The pH was adjusted to 3.0 using H_2SO_4. Lastly, the solution was placed into a Pyrex glass closed irradiation cell. The reactor, covered with aluminium foil, was placed inside the Solarbox for 15 minutes in order to reach the same temperature as the Solarbox before starting the irradiation. Three H_2O_2 concentrations have been tested (0.1, 0.8 and 1.5 mmol/L of H_2O_2 in the final solution). H_2O_2 was added as the last reagent and experiments started immediately after that.

2.5.   Caffeine measurement

To monitor the concentration of caffeine in treated water, samples were taken using the "Take sample" command of the robot. Then, 1 mL of sample was manually added with 0.2 mL of methanol in a vial in order to stop the degradation reaction. The solutions were analysed by HPLC.

2.6. H_2O_2 measurement

To perform the colorimetric reaction of H_2O_2, the reagent solution and the sample were automatically mixed, using the developed device, in a 3:2 ratio. The colorimetric reagent was prepared with 0.7112 g of $NaH_2PO_4 \cdot H_2O$, 0.2760 g of $Na_2HPO_4 \cdot 2H_2O$, 0.2340 g of phenol, 0.1000 g of 4-amminoantipiridine and 0.0010 g of peroxidase (VI) for 100 mL of colorimetric reagent. The solution was measured using both the new device and a spectrophotometer. The measure by the spectrophotometer was carried out manually, obtaining the absorbance at 505 nm.

The measure by the new device was carried out automatically, obtaining the colour parameters by the sensor. Due to the kinetics of the colorimetric reaction, a delay of 6 minutes was added before obtaining the absorbance/colour data to wait for proper colour development.

3. Results and discussion

3.1. Peristaltic pump flow

In order to optimize the flow of the system, different tubes with different internal diameter (i.d.) and external diameter (e.d.) were tested. The tubes (PVC-Standard, SPECTEC) were identified with colour codes: Grey-Grey (G-G, i.d.: 1.295 mm, ref:38-0046), Orange-Yellow (O-Y, i.d.: 0.508 mm, ref:38-0025), Blue-Yellow (B-Y, i.d.: 1.524 mm, ref:38-0052), Black-Black(B-B, i.d.: 0.762 mm, ref:38-0032), White-White (W-W, i.d.: 1.016 mm, ref:38-0040). Three experiments were carried out. The first one was to study the potential of the transformer employed to plug in the device. The second was to study if there were differences in the flow using different peristaltic pumps. The last one was to study the flow of each type of tube with the optimal parameters.

To carry out the first study, the G-G tube was employed. The total volume carried by the peristaltic pump was collected for 10 and 20 s using a power supply voltage of 6, 9 and 12 V. The Table 14.1 collects the data obtained for the experiments. As it can be seen, a higher voltage (12 V) provides a high carried volume but high error too. For this reason, to carry the higher amount of solution with the lower error, the preferred voltage was 9 V.

Table 14.1: Volumes obtained for the peristaltic pump for 10 or 20 seconds working applying a voltage of 6, 9 or 12.

Measure	6 V		9 V		12 V	
Time	10 s	20 s	10 s	20 s	10 s	20 s
1	1.00	2.17	2.03	3.76	3.07	5.80
2	1.13	2.16	2.01	3.67	2.93	5.72
3	1.13	2.03	2.02	3.72	2.98	5.56
4	1.13	1.97	2.04	3.72	2.86	5.23
5	1.11	1.92	1.94	3.69	2.91	4.83
Mean	1.12	2.04	2.01	3.71	2.95	5.42
Standard deviation	0.01	0.1	0.04	0.03	0.08	0.40
Error (%)	0.93	5.04	1.95	0.89	2.67	7.38

Once the voltage was selected, the peristaltic pumps were studied, using the G-G tube, in order to evaluate if there are differences between different of them. The

volume carried for three pumps were studied 5 times at 10, 20 and 30 seconds and curve calibration were made for each pump. The Figure 14.3 shows the results obtained. As can be seen, the differences between the pumps are minimal. For this can be said that the volume carried for each peristaltic pump is very similar and do not provide an error source in the chemical reaction. After that the flow of each type of tube was evaluated with the amount of water carried in 10 seconds. This was made 5 times for each tube. Table 14.2 shows the mean of the flow obtained.
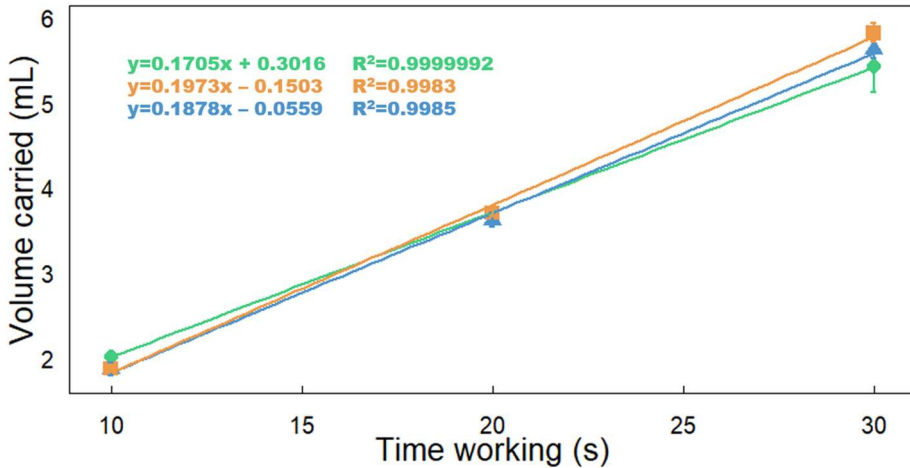
Figure 14.3: Curve calibration of the average volume carried for each peristaltic pump at each time and their errors.

Table 14.2: Flow that provide each tube obtained using a potential of 9 V.

Tube	G-G	O-Y	B-Y	B-B	W-W
flow (mL/s)	0.187	0.035	0.240	0.076	0.116

3.2.   Comparison between UV-vis spectrophotometer and TCS34725 sensor

In order to check if the robot was correctly carrying out a colorimetric measure of H_2O_2, a calibration curve was prepared. Standard solutions of 0, 0.01, 0.05, 0.1, 0.25, 0.5, 0.75, 1, 1.25, 1.5 and 2 mM of H_2O_2 were prepared. The reaction was performed, mixing the colorimetric reactive and the sample in a 3:2 ratio. As colour of the solution increase with the time, the moment in which the measure is taken is a crucial parameter. For this reason the colorimetric measure by UV-vis spectrophotometry was obtained at 6 and 10 minutes to evaluate when the optimal moment occurs (Figure 14.4).
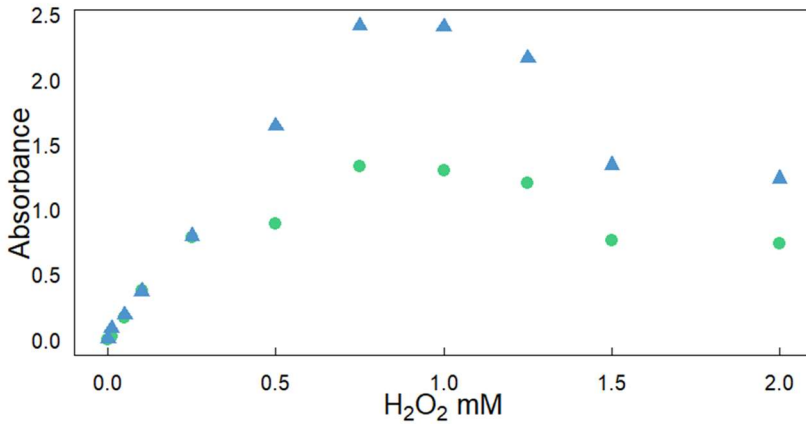
Figure 14.4: Absorbance of the colorimetric reaction for H_2O_2 determination at different times: 6 minutes (Green[●]) and 10 minutes (Blue[▲]).

The sensor employed provides colour information using the R, G, B channels. Although it is possible to obtain calibration curves with the raw data, the ratios between colour parameters provide more stable readings, with lower coefficient of variation and larger linear calibration range. The results obtained using the R/G ratio have the same trend as the results obtained with the spectrophotometer (Figure 14.5). This ratio is used to show the behaviour, not for making the subsequent analysis, for this purpose the G/B colour ratio provides better results and a higher linear range. For this reason, it is possible to say that the colour sensor provides the same information as the spectrophotometer. As it can be seen, waiting 10 minutes before measuring the colour, provides a better sensibility, but for monitoring the reaction this takes a long time. For that, 6 minutes are taken to make the measure.

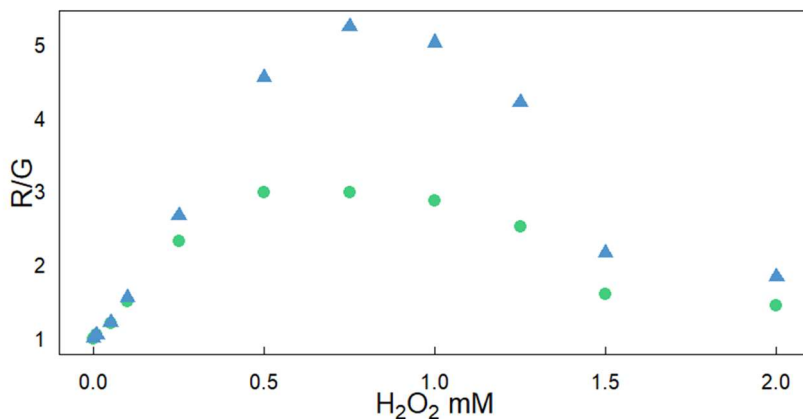Figure 14.5: Colour ratio obtained from the colorimetric reaction for H_2O_2 determination employing the TCS34725 colour sensor at different times: 6 minutes (Green[●]) and 10 minutes (Blue[▲]).

In this study, we compared the limits of detection (LOD) and quantification (LOQ) of the colorimetric method obtained using the robot and UV-vis spectrophotometer. It is important to note that the colour measurement requires waiting for a while, and this time is automated with the robot, but it is manually controlled with the spectrophotometer measurement. The LOD and LOQ were determined as LOD = 3·s_y/slope and LOQ = 10·s_y/slope, where S_y is the deviation of the linear calibration. Our results showed that the colour sensor had an LOD of 0.032 mM and an LOQ of 0.106 mM for hydrogen peroxide measurement, while the spectrophotometer had an LOD of 0.064 mM and an LOQ of 0.213 mM. These results suggest that the colour sensor has a higher sensitivity for hydrogen peroxide detection than the spectrophotometer, that can be explained due the automated control in the waiting time of the colorimetric reaction by the robot.

To further evaluate the performance of the colour sensor, we measured the signal and standard deviation for hydrogen peroxide concentrations near the LOD. The results are showed in the Figure 14.6. Based on these results, it appears that hydrogen peroxide concentrations lower than 30 mM cannot be reliably detected with the colour sensor, while concentrations of 30 mM and higher can be detected with reasonable confidence. This is consistent with the LOD and LOQ values obtained from the calibration line. Overall, these results suggest that the TCS3425 colour sensor is a sensitive and reliable tool for hydrogen peroxide colorimetric measurement. The linear range of the procedure is between 0.11 - 0.80 mM.
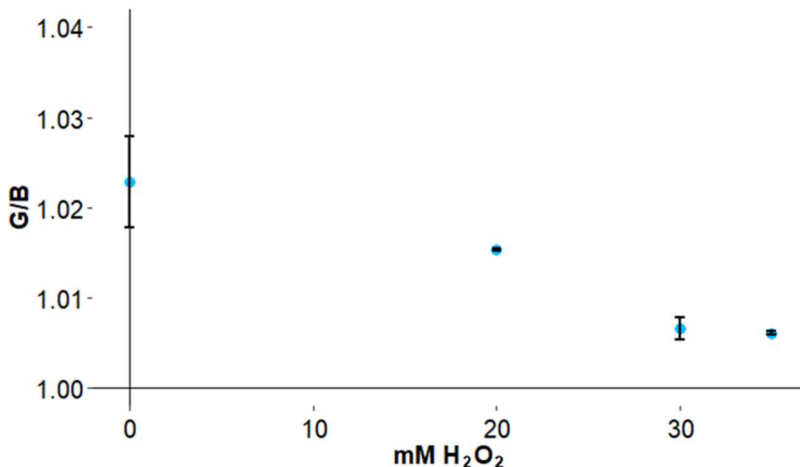

Figure 14.6: Average and standard deviation obtained of the measurements signal for low amounts of H_2O_2 obtained by the new device.

3.3. Studies of the use of the new device in H_2O_2 and caffeine monitoring

To carry out the Photo-Fenton process, 100 mL of the contaminant solution (20 mg/L of caffeine) were used. The reaction was carried out with a concentration of 0.1 mg/L of Fe(II) and 0.8 mM of H_2O_2. The robot was employed to obtain a sample of the solution, as is explained in the 2.3 section at 0, 10, 20, 30, 60 and 90 minutes.at that same time, the robot was used to determine the content of H_2O_2, using the colour sensor. The Figure 14.7.A shows the results of the concentration of both analytes at those times.

The experiment has been repeated, increasing the concentration of Fe(II) (0.5 mg/L of iron). Figure 14.7.B shows that the increase of iron increases the velocity of the degradation of caffeine. Moreover, the study of the consumption of H_2O_2 has been carried out. In this case, the H_2O_2 is reduced to half after 75 minutes of irradiation. Figure 14.7.C shows that reducing the amount of H_2O_2 does not have a significant effect on the degradation of caffeine. The results show that the robot can take the sample from the reactor and perform the colorimetric reaction.
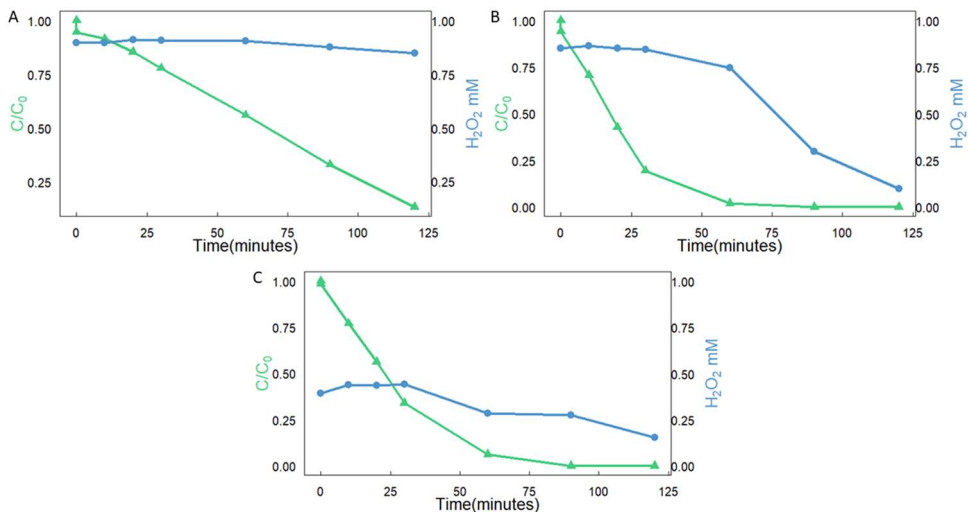
Figure 14.7: Results obtained for monitoring of H_2O_2 (Blue[●]) and caffeine (Green[▲]) in a Photo-fenton process at conditions of: A)20 mg/L of caffeine, 0.8 mM of H_2O_2 and 0.1 mg/L of Fe(II); B) 20 mg/L of caffeine, 0.8 mM of H_2O_2 and 0.5 mg/L of Fe(II); C) 20 mg/L of caffeine, 0.4 mM of H_2O_2 and 0.5 mg/L of iron.

3.4. Design of Experiments (DoE)

To study the behaviour of the Photo-Fenton reaction depending on the concentration of the reagents and contaminant, a DoE was carried out. According to other works (El Shahawy et al., 2021; Mohadesi & Shokri, 2019; Tayeb et al.,

2018), a Box-Benhken is a good option to carry out the DoE in Photo-Fenton reaction. In this case, a 3-levels 3-factors Box-Behnken was performed. The three factors studied were the concentration of contaminant, the concentration of H_2O_2 and the concentration of Fe(II). In Table 14.3 are displayed the experimental conditions in which the 15 experiments of the DoEwere performed. As response parameters the content of caffeine and H_2O_2, expressed as C/C_0, at 30, 60 and 90 were employed. Out of a total of 18 contour graphs, 9 graphs of interest have been obtained (Figures 14.A.3 to 14.A.11).

Table 14.3: Parameters and experiments carried out in the Box-Benhken study.

Factor	Level -1	Level 0	Level 1
Caffeine (mg/L)	5	20	35
H2O2 (mM)	0.1	0.8	1.5
Fe(II) (mg/L)	0.1	0.5	0.9

Exp.	Caff.	H_2O_2	Fe(II)	Exp.	Caff.	H_2O_2	Fe(II)
1	-1	-1	0	9	0	-1	-1
2	1	-1	0	10	0	1	-1
3	-1	1	0	11	0	-1	1
4	1	1	0	12	0	1	1
5	-1	0	-1	13	0	0	0
6	1	0	-1	14	0	0	0
7	-1	-1	1	15	0	0	0
8	1	-1	1				

Firstly, the amount of caffeine remaining at different times was evaluated according to the initial content of H_2O_2 and Fe(II) (Figures 14.A.3-14.A.5). As it can be seen, the parameter that has a higher influence is the Fe(II). At short irradiation times, the peroxide does not have an important influence in the degradation of caffeine. At longer irradiation times, H_2O_2 acquire a more significant effect. Moreover, at later times, it is possible to find a ratio between the H_2O_2 and the Fe(II) that allows a higher degradation ratio (Figure 14.A.6). When the amount of H_2O_2 that is consumed is evaluate according to the same parameters, it is possible that the parameter with the most influence is the Fe(II) (Figures 14.A.6-14.A.8). On the other hand, when higher is the initial concentration of H_2O_2, fast is the H_2O_2 consumption.

Other analysis was performed to study the consumption of H_2O_2 depending on the initial concentration of H_2O_2 and the initial content of caffeine (Figures 14.A.9-14.A.11). In the surface graphs, it is possible to check that is a relation between

them. For lower and higher concentrations of contaminant, the consumption of H_2O_2 is higher. On the other hand, for significant amount of H_2O_2 the content does not change significantly with the time. As could be seen in the preliminary studios (3.3 section) the H_2O_2 is not fast consumed as was thought.

At last, the results of this DoE allow knowing the best conditions, in this range of concentration of these parameters, to achieve the higher caffeine degradation using the lowest amount of reagents. The Figure 14.8 shows the surface graph obtained for the caffeine degradation, for the H_2O_2 consumption and the overlapping of both at 90 minutes. The overlapping shows that to achieve the higher degradation of caffeine, it is possible to use a different amount of the reagents. it is important bearing in mind that it is preferable to use less amount of H_2O_2 than Fe(II) and it is preferable to consume the higher amount of H_2O_2 possible. The best conditions for that requirements are a concentration of 0.85 mg/L of Fe(II) and 0.5 mM of H_2O_2.
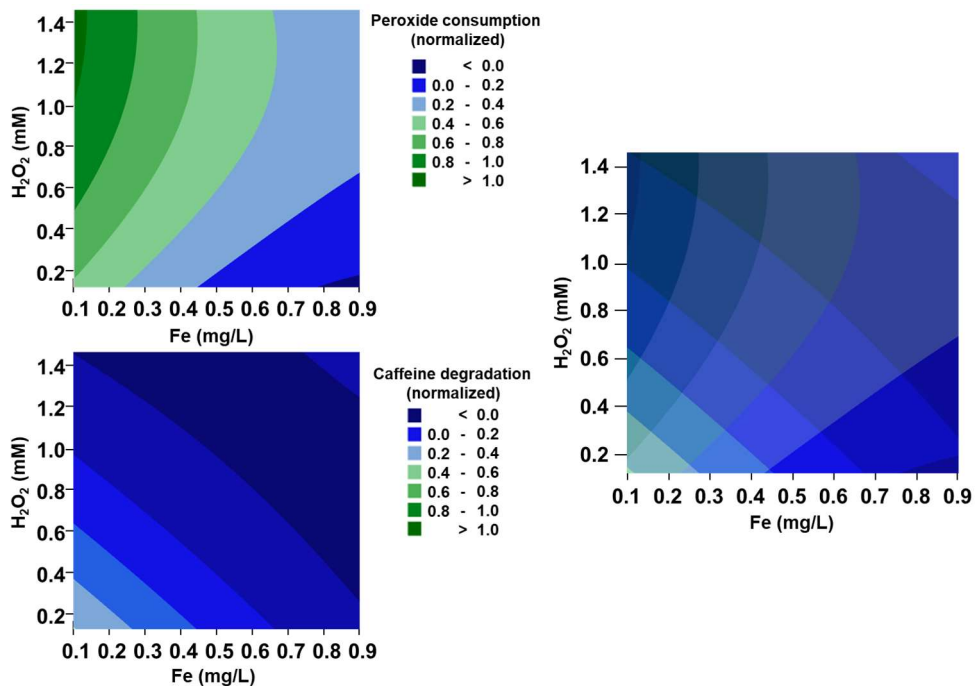

Figure 14.8: Overlapping of the contour graph obtained for caffeine degradation and peroxide consume obtained with [peroxide]vs[Fe] for a fixed content of caffeine (20 mg/L) at 90 min.

4. Conclusions

In conclusion, we have successfully demonstrated the effectiveness of a low-cost Arduino system in conducting a chemical measurement that typically requires extensive manual labour. For the H_2O_2 measurement, the developed robot has been demonstrate reaching a LOD and a LOQ of 0.03 and 0.11 mM respectively with a linear range of 0.11-0.80 mM using the G/B colour parameters ratio. Our results have revealed that this automated system is more sensitive compared to the traditional manual method. Moreover, it has been possible to monitoring a photo-Fenton reaction modifying different parameters as the pollutant content, the iron and H_2O_2 concentration and different times of irradiation. By incorporating robots into laboratory settings, we can not only reduce the amount of waste produced, but also minimize the resources required for experimentation. This technology also enhances operator safety by decreasing direct exposure to reagents, UV radiation, and samples.

To further reduce the number of experiments and generated waste, such devices can be combined with other tools like Design of Experiments (DoE). Our findings highlight the significant potential of automated systems like the one presented here, as they can significantly streamline laboratory processes while enhancing efficiency, accuracy, and safety.

Beyond chemical measurements, this technology can be applied across multiple scientific fields. Therefore, the exploration and integration of such automated devices in laboratory settings to enable more efficient and sustainable scientific research must be inquired. Overall, the use of low-cost automated systems has immense potential to transform the way we conduct experiments and improve the scientific process.

5.   References

Abdulraheem, A. S., Salih, A. A., Abdulla, A. I., Sadeeq, M. A., Salim, N. O., Abdullah, H., ... & Saeed, R. A. (2020). Home automation system based on IoT. *Technology Reports of Kansai University*, *62*(5).

Antela, K. U., Sáez-Hernández, R., Cervera, M. L., Morales-Rubio, A., & Luque, M. J. (2023). Development of an automated colorimeter controlled by Raspberry Pi4. *Analytical Methods*. DOI: 10.1039/d2ay01532c

Asadullah, M., & Raza, A. (2016). An overview of home automation systems. In *2016 2nd international conference on robotics and artificial intelligence (ICRAI)* (pp. 27-31). IEEE. Singapore. DOI: 10.1109/ICRAI.2016.7791223

Badamasi, Y. A. (2014). The working principle of an Arduino. In *2014 11th international conference on electronics, computer and computation (ICECCO)* (pp. 1-4). IEEE. Kaskelen, Kazakhstan. DOI: 10.1109/ICECCO.2014.6997578

Boczkaj, G., & Fernandes, A. (2017). Wastewater treatment by means of advanced oxidation processes at basic pH conditions: a review. *Chemical Engineering Journal*, *320*, 608-633. DOI: doi.org/10.1016/j.cej.2017.03.084

Deng, Y., & Zhao, R. (2015). Advanced oxidation processes (AOPs) in wastewater treatment. *Current Pollution Reports*, *1*(3), 167-176. DOI: 10.1007/s40726-015-0015-z

El Shahawy, A., Mohamadien, R. H., El-Fawal, E. M., Moustafa, Y. M., & Dawood, M. M. K. (2021). Hybrid Photo-Fenton oxidation and biosorption for petroleum wastewater treatment and optimization using Box–Behnken Design. *Environmental Technology & Innovation*, *24*, 101834. DOI: 10.1016/j.eti.2021.101834

Garrido-Cardenas, J. A., Esteban-García, B., Agüera, A., Sánchez-Pérez, J. A., & Manzano-Agugliaro, F. (2020). Wastewater treatment by advanced oxidation process and their worldwide research trends. *International Journal of Environmental Research and Public Health*, *17*(1), 170. DOI: 10.3390/ijerph17010170

Goon, L. H., Isa, A. N. I. M., Choong, C. H., & Othman, W. A. F. W. (2019). Development of Simple Automatic Floor Polisher Robot using Arduino. *International Journal of Engineering Creativity & Innovation*, *1*(1), 17-23.

Gunge, V. S., & Yalagi, P. S. (2016). Smart home automation: a literature review. *International Journal of Computer Applications*, *975*(8887-8891).

Kumar, V., Singh, K., & Shah, M. P. (2021). Advanced oxidation processes for complex wastewater treatment. In *Advanced Oxidation Processes for Effluent Treatment Plants* (pp. 1-31). Elsevier. DOI: 10.1016/B978-0-12-821011-6.00001-3

Liu, X., Zhou, Y., Zhang, J., Luo, L., Yang, Y., Huang, H., Peng, H., Tang, L., & Mu, Y. (2018). Insight into electro-Fenton and photo-Fenton for the degradation of antibiotics: mechanism study and research gaps. *Chemical Engineering Journal*, *347*, 379-397. DOI: 10.1016/j.cej.2018.04.142

Ma, D., Yi, H., Lai, C., Liu, X., Huo, X., An, Z., Li, L., Fu, Y., Li, B., Zhang, M., Qin, L., Liu, S., & Yang, L. (2021). Critical review of advanced oxidation processes in organic wastewater treatment. *Chemosphere*, *275*, 130104. DOI: 10.1016/j.chemosphere.2021.130104

Miklos, D. B., Remy, C., Jekel, M., Linden, K. G., Drewes, J. E., & Hübner, U. (2018). Evaluation of advanced oxidation processes for water and wastewater treatment–A critical review. *Water research*, *139*, 118-131. DOI: 10.1016/j.watres.2018.03.042

Minella, M., Sappa, E., Hanna, K., Barsotti, F., Maurino, V., Minero, C., & Vione, D. (2016). Considerable Fenton and photo-Fenton reactivity of passivated zero-valent iron. *Rsc Advances*, *6*(89), 86752-86761. DOI: 10.1039/C6RA17515E

Mohadesi, M., & Shokri, A. J. I. J. O. E. S. (2019). Treatment of oil refinery wastewater by photo-Fenton process using Box–Behnken design method: kinetic study and energy consumption. *International Journal of Environmental Science and Technology*, *16*(11), 7349-7356. DOI: 10.1007/s13762-018-2153-5

Palma, D., Bianco Prevot, A., Brigante, M., Fabbri, D., Magnacca, G., Richard, C., Mailhot, G., & Nisticò, R. (2018). New insights on the photodegradation of caffeine in the presence of bio-based substances-magnetic iron oxide hybrid nanomaterials. *Materials*, *11*(7), 1084. DOI: 10.3390/ma11071084

Palma, D., Papagiannaki, D., Lai, M., Binetti, R., Sleiman, M., Minella, M., & Richard, C. (2021). PFAS degradation in ultrapure and groundwater using non-thermal plasma. *Molecules*, *26*(4), 924. DOI: 10.3390/molecules26040924

Tayeb, A. M., Tony, M. A., & Mansour, S. A. (2018). Application of Box–Behnken factorial design for parameters optimization of basic dye removal using nano-hematite photo-Fenton tool. *Applied Water Science*, *8*(5), 1-9. DOI: 10.1007/s13201-018-0783-x

Wang, J., & Wang, S. (2021). Toxicity changes of wastewater during various advanced oxidation processes treatment: An overview. *Journal of Cleaner Production*, *315*, 128202. DOI: 10.1016/j.jclepro.2021.128202

Wu, H., Dyson, M., & Nazarpour, K. (2021). Arduino-based myoelectric control: towards longitudinal study of prosthesis use. *Sensors*, *21*(3), 763. DOI: 10.3390/s21030763

Annexes

Color	Corresponding
Red	Light module
Yellow	Flow Cell module
Green	Color sensor module
Orange	White LED
Blue	Flow Cell
Purple	Color Sensor
White	Optic path
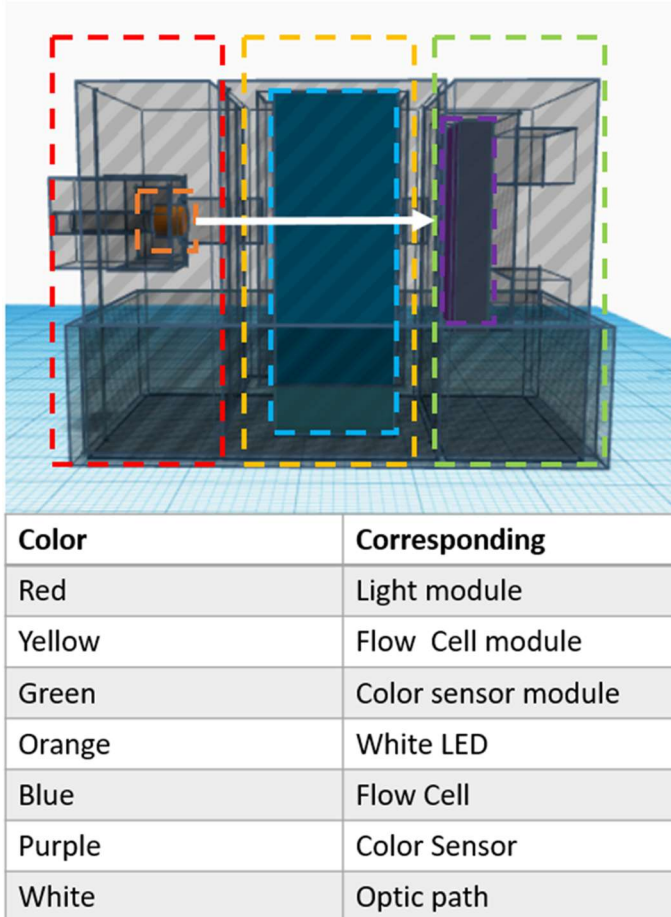
Figure 14.A.1: Scheme of the colour measurement module
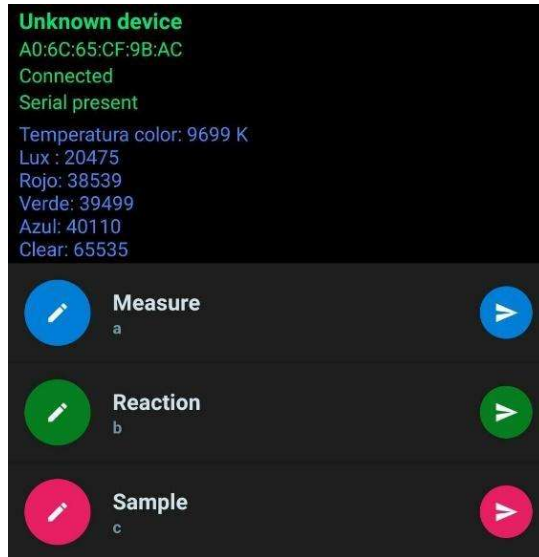
Figure 14.A.2: Screenshot of the app obtaining the colour measure data.

Figure 14.A.3: Contour graph obtained for caffeine degradation obtained with [peroxide]vs[Fe] for a fixed content of caffeine (20 mg/L) at 30 minutes.
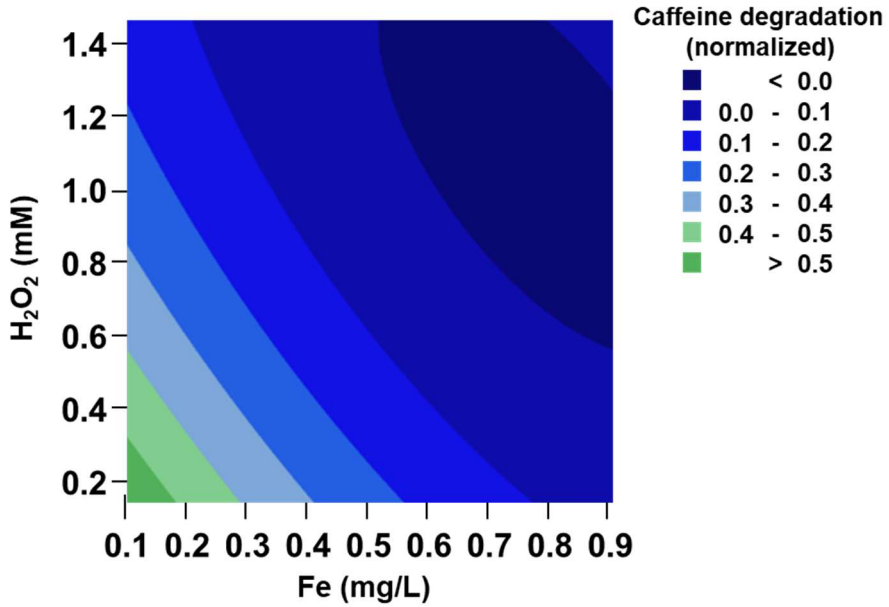
Figure 14.A.4: Contour graph obtained for caffeine degradation obtained with [peroxide]vs[Fe] for a fixed content of caffeine (20 mg/L) at 60 minutes.
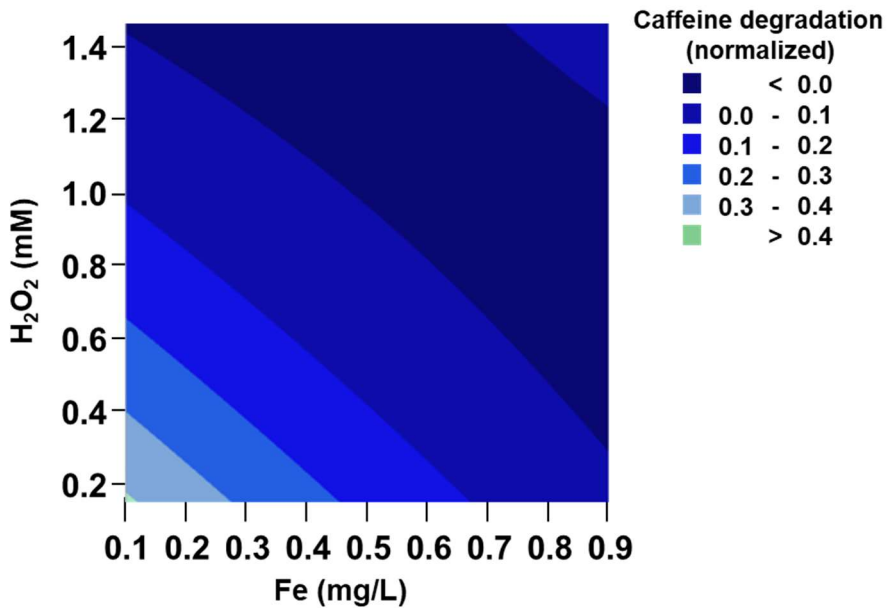
Figure 14.A.5: Contour graph obtained for caffeine degradation obtained with [peroxide]vs[Fe] for a fixed content of caffeine (20 mg/L) at 90 minutes.

Figure 14.A.6: Contour graph obtained for peroxide consumption obtained with [peroxide]vs[Fe] for a fixed content of caffeine (20 mg/L) at 30 minutes.

Figure 14.A.7: Contour graph obtained for peroxide consumption obtained with [peroxide]vs[Fe] for a fixed content of caffeine (20 mg/L) at 60 minutes.
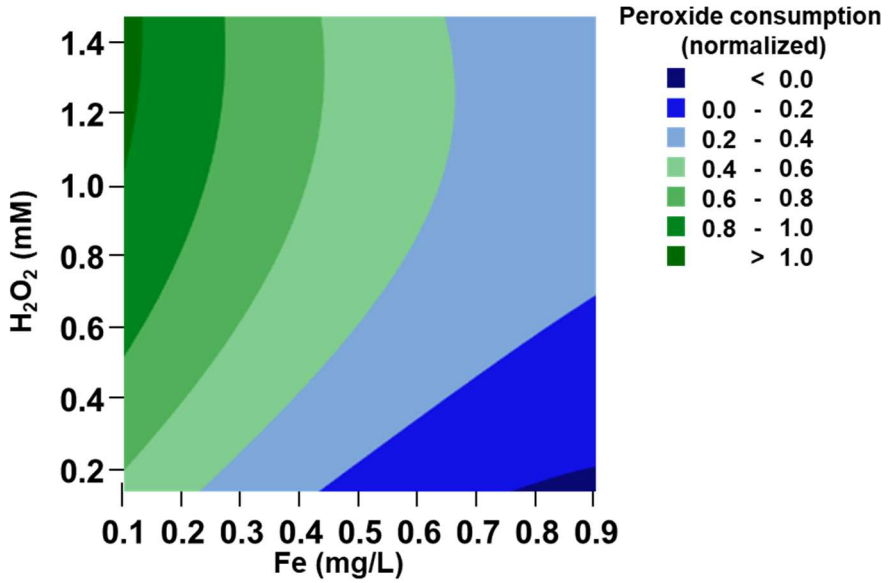
Figure 14.A.8: Contour graph obtained for peroxide consumption obtained with [peroxide]vs[Fe] for a fixed content of caffeine (20 mg/L) at 60 minutes.
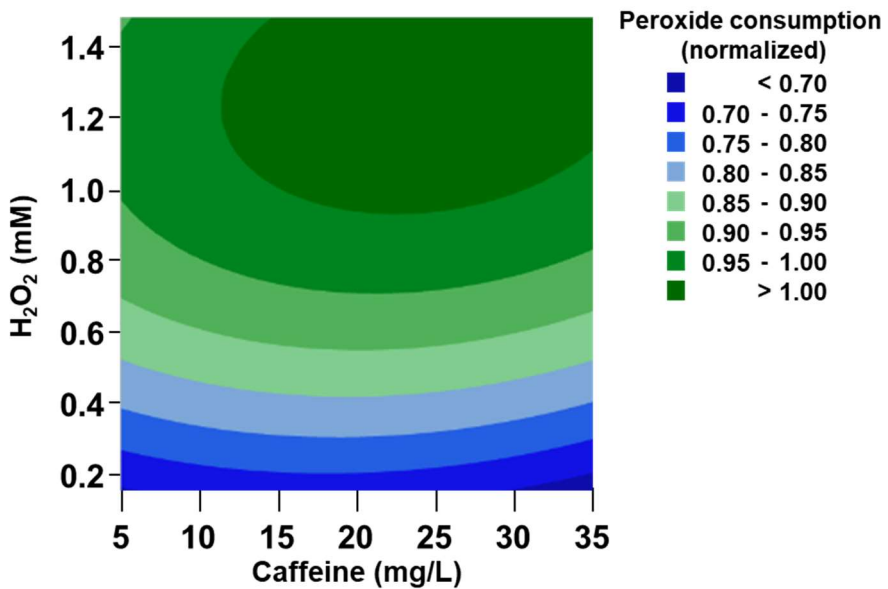
Figure 14.A.9: Contour graph obtained for peroxide consumption obtained with [caffeine]vs[Fe] for a fixed content of iron (0.5 mg/L) at 30 minutes.
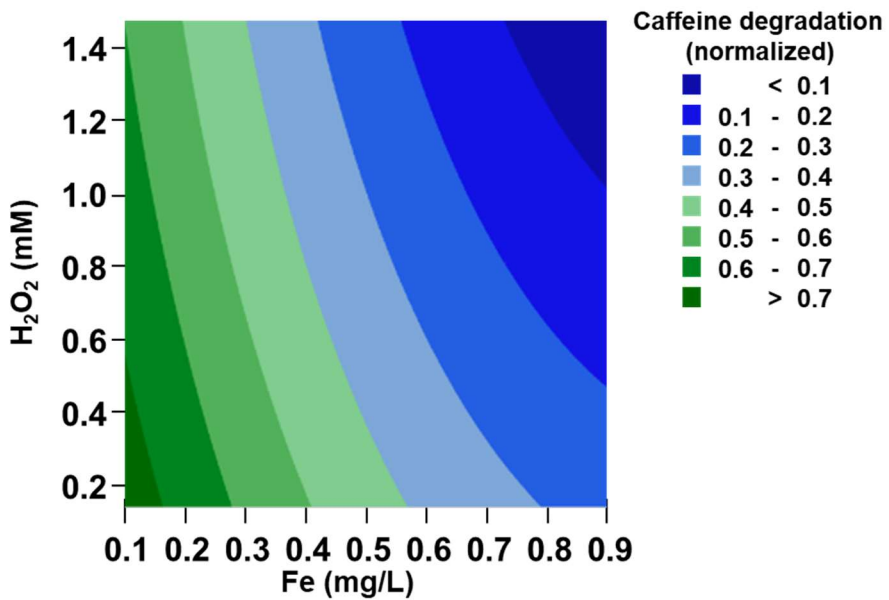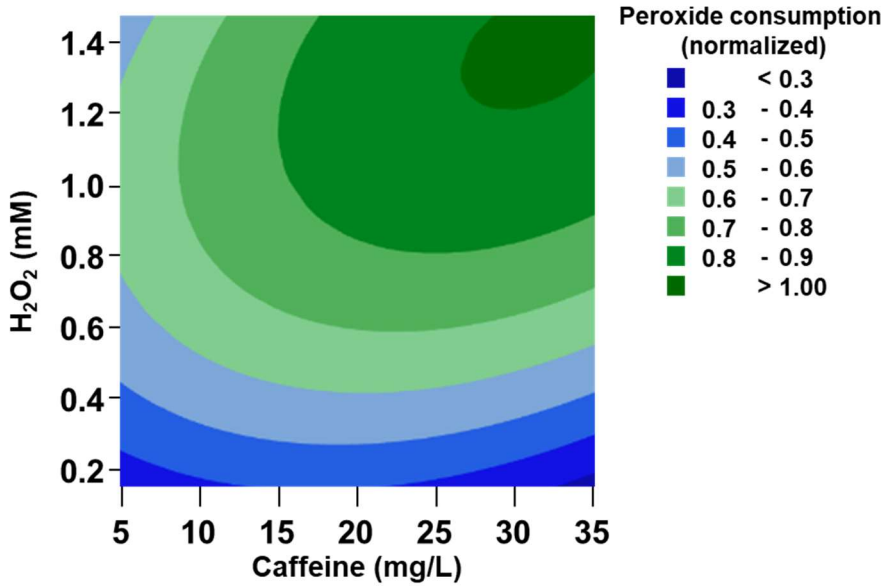
Figure 14.A.10: Contour graph obtained for peroxide consumption obtained with [caffeine]vs[Fe] for a fixed content of iron (0.5 mg/L) at 60 minutes.
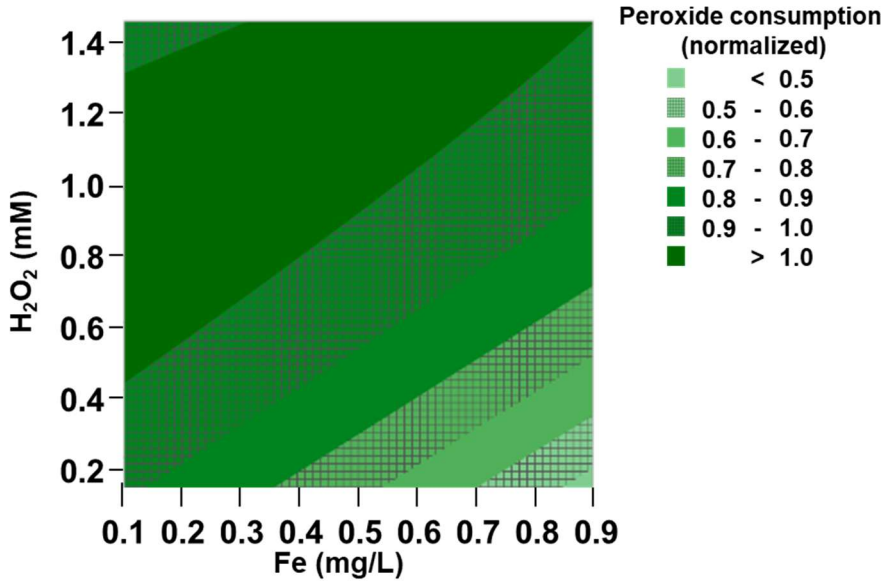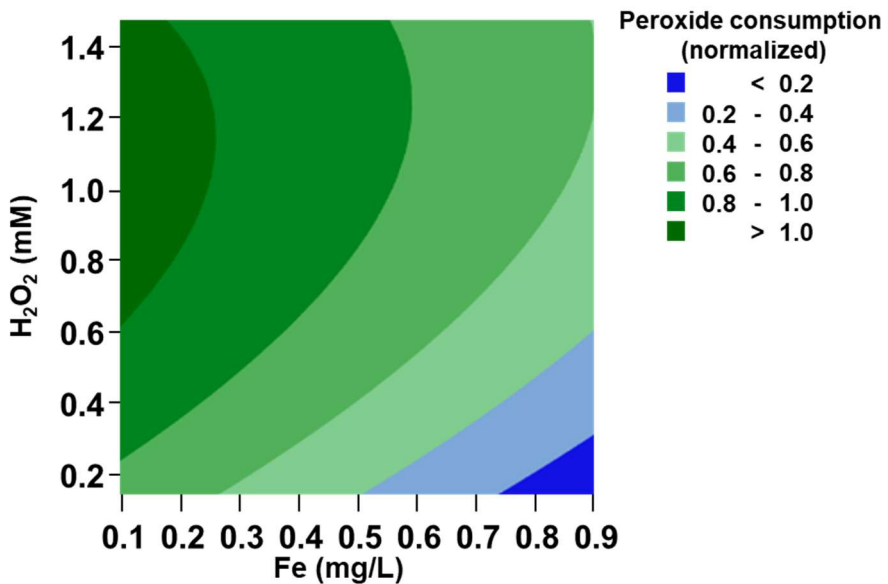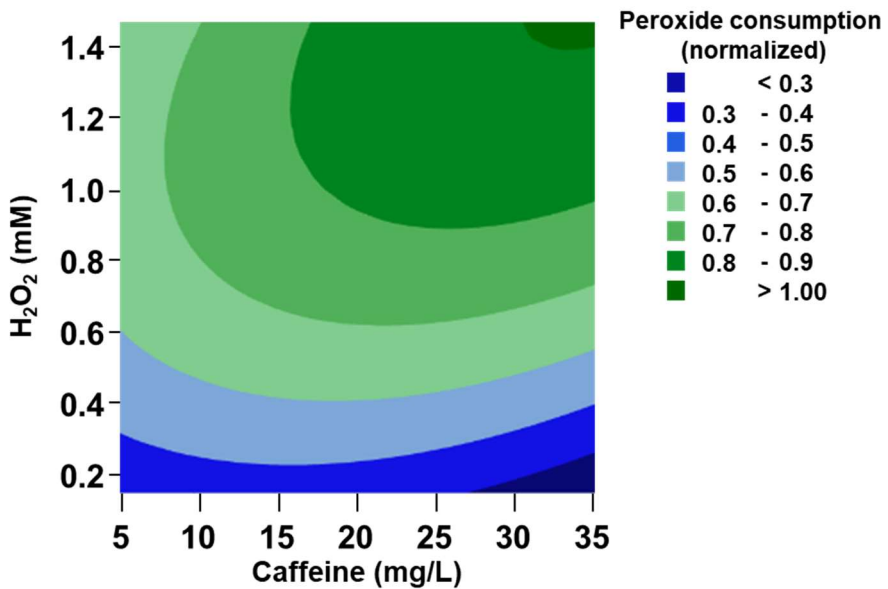

Figure 14.A.11: Contour graph obtained for peroxide consumption obtained with [caffeine]vs[Fe] for a fixed content of iron (0.5 mg/L) at 90 minutes.
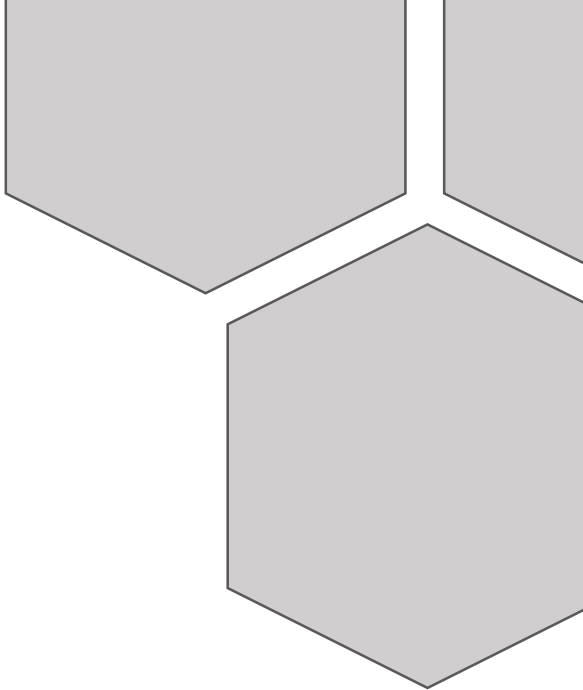
SECTION 3

LEARNING RESEARCH: GAME-BASED LEARNING
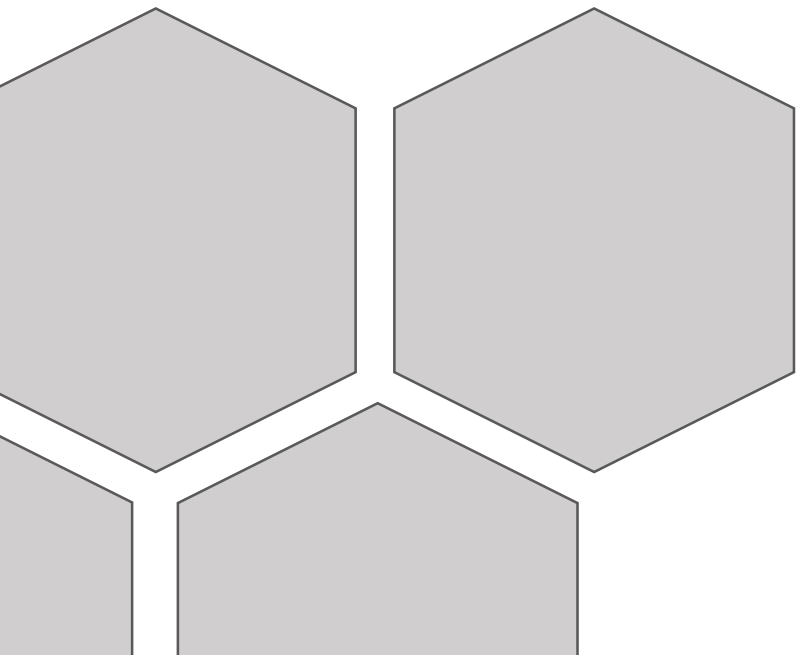
CHAPTER 15: Game-based learning: a chemistry videogame as reinforcement for higher education
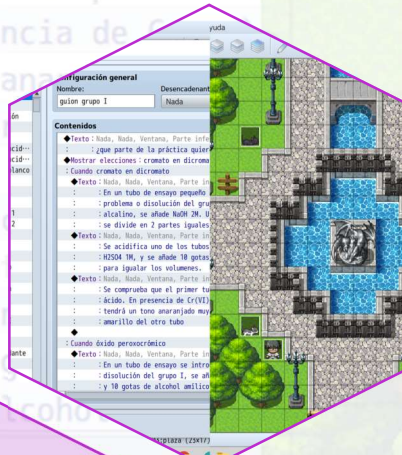
ABSTRACT

In this chapter, the RPG maker® MZ program which allows creating 8-bit aesthetic video games with a simplified program code has been used to develop a game-based learning (GBL). The developed game, available for free, on the website laboratoriorpgdocente.webnode.es, includes laboratory practices of analytical chemistry from the second year of the chemistry degree from the University of Valencia, numerical exercises of chemistry from high school and college, videos and a laboratory waste management minigame. The laboratory practices developed in the game are the identification of 17 cations in an unknown sample and an amoxicillin acid-base titration. In addition, player satisfaction surveys have been collected for each part of the game. The results of the surveys show that the students receive the use of these tools in a good way. According to the surveys, the players indicate that is easy to use, and it is like the reality. The students indicate that the game is original, amusing and is useful as learning tool, and state that they would repeat this experience.

Keywords: Game-Based Learning, RPG Maker, Chemistry, Gamification, Laboratory.

1.   Introduction

In recent years, new learning active methodologies, that allow students to be more active in their education, have been employed achieving those students turns from passive subjects to be an active and engaged part with their learning (Armellini & Rodriguez, 2021, Hartt et al., 2020).

Gamification is one of these active learning techniques and can be defined as a strategy that implies the incorporation of dynamics or elements from a game in other environments different from itself (Kapp, 2012, Pegalajar, 2021). This can help to get the students involved and promote a positive evolution in the apprenticeship results (Ofosu-Ampong et al., 2020). The main objective in any current learning system is that the students were find motivated (Bridgeland et al., 2006). Gamification studies have reported that the employment of game elements achieve an improvement in the intrinsic (due to the own student) and extrinsic (due to the external factors) motivation, in engagement and in achievements of the apprenticeship of the students (Zainuddin et al., 2020).

One of the variants of the gamification is game-based learning (GBL), in which video games are considered as learning tools (Hartt et al., 2020, Subhash & Cudney, 2018). Nowadays, rapidly growing technologies and cultural changes have meant that educational institutions cannot easily adapt to the realities of the today's students (Pérez, 2016). Research shows us that the employment of digital tools, with a lower focus on the traditional learning, has promoted the student's stimulation (Shi & Shih, 2015), and the "2014 NMC Horizon" report has shown that the use of video games and gamifications is a trend in the higher education (Pho & Dinscore, 2015). Games allow to integrate the intrinsic and extrinsic motivational components to create an environment where students are encouraged to participate in the target activities (Hartt et al., 2020). Educators agree that the games can improve the capability of the students to get new perspectives through the active participation in making decisions and problem resolutions (Tu et al., 2015). On the other hand, GBL allows to create adaptive and secure environment for learning (Shi & Shih, 2015), and help students to develop additional skills such as strategy thought, resources managing, planning and implementation skills (Greipl et al., 2020).

To create a GBL it is necessary to follow some steps. The first step is analysing the target public, since a very simple activity could generate disinterest and a very complex procedure could induce frustration. The next step is stablishing objectives, and in this case, the gamification and GBL techniques intend to achieve a

motivation increase in the student learning (Kiryakova et al., 2014). To achieve this, in 2003 Pivec et al. have proposed the use of techniques such as interactivity, visual dynamics, the foundation of the challenge, fantasy, curiosity, and the control (Pivec et al., 2003). Even though a realistic environment is preferred when creating a GBL, involving fantasy worlds could increase student's interest, since pedagogical benefits are not limited to real environments simulation (Hartt et al., 2020). On the other hand, it is necessary to use surprise elements, promote the investigation, movement liberty and ability to choose to hold the interest of the student.

Next step involves structuring the content. A GBL must be created to advance in the game step by step, with an increasing in the difficult of the game. In this way, the progress, and the self-confidence in the student increase (Mayo, 2009). By last, releasing the game and getting feedback allow to collect data and opinions to correct errors, improving the mechanism and the experience of play the GBL (Huang & Soman, 2013).

The application of active learning methodologies opens new possibilities and opportunities if properly done. GBL can partially substitute the lack of some experimental techniques, that due to their cost, complexity, or dangerousness, are not available (Bonde et al., 2014). In addition, GBL have the advantage of reducing students test anxiety (Stănescu et al., 2020).

The link between the cognitive, emotional, and behavioural results derived from gamification is complex, since gamification helps to retain knowledge and improve student self-efficiency (Rabah et al., 2018), but it is important to highlight that although the application of the GBL methodology induces an improvement in the student himself/herself, this improvement depends on its correct use and approach (Mayo, 2009). In addition, it is possible to find a higher efficiency when the traditional learning and the use of gamification and GBL are combined in a cohesive and consistent way (Bonde et al., 2014)

This is an emerging trend that applies game mechanicals to motivate, bring closer and improve the student experience, and is a fast growth phenomenon that shows that has been proven to provide attraction and satisfying solutions for educational and learning contexts (Zainuddin et al., 2020).

The objective of this chapter is to integrate a chemistry campus inside one GBL, that could be useful as supplementary tool for traditional learning. The following parts are included in the development of this GBL: I) development of a chemistry practices simulator; II) development of a theoretical reinforce to solve numerical

exercises; III) videos access of detailed explanation of how to solve more complex numerical exercises; IV) development of supplementary mini games to improve the student's skills in different jobs.

2.   Methodology

The RPG maker® MZ program, used for the development of the GBL, requires a single license for use, and it is a pay-wall protected program. It is focused on the creation of 8-bits aesthetics games, which provide a retro and eye- catching look. The program uses Ruby programming code. Since this software is thought for amateur users, a simplified codification is employed with predefined actions, that do not require write the raw code to carry out the process. In this way, the user can develop a code in which the actions that wants them to be carried out are programmed sequentially.

The first step is the development of the programming of the game to become a teaching tool, considering the different aspects of the game. On the one hand, the aesthetic of the environments has been created simulating the real sciences campus of the University of Valencia. On the other hand, the functionalities of the game to achieve a recreation of the different practices and numerical exercises have been programmed.

To create the GBL it is necessary to focus on two sections. The first one is the creation of the environments. To carry out this, the tileset system is used, that employ images based in pixelart. The map of the game is a grid where in each square it is possible to include a tile. Tiles can be programmed to be the floor where the player can walk, and it is possible to set the available directions. Tiles can be walls or roof too, to create buildings. While the first layer of this system is the floor, wall, or roof, the second and third layers are used to put decorative elements as plants, furniture, signs, statues… (Figure 15.1).

The second section is the programming of common events. These elements are codes that can produce certain situations that induce changes in the game. The common events can be used to perform the laboratory practices and, when some conditions are achieving, can be activated to advance in the game (Figure 15.2).

Once the video game has been released, satisfaction surveys have been created to collect users' opinions to improve the video game in new versions and to know the reception of the game by the users.
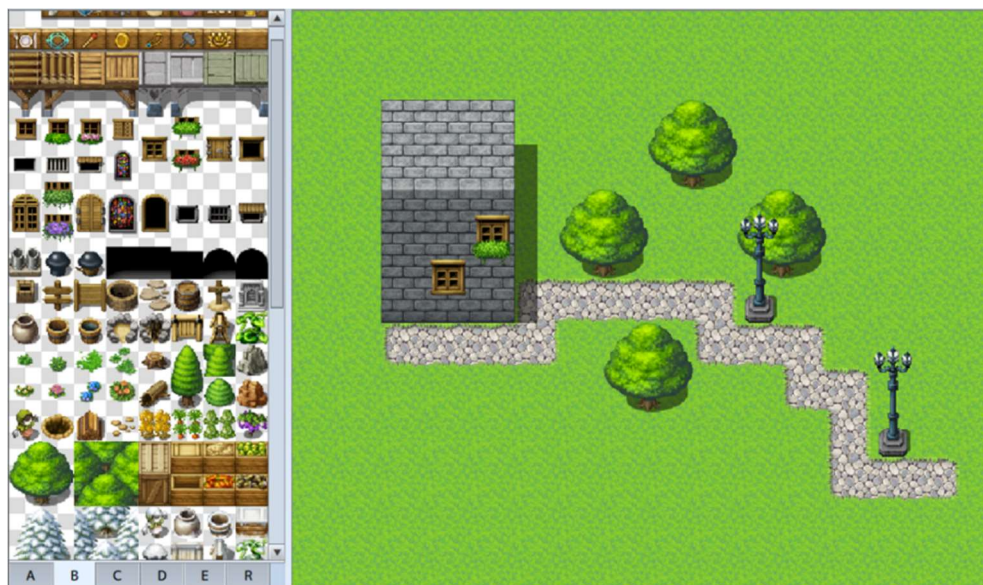
Figure 15.1: Tileset system of RPG maker® MZ program for environment design.
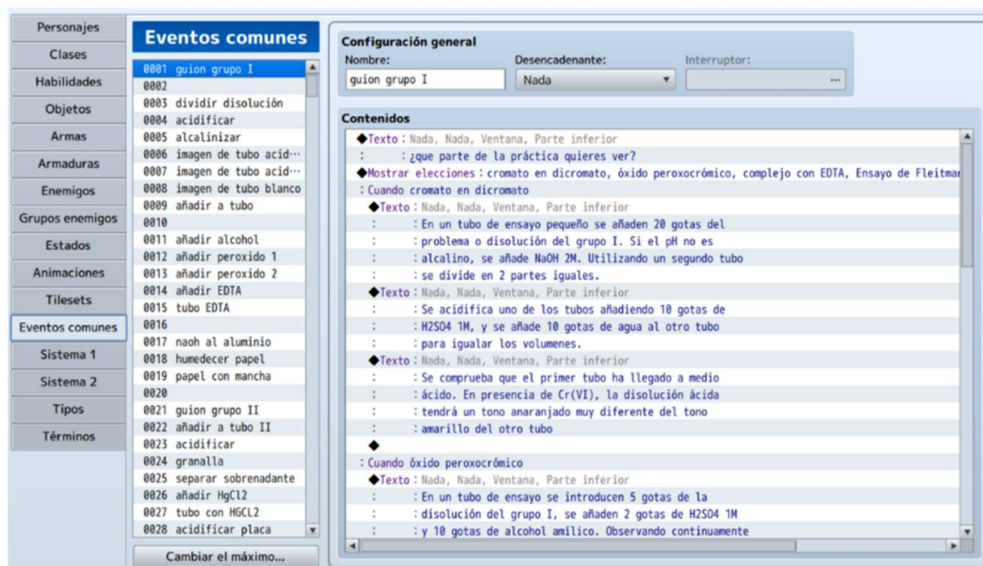
Figure 15.2: Common events window of RPG maker® MZ program.

2.1.   Chemistry laboratory

The GBL has been designed according to the practices that are carried out in the analytical chemical laboratory subject of the second year of the chemical degree at the University of Valencia. In this case two practices have been developed: the

qualitative separation of 17 cations and an acid-base titration for the determination of amoxicillin.

To create the aesthetic of this section, the analytical chemistry practices laboratory has been recreated in the game (Figure 15.3). In this place, student can work in a bench where can carry out the experimental procedures. There are benches with laboratory material and fume hoods for acids and bases, and in addition, there is a room with precision scales.

Figure 15.3: Design of the analytical chemistry practices laboratory.

To play in the chemistry laboratory, the student must talk with the teacher in the room next to the laboratory, located in the lower right corner of Figure 15.3. The teacher asks the student what is the practice that wants to carry out.

The separation of the 17 cations is divided into 6 sequential groups according to their chemical properties (Laboratory guide, Analytical chemistry department). Students must finish one group before being able to do the next one, so this practice is programmed sequentially. Firstly, must select the cation group that they

are going to study in the assay and later, in the laboratory, they have to collect the reagents and do the experiment in their bench workplace.

When the student carries out the experiment and gets the results of all the essays, he/she must talk with the laboratory instructor to finish the group and to be able to access to the next one, and finally when all six groups has been finished, an unknown sample analysis can be done.

To access to this game mode the student must have met three conditions: I) having finished all six groups in the essay mode; II) receiving the password to be able to play this mode (from the subject teacher); III) receiving a code of the sample that he/she must analyse (from the subject teacher). When the student has finished the analysis of the unknown sample, he/she has to handle the result to the teacher, that knows the correct answer, to be evaluated. The student, when carrying out the procedures, obtains an object in the inventory where he/she can see the result as a real image of the laboratory, as can be seen in the Figure 15.4.
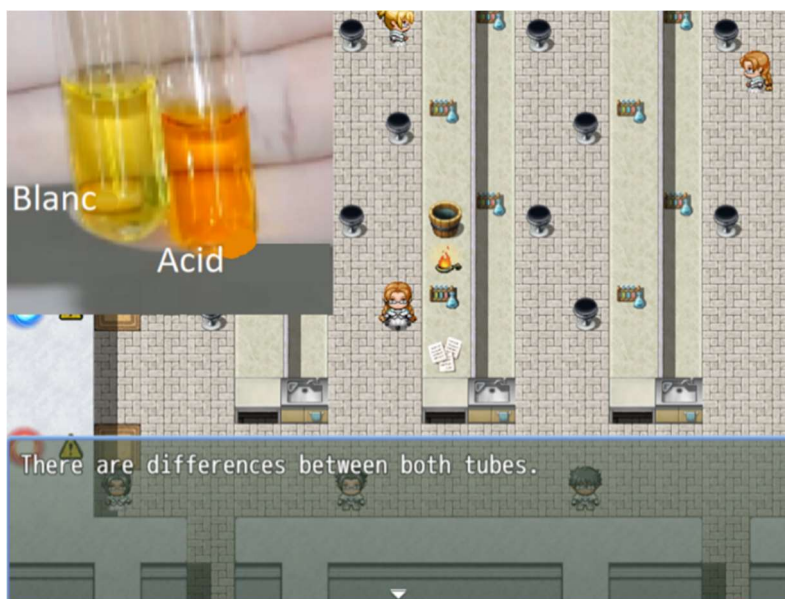
Figure 15.4: Image of the game where the student can see the result of one of the experiments.

When the students select the acid-base titration practice, they are going to carry out the amoxicillin determination and involves the use of a calculator to make the calculations to obtain the result. In this case they must follow the real procedure. First, students should weigh the sample and adequate reagents in the balance room and record the weights for later calculations. The game provides the weight of the

sample and the weight of the standard by triplicate. To carry out the titration, the students must select the reagents in order, and they must evaluate if the colour of the solution that is being titrated indicates the final of the procedure. They must also make a reagent blank. On the other hand, the game provides the spent volume in the titration of the blank, the normalization of the perchloric acid and the titration of the sample. With this data, students can make the calculation of the concentration of amoxicillin in the sample. When the user has finished, he/she must talk with the teacher in the game and provide the result. If the result is correct, the practice has finished, if not, the student must recalculate the result.

When the student finishes the practices, he/she receives two medals, one for each finished practice.

In both practices, the necessary documents appear on the workbench that show the student information about the reactions carried out or characteristics about the procedures within the game. Moreover, instructions for performing the experiments appear in their inventory.

2.2. Chemistry laboratory

Other section that has been developed in the game is the creation of reinforcement tools to solve numerical exercises. In this case, the game provides to the students an exercise and asks them to answer simple questions to achieve the result. The students must find the solution step by step. In this way, this tool has been programmed in the game in an educational way, created as a guide for the student to be able to solve the exercise by himself/herself and allow them to solve similar exercises.

Since it is recommended that unreal elements are used in the GBL to increase the student's involvement (Pivec et al., 2003), a theatre to simulate fantasy elements has been created. To enter in this section of the game, the student must go to the theatre room, located at the first floor of the Chemistry Faculty. Here, the student must select the difficulty level, for high school or university students. Once the level of difficulty is selected, students enter a dungeon, which has been designed as if it were a theatre set (Figure 15.5). Here the student enters in the battle mode and must battle against "monsters". While in other games, the user must battle with monster to defeat it, in our case, the battle mode provides a numerical exercise and to defeat the monster the student has to find the solution. Each monster proposes a different type of exercise. When students finish the dungeon, they can enter again but with the possibility to select the exercise that wants to solve.
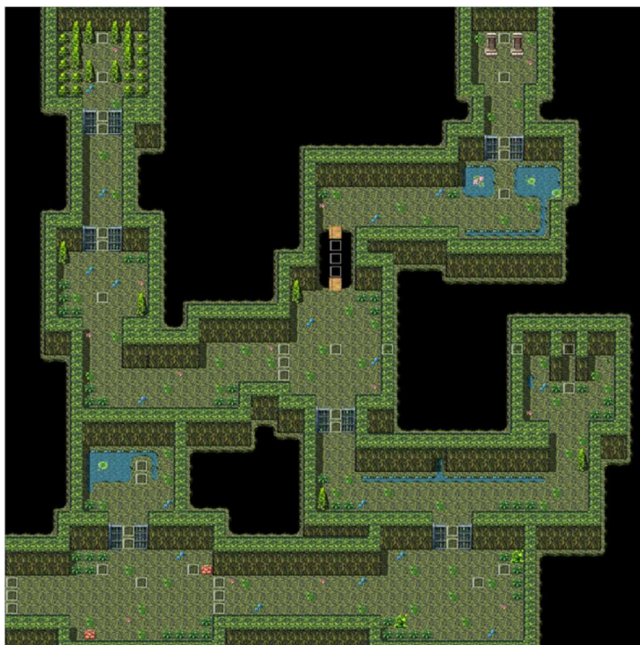
Figure 15.5: Design of the dungeon for numerical exercises resolution.

The intention with this idea is that the students, that have the basic knowledge about the subject, would be able to solve any exercise similar to the game. This mechanic allows to give tips or suggestions to the student to help him to understand how to solve that type of exercises. Each dungeon has an increase in the level of difficulty of the exercises, according to the teaching guide for that educational level. The exercises programmed for each level are in the Table 15.1.

Table 15.1: Types of exercises and difficulty levels of each dungeon.

Exercise type	High school level	College level
Determination of acidity constants	X	
Dissociation constants of weak acids and bases	X	
Mixtures of strong acids or bases with weak acids or bases	X	
Exercises of dissociation	X	X
Mass and charge balances		X
Protonation constants		X
Precipitation exercises	X	X
Redox adjustment	X	X
Acid-Base titrations		X
Redox titration		X
Exercises with two protonation constants		X

2.2.1.   High school level

2.2.1.1. Acidity constant determination

In this exercise, the statement of the exercise gives to the student the concentration of an acetic acid solution and asks for the pH. First, the student needs to adjust the reaction, then they must answer some questions about the calculations, and finally, the student must provide the pH value.

2.2.1.2. Dissociation constant for weak acids and bases

The exercise provides the protonation constant and ask the concentration of the different species of sulfuric acid in the solution. First it is necessary that the student provide the number of reactions that have place. Later, it is necessary to know the difference between a total or a partial dissociation. The last question is which concentrations are provided with the statement information, and finally, the player calculates the sulphate species concentrations.

2.2.1.3. Weak acid or base with strong base or acid mixtures

The exercise explains the Le Châtelier principle. The student must provide the pH value of the solution obtained by mixing ammonia with sodium hydroxide in a known volume of water. The volume and concentration of both compounds is provided. To start, the student must answer which is the basic force of the species. Later, the student must indicate if the reactions showed are correct. To finish, the equations necessary to find the solutions are provided, and the student must indicate the number of hydroxyl mols, the concentration and the pH of the mixture.

2.2.1.4. Dissociation exercises

To defeat the monster in this dungeon level, the student has to indicate the dissociation grade and the pKa value of a valeric acid solution. The exercise indicates that the pH of the solution is the same that a nitric acid solution with a known concentration. Firstly, to ensure that the student understands the statement, the exercise ask student to give the pH value. Later, the student has to provide the dissociation grade using the equation showed in the screen. By last, the player introduces the pKa value of the acid.

2.2.1.5. Acidity constant determination

To complete this exercise, the student must answer in two stages. In the first, the student must calculate the calcium fluoride solubility using the solubility constant. The game provides a scheme about how to calculate the solubility, the player will adjust the reaction and then will introduce the solubility value. The second part requires calculate the amount of sodium fluoride that it is necessary to add to a calcium chloride solution with a known amount of calcium to induce the

precipitation. To do this the user has to introduce the concentration of calcium in the solution and the concentration of fluoride ions using the equations provided by the game. To finish the battle, he/she has to provide the sodium fluoride milligrams that it is necessary to add to the solution.

2.2.1.6. Redox reaction in acid medium

The last exercise of this dungeon ask that the student has to adjust a redox reaction. Firstly, the student must indicate the oxidation state of each atom. Later oxidation and reduction theory is explained to help student to adjust the semi reactions following the next 3 steps: I) adjust the element that vary its oxidation state; II) adjust oxygen atoms with water molecules; III) adjust the electron change. By last, the student has to write the correct adjusted reaction.

2.2.1. College level

In this dungeon, there are exercises from the first and second year of chemistry degree, and the exercises that are programmed in this dungeon has been shown in the Table 15.1.

2.2.2.1. A protonation constant

In this exercise, the statement gives to the student the general scheme to solve any exercise of this type. In this case, it is necessary to calculate the concentration of acetic acid and acetate in the solution. Firstly, the student must provide the pH value of the solution and later must calculate the concentration of both species.

2.2.2.2. Two protonation constants

To defeat the monster in this case, the student has to calculate the concentration of the species in an oxalic acid solution using its protonation constants. In first place, the game provides a resolution scheme to be follow by the student to solve this type of exercises. The game asks to student to calculate the protons concentration and later the oxalic acid concentration and its derivative species.

2.2.2.3. Acid-base titration

Titration of hydrochloric acid with sodium hydroxide is proposed in this case. The exercise helps to student to obtain the titration curve and to calculate the pH when different volumes of standard is added. To start, it is necessary to write the reaction, later the student must calculate the equivalence point using the equations provided. Each time that the asked pH is calculated the curve titration is drawn in the screen.

2.2.2.4. Redox titration

In this exercise it is necessary to determine the amount of hydrogen peroxide that there are in a solution. To do this a titration with potassium permanganate will be carried out. The first step is drawing a scheme to understand the problem. Later the reactions are adjust using the procedure that they have reinforce using the exercise of the redox adjust. The next step is that the student calculates the hydrogen peroxide concentration, and by last, must indicate how many grams of hydrogen peroxide per litre there is in the solution.

2.2.2.5. Mass and charge balance

To complete this exercise, the student has to calculate the pH of an acetic acid and sodium hydroxide mixture solution using the mass and charge balance fundament. Firstly, a scheme is described. Later, the concentration of both species in the mixture is calculated. The game shows the equations that the student must use to make the calculations. To finish, the student has to provide the pH value of the solution.

2.2.2.6. Complex formation exercise

The last exercise of this dungeon is divided in different steps. The first step is preparing a EDTA solution, that is normalized with a calcium standard. The EDTA normalized solution is used for three procedures: I) determination of calcium percentage in a limestone sample; II) determination of heptahydrate magnesium sulphate in a sample; III) determination of the partial and total hardness in a water sample.

2.3. Videos

To help student solve numerical exercises, some videos with a more detailed explanation about how to solve more complex exercises have been recorded, and to visualise them, an audio-visual room has been created in the GBL (Figure 15.6). In this case three videos have been created: I) determination of the content of magnesium in a steel; II) water hardness; III) weak base titration with a strong acid. The creation of this videos includes the use of slides to how the information and digital tablet to write notes or show important data that it is necessary that the student bear in mind. Videos have a high weight to be added in the game or include full videos inside the game as multimedia data require to use a lot of memory to save them inside the program game. To solve this problem, the audio-visual room allows student to access the videos from QR codes. In this way, the game provides the videos minimizing the memory resources needed.
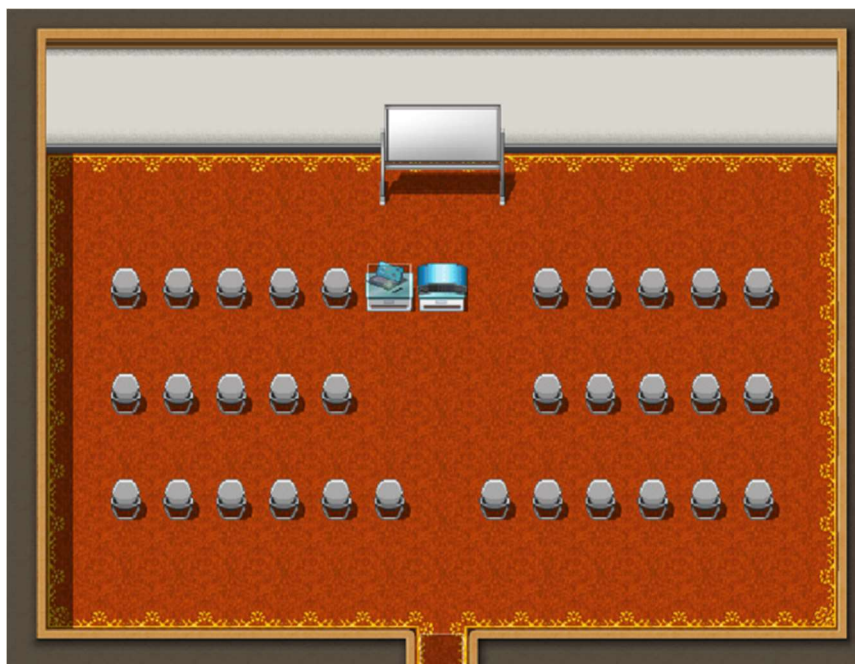
Figure 15.6: Design of the audio-visuals room on the first floor of the chemistry faculty.

2.4. Minigames

The last element created in the game is a minigame to guide the student how to manage the generated laboratory wastes. In the game, the student must go to the north to access to the waste management building that has been recreated inside the GBL (Figure 15.7). In this place students must talk with the technician (non-player character [NPC]) to help they with the wastes classification. In this minigame, the NPC provides one waste that the students have to classify in the corresponding waste group according the normative (Servicio de Prevención y Medio Ambiente, 2022). When the player classifies the first waste, the technician provides a second waste. To finish the minigame, students must manage 5 wastes. One medal has been programmed, and in the case that the student plays 10 times to the minigame (50 wastes) he/she will receive it.

Figure 15.7: Design of the exterior of the wastes management building.

2.5.   Satisfaction surveys

To evaluate the videogame as teaching tool, students answered surveys about the different game modes that the GBL has. Firstly, information about the student is asked to make a demographic study. Later, students have to evaluate different aspects of the game giving a score between 1 and 9 being 9 high score and 1 low score. The score of 5 is in the middle, for that, this value show that the parameter is not high or low, there is not a strong opinion about that. There is not satisfaction surveys from the mini game. This part of the game is not the main and for that information about the satisfaction of the user was not collected. The student can play it if they want. The incentive for that they play this part is to get the medal as the basis of the challenge. The GBL is available for them in the project´s web page for free for everyone that wants to try the game (Figure 15.8).

Figure 15.8: QR code to access to the project´s web page.

3. Results and discussion

3.1. Chemistry laboratory satisfaction surveys

The two practices have been evaluated separately with surveys. The demographic results for both practises are shown in the Figures 15.9 and 15.10. The results are similar, and it is important to focus that the game have been tested by people that play video games and, in their majority, are from sciences fields with knowledge about the exercises that have been programmed in the game.

In the evaluation survey, questions about the game, such as the satisfaction level, how similar is with the practice in the real live, how easy is move through the game and how much time is necessary to complete the practice has been asked. In the case of the time that is necessary invest to complete the practice, the results have a normal distribution, for high scores, the student has to invest too much time, and for low scores, the student has to spend so few amounts of time. So, a score of 5 means that the student employs the adequate time. On the other hand, some questions about how useful the GBL as tool is, are asked. The Figures 15.11 and 15.12 shown the results obtained in the satisfaction surveys for the game, and Table 15.2 summarises the mean values of these results.
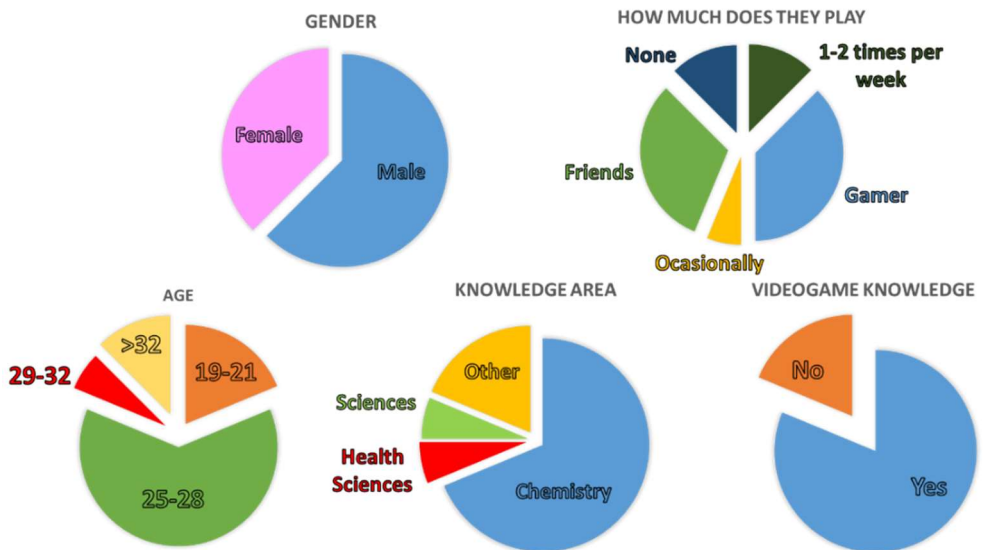

Figure 15.9: Demographic study of the surveys from the separation of the 17 cations practice (n=16).
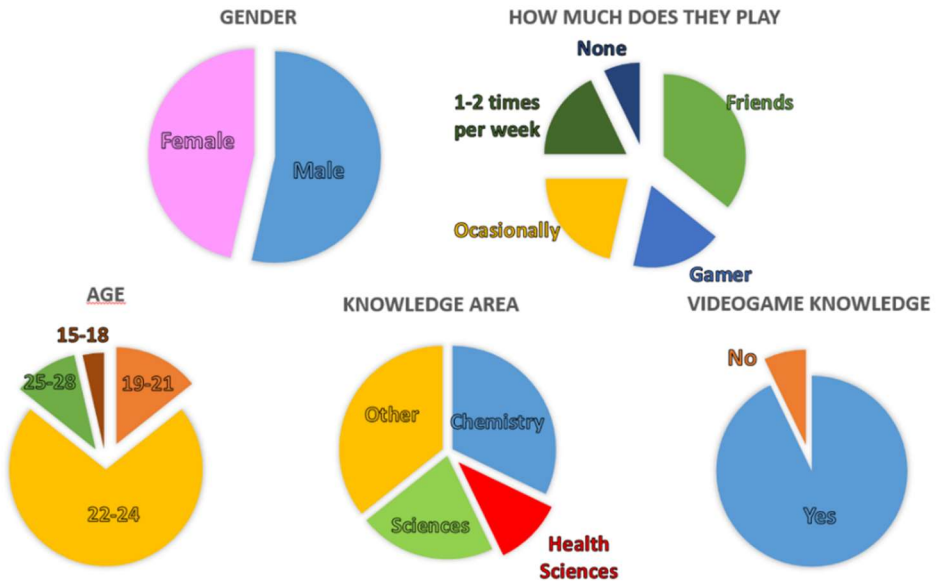
Figure 15.10. Demographic study of the surveys from the acid-base titration practice (n=28).
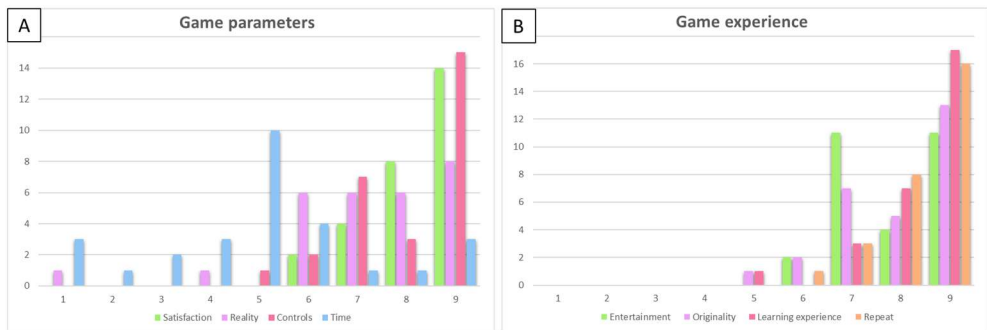
Figure 15.11: Statistical study about the 17 cations separation practice.
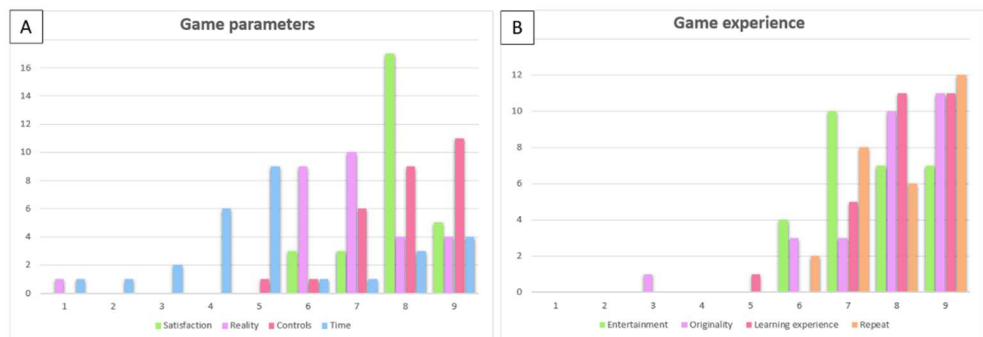
Figure 15.12: Statistical study about the acid-base titration practice.

Table 15.2: Mean value of answers from the satisfaction surveys about the game.

Parameter	Separation practice	Acid-base titration
Satisfaction level	8.2	7.9
Similarity with the reality	7.3	6.9
Controls	8.0	8.0
Time investment	5.0	5.4
Originality	8.0	7.9
Entertainment	7.9	7.6
Learning experience	8.4	8.1
Intention of repeat	8.4	8.0

3.2.   Numerical exercises satisfaction surveys

The demographic results for the satisfaction survey are shown in the Figure 15.13, including the question what dungeons they have played. The results obtained for this section are like the obtained for the acid-base titration practice.

In the satisfaction survey about the game experience, moreover the other parameters, is asked to the students how useful this section of the game as teaching tool is. The results are shown in the Figure 15.14. According to the results about the satisfaction and the reality of the game, the average values are 8.1/9 and 7.1/9, respectively. In this case, most of the results are that the time required is slightly higher than the expected by the student being the average value is 5.7/9. Moreover, the controls of the game were well evaluated with a score of 7.9/9 (Figure 15.14A).

The parameters related with the game experience provide very good results. The students evaluate the entertainment and the originality with 7.4/9 and 8.0/9 scores respectively. The learning experience that provides the game and the utility as teaching tool were evaluated with an 8.1/9 and 8.0/9 score respectively. By last, the intention of the students of repeat this type of experience was scored with 8.3/9 (Figure 15.14B).
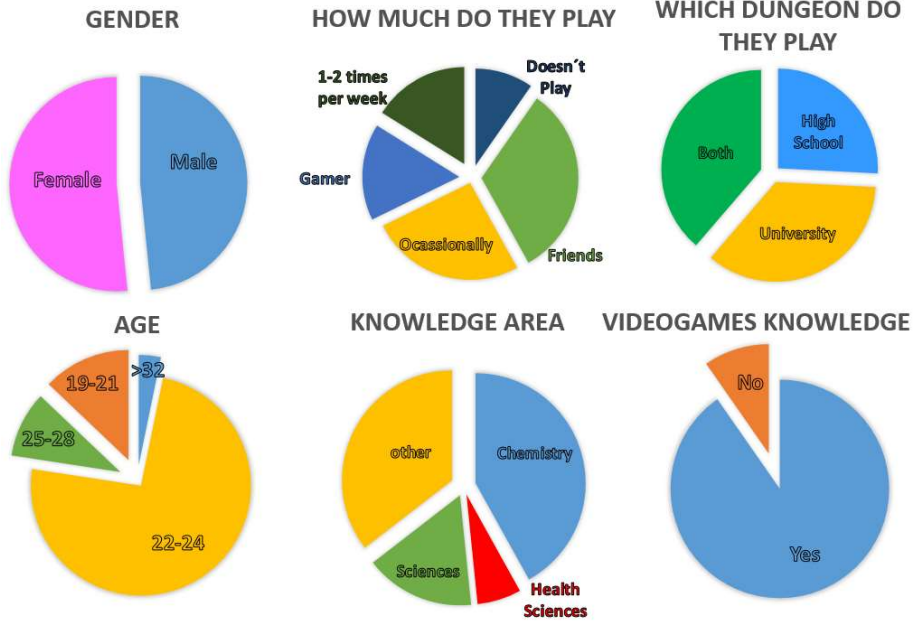
Figure 15.13. Demographic study of the surveys from the numerical exercises dungeons (n=31).
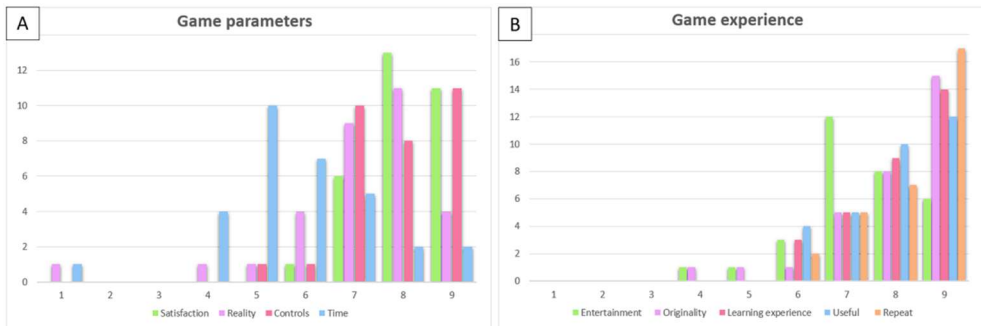
Figure 15.14. Statistical study about the numerical exercises dungeons.

3.3. Numerical exercises satisfaction surveys

Like the other surveys, the demographic studio is showed in the Figure 15.15. In this case the information about the gamer behaviour of the student is not relevant. The results are similar than the previous surveys. The satisfaction survey of this section is focused in know how useful the videos and their implementation in the game are (Figure 15.16). The results provide an average evaluation of 7.9/9 for the satisfaction and the usefulness of include an explanatory video was evaluated with a 7.7/9, the learning experience had a score of 8.3/9 and the intention of repeat an 8.0/9.

414
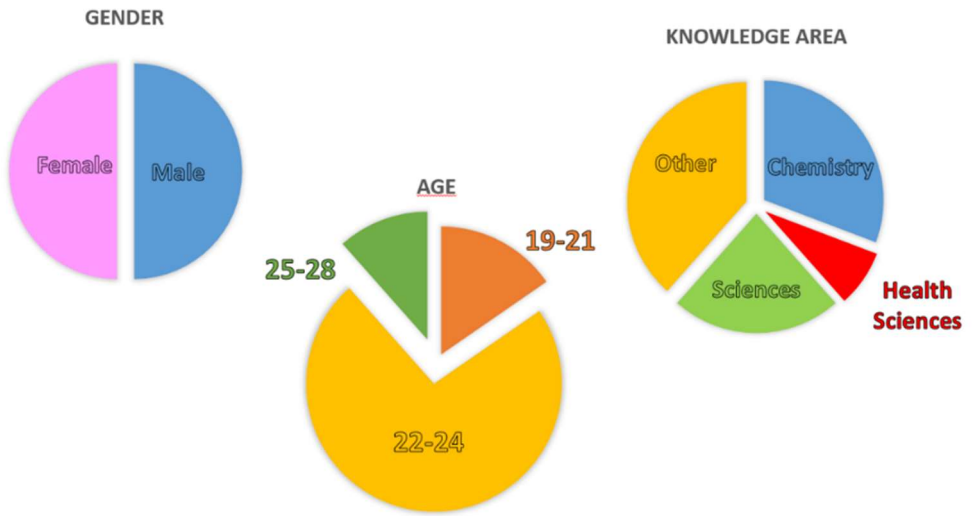
Figure 15.15. Demographic study of the surveys from the videos in the audio-visuals room (n=26).
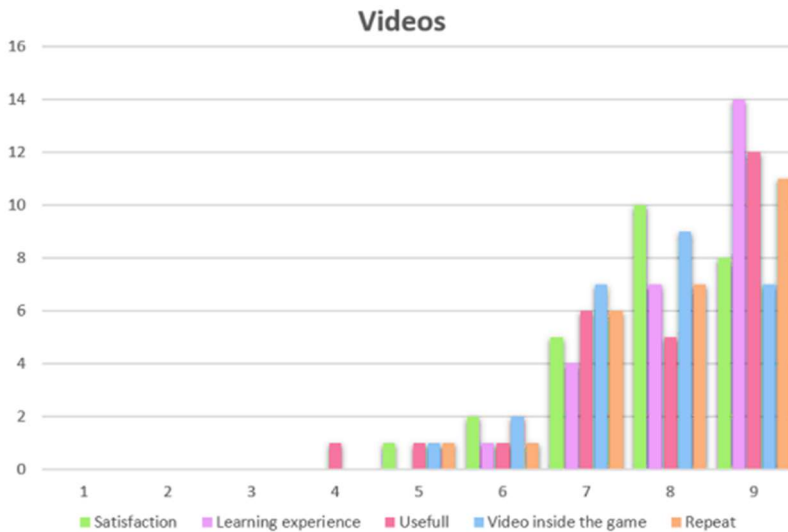
Figure 15.16: Statistical study about the videos available in the game.

4.   Conclusions

In this chapter, a free GBL has been programmed with RPGMAKER MZ and evaluated by students. The GBL include practical and theoretical contents. Moreover, include a minigame to incentive to students to learn in a fun way. The practices included in the game allow to student to reinforce the content that is approached in the laboratory when this has finished and practice the procedure of the experiment before going to the laboratory.

The theoretical content allows students to study playing games. In this way students can play a RPG game that ask that players answer some questions in order to solve a numerical exercise. The addition of virtual prices as medals when the student finishes the dungeon, or the laboratory practices increases the motivation in the users.

All surveys show us that the GBL of chemistry have a good reception by students. Due these results, in the future, the game is going to increase the available content. The next step is to add other laboratory practices and program other theoretical content. Moreover, there is another educative innovation project in collaboration with the Optic and Optometric department to add a clinic diagnosis practice in this GBL. the objective of this project is to obtain an interdisciplinary in collaboration with other universities nationals and internationals to allow students to get access to university content in an amusing way.

5.   References

Armellini, A., & Rodriguez, B. C. P. (2021). Active blended learning. *Cases on Active Blended Learning in Higher Education Advances in Educational Technologies and Instructional Design*, 1-22. DOI: 10.4018/978-1-7998-7856-8.ch001.

Bonde, M. T., Makransky, G., Wandall, J., Larsen, M. V., Morsing, M., Jarmer, H., & Sommer, M. O. A. (2014). Improving biotech education through gamified laboratory simulations. *Nature Biotechnology*, 32(7), 694–697. DOI: 10.1038/nbt.2955.

Bridgeland, J. M., DiIulio Jr, J. J., & Morison, K. B. (2006). The silent epidemic: Perspectives of high school dropouts. Civic Enterprises.

Greipl, S., Moeller, K., & Ninaus, M. (2020). Potential and limits of game-based learning. Loughborough University. Journal contribution. https://hdl.handle.net/2134/13621973.v1

Hartt, M., Hosseini, H., & Mostafapour, M. (2020). Game on: Exploring the Effectiveness of Game-based Learning. *Planning Practice & Research*, 35(5), 589-604. DOI: 10.1080/02697459.2020.1778859.

Huang, W. H. Y., & Soman, D. (2013). Gamification of education. Research Report Series: Behavioural Economics in Action. Rotman School of Management, University of Toronto.

Kapp, K. M. (2012). The gamification of learning and instruction: game-based methods and strategies for training and education. John Wiley & Sons.

Kiryakova, G., Angelova, N., & Yordanova, L. (2014). Gamification in education. Proceedings of 9th International Balkan Education and Science Conference, Edirne, Turkey.

Laboratory guide, Analytical Chemistry Department. (2020). Practice Guide for Classic Qualitative Analysis of the Analytical Chemistry Laboratory-I Subject of the Degree in Chemistry of the University of Valencia.

Mayo, M. J. (2009). Video Games: A Route to Large-Scale STEM Education? *Science*, 323(5910), 79-82. DOI: 10.1126/science.1166900.

Ofosu-Ampong, K., Boateng, R., Anning-Dorson, T., & Kolog, E. A. (2020). Are we ready for Gamification? An exploratory analysis in a developing country. *Education and Information Technologies*, 25(3), 1723-1742. DOI: 10.1007/s10639-019-10057-7.

Pegalajar, M.C. (2021) Implicaciones de la gamificación en Educación Superior: una revisión sistemática sobre la percepción del estudiante. *Revista de Investigación Educativa*, 39(1), 169-188. DOI: 10.6018/rie.419481.

Pérez, F. Q. (2016). Aplicación de herramientas de gamificación en física y química de secundaria. *Opción*, 32 (12), 327-348.

Pho, A., & Dinscore, A. (2015). Game-based learning. *Tips and trends*, 1-5.

Pivec, M., Dziabenko, O., & Schinnerl, I. (2003). Aspects of game-based learning. In 3rd International Conference on Knowledge Management, Graz, Austria.

Rabah, J., Cassidy, R., & Beauchemin, R. (2018). Gamification in education: Real benefits or edutainment. In proceedings of European Conference on E-Learning (pp. 1-12). Greece: Academic Conferences and Publishing International.

Servicio de Prevención y Medio Ambiente (2022). Sistema de recogidas. Universitat de València. https://www.uv.es/uvweb/servicio-prevencion-medioambiente/es/medio-ambiente/area-medio-ambiente/residuos-laboratorio/sistema-recogidas-1285902695195.html

Shi, Y. R., & Shih, J. L. (2015). Game factors and game-based learning design model. *International Journal of Computer Games Technology*, 2015(1), 1-11. DOI: 10.1155/2015/549684.

Stănescu, D. F., ioniță, C., & ioniță, A. M. (2020). Game-thinking in Personnel Recruitment and Selection: Advantages and Disadvantages. Postmodern Openings/Deschideri Postmodern, 11(2), 267-276. DOI: 10.18662/po/11.2/174.

Subhash, S., & Cudney, E. A. (2018). Gamified learning in higher education: A systematic review of the literature. *Computers in human behavior*, 87, 192-206. DOI: 10.1016/j.chb.2018.05.028.

Tu, C. H., Sujo-Montes, L. E., & Yen, C. J. (2015). Gamification for learning. In Media Rich Instruction: Connecting Curriculum to All Learners (pp. 203-217). Springer International Publishing. DOI: 10.1007/978-3-319-00152-4_13.

Zainuddin, Z., Kai Wah Chu, S., Shujahat, M., & Perera, C.J. (2020). The impact of gamification on learning and instruction: A systematic review of empirical evidence. *Educational Research Review*, 30, 100326. DOI: 10.1016/j.edurev.2020.100326.
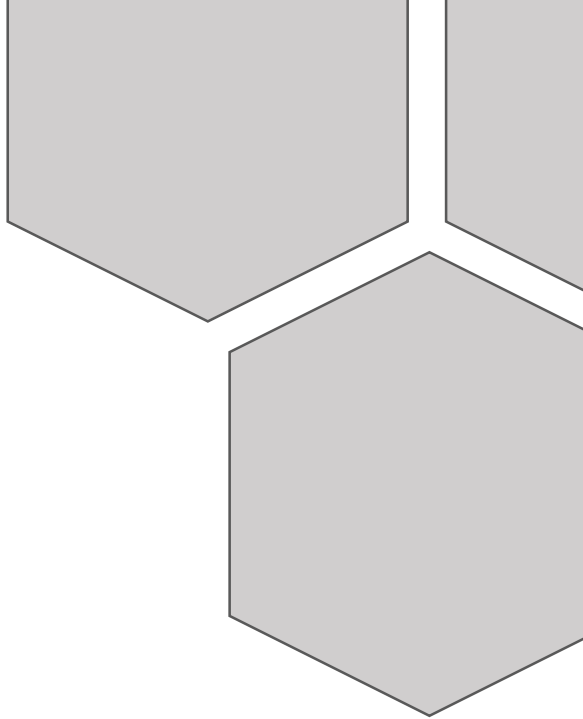
RESUMEN
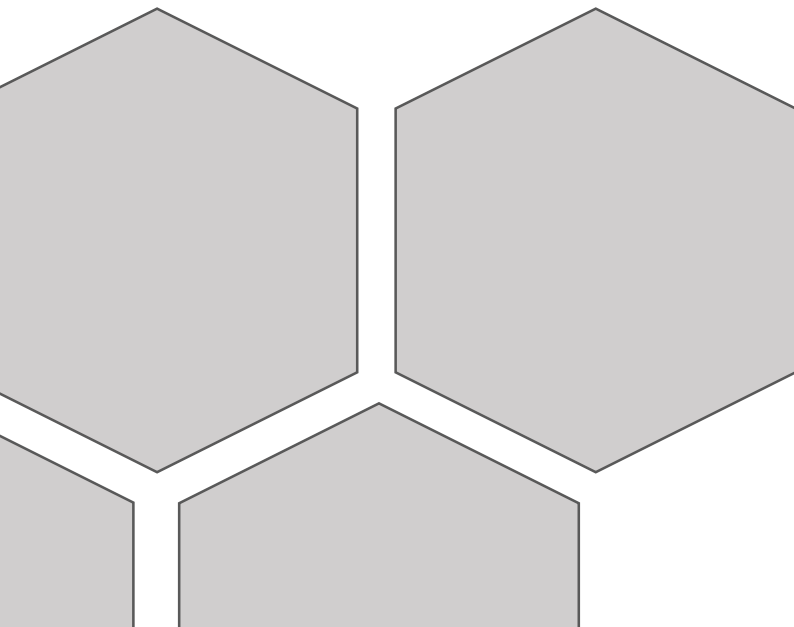
El avance de la tecnología en los últimos años ha sido muy notable, y su desarrollo continúa estando en aceleración. Situaciones que eran impensables hace 30 años, gracias a la tecnología, no solo son una realidad, sino que además están al alcance de cualquier usuario. Esto puede apreciarse en el empleo de los *smartphones*, que permiten a los ciudadanos tener en sus manos múltiples herramientas que normalmente requerirían de un instrumento específico. También se ha visto que la robótica ha pasado de requerir herramientas complejas y un personal especializado a simplemente necesitar curiosidad e interés para aprender su funcionamiento, llegando a encontrarse cursos de iniciación en robótica incluso para niños.

El objetivo principal de esta tesis es mostrar las ventajas de la interconexión entre la rama de conocimiento de la química con las nuevas tecnologías, enfocándose en la importancia de la programación, tratamiento del color de las imágenes o la impresión 3D. La tesis comprende 15 capítulos divididos en 3 secciones:

1. El primer bloque se basa en el uso del *smartphone* como herramienta de análisis y se divide en 10 capítulos. Uno de los aspectos más destacables de un *smartphone* es su cámara, y dado que las cámaras captan información referente al color del entorno, se pueden utilizar para realizar análisis colorimétricos después de filtrar y tratar, mediante códigos de programación adecuados, la información recogida en las imágenes.

2. El segundo bloque comprende 4 capítulos y está enfocado en el desarrollo de robots para la realización de análisis de manera automatizada. El desarrollo tecnológico ha logrado que aparezcan plataformas sencillas para programar, de manera que hasta el usuario más novato lo puede hacer e incluso puede crear dispositivos electrónicos. Entre estas plataformas podemos encontrar las placas Arduino y los dispositivos Raspberry Pi. Con la correcta programación de dichas placas y las conexiones a los sensores y dispositivos adecuados se puede lograr una automatización del laboratorio a bajo coste y acorde a las necesidades del operador.

3. Por último, el tercer bloque está centrado, en un único capítulo, en la investigación docente. Entre las actividades realizadas dentro de la comunidad universitaria no solo está la investigación del conocimiento básico o su aplicación, sino que sobre la docencia también recae una importancia considerable. Debido a esto se ha planteado el desarrollo y evaluación de un videojuego como instrumento docente desde el punto de vista de la gamificación y el *Game-Based Learning* (GBL).

El primer capítulo de esta tesis trata la problemática de la información de color recibida por los *smartphone* y se compara la información captada por diversos teléfonos con la información obtenida por instrumentos de medida de color de referencia. Los siguientes 4 capítulos están basados en la obtención de información

mediante la imagen directa obtenida con el *smartphone*. En estos capítulos se obtiene información sobre el contenido de hierro foliar y clorofila en hojas y entornos acuáticos sin necesidad de tratamiento de la muestra. Los 4 capítulos posteriores obtienen información de la imagen tras realizar un tratamiento o una reacción química sobre la muestra. En estos se ha trabajado con colorantes alimentarios y quinina en muestras alimentarias y en el desarrollo de un kit para la cuantificación de cobre en aguas tratadas. El último capítulo se basa en el desarrollo de una transformación de la imagen captada con el teléfono para permitir establecer diferencias organolépticas de madurez en el tomate por parte de personas dicrómatas.

El primer capítulo del segundo bloque (Capítulo 11) hace una revisión de los sensores electrónicos acoplables a Arduino y Raspberry Pi que están siendo aplicados en la realización de análisis. En este capítulo no solo se plantea la revisión de dichos sensores, sino que también expone su montaje y la forma de programarlos. El segundo capítulo de este bloque desarrolla un dispositivo para el análisis de color con un sensor de color empleando Raspberry Pi. Este dispositivo no solo realiza un análisis automatizado, sino que se ha acoplado a un muestreador construido con impresión 3D y programado con la placa Raspberry Pi para poder realizar el análisis automatizado de diversas muestras. Los siguientes dos capítulos tratan sobre dispositivos para automatizar la preparación y análisis de muestras empleando Arduino. En estos casos los análisis se realizan mediante el empleo de sensores de color.

El último capítulo de la tesis (Capítulo 15) se enfoca en la investigación docente con un GBL. Se ha programado un videojuego para contener prácticas de laboratorio simuladas y con ejercicios para ayudar a los estudiantes a reforzar los conocimientos. Además, el videojuego presenta un minijuego de gestión de residuos del laboratorio y videos para explicar aquellos apartados más complejos de los contenidos de la planificación docente.

1.   El smartphone en análisis instrumental

El gran desarrollo de las técnicas instrumentales data de la segunda guerra mundial. A partir de esta, los métodos instrumentales de análisis comenzaron a emplearse con más frecuencia frente a los métodos clásicos de análisis (Karayannis & Efstathiou, 2012). En un análisis, los instrumentos empleados hacen uso de las radiaciones electromagnéticas o de alguna propiedad física de la materia para obtener información que, tras ser manipulada e interpretada, genera resultados de los parámetros de interés. De acuerdo con esta definición se puede entender que los aparatos empleados para conseguir dicha información sirve como medio de comunicación entre la muestra estudiada y el operador (Skoog et al., 2017; Robinson et al., 2005). En la Figura R.1 se puede observar una breve cronología sobre la evolución en el desarrollo de algunas de las diferentes técnicas conocidas.
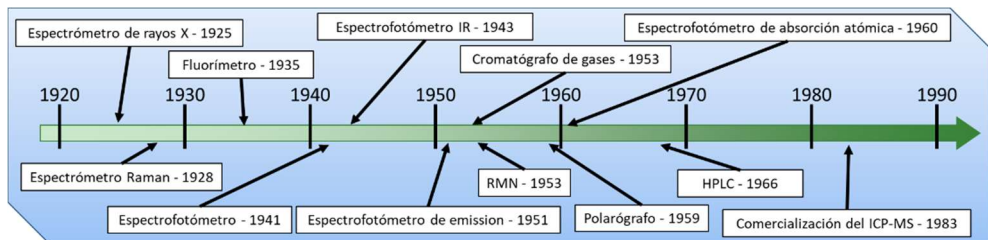
Figura R.1: Breve cronología sobre el avance en las técnicas instrumentales (Clark et al., 1925; Engelhardt, 1999; Karayannis & Efstathiou, 2012; Pyke, 1937; Raman & Krishnan, 1928).

Dado que los instrumentos analíticos permiten recoger datos sobre las propiedades físicas de las muestras de estudio, el *smartphone* puede encajar dentro de esta definición. Este dispositivo, también conocido como teléfono inteligente, es un aparato pequeño, que ha logrado la accesibilidad de las personas a la información y a las redes sociales. Dadas sus características, es un objeto ampliamente distribuido entre la población (Organista-Sandoval et al., 2013). Un *smartphone* se define como un teléfono móvil que ofrece prestaciones similares a la que puede proporcionar un ordenador y destaca por la posibilidad de conectarse a la red. Estos suelen incluir un teclado tipo QWERTY, con la posibilidad de acceso a los servidores de búsqueda de internet o al correo personal, de efectuar llamadas o enviar mensajes entre otras. Sin embargo, lo más destacable de este tipo de teléfonos es la presencia de diferentes tipos de sensores y la posibilidad de trabajar en diferentes aplicaciones accesibles desde la tienda del teléfono.

Si estos dispositivos presentan sensores, podrán recoger información del medio, y con esta información, un usuario puede hacer interpretaciones del entorno. Por lo tanto, este aparato actúa como intermediario entre la información proporcionada

por el objeto de estudio y el operador. El smartphone puede actuar como herramienta en las técnicas instrumentales, y entre las diferentes posibilidades que ofrece un teléfono inteligente para ser empleado en la obtención de información destaca la cámara fotográfica para la toma de imágenes.

De acuerdo con la Comisión Internacional sobre la Iluminación (CIE), la colorimetría es "La medida de los estímulos de color basadas en una serie de convenciones" (CIE, 2011). En química, la colorimetría es una técnica que se emplea para determinar la concentración de diferentes compuestos a partir del color de la muestra (Housecroft & Constable, 2010). Para evaluar el color de un objeto, este tiene que ser iluminado y medir la luz reflejada (Figura R.2A), sin embargo, en el caso de los líquidos que son transparentes, el color se evalúa mediante la transmisión de la luz a través del fluido (Figura R.2B). Esto queda reflejado en la ecuación de la Ley de Lambert-Beer (Ecuación 1) en donde se muestra una relación entre la absorbancia de la muestra líquida y la concentración del compuesto que absorbe la radiación (Shellhammer, 2009). Esto se puede traducir en que hay una correlación entre los compuestos presentes en la muestra y el color que presenta. El *smartphone*, al disponer de una cámara fotográfica, es capaz de obtener información sobre el color del entorno. Si es capaz de obtener información del color, podría ser capaz de obtener información sobre su composición química. Por lo tanto, el *smartphone* puede ser usado como instrumento colorimétrico mediante el análisis de imagen de las fotografías.

Cuando se toma una fotografía con el *smartphone* este suele proporcionar una imagen en formato jpg. o jpeg. (Joint Photographic Experts Group). Estos formatos son un tipo de compresión del archivo de imagen que permite almacenar los datos de color mediante los canales RGB y estos mismos datos en escala de grises. Hay numerosas aplicaciones y softwares que permiten obtener la información de los diferentes canales de la imagen para poder trabajar con los datos. De esta manera a partir de una imagen podemos obtener los parámetros de color descompuestos en las componentes Roja, Verde y Azul (RGB) (Rezazadeh et al., 2019). Con estos parámetros de color y la concentración conocida de un analito se pueden crear curvas de calibración para calcular el contenido de dicho analito en una muestra problema. A pesar de los numerosos programas para obtener los parámetros de color, en esta tesis se ha empleado el programa Matlab para trabajar con los datos. Mediante el empleo de este software y de la librería ColorLab (Malo & Luque, 2002), no solo se puede obtener la información codificada en el espacio de color RGB, sino que es posible realizar transformaciones para obtener la información en otros espacios de color como el CIELab o el CIELhC, los cuales expresan la misma información de formas diferentes, que en función de la situación pueden ser más útiles a la hora de crear modelos de calibración.
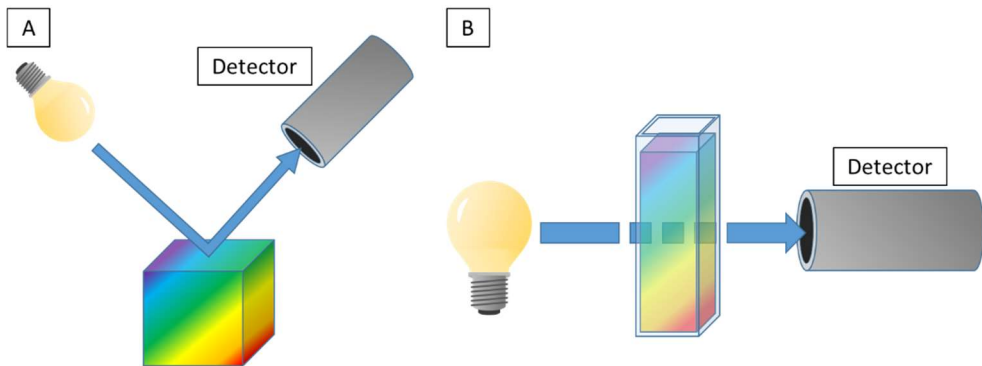
Figura R.2: Disposición de la fuente-muestra-detector para una determinación por reflectancia (A) o por transmitancia (B).

$$A = \propto \cdot l \cdot c \qquad \text{(Ecuación 1)}$$

A=absorbancia; α= absortividad molar; λ= longitud de onda; l= paso óptico; c= concentración del compuesto.

1.1. Espacios de color

Un espacio de color es una organización específica de los colores (Kerr, 2010; Ragain, 2016). El color no es una propiedad física primaria de la materia y, lo que proporciona el color es el espectro de absorbancia/reflectancia que es dependiente de las características de la fuente de iluminación (Kerr, 2010). Estos espectros pueden ser descritos como funciones de la longitud de onda a través del espectro visible. Sin embargo, para describir estas funciones se requeriría un número de parámetros prácticamente infinito. A pesar de esto, varios autores han sugerido que las curvas de reflectancia espectral podrían ser ajustadas a un modelo lineal con un número reducido de parámetros (Billmeyer & Fairman, 1987). A lo largo de los años se han desarrollado una serie de espacios de color que mediante la utilización de 3 parámetros son capaces de describir un color, siendo de los más empleados el RGB, CIEL*a*b*, y CIEL*h*C*.

1.1.1. RGB

La expresión del color mediante RGB es la más común en los dispositivos de captura. Este modelo describe el color mediante 3 canales, los correspondientes al Rojo (R), Verde (G) y Azul (B). Los valores que puede adoptar cada canal varían entre [0, 0, 0], correspondiente al negro, y [2n-1, 2n-1, 2n-1], correspondiente al blanco. El valor de n se corresponde con el número de bits de digitalización del color. El modelo RGB es aditivo, es decir, los colores se obtienen mediante la suma de las

componentes de los 3 canales (Capitán-Vallvey et al., 2015). La representación visual de cómo funciona este modelo se muestra en la Figura R.3.
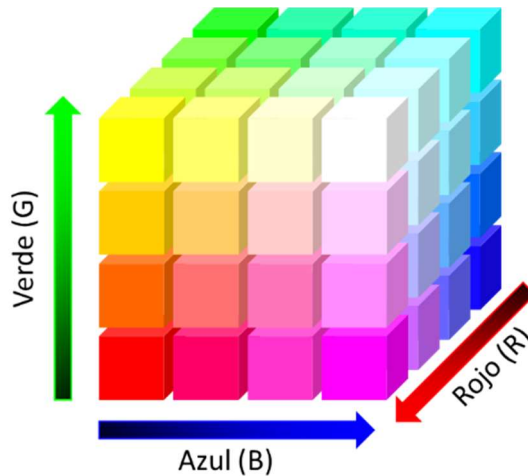
Figura R.3: Representación visual del modelo de color RGB.

En la presente tesis esta forma de expresar el color ha sido utilizada en la calibración de colorantes empleando lanas (Capítulo 7) y en la creación de modelos para la obtención del contenido de clorofila en aguas mediante soporte sólido (Capítulo 4).

En el contexto de los dispositivos digitales que proporcionan la información sobre el color expresado en RGB, delimitados por los pixeles Rojo, Verde y Azul del dispositivo, los colores percibidos por estos dispositivos están restringidos a los colores que pueden ser generados a partir de la combinación de dichos pixeles. En la Figura R.4 se presenta el locus espectral con el triángulo de generación de colores a partir de los tres pixeles de un dispositivo aleatorio. El locus espectral es una representación de los valores triestímulo espectrales de las longitudes de onda de los colores monocromáticos entre 380 y 780 nm. Dentro de esta región representada se encuentran todos los colores, obtenidos mediante combinación de diferentes longitudes de onda (Zharinov & Zharinov, 2017).
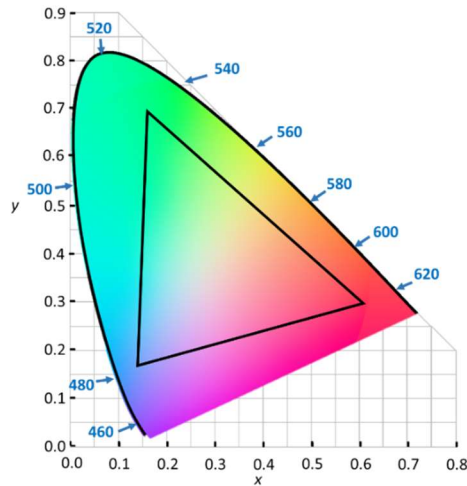
Figura R.4: Locus espectral con la representación de un triángulo de colores generables a partir de un pixel verde, un pixel rojo y un pixel azul (gamut).

Como se puede observar, los pixeles no son colores puros, por lo tanto, hay muchos colores existentes que no pueden ser ni captados ni reproducidos por los dispositivos. En este caso, los dispositivos lo que perciben es el color generable o captable más cercano al color real. Esto podría provocar un problema a la hora de utilizar diferentes smartphones. Cada dispositivo es capaz de percibir unos colores diferentes dependiendo de la cámara empleada por lo que para empezar sería necesario emplear siempre las mismas condiciones lumínicas para tener una reproducibilidad en las medidas. Sin embargo, aunque tengamos dichas condiciones el empleo de otros dispositivos podría proporcionar otros resultados. Esto no solo se aplica entre los dispositivos, sino que también podrían diferir de los resultados obtenidos con dispositivos de referencia como un colorímetro o un espectrorradiómetro. Todo el estudio de los datos de color obtenidos por diferentes dispositivos y su posibilidad de empleo para obtener los colores reales es tratado en el capítulo 1 de la presente tesis.

1.1.2. CIEL*a*b*

Para poder trabajar en términos de uniformidad, la CIE ha recomendado ciertos espacios de color entre los que se encuentra el CIEL*a*b* (Robertson, 1977). Este es un espacio tridimensional que está diseñado para aproximarse a la visión humana (Bansal & Aggarwal, 2011). Las tres coordenadas de este espacio son la coordenada L*, la coordenada a* y la coordenada b*. La primera de ellas hace referencia a la luminosidad siendo un valor de L*= 0 el color negro y un valor de L*= 100 el blanco difuso. La coordenada a* hace referencia a la diferencia de luz reflejada entre el verde y rojo, siendo un valor de a*=-100 el verde y un valor de

a*=+100 el rojo. La última coordenada hace referencia a la diferencia de luz reflejada entre el azul y amarillo, siendo un valor de b*=-100 el azul y un valor de b*=+100 el amarillo (Bansal & Aggarwal, 2011; Robertson, 1977). Como se puede ver en la Figura R.5, es un espacio tridimensional con geometría esférica. Aunque este espacio de color es muy útil, los dispositivos digitales no son capaces de proporcionar los datos en este formato. Para solucionar este inconveniente en los estudios presentados en la tesis, los datos de color son transformados mediante Matlab con el uso de la librería ColorLab (Malo & Luque, 2002). El empleo de la función de la ecuación 2 en un script del programa permite transformar los parámetros de color de RGB a L*a*b*, siendo "rgb" nuestra matriz Nx3 de colores en RGB.
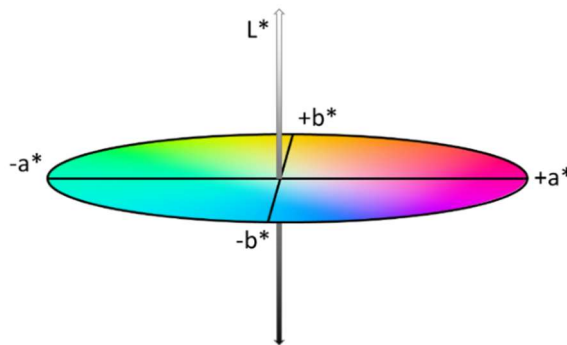
Figura R.5: Representación visual del espacio de color L*a*b*.

$$lab = rgb2lab\ (rgb)$$
(Ecuación 2)

Para poder realizar correctamente este análisis hay que seguir el siguiente procedimiento.

Primero se selecciona la zona de la fotografía que nos interesa analizar, ya sea mediante selección manual o con el empleo de máscaras que escojan una región en función de las características buscadas. Una vez separada nuestra zona de estudio se obtiene el color promedio teniendo en cuenta el color de todos los pixeles de dicha zona. Esto se logra mediante el empleo de una imagen indexada, que consta de dos partes: Por un lado, tenemos la imagen en la que cada zona que presenta un color concreto es identificada con un código, y, por otro lado, tenemos la paleta de colores en la que se identifica cada código con el color que gobierna dichos pixeles/regiones. Esto se logra mediante el empleo de la función representada en la ecuación 3, donde: 1) "im" es la matriz de datos correspondiente a nuestra región de estudio, 2) "col" sería el número de colores que queremos que tenga nuestra paleta, 3) "imind" sería la matriz de datos de nuestra región de

estudio, pero asociando a cada pixel un código y 4) "palRGB" sería nuestra paleta de colores en forma de matriz N*3, siendo N el número de colores, asociada a nuestra imagen indexada.

$$[imind, palRGB] = true2pal(im, col) \qquad \text{(Ecuación 3)}$$

Teniendo la imagen indexada se podría sacar el promedio de color empleando el espacio RGB, sin embargo, en este espacio no es posible al ser aditivo, y es necesario pasar a un espacio de color intermedio, en este caso el XYZ que corresponde a los valores triestímulo. Para esto sería necesario aplicar el cambio de espacio de color a la paleta de colores en RGB y realizar el promedio de color en el espacio de color XYZ, como se puede observar en las funciones de las ecuaciones 4 y 5. En la ecuación 4, "palXYZ" corresponde a nuestra paleta de colores en el espacio de color XYZ. En la ecuación 6 se está realizando el promedio de color en el espacio de color XYZ, utilizando todos los pixeles correspondientes a la imagen indexada que pertenecen a la región que queremos estudiar (masc==1). De esta manera si un color está presente en un determinado número de pixeles, en el promedio se emplea ese color tantas veces como pixeles con ese color estén presentes. Cuando se tiene el color promedio en XYZ sólo hay que pasarla al espacio de color L*a*b* mediante el empleo de la función presente en la ecuación 6, siendo "xyz" nuestra matriz Nx3 de colores y "xyzb" nuestro valor del blanco de referencia en el espacio de color XYZ.

$$palXYZ = rgb2xyz(palRGB) \qquad \text{(Ecuación 4)}$$
$$xyz = mean(palXYZ(imind(masc == 1),:)) \qquad \text{(Ecuación 5)}$$
$$lab = xyz2lab(xyz, xyzb) \qquad \text{(Ecuación 6)}$$

Este espacio de color ha sido útil cuando se ha querido trabajar con un color concreto o con la cantidad de luz. En el capítulo 2 de la tesis se ha logrado determinar el contenido de hierro en hojas mediante una fotografía empleando el parámetro L* de la imagen. La falta de hierro en las hojas provoca una condición denominada clorosis férrica que deriva en un amarilleo de las hojas y por lo tanto en un aumento de luminosidad del color. También ha sido útil el parámetro L* en la determinación fluorimétrica de quinina mediante el análisis de imagen, ya que a mayor contenido de quinina mayor es la fluorescencia. Este espacio no solo proporciona buena información respecto a la luminosidad, sino que también sobre el color, como se puede observar en los capítulos 5 y 10. En el capítulo 5 se ha logrado cuantificar la clorofila en agua mediante la fotografía directa de una columna de agua empleando el parámetro a* que se corresponde con el color verde del analito. Por otro lado, en el capítulo 10 se trabaja con la problemática de la distinción del color verde-rojo, asociada a la madurez del tomate, en personas dicrómatas. Esta dificultad se corresponde con la coordenada a* del presente

espacio. Mediante un intercambio en los valores de las coordenadas a* y b* de la imagen es posible que estas personas encuentren diferencias en la madurez del tomate con los colores azul-amarillo.

1.1.3. CIEL*h*C*

El espacio de color CIEL*h*C* presenta la misma forma que el espacio de color CIEL*a*b*, pero con la diferencia de que en el primero son coordenadas cilíndricas y en el segundo son coordenadas cartesianas (Rossel et al., 2006). En este espacio de color la L* seguiría representando la Luminosidad, la coordenada h* representaría el tono (hue) y la coordenada C* representaría la cromaticidad. La Figura R.6 muestra una representación de este espacio. Para obtener los datos de color perteneciente a este espacio de color mediante el empleo de Matlab, sólo hay que aplicar la función presente en la ecuación 7. Esta función simplemente realiza la transformación de coordenadas cartesianas a coordenadas polares.

Este espacio de color ha sido empleado en los capítulos 6 y 9 de la tesis, en donde para realizar los análisis ha sido necesario trabajar con la cantidad de color, asociado al croma, y la tonalidad de color, estudiada con el parámetro h*. En el capítulo 6 este espacio ha sido fundamental para obtener buenos resultados dado que se ha trabajado con colorantes alimentarios en dulces. Normalmente los dulces presentan uno o dos colorantes para crear toda la gama de colores. Para evaluar un único color solo es necesario trabajar con el croma, sin embargo, en los casos que había una mezcla de colorantes, la proporción de colorantes venia dada por el tono. Una vez que se tenía la proporción de colorantes solo era necesario utilizar la cromaticidad para obtener el contenido total de colorantes. En el capítulo 9 de la presente tesis, el parámetro que se utilizó para realizar el análisis químico mediante análisis de imagen fue el parámetro C*. En este caso se quería evaluar el color de una reacción química ante la presencia de cobre. La disolución sin cobre era incolora y a mayor contenido de cobre más violeta se volvía la disolución. Dado que estamos ante un aumento de color, la cromaticidad es un muy buen parámetro para este análisis.
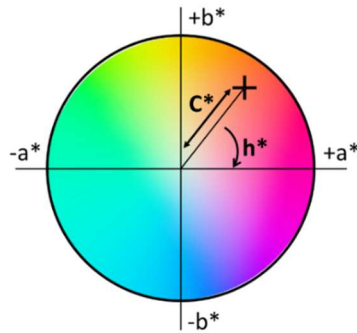
Figura R.6: Representación visual del espacio de color L*h*C*.

$$lhc = lab2perc(lab)$$ (Ecuación 7)

2. Sensores electrónicos en análisis químico

El *smartphone* es un instrumento adecuado para la toma de medidas colorimétricas, como se ha podido observar en esta tesis, siendo necesario realizar un tratamiento de imagen apropiado para llevar a cabo el análisis químico. Si bien estos dispositivos son comunes entre la población hay otro tipo de herramientas que están menos difundidas: los sensores electrónicos.

Los sensores son dispositivos que convierten una variable física en otra variable que puede ser interpretada. En el caso de los sensores electrónicos estaríamos hablando de señales eléctricas (Ebel & Nestel, 1993). Existe una gran variedad de sensores entre los que se pueden encontrar sensores físicos como de presión (Hetprostore, 2022) o inclinación (Llamas, 2022). Sin embargo, estos sensores no son de gran utilizad a la hora de realizar análisis químicos. Por otro lado, se puede encontrar otro tipo de sensores como los de temperatura (Parihnar et al., 2017), de gas (Sahu et al., 2017), de humedad (Bhadani & Vashisht, 2019) o, en los que se centra esta tesis, los sensores de luz (Ashwin & Harish, 2020) y color (de Carvalho et al., 2022). El capítulo 11 de esta tesis realiza una revisión más profunda de los diferentes sensores que pueden ser utilizados para realizar monitoreo o análisis de diversa índole.

Entre los sensores de luz y color el más sencillo de todos es el fotorresistor. Esta herramienta permite obtener información a partir de la luz. Los fotorresistores son dispositivos que varían su resistencia de acuerdo con la cantidad de luz que incide sobre él (Llamas, 2022). A priori estos dispositivos podrían ser útiles, sin embargo, presentan un gran número de desventajas. A pesar de ser muy económicos, menos de 1€, solo pueden medir cantidad de luz, y esto podría ser un problema cuando lo

que ocurre es un cambio de color que no llegue a modificar la cantidad de luz, ya que el sensor no sería capaz de cambiar la resistencia y, por lo tanto, tampoco variaría el valor de la señal analógica. Por otro lado, el rango de valores que puede adoptar esta limitado a 1024 (10 bits). Como alternativa a este sensor de luz, se puede encontrar el sensor BH1750, que no da el valor analógico de la intensidad de corriente, sino que proporciona directamente la medida de la luz en lumen/m^2 y tiene un rango de valores comprendido entre 1 y 65535 (16 bits) (Naylampmechatronics, 2022). A pesar de seguir siendo barato y presentar una mayor exactitud y precisión, volvemos a encontrar el problema de que estos dispositivos sólo son capaces de detectar los cambios asociados a la cantidad de luz. Para ser capaces de realizar medidas de la variación de la luz más eficientes, ya sea de cantidad de luz o de color de la luz, sería recomendable el empleo de sensores de color como el TCS34725. Este sensor presenta 3 filtros para la recepción de información correspondiente a cada canal (rojo, verde, azul y clear), por lo que es capaz no solo de diferenciar la cantidad de luz, sino que también el color (Ams, 2022).

A la hora de poder trabajar con los sensores es necesario contar con un soporte que permita la programación de estos instrumentos con el fin de ser capaces de obtener la información adecuada de ellos. Para poder desarrollar un código de programación y trabajar en las diversas plataformas disponibles normalmente se cree que se necesita un conocimiento extenso del campo, sin embargo, esto no es realmente así. En los últimos años, y con el rápido crecimiento de las nuevas tecnologías, los entornos de programación están siendo más accesibles para un usuario que está iniciándose en este mundo. Tal es la situación que cualquiera puede encontrar a su disposición un gran número de cursos de iniciación en los diversos lenguajes de programación como pueden ser el C++ (Carrillo, 2005), Python (Challenger-Pérez et al., 2014) o R (García et al., 2010). A pesar de la importancia del código, el soporte físico con el cual se va a trabajar es también importante. Para poder programar se necesita un dispositivo a programar y para ello un soporte que traduzca el código en órdenes. Entre los soportes más aptos para un usuario sin experiencia y que, a su vez, son muy versátiles debido a su aplicación en empresa o en el desarrollo de prototipos, se pueden encontrar los dispositivos Arduino y Raspberry Pi.

Arduino es una placa microcontroladora reprogramable que presenta diferentes pines de conexión (tipo hembra) que facilita la creación de los circuitos y la conexión de sensores y controladores. Arduino surgió en 2005 de la mano del instituto de diseño interactivo de Ivrea, en Italia, para facilitar, a bajo costo, la comunicación entre los estudiantes y los diferentes dispositivos (Artero, 2013). Arduino fue creado con la intención de que usuarios no especializados pudieran utilizarla para lograr diferentes objetivos. Fue una plataforma para diseñadores y

artistas con el fin de que pudieran modificar y usar elementos del hardware de manera sencilla y barata (Gibb, 2010). Por otro lado, el dispositivo Raspberry Pi es un ordenador monoplaca de pequeño tamaño que presenta un sistema operativo como un ordenador, pero a pequeña escala. También es posible conectarle periféricos, como un monitor, y poder trabajar dentro de la placa. Además de actuar como un ordenador, presenta pines de conexión al igual que Arduino y, por lo tanto, se pueden conectar diferentes sensores y controladores que son programados por la propia Raspberry (Zhao et al., 2015).

Tanto el sensor de color TCS34725 como las placas Arduino y Raspberry Pi han sido utilizados como herramientas para obtener la información necesaria para llevar a cabo análisis químicos en los capítulos 12, 13 y 14 de la presente tesis. En el capítulo 12 este sensor ha sido programado empleando un ordenador monoplaca Raspberrry Pi4 mediante lenguaje Python. El dispositivo desarrollado consistía en un automuestreador controlado con servos, una bomba peristáltica para impulsar la disolución por el circuito y un sensor TCS34725. Este dispositivo permite la automatización de la medida colorimétrica de diferentes muestras obteniéndose un informe con los valores de color de la disolución. Los analitos estudiados fueron colorantes alimentarios como Tartrazina, Azul brillante FCF y Rojo Allura. En el capítulo 13 de la presente tesis este sensor fue acoplado a un dispositivo empleado para llevar a cabo reacciones colorimétricas de manera automática. El robot fue controlado mediante lenguaje C++ empleando una placa Arduino uno. Este dispositivo, mediante el empleo de microbombas, impulsa la muestra y los diferentes reactivos hasta el detector mediante secuencias de códigos de programación. En el detector se encuentra el resultado de la reacción colorimétrica y mediante el empleo del sensor TCS34725 es posible realizar un calibrado y el análisis químico de diferentes muestras. La reacción empleada para el estudio de la capacidad de estos dispositivos robóticos es la obtenida entre el cobre y el ácido bicinconínico, desarrollada en el capítulo 9 de la presente tesis. Por último, en el capítulo 14 de la presente tesis se han utilizado tanto el sensor TCS34725 como la placa Arduino y código de programación en lenguaje C++ para llevar a cabo el monitoreo del consumo de peróxido de hidrógeno en una reacción de degradación de contaminantes con el método foto-fenton. En este proceso se emplea el hierro y el peróxido de hidrógeno para llevar a cabo un proceso de oxidación avanzada para degradar contaminantes orgánicos. El peróxido de hidrógeno actúa como precursor de radicales hidroxilo que inician la reacción de degradación. De esta manera, con el uso de estas técnicas se puede rehabilitar el agua para su posterior uso.

Todas estas investigaciones dejan entrever la importancia de la interdisciplinariedad con otros campos. La incorporación de conocimientos básicos en programación permite el desarrollo de robots que pueden ser aplicados en

435

química analítica. Sin embargo, esta no es la única tecnología que puede ser utilizada como soporte, la impresión 3D es un tipo de avance tecnológico muy distribuido tanto a nivel profesional como a nivel de usuario que permite crear diferentes estructuras con plástico de tipo PLA, principalmente, de acuerdo con las necesidades del usuario. En la presente tesis se puede observar a lo largo de los diferentes capítulos su utilidad para el desarrollo de soportes personalizados que faciliten las tareas de análisis o permitan llevar a cabo mediciones que de otra forma serían más complicadas o costosas en términos de tiempo invertido.

3.   La investigación docente y el GBL

Como se puede observar, la interdisciplinariedad es algo que está a la orden del día cuando se habla de investigación. Sin embargo, esto no solo se tiene que aplicar a la investigación del conocimiento básico. Las universidades, como lugares de divulgación de conocimiento, también tienen la función de transmitir los conocimientos a los futuros investigadores (Turugare & Rudhumbu, 2020). Por lo tanto, la labor docente es algo que ocupa una gran parte del tiempo invertido en la institución universitaria. Esto se puede comprobar en el número de clases impartidas por los investigadores de las diferentes ramas, los trabajos de final de carrera de investigación que los estudiantes tienen que llevar a cabo adscritos a uno de los departamentos asociados a los estudios impartidos o en los proyectos de innovación docente. Los proyectos de innovación educativa consisten en el desarrollo y la implementación de nuevas herramientas en la enseñanza con la finalidad de lograr una mejora en la adquisición de los contenidos impartidos por parte del estudiantado (Feixas et al., 2018).

Una de las estrategias más comentadas en los últimos años dentro de la investigación en innovación educativa es la gamificación (Kapp, 2012; Pegalajar, 2021). La gamificación es una metodología de aprendizaje en la que el docente aplica técnicas tradicionales de los juegos, como puntos, premios, misiones o tablas de puntuación, dentro del aula y por tanto fuera del contexto propio de un juego (Pivec et al., 2003). De este tipo de metodologías deriva la que se llama Game-Based Learning (GBL). Esta metodología, al contrario de la gamificación que no usa juegos como herramientas docentes, utiliza los juegos como instrumento para transmitir y facilitar la adquisición del conocimiento (Hartt et al., 2020; Perez, 2015).

En el capítulo 15 de la presente tesis se habla de un trabajo de innovación docente que consiste en el desarrollo de un GBL como herramienta de enseñanza en los estudios de química. Este videojuego ha sido creado con el empleo del programa RPGMaker MZ® (Figura R.7). Al hablar de un videojuego estamos hablando de la

necesidad de escribir códigos de programación para llevar a cabo las acciones del juego. Este programa está basado en lenguaje Ruby (Muñoz Alejandre, 2022), pero a pesar de necesitar de conocimientos básicos de programación, el programa está hecho con la idea de que cualquier persona pueda desarrollar un videojuego sin ser un profesional. Esto se ha logrado mediante la codificación de códigos preestablecidos nombrados como acciones. De esta manera el usuario solo tiene que seleccionar las acciones que quiere que el personaje lleve a cabo para obtener el código del juego. El juego desarrollado intenta abordar temas como la preparación y refuerzo de prácticas de laboratorio, la formalización de conceptos y procedimientos para resolver ejercicios numéricos y la incorporación de material soporte para reforzar los contenidos del temario. El proyecto de innovación docente se encuentra en su tercer año siendo estos: UV-SFPIE_PID-1356255 (primer año), UV-SFPIE_PID-1641484 (segundo año) y UV-SFPIE_PID-2079679 (tercer año).

Figura R.7: Captura de pantalla de la pantalla de carga del programa.

4. Conclusiones

Como se puede comprobar, esta tesis deja entrever la utilidad de los conocimientos informáticos en una era regida por los avances tecnológicos. Dada la gran cantidad de herramientas a disposición de los usuarios para el control de dispositivos y creación de contenido, unos conocimientos básicos en programación pueden sentar la base de proyectos que, sin estos conceptos, no podrían llevarse a cabo. Este crecimiento tecnológico de la sociedad hace que la interrelación entre los conocimientos químicos e informáticos sea más palpable. Gracias a unas bases en la programación de códigos se ha logrado elaborar procedimientos de análisis de imagen, desarrollar dispositivos de automatización y herramientas docentes más actualizadas y cercanas a los estudiantes, todas enfocadas hacia el punto de vista

químico y siendo creadas por personal *amateur*. Con esto se evidencia la utilidad que puede tener la informática y las nuevas tecnologías en cualquier campo de investigación para el desarrollo de equipos o softwares personalizados y adaptados a las necesidades del investigador.

5.   Bibliografía

Ams. (Accessed September 26, 2022). Colour Sensor – Colour Light-To-Digital Converter – TCS34725 ams | ams, (n.d.). https://ams.com/tcs34725#tab/description

Artero, Ó. T. (2013). Arduino. Curso práctico de formación. RC libros. Madrid.

Ashwin, S. H., & Harish, S. V. (2020). Titration machine: A new approach using Arduino. In Kalam, A., Niazi, K.R., Soni, A., Siddiqui, S.A., & Mundra, A. (Eds.), Intelligent Computing Techniques for Smart Energy Systems. Springer, Singapore.

Bansal, S., & Aggarwal, D. (2011). Colour image segmentation using CIELab colour space using ant colony optimization. *International Journal of Computer Applications*, 29(9), 28-34. DOI:10.5120/3590-4978.

Bhadani, P., & Vashisht, V. (2019). Soil moisture, temperature and humidity measurement using arduino. In 9th International Conference on Cloud Computing, Data Science & Engineering. IEEE.

Billmeyer Jr, F. W., & Fairman, H. S. (1987). CIE method for calculating tristimulus values. *Colour Research & Application*, 12(1), 27-36. DOI:10.1002/col.5080120106.

Capitán-Vallvey, L. F., Lopez-Ruiz, N., Martinez-Olmos, A., Erenas, M. M., & Palma, A. J. (2015). Recent developments in computer vision-based analytical chemistry: A tutorial review. *Analytica Chimica Acta*, 899, 23-56. DOI: 10.1016/j.aca.2015.10.009.

Carrillo, A. G. (2005). Fundamentos de programación en C++. Primera edición. García, F. M. (Ed.). Delta Publicaciones. Madrid.

Challenger-Pérez, I., Díaz-Ricardo, Y., & Becerra-García, R. A. (2014). El lenguaje de programación Python. *Ciencias Holguín*, 20(2), 1-13.

CIE. (Accessed September 20, 2022). https://cie.co.at/eilvterm/17-25-014

Clark, G. L., Weber, H. C., & Hershey, R. L. (1925). A Precision X-Ray Spectrometer for Chemical Investigations. *Industrial & Engineering Chemistry*, 17(11), 1147-1150.

de Carvalho, G., Machado, C. C. S., Inácio, D. K., da Silveira Petruci, J. F., & Silva, S. G. (2022). RGB colour sensor for colorimetric determinations: Evaluation and

quantitative analysis of coloured liquid samples. *Talanta*, 241, 123244. DOI: 10.1016/j.talanta.2022.123244.

Ebel, F., & Nestel, S. (1993). Sensores para la técnica de procesos y manipulación: sensores de proximidad. Festo Didactic. Esslingen.

Engelhardt, H. (1999). GC und HPLC—die letzten 50 Jahre. *Nachrichten aus Chemie, Technik und Laboratorium*, 47(12), 1451-1452. DOI: 10.1002/nadc.19990471229.

Feixas, M., Martínez-Usarralde, M. J., & López-Martín, R. (2018). Do teaching innovation projects make a difference? Assessing the impact of small-scale funding. *Tertiary Education and Management*, 24(4), 267-283. DOI: 10.1080/13583883.2017.1417470.

García, J. M. C., Portillo, E. M., & Cezón, P. A. (2010). Introducción a la programación estadística con R para Profesores.

Gibb, A. M. (2010). New media art, design, and the Arduino microcontroller: A malleable tool. Thesis. Pratt Institute.

Hartt, M., Hosseini, H., & Mostafapour, M. (2020). Game on: Exploring the Effectiveness of Game-based Learning. *Planning Practice & Research*, 35(5), 589-604. DOI: 10.1080/02697459.2020.1778859.

Hetprostore. (Accessed September 26, 2022). Sensor de Fuerza o Presión MF01. https://hetpro-store.com/TUTORIALES/sensor-de-fuerza-o-presion-mf01/#:~:text=El%20sensor%20de%20fuerza%20o,sensor%20cambia%20su%20resistencia%20interna.

Housecroft, C. E., & Constable, E. C. (2010). Chemistry: an introduction to organic, inorganic and physical chemistry. Fourth edition. Pearson education. Harlow.

Kapp, K. M. (2012). The gamification of learning and instruction: game-based methods and strategies for training and education. Taff, R. (Ed.). John Wiley & Sons. San Francisco.

Karayannis, M. I., & Efstathiou, C. E. (2012). Significant steps in the evolution of analytical chemistry—Is the today's analytical chemistry only chemistry? *Talanta*, 102, 7-15. DOI: 10.1016/j.talanta.2012.06.003.

Kerr, D. A. (2010). The CIE XYZ and xyY colour spaces. *Colourimetry*, 1(1), 1-16.

Llamas, L. (Accessed September 26, 2022). Medir inclinación con arduino y sensor TILT SW-520D. https://www.luisllamas.es/medir-inclinacion-con-arduino-y-sensor-tilt-sw-520d/#:~:text=%C2%BFQue%20es%20un%20sensor%20tilt,partir%20de%20una%20cierta%20inclinaci%C3%B3n.

Llamas, L. (Accessed September 26, 2022). https://www.luisllamas.es/medir-nivel-luz-con-arduino-y-fotoresistencia-ldr/.

Malo, J., & Luque, M. J. (2002). ColourLab: the Matlab toolbox for Colourimetry and Colour Vision. Univ. Valencia. http://isp.uv.es/code/visioncolour/colourlab.html.

Muñoz Alejandre, S. (2022). PAWN: Del tablero a videojuego en 3D con UnityDesarrollo del modo multijugador online, Tesis doctoral, Universitat Politècnica de València.

Naylampmechatronics. (Accessed September 26, 2022). https://naylampmechatronics.com/blog/44_tutorial-modulo-sensor-de-luz-bh1750.html.

Organista-Sandoval, J., McAnally-Salas, L., & Lavigne, G. (2013). El teléfono inteligente (smartphone) como herramienta pedagógica. *Apertura*, 5(1), 6-19.

Parihar, V. R., Tonge, A. Y., & Ganorkar, P. D. (2017). Heartbeat and temperature monitoring system for remote patients using Arduino. *International Journal of Advanced Engineering Research and Science*, 4(5), 237161. DOI: 10.22161/ijaers.4.5.10.

Pegalajar, M. C. (2021) Implicaciones de la gamificación en Educación Superior: una revisión sistemática sobre la percepción del estudiante. *Revista de Investigación Educativa*, 39(1), 169-188. DOI: 10.6018/rie.419481

Perez, D. (2015). Make a 2D RPG in a Weekend: With RPG Maker MV. Second edition. Renow-Clarke B. (Ed.) Apress.

Pivec, M., Dziabenko, O., & Schinnerl, I. (2003). Aspects of game-based learning. In 3rd International Conference on Knowledge Management, Graz, Austria.

Pyke, M. A. (1937). The chemical measurement of vitamin B1 in foodstuffs and biological material by means of the thiochrome reaction. *Biochemical Journal*, 31(11), 1958. DOI: 10.1042/bj0311958.

Ragain, J. C. (2016). A review of colour science in dentistry: Colourimetry and colour space. *Journal of Dentistry, Oral Disorders & Therapy*, *4*, 1-5. DOI: 10.15226/jdodt.2016.00148.

Raman, C. V., & Krishnan, K. S. (1928). A new class of spectra due to secondary radiation. *Indian Journal of Physics*, 2, 399-419.

Rezazadeh, M., Seidi, S., Lid, M., Pedersen-Bjergaard, S., & Yamini, Y. (2019). The modern role of smartphones in analytical chemistry. *Trends in Analytical Chemistry,* 118, 548-555. DOI: 10.1016/j.trac.2019.06.019.

Robertson, A. R. (1977). The CIE 1976 colour-difference formulae. *Colour Research & Application*, 2(1), 7-11. DOI: 10.1002/j.1520-6378.1977.tb00104.x.

Robinson, J. W., Frame, E. M. S., Frame, G. M., Eileen, M., & Skelly, F. (2005). Undergraduate instrumental analysis. Seventh edition. CRC Press. Boca Raton.

Rossel, R. V., Minasny, B., Roudier, P., & Mcbratney, A. B. (2006). Colour space models for soil science. *Geoderma*, 133(3-4), 320-337. DOI: 10.1016/j.geoderma.2005.07.017.

Sahu, P., Dixit, S., Mishra, S., & Srivastava, S. (2017). Alcohol detection based engine locking system using MQ-3 sensor. *International Research Journal of Engineering and Technology*, 4(4), 979-981.

Shellhammer, T. H. (2009). Beer colour. In Bamforth, C.W. (Ed.). Beer: a quality perspective (pp. 213-227). Elsevier Inc.

Skoog, D. A., Holler, F. J., & Crouch, S. R. (2017). Principles of instrumental analysis. Seventh edition. Cengage learning. Boston.

Turugare, M., & Rudhumbu, N. (2020). Integrating technology in teaching and learning in universities in Lesotho: opportunities and challenges. *Education and Information Technologies*, 25(5), 3593-3612. DOI: 10.1007/s10639-019-10093-3.

Zhao, C. W., Jegatheesan, J., & Loon, S. C. (2015). Exploring iot application using raspberry pi. *International Journal of Computer Networks and Applications*, 2(1), 27-34.

Zharinov, I. O., & Zharinov, O. O. (2017). Spectral locus interpolation with splines in optical instruments. In IOP Conference Series: *Materials Science and Engineering* (286, 012013). DOI 10.1088/1757-899X/286/1/012013.